

**COCAINE-AND AMPHETAMINE-REGULATED TRANSCRIPT
(CART) PEPTIDE AS A COMMON MESSENGER IN
NEURAL PATHWAYS THAT MEDIATE
ENERGY BALANCE AND REPRODUCTION**

By

SANTOSH KUMAR

LIFE11201104003

**National Institute of Science Education and Research (NISER),
Bhubaneswar**

A thesis submitted to the

Board of Studies in Life Sciences

In partial fulfillment of requirements

for the Degree of

DOCTOR OF PHILOSOPHY

of

HOMI BHABHA NATIONAL INSTITUTE



April, 2018

Homi Bhabha National Institute¹

Recommendations of the Viva Voce Committee

As members of the Viva Voce Committee, we certify that we have read the dissertation prepared by Mr. Santosh Kumar entitled "Cocaine-and amphetamine-regulated transcript (CART) peptide as a common messenger in neural pathways that mediate energy balance and reproduction" and recommend that it may be accepted as fulfilling the thesis requirement for the award of Degree of Doctor of Philosophy.



Chairman – Dr. A. Srinivasan, NISER, Bhubaneswar

Date: 27.4.18



Guide / Convener – Dr. Praful Singru, NISER, Bhubaneswar

Date: 27.4.2018

Co-guide - None

Date:



External Examiner- Dr. Aurnab Ghose, IISER, Pune

Date: 27-4-2018



Member 2- Dr. Chandan Goswami, NISER, Bhubaneswar

Date:

27-04-2018



Member 3- Dr. V Badireenath Konkimalla, NISER, Bhubaneswar

Date: 27-04-2018



Member 1- Dr. Avinash Sonawane, School of Biotechnology,
KIIT University, Bhubaneswar

Date: 27.04.2018

Final approval and acceptance of this thesis is contingent upon the candidate's submission of the final copies of the thesis to HBNI.

I/We hereby certify that I/we have read this thesis prepared under my/our direction and recommend that it may be accepted as fulfilling the thesis requirement.

Date: 27.04.2018

Place: NISER, Bhubaneswar



Dr. Praful Singru

Co-guide (if applicable)

Guide

¹ This page is to be included only for final submission after successful completion of viva voce.

STATEMENT BY AUTHOR

This dissertation has been submitted in partial fulfillment of requirements for an advanced degree at Homi Bhabha National Institute (HBNI) and is deposited in the Library to be made available to borrowers under rules of the HBNI.

Brief quotations from this dissertation are allowable without special permission, provided that accurate acknowledgement of source is made. Requests for permission for extended quotation from or reproduction of this manuscript in whole or in part may be granted by the Competent Authority of HBNI when in his or her judgment the proposed use of the material is in the interests of scholarship. In all other instances, however, permission must be obtained from the author.

Santosh Kumar
Santosh Kumar

Date: 27/04/2018

DECLARATION

I, hereby declare that the investigation presented in the thesis has been carried out by me. The work is original and has not been submitted earlier as a whole or in part for a degree/diploma at this or any other Institution/University.

Santosh Kumar
Santosh Kumar

Date: 27/04/2018

LIST OF PUBLICATIONS ARISING FROM THE THESIS

JOURNALS

1. “Transient receptor potential vanilloid 5 (TRPV5), a highly Ca²⁺-selective TRP channel in the rat brain: relevance to neuroendocrine regulation”, **Kumar S**, Singh U, Goswami C, Singru PS, *Journal of Neuroendocrinology*, **2017**, 29, 4, DOI: 10.1111/jne.12466
2. “Transient receptor potential vanilloid 6 (TRPV6) in the mouse brain: Distribution and estrous cycle-related changes in the hypothalamus”, **Kumar S**, Singh U, Singh O, Goswami C, Singru PS, *Neuroscience*, **2017**, 344: 204-216.
3. “Transient receptor potential vanilloid 1-6 (TRPV1-6) gene expression in the mouse brain during estrous cycle”, **Kumar S**, Singh O, Singh U, and Singru PS, **2018**, (under review).

CHAPTERS IN BOOKS AND LECTURES NOTES

None

CONFERENCES

1. “Estrous cycle-related changes in transient receptor potential vanilloid (TRPV) ion channels gene expression in mouse brain”, **Kumar S** and Singru PS, *International Society of Neurochemistry (ISN) and the European Society for Neurochemistry (ESN), Paris, France, 2017 (Poster presentation)*
2. “Transient receptor potential vanilloid 5 (TRPV5), a highly Ca²⁺-selective TRP channel in the rat brain: organization and role in the regulation of CART-containing neurons of the hypothalamic arcuate nucleus”, **Kumar S**, Singh U, Goswami C, and Singru PS, *Second Meeting of the Indian Sub-Continental Branch of the International*

Neuropeptide Society, National Institute of Science Education and Research (NISER) and Institute of Life Sciences (ILS), Bhubaneswar, India, 2015 (Poster presentation)

3. “Role of isotocin in the regulation of the hypophysiotropic dopamine neurons in the preoptic area of the catfish, *Clarias batrachus*”, Singh O, **Kumar S**, Singh U, Singru PS, *National Symposium on Comparative Endocrinology and Reproductive Biology (CERB), India, 2015*
4. “Expression and distribution of transient receptor potential vanilloid 5 (TRPV5), a highly Ca²⁺-selective TRP channel in the rat brain”, **Kumar S**, Singh U, Goswami C, and Singru PS, *International Symposium on Translational Neuroscience & XXXII Annual Conference of the Indian Academy of Neurosciences, National Institute of Mental Health and Neurosciences (NIMHANS), Bangalore, India, 2014 (Poster presentation)*
5. “CART neurons of the hypothalamic arcuate nucleus are equipped with TRPV3: role in driving CART-GnRH pathway”, **Kumar S** and Singru PS, *International Meeting on Neuromodulation of Behaviour, National Centre for Biological Sciences (NCBS), Bangalore, India, 2014 (Poster presentation)*
6. “Interaction between neuropeptide Y and dopamine in the ventral telencephalon of the Indian major carp, *Cirrhinus cirrhosus*”, Saha S, **Kumar S**, Singh U, Singru PS, *International Conference on Comparative Endocrinology and Physiology (ICCEP), RTM Nagpur University, Nagpur, India, 2013*
7. “TRPV6 in the forebrain of the catfish, *Clarias batrachus*”, **Kumar S**, Singh U, Goswami C, Singru PS, *International Conference on Comparative Endocrinology and Physiology (ICCEP), RTM Nagpur University, Nagpur, India, 2013 (Best oral presentation award)*

8. “Neural circuitry and neuromodulators regulating LH cells and reproduction of teleost”, Singru PS, Singh U, **Kumar S**, Saha S, *National Symposium on Emerging Trends in Biotechnology: Present Scenario and Future Dimensions*, **2012**
9. “Organization of dopamine in the forebrain and pituitary of the catfish, *Clarias batrachus*: Relevance to reproduction”, Singh U, **Kumar S**, Singru PS, *National Colloquium on Recent Advances in Molecular and Cellular Endocrinology, Department of Zoology, Banaras Hindu University, Varanasi, India*, **2011**

OTHER PUBLICATIONS

1. “Tyrosine hydroxylase in the olfactory system, forebrain and pituitary of the Indian major carp, *Cirrhinus cirrhosus*: organisation and interaction with neuropeptide Y in the preoptic area”, **Kumar S**, Singh U, Saha S, Singru PS, *Journal of Neuroendocrinology*, **2014**, 26 (6): 400-411.
2. “Role of isotocin in regulation of the hypophysiotropic dopamine neurons in the preoptic area of the catfish, *Clarias batrachus*”, Singh O, **Kumar S**, Singh U, Bhute Y, Singru PS, *Journal of Neuroendocrinology*, **2016**, 28, 12, DOI: 10.1111/jne.12441
3. “Cocaine- and amphetamine-regulated transcript peptide (CART) in the brain of zebra finch, *Taeniopygia guttata*: Organization, interaction with neuropeptide Y, and response to changes in energy status”, Singh O, **Kumar S**, Singh U, Kumar V, Lechan RM, Singru PS, *Journal of Comparative Neurology*, **2016**, 524 (15): 3014-3041.
4. “Transient receptor potential vanilloid 3 (TRPV3) in the ventral tegmental area of rat: Role in modulation of the mesolimbic-dopamine reward pathway”, Singh U, **Kumar S**, Shelkar GP, Yadav M, Kokare DM, Goswami C, Lechan RM, Singru PS, *Neuropharmacology*, **2016**, 110 (Pt A): 198-210.

5. "Noradrenergic inputs from locus coeruleus to posterior ventral tegmental area are essential to support ethanol reinforcement", Shelkar GP, **Kumar S**, Singru PS, Subhedar NK, Kokare DM, *Addiction Biology*, **2015**, 22 (2): 291-302.
6. "Elucidating the role of disulfide bond on amyloid formation and fibril reversibility of somatostatin-14: relevance to its storage and secretion", Anoop A, Ranganathan S, Das Dhaked B, Jha NN, Pratihar S, Ghosh S, Sahay S, **Kumar S**, Das S, Kombrabail M, Agarwal K, Jacob RS, Singru P, Bhaumik P, Padinhateeri R, Kumar A, Maji SK, *Journal of Biological Chemistry*, **2014**, 289 (24): 16884-16903.
7. "Interaction between dopamine and neuropeptide Y in the telencephalon of the Indian major carp, *Cirrhinus cirrhosus*", Saha S, **Kumar S**, Singh U, Singh O, Singru PS, *General and Comparative Endocrinology*, **2014**, 220: 78-87.
8. "Interaction between dopamine- and isotocin-containing neurones in the preoptic area of the catfish, *Clarias batrachus*: role in the regulation of luteinising hormone cells", Singh U, **Kumar S**, Singru PS, *Journal of Neuroendocrinology*, **2012**, 24 (11): 1398-1411.

Santosh Kumar

Santosh Kumar

Date: 27/04/2018

DEDICATION

The faith of my parents in me is the actual driver which keeps me going. It's their evergreen love and endless support that today I am submitting this thesis for the award of doctoral degree. I heartily dedicate my thesis to my beloved parents without whom this happy moment is incomplete.

ACKNOWLEDGEMENTS

Words seem small while thanking my Ph.D. thesis supervisor Dr. Praful Singru, NISER, Bhubaneswar, India who gave me opportunity to work in the Laboratory of Neural Circuits and Behavior as a Ph.D. student under his supervision despite being my different academic background. Being his second Ph.D. student, I am extremely lucky in learning neuroanatomy and behaviour directly from him. I learnt key techniques in neuroanatomy and manuscript writing from him. His friendly nature and freedom to design and perform my own experiments helped me formulate and address my research question in a better way. I would like to thank my Doctoral Committee members, Drs. A. Srinivasan, Avinash Sonawane, Chandan Goswami, and V. Badireenath Konkimalla for continuously evaluating my Ph.D. research work and findings. Their suggestions as well as criticisms during the annual thesis monitoring committee meetings were valuable and helpful in improving the quality of my work. I am highly thankful to Dr. Saurabh Chawla for his help in animal protocol approvals and experiments on animals, Dr. Manjusha Dixit and Mr. Khurshid for providing the HEK 293T cell line for transfection studies, and Dr. Chandan Goswami for providing TRPV antibodies used in my pilot studies. I thank the faculty members and all the students of the School of Biological Sciences for their encouragement and help. I also wish to record my thanks to the Institute of Life Sciences, Bhubaneswar for availing their DNA sequencing and mass spectrometry facilities. The journey might have been joyless without my lab members especially Dr. Uday Singh and Omprakash Singh in establishing and maintaining the lab and my friends who are always ready to take me out of this world. The funds provided by NISER, Department of Biotechnology (DBT), and Science and Engineering Research Board (SERB) for research and infrastructure made this research work possible. I am heartily thankful for the scholarship provided by NISER, Bhubaneswar and DAE, Government of India, without which I may be extinct.

CONTENTS

	Page No.
ABBREVIATIONS	1
SYNOPSIS	6
LIST OF FIGURES	15
LIST OF TABLES	20
GENERAL INTRODUCTION	22
PLAN OF WORK	36
CHAPTER 1: ELUCIDATING THE ROLE OF CART AS COMMON MESSENGER IN THE NEURAL PATHWAYS REGULATING ENERGY BALANCE AND REPRODUCTION	
INTRODUCTION.....	39
MATERIALS AND METHODS.....	42
RESULTS.....	48
DISCUSSION.....	67
CHAPTER 2: TRANSIENT RECEPTOR POTENTIAL VANILLOID 1-6 (TRPV1-6) GENE EXPRESSION IN THE MOUSE BRAIN DURING ESTROUS CYCLE	
INTRODUCTION.....	74
MATERIALS AND METHODS.....	77
RESULTS.....	81
DISCUSSION.....	100

**CHAPTER 3: TRANSIENT RECEPTOR POTENTIAL VANILLOID 5 (TRPV5), A
HIGHLY Ca^{2+} -SELECTIVE TRP CHANNEL IS WIDELY
DISTRIBUTED IN THE BRAIN AND MAY SERVE AS POTENTIAL
MODULATOR OF ARCUATE NUCLEUS CART NEURONS**

INTRODUCTION.....	105
MATERIALS AND METHODS.....	109
RESULTS.....	123
DISCUSSION.....	142

**CHAPTER 4: ORGANIZATION OF TRANSIENT RECEPTOR POTENTIAL
VANILLOID 6 (TRPV6)-EQUIPPED ELEMENTS IN THE BRAIN,
ESTROUS CYCLE-RELATED CHANGES IN THE
HYPOTHALAMUS, AND ROLE IN REGULATION OF ARCUATE
NUCLEUS NEURONS**

INTRODUCTION.....	149
MATERIALS AND METHODS.....	151
RESULTS.....	158
DISCUSSION.....	173

**CHAPTER 5: CART- AND TRPV1-INDUCED GROWTH HORMONE
SECRETION MAY SERVE AS NOVEL COMPONENT OF THE
CENTRAL REGULATION OF ENERGY BALANCE AND
REPRODUCTION**

INTRODUCTION.....	179
MATERIALS AND METHODS.....	183

RESULTS.....	192
DISCUSSION.....	205
SUMMARY AND CONCLUSIONS.....	210
REFERENCES.....	217
APPENDIX.....	261

ABBREVIATIONS

3V	3 rd ventricle
4/5Cb	lobules 4 and 5 of the cerebellar vermis
4n	trochlear nerve
4V	4 th ventricle
ACo	anterior cortical amygdaloid area
AHA	anterior hypothalamic area, anterior part
AHC	anterior hypothalamic area, central part
AHiHL	amygdalohippocampal area, anterolateral part
Aq	aqueduct
ARC	hypothalamic arcuate nucleus
Arc	hypothalamic arcuate nucleus
ArcP	arcuate hypothalamic nucleus, posterior part
BMA	basomedial amygdaloid nucleus, anterior part
BMP	basomedial amygdaloid nucleus, posterior part
bv	blood vessel
C1/A1	A1 noradrenaline cells
CA1	field CA1 of the hippocampus
CA2	field CA2 of the hippocampus
CA3	field CA3 of the hippocampus
cc	corpus callosum
CeC	central amygdaloid nucleus, capsular part
CeM	central amygdaloid nucleus, medial division
cg	cingulum
chp	choroid plexus

Cop	copula of the pyramis
cp	cerebral peduncle
CPu	caudate putamen (striatum)
Crus1	crus 1 of the ansiform lobule
Crus2	crus 2 of the ansiform lobule
csc	commissure of the superior colliculus
D3V	dorsal 3 rd ventricle
DA	dorsal hypothalamic area
DC	dorsal cochlear nucleus
DCFu	dorsal cochlear nucleus, fusiform layer
DCMo	dorsal cochlear nucleus, molecular layer
DG	dentate gyrus
DLPAG	dorsolateral periaqueductal gray
DMD	dorsomedial hypothalamic nucleus, dorsal part
DMV	dorsomedial hypothalamic nucleus, ventral part
DTT	dorsal tenia tecta
EW	Edinger-Westphal nucleus
EZ	external zone of the median eminence
f	fornix
GiA	gigantocellular reticular nucleus, alpha part
icf	intercrural fissure
icp	inferior cerebellar peduncle
IF	interfascicular nucleus
IOD	inferior olive, dorsal nucleus
IPC	interpeduncular nucleus, caudal subnucleus

IPR	interpeduncular nucleus, rostral subnucleus
IRt	intermediate reticular nucleus
IZ	internal zone of the median eminence
LEnt	lateral entorhinal cortex
LH	lateral hypothalamic area
LMol	lacunosum moleculare layer of the hippocampus
LPO	lateral preoptic area
LR4V	lateral recess of the 4 th ventricle
LV	lateral ventricle
M1	primary motor cortex
M2	secondary motor cortex
ME	median eminence
MeAD	medial amygdaloid nucleus, anterodorsal part
MePD	medial amygdaloid nucleus, posterodorsal part
MePV	medial amygdaloid nucleus, posteroventral part
ml	medial lemniscus
mlf	medial longitudinal fasciculus
MoDG	molecular layer of the dentate gyrus
MPA	medial preoptic area
mt	mammillothalamic tract
MTu	medial tuberal nucleus
MVe	medial vestibular nucleus
ns	nigrostriatal tract
oc	optic chiasm
opt	optic tract

pfs	parafloccular sulcus
Pir	piriform cortex
PLH	peduncular part of lateral hypothalamus
PM	paramedian lobule
PMCo	posteromedial cortical amygdaloid area
PN	paranigral nucleus of the ventral tegmental area
ppf	prepyramidal fissure
prf	primary fissure
psf	posterior superior fissure
PV	paraventricular thalamic nucleus
PVA	paraventricular thalamic nucleus, anterior part
PVN	paraventricular hypothalamic nucleus
py	pyramidal tract
RCh	retrochiasmatic area
RChL	retrochiasmatic area, lateral part
Re	reuniens thalamic nucleus
Rh	rhomboid thalamic nucleus
RLi	rostral linear nucleus of the raphe
RMg	raphe magnus nucleus
RPa	raphe pallidus nucleus
rs	rubrospinal tract
RSD	retrosplenial dysgranular cortex
RSGa	retrosplenial granular cortex, a region
RSGb	retrosplenial granular cortex, b region
S1BF	somatosensory barrel cortex

S1DZ	primary somatosensory cortex, dysgranular region
SCh	suprachiasmatic nucleus
scp	superior cerebellar peduncle
SFO	subfornical organ
SHy	septohypothalamic nucleus
Sim	simple lobule
SNC	substantia nigra, compact part
SNR	substantia nigra, reticular part
SO	supraoptic nucleus
sol	solitary tract
solM	nucleus of the solitary tract, medial part
SON	supraoptic nucleus
SOR	supraoptic nucleus, retrochiasmatic area
sox	supraoptic decussation
Sp5I	spinal trigeminal nucleus, interpolar part
Sub	submedius thalamic nucleus
ts	tectospinal tract
VMH	ventromedial hypothalamic nucleus
vsc	ventral spinocerebellar tract
VTA	ventral tegmental area
VTT	ventral tenia tecta
ZI	zona incerta
ZID	zona incerta, dorsal part
ZIV	zona incerta, ventral part

SYNOPSIS

Energy status plays a major role in reproductive success of the species. In rodents, acute or chronic food deprivation or food restriction delays puberty, lengthens estrous cycles and reduces reproductive behaviour [1,2]. One of the important factors responsible for the infertility due to inadequate nutrition is the suppression of pulsatile luteinizing hormone (LH) secretion from the pituitary [3]. There are distinct neural circuitries in the brain for regulating reproduction and energy balance and it is therefore important to understand the central mechanism that link reproduction and energy balance. Hypothalamus, a complex and compartmentalized structure consisting of several discrete neuronal groups with large number of neuronal pathways and neurotransmitters, has been identified as crucial centre in the brain involved in the regulation of energy balance. Preoptic area (POA) located rostral to the hypothalamus harbours crucial elements of the neuronal pathways involved in the regulation of reproduction [4,5]. The GnRH neurons residing in POA project to the median eminence, regulate LH secretion, and serve as the principal regulator of hypothalamic-pituitary-gonadal (HPG) axis [6,7]. The neural circuitry that regulates food intake and energy balance resides in the hypothalamus [8,9]. The thyrotropin releasing hormone (TRH) neurons in the hypothalamic paraventricular nucleus (PVN) control the synthesis/secretion of thyroid stimulating hormone (TSH) from the pituitary gland [10]. TSH acts on thyroid gland and stimulates thyroid hormone production, which in turn regulates energy expenditure [11]. Although TRH neurons have been identified as the principal regulator of the energy balance, these neurons are under direct regulatory control of the orexigenic and anorexigenic neurons of the hypothalamic arcuate nucleus (ARC) [12]. The anorexigenic neuropeptides- [cocaine- and amphetamine regulated transcript (CART) and alpha-melanocyte stimulating hormone (α -MSH)] and orexigenic neuropeptides [agouti-related protein (AgRP) and neuropeptide Y (NPY)] containing axons innervates PVN, contact TRH neurons and regulate TRH

biosynthesis/secretion and energy balance [12]. The ARC serve as direct target for leptin, insulin, glucose, and gut hormones, and the expression of the neuropeptides in ARC are modulated by changes in energy status of the animal [13]. Although the GnRH-LH axis is modulated by circulating levels of gonadal steroids, GnRH in turn is regulated by a complex neural circuitry in the hypothalamus. Estrogen receptor alpha (ER α) in ARC has been suggested to be involved in the regulation of food intake by acting on the feeding-related neurons in ARC [14]. Although the GnRH neurons are regulated by gonadal steroids feedback [15], the absence of ER α in GnRH neurons [16] raised a question as how the gonadal steroids interact with GnRH neurons [17]. Other neurotransmitters containing systems in the brain that express ER α have been suggested to mediate the effects of gonadal steroids to GnRH neurons [18]. CART is recently discovered novel neuropeptide [19]. While the axon terminals containing CART innervate POA GnRH neurons [20], these axons seem to originate from ARC and premammillary ventral nucleus [20]. The evidence like the GnRH cells expressing cFos in the afternoon of the proestrus are contacted by CART-containing axons [20], and increased GnRH pulse amplitude in cycling females and decreased GnRH pulse intervals in prepubertal rats following CART treatment, suggest role of CART in the regulation of GnRH neuronal activity [21]. CART neurons in ARC have been suggested important in the regulation of feeding and energy balance [22]. The CART mRNA expression in ARC is suppressed during fasting [22] and central administration of CART decreases food intake [23] and stimulates cFos expression in the areas of the brain involved in the regulation of food intake [24]. CART neurons are equipped with leptin receptors, respond to leptin treatment [22,25] and mediate leptin actions on GnRH neurons [26]. Prolonged food deprivation suppresses steroid-induced lordosis and decrease estrogen receptors in the brain [3]. In rats, decrease in mean plasma LH levels, LH pulse frequency, and LH pulse amplitude was observed after food deprivation [27]. The GnRH neurons in

POA are sensitive to glucose, and this sensitivity show alteration with gonadal steroids [28]. Recent evidence suggests modulation of CART by estrogen. Estradiol treatment in the ovariectomized rats reduced CART mRNA expression in ARC and lateral hypothalamic area, but increased in PVN [29]. The antiobesity drug, oleyl estrone as well as ovariectomized animals treated with estrogen showed reduced food intake and hypothalamic CART mRNA expression [29,30]. Whether CART serves as common messenger in the neural pathways regulating these functions, however has remained unexplored.

Growing evidence suggest an important role of transient receptor potential vanilloid (TRPV) ion channels in neural and neuroendocrine regulation, synaptic plasticity, Ca^{2+} -mediated cellular signalling and modulation of behaviour [31]. In TRPV subfamily, while TRPV1-4 are non-selective cation channels, TRPV5 and TRPV6 are highly Ca^{2+} -selective [32]. The organization of TRPV1-4-expressing elements has been described in the brain and their relevance to neuroendocrine regulation demonstrated [33], but the relevant aspect about TRPV5 and TRPV6 has remained unexplored. The promoters of TRPV genes contain estrogen response elements (ERE), and estradiol regulates TRPV5/6 mRNA expression in peripheral tissues [34]. The ARC neurons express $ER\alpha$, contain CART, and are modulated by estradiol. Whether ARC CART neurons are equipped with TRPV5 and TRPV6, and the expression of these ion channels in ARC is modulated by circulating levels of estradiol, however is not known. In addition to thyroid hormones, growth hormone (GH) secreted from the pituitary gland also plays an important role in energy balance [35] as well as reproduction [36]. GH regulates gluconeogenesis, glycogenolysis, lipolysis in the adipose tissue, and free fatty acid uptake in skeletal muscles [37]. Compared to wild type mice, the GH receptor knockout mice showed longer estrous cycle, reduced number of preovulatory follicles, corpora lutea, and plasma estradiol level [36]. The effect of GnRH on LH secretion and testicular function is also altered in GH receptor knockout mice [38]. The role of CART in

the regulation of GH secretion has been suggested. While the CART-ir cells present in the pituitary co-express GH, icv CART peptide treatment has resulted in significant increase in GH secretion [39,40]. The dense innervation of the external zone of median eminence by CART axon terminals, suggests its role in hypophysiotropic regulation of GH. Whether ARC CART contributes to the hypophysiotropic regulation and by controlling GH release contributes to energy balance has remained unexplored.

In this background, the aim of my thesis was to find out if ARC CART neurons serve as common neural substrate for connecting pathways regulating reproduction and energy balance, and role of TRPV ion channels in the regulation of these neurons and GH secretion. Experiments were conducted on the adult, male and female, Sprague Dawley rats and BALB/c mice and the results are presented in five chapters. Using double immunofluorescence, we have identified the ER α expressing CART neurons and their response to changes in energy balance. The trajectories of ARC CART neurons in the brain were mapped and the innervation on GnRH neurons in POA determined. Attempt was made to find out if CART-GnRH association is modulated by estrous cycle and changes in energy balance. These results are given in chapter 1. In chapter 2, we present our results on identification of putative functional ERE in the promoters of TRPV1-6 genes and estrous cycle-related changes in TRPV1-6 gene expression in different compartments of the brain. Results on neuroanatomical organization of TRPV5- and TRPV6-expressing elements in the brain, and their relevance in regulation of ARC CART neurons are presented in chapters 3 and 4, respectively. While delineating the role of hypothalamic CART in GH secretion, we observed interesting aspects of TRPV ion channels in the pituitary gland and determined the role of TRPV1 in GH secretion. These results are presented in chapter 5. A brief outline of the results presented in each chapter is given below.

CHAPTER 1

Elucidating the role of CART as common messenger in the neural pathways regulating energy balance and reproduction

CART neurons were observed in the ARC and a great majority of these neurons contained ER α . The ARC CART neurons also responded to changes in energy status of the animal and showed cFos activation after refeeding following a prolonged fast. CART and α -MSH are exclusively colocalized in the ARC neurons and the double labelled axons may serve as evidence of their ARC origin. Using this approach, we mapped the projections of ARC CART neurons in the brain. While the CART fibers of ARC origin were observed in different brain regions, dense innervation was seen in POA. The CART/ α -MSH double labelled axons were seen in close apposition to the GnRH cell bodies in POA. In POA, the CART-ir fibers from ARC showed estrous cycle- and energy status-dependent changes. Semi-quantitatively, no significant difference in the mean number of GnRH neurons was observed in POA during estrous cycle. However, the intensity of GnRH-ir in MnPO neurons showed significant reduction during estrus compared to proestrus, metestrus, and diestrus. In addition, compared to proestrus a reduction in the percentage of MnPO GnRH neurons contacted by CART-ir fibers originating from ARC was noticed during estrus.

CHAPTER 2

Transient receptor potential vanilloid 1-6 (TRPV1-6) gene expression in the mouse brain during estrous cycle

Given the emerging importance of TRPV channels in neuroendocrine regulation and the evidence suggesting their regulation by estradiol, we explored changes in TRPV1-6

mRNA expression in different brain regions during estrous cycle. In the mouse brain, the TRPV1-6 mRNA expressions were observed in the olfactory bulb, cortex, hypothalamus, hippocampus, brainstem, and cerebellum. Analysis using Dragon ERE Finder version 3.0 showed the presence of putative functional ERE patterns in the promoter regions of TRPV1-6. The TRPV1-6 mRNA levels showed estrous cycle related changes. During proestrus, where TRPV1 and TRPV5 mRNA levels were lower, higher mRNA levels of TRPV2, TRPV4, and TRPV6 were observed. Reduced expression of TRPV3 mRNA was apparent during estrus compared to other stages of the estrous cycle. TRPV2 mRNA showed abundant expression during all the four stages of the estrous cycle.

CHAPTER 3

Transient receptor potential vanilloid 5 (TRPV5), a highly Ca²⁺-selective TRP channel is widely distributed in the brain and may serve as potential modulator of arcuate nucleus CART neurons

TRPV5-immunoreactive neurons were conspicuously seen in PVN, supraoptic (SON), accessory neurosecretory, retrochiasmatic area of SON, ARC, medial tuberal nuclei, and other brain regions. Glial cells also showed TRPV5-immunoreactivity. To test the neuroendocrine relevance of TRPV5, we focused on vasopressin, oxytocin, and cocaine- and amphetamine-regulated transcript (CART) as representative candidate markers. In hypothalamic neurons, we find the co-expression of TRPV5 with vasopressin and oxytocin. While ARC neurons express estrogen receptors, 17 β -estradiol regulates TRPV5, and CART neurons and astrocytes in ARC. Using double immunofluorescence, GFAP-labeled astrocytes and majority of CART neurons in ARC showed TRPV5-immunoreactivity. Retrograde neuronal tracing showed projections of TRPV5-equipped ARC CART neurons to

the anteroventral periventricular nucleus and median preoptic nucleus. Compared to proestrus, a significant increase in the percentage of TRPV5-expressing CART neurons was observed during estrus, metestrus, and diestrus. TRPV5-immunoreactivity in the astrocytes, however, showed a significant increase during metestrus and diestrus.

CHAPTER 4

Organization of transient receptor potential vanilloid 6 (TRPV6)-equipped elements in the brain, estrous cycle-related changes in the hypothalamus, and role in regulation of arcuate nucleus neurons

TRPV6-immunoreactive cells/fibers were observed in vascular organ of the lamina terminalis, olfactory bulb, amygdala, hippocampus, septohypothalamic, SON, ARC, dorsomedial, and subincertal nuclei. TRPV6-immunoreactive cells/fibers were also observed in the brainstem and cerebellum. Estrogen has emerged as a potential regulator of TRPV6 in peripheral tissues. Estrogen activates TRPV6 via ER α , and ER α -expressing ARC neurons in mediobasal hypothalamus (MBH) serve as primary site for estradiol feedback. Using double immunofluorescence, co-expression of TRPV6 and ER α was observed in several ARC neurons. MBH of mice during different phases of estrous cycle were subjected to Western blot analysis of TRPV6. Compared to proestrus, a significant reduction in intensity of TRPV6-immunoreactive band was observed in MBH during metestrus and diestrus phases. Using retrograde neuronal tracing, several TRPV6-equipped ARC neurons were found projecting to AVPe and MnPO. Application of double immunofluorescence showed few TRPV6-ir neurons co-expressing CART but majority were NPY-immunoreactive.

CHAPTER 5

CART- and TRPV1-induced growth hormone secretion may serve as novel component of the central regulation of energy balance and reproduction

Isolated CART and α -MSH fibers were seen in the median eminence suggesting the involvement of non-ARC CART neurons in the regulation of pituitary. In the rat pituitary, compared to other members in the TRPV subfamily, TRPV1 showed higher expression. Application of TRPV1-6 antisera on rat pituitary sections showed discrete organization of these ion channels in pars nervosa, pars intermedia and pars distalis of the pituitary. Compared to controls, treatment of the rat pituitary primary cells either with CART or resiniferatoxin (a TRPV1 agonist) significantly elevated GH release. We have also observed that the TRPV1-mediated GH release was more potent than CART-mediated response. To determine whether CART-induced GH secretion is mediated *via* TRPV1, pituitary cells were treated with iodoresiniferatoxin (a TRPV1 antagonist) followed by CART. Pre-treatment with iodoresiniferatoxin did not block the stimulatory effect of CART on GH secretion.

The major findings of my thesis are:

- ARC CART neurons co-express ER α , respond to changes in energy status, and may link neural pathways regulating reproduction and energy balance.
- ARC CART neurons densely innervate POA, contact GnRH neurons and their association show reproduction stage- and energy status-dependent plasticity.
- Highly Ca²⁺ selective TRP channels *viz.* TRPV5 and TRPV6-equipped elements were widely distributed in the brain.

- ARC CART neurons equipped with estradiol-sensitive TRPV ion channels may serve as novel component of the neural pathways regulating reproduction/energy balance.
- During estrous cycle, while TRPV5 seems to regulate anorexigenic ARC CART neurons, TRPV6 may regulate orexigenic ARC NPY neurons.
- Effects of CART on GH secretion seem independent of TRPV1 activation.

LIST OF FIGURES

GENERAL INTRODUCTION

- Figure 1:** Organization of the hypothalamus, PVN and its hypophysiotropic connections.....23

CHAPTER 1

- Figure 1:** CART neurons in the preoptic area and hypothalamus of rat co-express estrogen receptor alpha.....49
- Figure 2:** Energy status-dependent activation of hypothalamic neurons.....50
- Figure 3:** Co-localization of CART and α -MSH neurons in the rat brain.....51
- Figure 4:** Organization of CART fibers of arcuate nucleus origin in the forebrain of rat.....54
- Figure 5:** Organization of CART fibers of arcuate nucleus origin in the midbrain and hindbrain of rat.....55
- Figure 6:** Organization of CART fibers of arcuate nucleus origin in the pituitary gland and spinal cord of rat.....56
- Figure 7:** Association between GnRH neurons and CART axons in the median preoptic nucleus.....60
- Figure 8:** Arcuate nucleus CART fibers innervation in preoptic area show estrous cycle-related changes.....61
- Figure 9:** Arcuate nucleus CART fibers innervation in preoptic area show energy status-related changes.....64
- Figure 10:** Arcuate nucleus CART innervation of GnRH neurons in the median preoptic nucleus show estrous cycle-related changes.....65

Figure 11: Arcuate nucleus CART innervation of GnRH neurons in the median preoptic nucleus show energy status-related changes.....66

CHAPTER 2

Figure 1: TRPV1-6 mRNA expression in the mouse brain.....82

Figure 2: Estrous cycle-related changes in TRPV1-6 mRNA expression in the olfactory bulb, cortex, and hypothalamus of mice.....92

Figure 3: Estrous cycle-related changes in TRPV1-6 mRNA expression in the hippocampus, brainstem, and cerebellum of mice.....93

Figure 4: Representation of estrous cycle-related changes in TRPV1-6 mRNA levels in different brain regions of mice.....94

Figure 5: Heat maps showing estrous cycle-related changes in TRPV1-6 mRNA levels in the olfactory bulb, cortex, hypothalamus, hippocampus, brainstem, and cerebellum of mice.....95

Figure 6: Estrous cycle-related changes in TRPV1-6 mRNA expression in the olfactory bulb, cortex, and hypothalamus of mice.....96

Figure 7: Estrous cycle-related changes in TRPV1-6 mRNA expression in the hippocampus, brainstem, and cerebellum of mice.....97

Figure 8: Representation of estrous cycle-related changes in TRPV1-6 mRNA levels in different brain regions of mice.....98

Figure 9: Heat maps showing estrous cycle-related changes in TRPV1-6 mRNA levels in the olfactory bulb, cortex, hypothalamus, hippocampus, brainstem, and cerebellum of mice.....99

CHAPTER 3

Figure 1:	TRPV5 mRNA expression in the rat brain.....	124
Figure 2:	Specificity of TRPV5 antiserum in the rat brain using preadsorption control and western blot.....	125
Figure 3:	Specificity of TRPV5 antiserum using TRPV5 siRNA approach.....	127
Figure 4:	Specificity of TRPV5/6 antisera using transfection protocol.....	131
Figure 5:	Schematics showing the organization of TRPV5-immunoreactive elements in the rat brain.....	132
Figure 6:	Organization of TRPV5-immunoreactive elements in the hippocampus and cortex.....	133
Figure 7:	Organization of TRPV5-immunoreactive elements in the hypothalamus, midbrain, brainstem, and cerebellum.....	134
Figure 8:	TRPV5-immunoreactive elements in the arcuate nucleus, brainstem, choroid plexus, around the brain blood vessel, and Pia mater.....	135
Figure 9:	TRPV5-immunoreactive astrocytes in the cerebral cortex.....	137
Figure 10:	Hypothalamic vasopressin neurons are equipped with TRPV5.....	138
Figure 11:	Hypothalamic oxytocin neurons co-express TRPV5.....	139
Figure 12:	TRPV5-immunoreactivity in the arcuate nucleus shows estrous cycle-related changes.....	140

CHAPTER 4

Figure 1:	Specificity of the TRPV6 antiserum in the mouse brain.....	159
Figure 2:	Schematics showing the organization of TRPV6-immunoreactive elements in the mouse brain.....	161

Figure 3: Organization of TRPV6-immunoreactive elements in the forebrain of mouse.....164

Figure 4: Organization of TRPV6-immunoreactive elements in the hypothalamus and pars tuberalis of mouse.....165

Figure 5: Organization of TRPV6-immunoreactive elements in the midbrain and cerebellum of mouse.....168

Figure 6: TRPV6-immunoreactive cells in the arcuate nucleus co-express ER α and TRPV6 protein in mediobasal hypothalamus show correlation with estrous cycle.....169

Figure 7: Majority of the TRPV6-immunoreactive cells in the arcuate nucleus co-express neuropeptide Y but not CART.....170

Figure 8: TRPV6-equipped neurons in the arcuate nucleus innervate AVPe in the preoptic area.....171

Figure 9: TRPV6-equipped neurons in the arcuate nucleus innervate MnPO in the preoptic area.....172

CHAPTER 5

Figure 1: TRPV1-6 mRNA expression in the pituitary gland of rat.....196

Figure 2: Specificity of the TRPV1-6 antisera in the pituitary gland of rat.....197

Figure 3: Schematics showing the organization of TRPV1-6 immunoreactive elements in the pituitary gland of rat.....199

Figure 4: TRPV1-6 immunoreactivity in the pituitary gland of rat.....200

Figure 5: TRPV1-6 immunoreactivity in the pars tuberalis of rat.....201

Figure 6: Growth hormone-secreting cells in the rat pars distalis and pituitary primary cells co-express TRPV1.....202

Figure 7: Effect of CART peptide treatment and TRPV1 agonist on growth hormone secretion.....203

Figure 8: Effect of TRPV1 agonist on $[Ca^{2+}]_i$ activity in the rat pituitary primary cells.....204

SUMMARY AND CONCLUSIONS

Figure 1: Organization and proposed mechanism of the regulation of neural pathways in the brain wherein the cocaine- and amphetamine-regulated transcript (CART)-containing neurons of the hypothalamic arcuate nucleus (ARC) serve as a common messenger in the crosstalk between circuits regulating energy balance and reproduction..... 216

LIST OF TABLES

CHAPTER 1

Table 1: Semi-quantitative analysis of the CART/ α -MSH double labelled fibers in the forebrain, midbrain, hindbrain, spinal cord, and pituitary gland of rat.....57

CHAPTER 2

Table 1: Quantitative real-time PCR primer sequences for mouse TRPVs (target genes) and HPRT (endogenous control gene).....79

Table 2: Estrogen receptor alpha (ER α) binding sites in the promoter region of mouse TRPV1-6 genes analysed using Champion ChiP Transcription Factor Search Portal.....83

Table 3: Putative functional estrogen response element (ERE) patterns in the promoter region of mouse TRPV1-6 genes analysed using Dragon ERE Finder version 3.0.....84

CHAPTER 3

Table 1: Organization of TRPV-expressing neurons in different areas of the brain....108

Table 2: Distribution of TRPV5-immunoreactive neuronal cell bodies and fibers/terminals in the rat brain.....122

Table 3: Semi-quantitative analysis of the percentage of hypothalamic oxytocin and vasopressin neurons co-expressing TRPV5.....141

CHAPTER 4

Table 1: Distribution of TRPV6-immunoreactive neuronal cell bodies and fibers/terminals in the mouse brain and pituitary gland.....162

CHAPTER 5

Table 1: Primer sequences used in quantitative real-time PCR of the rat TRPVs (target genes) and HPRT (endogenous control gene).....185

Table 2: Qualitative analysis of TRPV1-6 immunoreactivity in the pituitary gland of rat.....198

APPENDIX

Table 1: Details of the primary antibodies/antisera used.....261

GENERAL INTRODUCTION

Pituitary gland serves as the principal regulator of the endocrine functions and controls a range of physiological processes. It is located beneath the tuberal region of the hypothalamus and consists of anterior, posterior and intermediate lobes. The posterior pituitary is directly connected with the hypothalamus and the neurosecretory neurons innervate this lobe [41]. Magnocellular neurons in the hypothalamic paraventricular (PVN) and supraoptic (SON) nuclei innervate the posterior pituitary and secrete the nonapeptides, oxytocin and vasopressin [42]. In contrast to posterior pituitary, the anterior pituitary is not directly connected to the hypothalamus and contains the hormone secretory cells including luteinizing hormone (LH), follicle stimulating hormone (FSH), growth hormone (GH), prolactin (PRL), and thyroid stimulating hormone (TSH) [43]. The hypothalamus is the hub where information from internal and external environments is integrated and transmitted to the posterior pituitary for peripheral action or secreted into the portal capillaries in the external zone of the median eminence [41]. These releasing factors are then transported to the anterior pituitary gland, which act on the specific cell types, and the picomolar signals are converted into nanomolar signals for further action [44].

The organization of hypothalamus, PVN and its hypophysiotropic connections is shown in Figure 1. The neuroendocrine neurons controlling the synthetic/secretory activity of cells in the anterior pituitary gland resides in the medial parvocellular subdivision of the PVN. The hypophysiotropic nature of these neurons was established using neuronal tracing studies. The retrograde neuronal tracer, horseradish peroxidase (HRP) or Fluoro-Gold (FG) was injected intravenously and their retrograde accumulations observed in neurons of the medial parvocellular as well as magnocellular subdivisions of the PVN and SON. The cellular distinction within the PVN regulating anterior and posterior pituitary was later

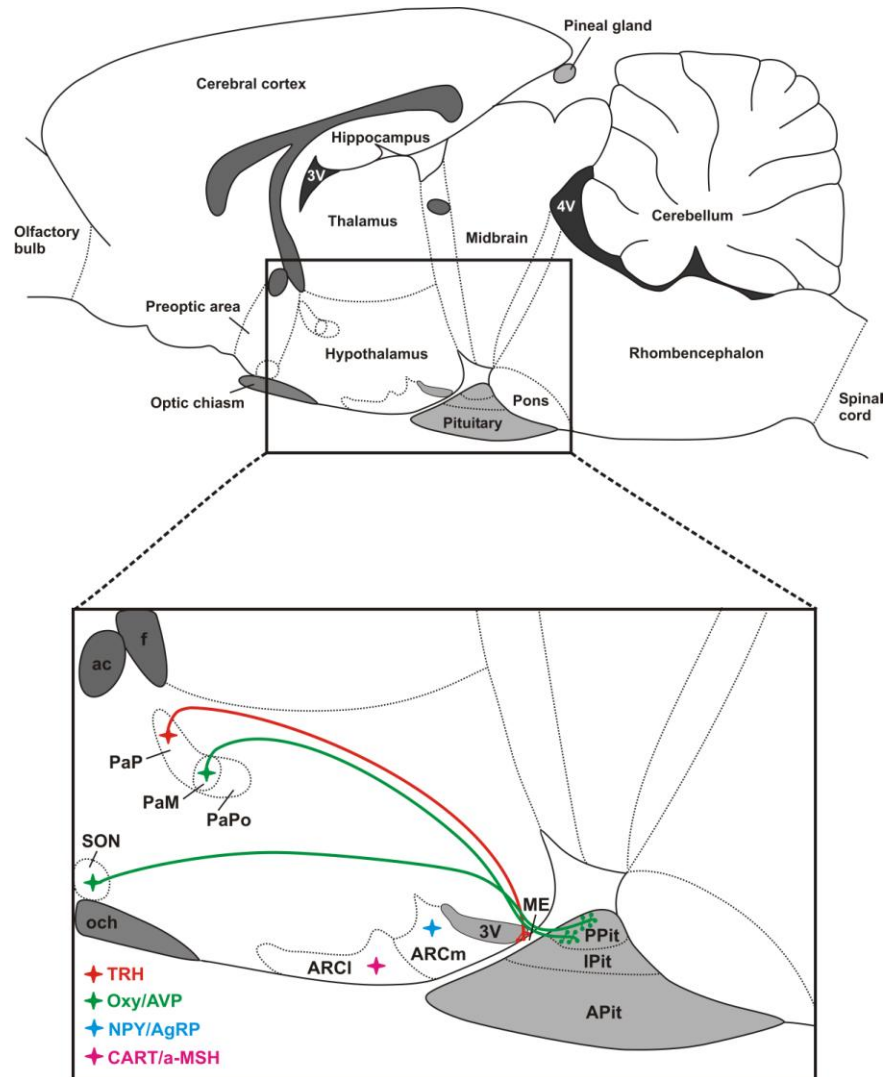


Figure 1: Organization of the hypothalamus, PVN and its hypophysiotropic connections. Pituitary gland is located beneath the tuberal region of the hypothalamus and consists of anterior (APit), posterior (PPit) and intermediate (IPit) lobes. Magnocellular neurons in the hypothalamic paraventricular (PaM) and supraoptic (SON) nuclei innervate the posterior pituitary and secrete oxytocin (Oxy) and vasopressin (AVP). The neuroendocrine neurons controlling the synthetic/secretory activity of cells in the anterior pituitary gland resides in the medial parvocellular subdivision of the paraventricular nucleus (PaP) and send their axons to the median eminence (ME) and terminate into its external zone in close proximity to the portal capillaries. The hypothalamic arcuate nucleus (ARC) is situated in the mediobasal hypothalamus on either side of the third ventricle (3V) and consists of two subdivisions viz. the lateral (ARCI) and medial (ARCm). While the neurons in the ARCI synthesize the neuropeptides viz. cocaine-and amphetamine regulated transcript (CART) and alpha-melanocyte stimulating hormone (α -MSH), the ARCm contains neurons producing neuropeptide Y (NPY) and agouti-related protein (AgRP). PaPo, hypothalamic paraventricular nucleus, posterior part; TRH, thyrotropin-releasing hormone; och, optic chiasm; ac, anterior commissure; f, fornix.

established using removal of the specific target glands and hormonal replacement [45,46]. Application of immunohistochemistry using specific antibodies raised against the hypothalamic releasing factors demonstrated that the neurons producing these factors resides in the medial parvocellular subdivision of the PVN, their axons travel laterally, swing over the fornix, enter the median eminence (ME) and terminate into its external zone in close proximity to the portal capillaries.

Similar to the range of physiological functions controlled by the hypothalamo-hypophyseal system, feeding and reproduction are also directly under the regulatory control of the hypothalamus and pituitary. Two releasing hormones viz. the thyrotropin-releasing hormone (TRH) and gonadotropin releasing hormone (GnRH) serve an important purpose in the regulation of the hypothalamus-pituitary-thyroid (HPT) and hypothalamus-pituitary-gonadal (HPG) axes, respectively. While the HPT axis regulates energy expenditure, HPG axis controls gonadotropic secretion, reproduction, and reproductive behaviour [15,47]. The TRH neurons residing in the PVN have been identified as the principal regulator of the HPT axis and energy balance [12]. Activation of these neurons secretes TRH into the external zone of ME and *via* hypophyseal portal system enters into the anterior pituitary and act on the thyrotrophs [12] as well as lactotrophs [48,49]. The TSH secreted from the thyrotrophs in the general circulation act on the thyroid gland and stimulate the synthesis/secretion of thyroid hormones, thyroxine (T4) and triiodothyronine (T3), which play crucial role in energy expenditure [12,50].

On the other hand, the GnRH neurons residing in the preoptic area (POA) have been identified as the principal regulator of the HPG axis [51]. Their activation results in the secretion of GnRH into the portal vessels in the external zone of ME and *via* hypophyseal portal system, enters into the anterior pituitary and acts on gonadotrophs [52,53]. The gonadotropins viz. follicle-stimulating hormone (FSH) and luteinizing hormone (LH) are

secreted in the general circulation, which further act on gonads and stimulate the production of gonadal steroid hormones [52,53]. These hormones play crucial role in the central regulation of reproduction and reproductive behaviour [52,53].

Although distinct components constitute the HPT and HPG axes, alteration in either of these pathways affect the function of other [15]. Evidences suggests the association and crosstalk between the HPT and HPG axes, but the neuroanatomical substrate and molecular players mediating the cross talk between the two axes are poorly understood [54]. Mechanisms are developed for the biological homeostasis of energy, a state known as energy balance (EB). Since the role of HPT axis in energy balance is well established, any perturbation in HPT axis results in either positive energy balance (PEB) or negative energy balance (NEB) depending upon the amount of calories consumed and calories burned over time [15,55]. The consumption of more calories than required results into PEB whereas the consumption of less calories produces NEB [55]. While PEB causes gain in weight, NEB results in weight loss. Both, PEB as well as NEB states adversely affect the fertility in humans and other mammals [56–58]. This clearly demonstrates the direct interaction between energy expenditure and reproduction and set a basis for exploring the cross-talk between neural pathways regulating these functions.

Hypophysiotropic TRH neurons are tightly regulated by neurons of the hypothalamic arcuate nucleus (ARC). The ARC is situated in the mediobasal hypothalamus on either side of the third ventricle and beneath the ventromedial nucleus. The neuroanatomical location of ARC in the rat brain and its organization is shown in Figure 1. The ARC consists of two subdivisions viz. the lateral (ARCl) and medial (ARCm). These subdivisions are not only anatomically distinct but contain distinct neuropeptides with specific function. While the neurons in the ARCl synthesize the neuropeptides viz. cocaine- and amphetamine regulated transcript (CART) and alpha-melanocyte stimulating hormone

(α -MSH), the ARCm contains neurons producing neuropeptide Y (NPY) and agouti-related protein (AgRP) [59–61]. While the NPY/AgRP are orexigenic, stimulate food intake and inhibit energy expenditure, the α -MSH/CART are anorexigenic in nature, inhibit food intake but promote energy expenditure [62–64]. The ARC neurons sense the peripheral cues related to energy reserves and accordingly exert orexigenic or anorexigenic effects. The adiposity signals, leptin and insulin have gained attention as peripheral cues of energy status because of their ability to cross the blood brain barrier and expression of their receptors on orexigenic/anorexigenic neuronal populations of ARC [65–67].

Leptin, the product of the obese (*ob*) gene, is a 16 kDa protein consisting of 146 amino acids and is secreted by adipocytes [68]. The concentration of leptin in the serum reflects the body fat content [69]. The leptin-deficient (*ob/ob*) mice are obese, diabetic, and exhibit reduced metabolism and body temperature [70]. The intraperitoneal injection of OB protein in *ob/ob* mice reduces their body weight, percent body fat, and food intake; and increases their metabolic rate and body temperature [70], suggesting its role in the regulation of the HPT axis. The individual deletion of leptin receptor (*LepR*) from the AgRP and POMC neurons of the ARC results into an increase in the body weight and adiposity [71]. These measures further increases following the simultaneous deletion of *LepR* from both the neuronal subpopulations [71], suggesting leptin-sensing by the orexigenic/anorexigenic neurons of the ARC is crucial for energy balance.

Insulin, a product of the preproinsulin gene, is a 5.8 kDa protein consisting of 51 amino acids and secreted by the pancreatic β cells in response to increased blood glucose levels [72,73]. Insulin promotes the uptake of glucose by the skeletal muscle and adipose tissue, and regulates lipid metabolism in the liver [73]. The neuron-specific disruption of the insulin receptor gene in mice (*NIRKO* mice) increases food intake, body fat and plasma leptin levels, thereby developing diet-sensitive obesity [74]. Insulin depolarizes POMC

neurons *via* TRPC5 channels activation in whole-cell recording, and increases c-Fos expression in ARC POMC neurons and inhibits food intake when given intracerebroventricularly [75].

Leptin and insulin acts on the brain *via* specific receptors. Leptin act *via* LepR whereas insulin's action is mediated by insulin receptors (InsR). These receptors are expressed in various brain regions and specifically localized in the hypothalamus. In the hypothalamus, higher expression of LepR as well as InsR was observed in the ARC AgRP and POMC neurons [65–67]. It has been proposed that the actions of leptin and insulin in POMC and AgRP neurons of ARC is crucial for central regulation of food intake, body weight, and energy balance [76]. LepR deletion or its overexpression in ARC neurons has been shown to alter the body weight and food intake [77,78]. The presence of LepR seem important for anorectic actions of POMC neurons since deletion of LepR from POMC neurons induces obesity [77,78]. It is interesting, however to mentioned that both AgRP and POMC neurons mediates the actions of leptin to regulate energy balance since deletion of LepR from both these neurons has resulted in severe obesity [71]. Binding of leptin to its receptors activates Janus kinase which phosphorylates the receptor and activates STAT3. The phosphor-STAT3 then binds to the promoters of *agrp* and *pomc* genes [76,79]. This leads to stimulation of POMC expression but AgRP expression gets inhibited [79]. In addition, leptin is also known to activate PI3K signalling, stimulate PIP3 and AKT [80,81]. The action of leptin and insulin has been shown to converge at some point during their actions on ARC neurons since insulin *via* insulin receptor substrate activate PI3K [82].

Neurons in the ARC densely innervate TRH neurons in the PVN and regulate the activity of these neurons [12]. In addition, ARC neurons have been shown to project to the POA and contact GnRH Neurons [20,83]. Therefore, the impaired signalling of leptin and insulin not only affects the metabolism and function of HPT axis, but may also alter

reproduction. While impaired leptin signalling in ob/ob mice results into infertility [84,85], leptin-treatment restores fertility both in the male and female ob/ob mice [86–88] and the leptin receptor-deficient (db/db) mice are infertile [89–91]. The expression of LepR in the brain of db/db mice however has been shown to restore the fertility [92]. This seems to be mediated by reverting leptin sensitivity of the POMC and AGRP/NPY neurons in the ARC [93]. To study the significance of insulin signalling in reproductive regulation, Bruning et al. [74] created a mice with neuron specific disruption of insulin receptor gene (NIRKO). In this mice, inactivation of insulin receptors resulted in the alteration of energy balance as well as reproductive regulation [74]. The mice developed obesity and showed impaired spermatogenesis, maturation of ovarian follicles and dysregulation of LH [74], suggesting role of insulin signalling in linking energy balance and reproduction.

Centrally, leptin and insulin may serve as common molecular players in the cross talk between pathways regulating energy balance and reproduction. The hormones may directly act on GnRH neurons in POA and regulate HPG axis [94] and may serve as important component of the energy status-dependent regulation of reproduction. Since the GnRH neurons do not express LepR [95], the possibility of direct actions of leptin on GnRH neurons is ruled out [94]. Unlike the indirect action of leptin, insulin seem to act on GnRH neurons directly. While the GnRH neurons express insulin receptor and insulin treatment stimulates these neurons [96,97], the deletion of insulin receptors selectively from the GnRH neurons did not alter fertility and displayed normal pubertal timing both in male and female mice [98]. This clearly suggest that the indirect action of peripheral cues of energy reserves on GnRH neurons serve as crucial regulators of these neurons during different energy states.

The neural pathways responding to metabolic cues also seem to be sensitive to circulating estradiol and the gonadal hormone may serve as yet another key molecular player in the cross talk between energy balance and reproductive pathways. The hormone and its

receptors are not only known to play a role in regulation of reproductive function but also affect a range of physiological processes including metabolism and feeding behaviour [99–101]. The discovery of membrane-associated steroid receptors suggests action of steroids at the level of membrane in controlling reproductive physiology. Estradiol membrane-initiated signalling modulates female sexual receptivity and estrogen feedback regulating LH surge [102]. Using single cell RT-PCR, more than 50% and approximately 10% of the GnRH neurons in the brain of female mouse were shown to express estrogen receptor (ER) viz. ER α and ER β transcripts, respectively [103]. The single GnRH cell analysis revealed lowest ER α and ER β transcripts during proestrus compared to estrus and diestrus [103]. However, other studies have reported absence of ER α in GnRH neurons [16,104–107]. While the neuronal deletion of ER α in the female mice did not show estrous cycles/negative feedback, ER β neuronal deletion did not affect the estrous cycle [108]. Further, the GnRH neuron-selective deletion of ER β has resulted in normal reproductive cycle and negative feedback in mice [108]. These findings suggest that the ER α -expressing neurons are essential and probably sufficient for the normal estrous cycle and estrogen negative feedback [108]. Neuron-specific ER α mutant mice failed to exhibit estrogen positive feedback, demonstrating that the neurons presence of ER α are critical [109]. Using GnRH neuron-specific Pseudorabies virus tracing approach, ER α -expressing neurons which innervate GnRH neurons have been shown to reside within the rostral periventricular region in the hypothalamus [109]. The results suggest that ovulation is driven by action of estrogen on ER α -expressing neuronal afferents to GnRH neurons [109]. Female mice lacking ER β gene in neuronal and glial cells showed normal estrous cycle and unaltered sexual behaviour in the adulthood [110]. These mice, however showed reduced ovarian weight and increased anxiety-like behaviour during the follicular phase, and in addition the number and distribution of GnRH-immunoreactive cells were also unaffected in these mice [110]. Although the GnRH neurons are regulated by the

gonadal steroid feedback mechanism [15], these neurons do not express ER α [16]. This has raised a question as how the gonadal steroids interact with GnRH neurons and suggested the role of other neurotransmitters-containing systems in the brain that express ER α to mediate the effects of gonadal steroids to GnRH neurons [18,111–113]. Estrogen inhibits adipose tissue deposition by regulating the food consumption and energy expenditure at the level of brain [114]. Estradiol regulates insulin sensitivity [115], reduces body weight and fat in the female mice in estrogen receptor element (ERE)-independent manner [116]. The role of estrogen in lipid homeostasis and glucose metabolism has been demonstrated using aromatase-knockout (ArKO) mouse, lacking ability to synthesize endogenous estrogens [100,117]. The role of estrogen and androgen receptors in the regulation of energy homeostasis have been described in both rodents and humans [99]. The estrogenic control of feeding behaviour and body weight regulation in mice depends on ER α gene expression [118]. During estrous cycle in rodents, compared to metestrus and diestrus, reduced food intake was observed during the proestrus and estrus phases [119–121]. There seems an inverse relationship between estradiol and ER α expression in the ARC. In the ovariectomized rats, estradiol treatment resulted in 64% reduction in ER α mRNA in the ARC [122]. Majority of the dopaminergic neurons in the ARC express ER α during diestrus phase but showed significant reduction during proestrus phase [123], when plasma estradiol levels remain elevated [124]. Although ER α in ARC has been suggested to be the crucial regulator of food intake, estrogen may regulate food intake by acting on the feeding-related neurons in ARC [14,125].

Although TRH neurons have been identified as the principal regulator of the energy balance, these neurons are under direct regulatory control of the orexigenic and anorexigenic neurons of the ARC. The axons containing CART/ α -MSH and AgRP/NPY innervate PVN, contact TRH neurons and regulate TRH biosynthesis/secretion and energy balance [12]. The

ARC neurons serve as direct target for leptin, insulin, glucose, and gut hormones, and the expression of the neuropeptides in ARC are modulated by changes in energy status of the animal. Although the GnRH-LH axis is modulated by circulating levels of gonadal steroids, GnRH in turn is regulated by a complex neural circuitry in the hypothalamus. CART is recently discovered novel neuropeptide [19]. CART derived its name after the discovery of a specific mRNA in the striatum of the rat which is transcriptionally regulated by cocaine and amphetamine [19]. The C-terminus region of the peptide encoded by CART mRNA was found to match with the peptide sequenced in 1981 by Spiess et al. [126] from the ovine hypothalamus. Later, Thim et al. [127] isolated and sequenced two CART peptides viz. CART (55-102) and CART (62-102) from rat tissue. The gene has assigned its name as “CART prepropeptide” and was named as “*CARTPT*” [128]. Further studies showed alternative splicing of CART prepropeptide which gave rise to two propeptides viz. proCART (1-89) and proCART (1-102) [128]. Although proCART (1-89) is the only CART propeptide reported in humans, rats have both proCART (1-89) as well as proCART (1-102) [128]. The long form proCART (1-102) in rats undergo post-translational processing and further gives rise to at least two biologically active peptides viz. CART (55-102) and CART (62-102) [128]. On the other hand, processing of the human proCART (1-89) gives rise to CART (42-89) and CART (49-89) fragments [128]. Interestingly, CART (55-102) and CART (62-102) are identical to CART (42-89) and CART (49-89), respectively in any species which expresses both the forms of proCART [128]. It should be noted that there may exist other bioactive CART peptides which needs further investigations [129]. In addition to humans, rats, and mouse, CART mRNA has been reported in the primates, bovine, swine, amphibians, and fish [129]. The CART gene and the predicted transcription factor binding sites in the promoter region are highly conserved across the species [129]. Despite several attempts, the CART receptors have still not been identified. Studies have suggested the

presence of a putative specific Gi/Go-protein-coupled receptor (GPCR) for the actions of CART peptides [128,129]. The mRNA and peptides of CART are abundantly expressed and widely distributed in the central as well as peripheral nervous systems, peripheral blood, pituitary portal blood, cerebrospinal fluid, as well as endocrine cells of the pituitary and adrenal glands [128,129]. Apart from the well-established role of CART in the regulation of food intake and energy balance, the peptide also plays a role in neuronal development and migration, anxiety and depression, stress, reward and addiction, as well as ischaemic stroke, dementia, Huntington's disease, and seizures [128,129].

The studies exploring cross talk between neural pathways regulating energy balance and reproduction became further exciting with the emergence of neuropeptide CART. The axon terminals containing CART were seen in close proximity of the GnRH neurons in POA [20] and these axons seem to originate from ARC and premammillary ventral nucleus [20]. The evidence like the CART axons innervating GnRH neurons during proestrus [20], increased GnRH activity in cycling females and decreased activity in the prepubertal rats following CART treatment, suggests role of CART in the regulation of GnRH neurons [21,130]. CART is an anorexigenic neuropeptide and abundantly expressed in areas of the brain regulating feeding and energy balance [24,128,131–133]. The CART neurons in ARC have been suggested important in the regulation of feeding and energy balance [22,134]. The CART mRNA expression in ARC is suppressed during fasting [22]. The central administration of CART has been shown to decrease food intake [23] and induce cFos expression in the areas of the brain known to regulate food intake [24]. While the CART neurons are equipped with leptin receptors and these neurons respond to leptin treatment [22,61], role of CART in mediating stimulatory effects of leptin on GnRH pulse generator has also been demonstrated [26]. Prolonged food deprivation suppresses steroid-induced display of lordosis in the adult female rats, which was associated with a decrease in estrogen

receptors in the brain [3]. In rats, a decrease in mean plasma LH levels, LH pulse frequency, and LH pulse amplitude was observed after food deprivation [27,135,136]. The GnRH neurons in POA are sensitive to glucose, and this sensitivity show alteration with changes in levels of gonadal steroids [28]. Recent evidence suggests modulation of CART by estrogen. Estradiol treatment in the ovariectomized rats reduced CART mRNA expression in ARC and lateral hypothalamic area, but was increased in PVN [29]. The antiobesity drug, oleyl estrone as well as ovariectomized animals treated with estrogen showed reduced food intake and hypothalamic CART mRNA expression [29,30].

While the neuropeptides execute the effects of the neural pathways, the signalling and components regulating these neurons/neuropeptide synthesis/release is not well established. Transient receptor potential (TRP) superfamily of cation channels may serve as crucial component of the neural pathways since these ion channels are known as cellular sensors for a wide range of physical and chemical stimuli [137]. They display greater diversity in activation mechanisms and selectivity compared to other group of ion channels [32]. TRP channels have been found in worms, fruit flies, zebrafish, mice, rats, and humans. Based on the sequence and topological differences, TRP superfamily is divided into two groups. The group 1 TRPs consist of five subfamilies viz. TRPC (canonical), TRPV (vanilloid), TRPM (melastatin), TRPA (ankyrin), and TRPN (no mechanoreceptor potential C, NOMP-C) [32]. Among these five subfamilies, TRPC subfamily has the strongest sequence homology with *Drosophila* TRP [138]. The group 2 TRPs consist of two subfamilies viz. TRPP (polycystin) and TRPML (mucolipin). TRPY (yeast) subfamily is different from group 1 and 2 TRPs and is only reported in yeast [32]. The TRPN expression was reported in the zebrafish but not observed in mammals [32]. TRPM proteins possess C-terminal enzyme domains and are therefore called as chanzymes [139]. Mutations in TRPP, TRPML, TRPC6, and TRPM6 genes have been observed to cause autosomal dominant

polycystic kidney disease (ADPKD) and mucopolysaccharidosis type IV (MLIV), autosomal dominant segmental glomerulosclerosis, hypomagnesemia/ hypocalcemia, respectively and thereby evidences the importance of TRP channels in human health [32]. TRP channels are polymodal in nature and serve as signal integrators. Their role in sensory physiology has been widely studied. All TRP channels are suggested to resemble voltage-gated potassium channels consisting of four subunits surrounding a centrally located ion permeation pore. Each subunit is a six transmembrane segment with a pore forming loop between S5 and S6, and intracellularly located N and C termini [137]. Growing evidence suggests an important role of transient receptor potential vanilloid (TRPV) ion channels in neural and neuroendocrine regulation [33]. These ion channels have emerged as novel players in neurotransmission, synaptic plasticity, Ca²⁺-mediated cellular signalling and modulation of behaviour. TRPV channels are gated by vanilloids, temperature, osmolality, phospholipids, and steroid hormones. The TRPV subfamily consists of six members viz. TRPV1-6 [32]. While TRPV1-4 are non-selective cation channels, TRPV5 and TRPV6 are highly Ca²⁺-selective [32]. The organization of TRPV1-4 expressing elements has been described in the brain and their relevance to neuroendocrine regulation demonstrated [33], but relevant information about TRPV5/TRPV6 is not available. The promoter of TRPV genes have been proposed to contain estrogen response elements (ERE), and estradiol regulates TRPV5/6 mRNA expression in peripheral tissues [34,140,141]. The ARC neurons express ER α , contain CART, and are modulated by estradiol [123]. Whether ARC CART neurons are equipped with TRPV5 and TRPV6, and the expression of these ion channels in ARC is modulated by circulating levels of estradiol, however is not known.

Apart from the role of gonadotrophs and thyrotrophs of pituitary gland in reproduction and energy balance respectively, somatotrophs also seem to play an important role in the regulation of these functions. The GH secreted from the somatotrophs of pituitary

gland which influences both energy balance [35] as well as reproduction [36]. Compared to wild type mice, estrous cycle/changes in estradiol levels are altered in the GH receptor knockout mice [36]. These mice further showed reduced testicular function [38]. GH regulates gluconeogenesis, glycogenolysis, lipolysis in the adipose tissue, and free fatty acid uptake in skeletal muscles [37]. Further, an increase in GH secretion by the central administration of CART peptide and dense innervations of CART in the external zone of ME, suggests role of hypophysiotropic CART in the modulation of GH secretion. Whether ARC CART contributes to the hypophysiotropic regulation, how CART controls GH release and control energy balance has remained unexplored.

In this background, my aim was to find out if ARC CART neurons serve as common neural substrate for connecting reproductive and energy balance pathways, and role of TRPV ion channels in the regulation of these neurons and GH secretion. Experiments were conducted on the adult, male and female, Sprague Dawley rats and BALB/c mice. Using double immunofluorescence, we have identified the ER α -expressing CART neurons and their response to changes in energy balance. The projections of ARC CART neurons in the brain were mapped and the innervation on GnRH neurons in POA determined. Attempts were made to find out if CART-GnRH association is modulated by estrous cycle and changes in energy balance. We studied the estrous cycle-related changes in TRPV1-6 gene expression in different compartments of the brain. Due to high Ca²⁺ selectivity and estradiol regulation of TRPV5/6, we focused on exploring the relevance of these ion channels in the brain. Given the importance of GH in the regulation of energy balance and reproduction, we explored the importance of CART in GH secretion and studied the hypophysiotropic and TRPV1-induced GH secretion.

PLAN OF WORK

Neural circuits regulating energy balance and reproduction are well established but the complex interplay between these circuitries is not well understood. I have investigated the role of hypothalamic CART neurons in bridging the pathways regulating energy balance and reproduction. I have presented the results obtained during my Ph.D. work in the following five chapters:

- Chapter 1: Elucidating the role of CART as common messenger in the neural pathways regulating energy balance and reproduction
- Chapter 2: Transient receptor potential vanilloid 1-6 (TRPV1-6) gene expression in the mouse brain during estrous cycle
- Chapter 3: Transient receptor potential vanilloid 5 (TRPV5), a highly Ca²⁺-selective TRP channel is widely distributed in the brain and may serve as potential modulator of arcuate nucleus CART neurons
- Chapter 4: Organization of transient receptor potential vanilloid 6 (TRPV6)-equipped elements in the brain, estrous cycle-related changes in the hypothalamus, and role in regulation of arcuate nucleus neurons
- Chapter 5: CART- and TRPV1-induced growth hormone secretion may serve as novel component of the central regulation of energy balance and reproduction

Our studies show that the CART neurons in ARC co-express estrogen receptor alpha and respond to changes in energy status. While CART-containing axons of ARC origin densely innervate GnRH neurons in the POA, CART-GnRH contacts showed reproduction stage- and energy status-dependent plasticity. These results are presented in chapter 1. TRPV ion channels may serve as potential regulators of ARC CART neurons. The promoter of TRPV1-6 genes contain estrogen response element and 17 β -estradiol modulates their expression in peripheral tissues. In chapter 2, we have presented our results on estrous cycle-

related changes in TRPV1-6 expression in different brain compartments. We explored the organization of TRPV5/6 in brain and their relevance in the regulation of CART neurons in the ARC. While a great majority of ARC CART neurons were equipped with TRPV5, only few neurons co-express TRPV6. Retrograde neuronal tracer iontophoresed into POA showed its accumulation in TRPV5- and TRPV6-equipped ARC CART neurons. TRPV5 and TRPV6 expression in these neurons showed correlation with estrous cycle but were not altered due to changes in energy status. TRPV5/6 may differentially regulate ARC neuronal populations. The results of TRPV5 and TRPV6 in the brain and their importance in the regulation of ARC CART neurons are presented in chapters 3 and 4, respectively. Finally, we elucidated the role of CART in regulation of GH cells, which controls energy balance. The external zone of median eminence was richly innervated CART-containing axons. Compared to control, CART-peptide treatment significantly elevated GH release in primary rat pituitary cells. While TRPV1-6 equipped elements showed discrete localization in different compartments of the pituitary, GH cells in the pituitary co-express TRPV1. TRPV1 agonist treatment resulted in GH secretion from primary rat pituitary cells and the CART-induced GH-secretion was not mediated via TRPV1. These results are presented in chapter 5.

CHAPTER 1

ELUCIDATING THE ROLE OF CART AS COMMON MESSENGER IN THE NEURAL PATHWAYS REGULATING ENERGY BALANCE AND REPRODUCTION

INTRODUCTION

CART is expressed in various brain regions and regulates range of physiological functions and behavior [22,133,142–146]. Well known for its anorectic action, CART-containing neurons were observed in the ARC, PVN, and dorsomedial nucleus (DMN) and lateral hypothalamus, and these areas are known to play important role in the central regulation of feeding and energy balance [24,128,131–133]. The CART-containing neurons in the ARC and PVN have been suggested important players of feeding and energy balance controlling pathways [22,134]. CART mRNA expression in the ARC is suppressed during fasting [22] and intracerebroventricular (icv) CART administration decreases food intake [23]. Injection of CART stimulates cFos expression in the areas of the brain involved in feeding [147]. CART neurons are direct targets for leptin. Leptin receptors are present on the CART neurons in the ARC [61] and these neurons respond to intracerebroventricular (ICV) administration of leptin [148]. CARTPT^{-/-} mice were shown to gain body weight [149–151]. The CART-containing system in the brain also seems to interact with NPY (orexigenic neuropeptide)-containing system and the NPY fibers were seen in close vicinity of PVN CART neurons [23].

Acute food deprivation or chronic food restriction delays puberty, lengthens estrous cycles, extends lactational diestrous and reduces reproductive behavior [1,2,152]. Food deprivation for 74 h suppresses steroid-induced display of lordosis in adult female rats, which was associated with a decrease in estrogen receptors in the brain [152]. Nutritional infertility is the result of several different factors, one being the suppression of pulsatile LH secretion from the pituitary. In rats, a decrease in mean plasma LH levels, LH pulse frequency and LH pulse amplitude was observed following 48 h of food deprivation [27,135,136]. The GnRH neurons in POA are sensitive to glucose and the sensitivity of the GnRH neurons to glucose show alteration with changes in gonadal steroids levels [28].

Recent evidence suggests the modulation of CART by estrogen. The midbrain CART neurons contains estrogen receptors and the gene expression of peptide was decreased following estrogen treatment in the rhesus monkey [153]. Estradiol treatment in the ovariectomized rats reduced CART mRNA expression in the ARC and lateral hypothalamic area, but increased in PVN [29]. Female odours stimulate CART neurons in the ventral premammillary nucleus of male rats [154]. Treatment with oleyl estrone, which is used as antiobesity drug seem to reduce food intake and CART mRNA expression in the hypothalamus [30]. In addition, ovariectomized animals treated with estrogen resulted in decreased food intake and CART mRNA expression in the ARC [29].

Although the role of ARC CART neurons in energy balance is well established, recent evidence demonstrate involvement of these neurons in the regulation of reproductive pathways in the brain [20,83]. CART-ir fibers were found in close apposition to GnRH cells and 100 nM CART-induced depolarization and spontaneous firing in GnRH-GFP neurons [83]. Using retrograde neuronal tracing, Rondini et al. [20] have demonstrated that the CART-ir fibers in anteroventral periventricular nucleus (AVPe) of female rats originate from ARC. In addition, the ARC CART neurons were also shown to project the dorsal raphe and locus coeruleus [155]. The ARC CART neurons innervate the sympathetic preganglionic neurons in the thoracic spinal cord [156]. Although these evidence suggest role of CART in the regulation of feeding and energy balance, whether CART serve as common messenger in the neural pathways regulating these functions has remained unexplored. The central projections of the ARC CART neurons involved in energy balance/reproduction, however are not known.

More than 95 % ARC CART neurons also express α -MSH [24]. In addition to ARC, α -MSH neurons are also found in nucleus of the solitary tract (NTS) in the brainstem

[157,158]. Although NTS contain neurons synthesizing CART, no colocalization of α -MSH and CART was observed in this region [157]. Therefore, the presence of CART/ α -MSH double labelled fibers would indicate their origin from the ARC and may serve as an important tool to trace the projections of ARC CART neurons in the CNS. As compared to the critical bilateral neuronal tracing with little success, CART/ α -MSH double immunofluorescence using sections of the brain a normal animal seems more accurate and simple approach to study the projections of ARC CART neurons. To find out whether the CART neurons in ARC involved in the regulation of energy balance also participate in regulation of reproduction, the sections of the hypothalamus were processed for CART/ $ER\alpha$ double immunofluorescence. Using CART/ α -MSH double immunofluorescence, an attempt has been made to trace and map the projections of ARC CART neurons in the CNS. In addition, we have explored the role of ARC CART neurons in modulation of GnRH neurons in the preoptic area by studying changes in CART/ α -MSH double-labelled fibers and their association with GnRH neurons in the preoptic area during estrous cycle and changes in energy status.

MATERIALS AND METHODS

Animals

Adult, male and female, Sprague-Dawley rats [200-250 g body weight (BW)] used in this study, were housed in the standard temperature and humidity on a cycle of 12 h light/12 h dark with *ad libitum* food and water. Experiments based on animal usage were reviewed and approved by the Animal Ethical Committee at the National Institute of Science Education and Research (NISER), Bhubaneswar, under the Committee for the Purpose of Control and Supervision of Experiments on Animals (CPCSEA), New Delhi, India.

Assessment of estrous cycle

The stages of estrous cycle were assessed by vaginal smear cytology as described previously [159,160]. In brief, the stages were identified by the presence of predominant nucleated epithelial cells in proestrus, cornified epithelial cells in estrus, mixture of leukocytes, nucleated epithelial cells and cornified cells in metestrus and predominant leukocytes in diestrus. The adult female rats were handled every morning between 8:00 and 9:00 am for a week prior to experiment to reduce the handling related stress. Vaginal smears were collected on glass slides between 8:00 and 9:00 am everyday by flushing vagina gently with 10 μ l 0.01 M PBS, pH 7.4 using pipette after cleaning with PBS-soaked cotton tipped wooden applicators. The unstained slides having vaginal smears were observed under the light microscope and stages were assigned to rats based on the cell types in the smears. Samples from three rats per stage of the estrous cycle were collected and processed as described below.

Fasting and refeeding

The fasting and refeeding of fasted animals is known to activate cFos in the brain regions involved in regulation of energy balance [161]. Adult female rats were divided into four groups (n = 3 rats/group) viz. fed, fasted for 65 h, and fasted for 65 h and refed for 2, 4 and 8 h. While the rats in fed group were supplied with food *ad libitum*, rats in fasted group had no access to food for 65 h. The animals in the refeeding group were fasted for 65 h and given free access to food for 2, 4 or 8 h. The animals in all groups received water *ad libitum*. The rats were anaesthetized and the brains were processed for immunofluorescence as described below.

Tissue collection and processing

Animals were anaesthetized using an intraperitoneal injection of a mixture of ketamine (100 mg/Kg BW) and xylazine (10 mg/Kg BW). The rats were perfused transcardially with phosphate buffered saline (PBS, pH 7.4) followed by 4 % paraformaldehyde in phosphate buffer (PB, pH 7.4). The brain, pituitary and spinal cord were dissected, post-fixed in 4 % paraformaldehyde and cryoprotected in 25% sucrose solution in PBS. Coronal sections (25 μ m thick) through the rostro-caudal extent of the brain, pituitary and spinal cord were cut on a cryostat (Leica CM3050 S, Leica Microsystems, Nussloch GmbH, Germany), collected in PBS, transferred to the anti-freezing solution, and stored at -20 °C until processed further.

Double immunofluorescence

To find out whether the hypothalamic CART neurons express ER α , double immunofluorescence protocol was employed, as described earlier [159]. In brief, coronal sections through the POA and hypothalamic regions from each brain (n = 3) were washed

several time in PBS to remove traces of anti-freezing solution. To improve antibody penetration, the sections were permeabilized with 0.5% Triton X-100 in PBS for 20 min at room temperature. The sections were incubated in 3% normal horse serum in PBS for 30 min. The sections were incubated overnight at 4°C in a mixture of diluted rabbit polyclonal anti-ER α antiserum (1:1000) and mouse monoclonal anti-CART antibody (1:2000). The sections were rinsed in PBS and incubated in a mixture of fluorescence conjugated secondary antibodies [Alexa Fluor 488-conjugated donkey anti-rabbit IgG and Alexa Fluor 594-conjugated goat anti-mouse IgG (Life technologies, 1:1000)] for 2 h at room temperature.

To find out the effect of dynamics of energy balance on CART neurons in the ARC, double immunofluorescence was employed. The rostrocaudal series of hypothalamic sections containing ARC from the rats in fed, fasted, and refed groups (n = 3/group) were incubated overnight at 4 °C in diluted rabbit polyclonal anti-cFos antiserum (1:50,000) and mouse monoclonal anti-CART antibody (1:2000). The sections were rinsed in PBS and incubated in a mixture of Alexa Fluor 488-conjugated donkey anti-rabbit IgG and Alexa Fluor 594-conjugated goat anti-mouse IgG (Life technologies, 1:1000) for 2 h at room temperature.

To map the innervations of hypothalamic CART immunoreactive fibers of ARC origin, rostro-caudal series of coronal sections through the brain, pituitary, and spinal cord from each animal (n = 6; 3 males and 3 females) were subjected to double immunofluorescence. The sections were prepared for immunofluorescence as described above and incubated in a mixture of mouse monoclonal anti-CART antibody (1:2000) and sheep polyclonal anti- α -MSH antiserum (1:10000) overnight at 4 °C. Following rinsing in PBS, sections were incubated in Alexa Fluor 594-conjugated goat anti-mouse IgG and Alexa Fluor 488-conjugated donkey anti-sheep IgG (Life technologies, 1:1000) for 2 h at room temperature.

Triple immunofluorescence

To determine whether the CART fibers of ARC origin innervate GnRH neurons in the POA, triple immunofluorescence protocol was employed. The coronal sections through the rostro-caudal extent of the median preoptic nucleus (MnPO) and AVPe were prepared for immunofluorescence protocol as described above. The sections were incubated overnight at 4 °C in a mixture of diluted mouse monoclonal anti-CART antibody (1:2000), sheep polyclonal anti- α -MSH antiserum (1:10000), and guinea pig polyclonal anti-GnRH antiserum (1:1000). Following incubation in primary antisera, sections were rinsed in PBS and incubated in a mixture of Alexa Fluor 594-conjugated goat anti-mouse IgG, Alexa Fluor 488-conjugated donkey anti-sheep IgG, and Alexa Fluor 648-conjugated donkey anti-guinea pig IgG (Life technologies, 1:1000) for 2 h at room temperature. After rinsing in Tris buffer (pH 7.6), sections were mounted on glass slides and coverslipped with Vectashield mounting medium.

Specificity of the antisera

The CART, ER α , cFos, α -MSH, and GnRH antisera used in this study have previously been shown to specifically recognize the respective antigens in the rat brain [134,161–164]. The details of the antisera are given in Appendix 1.

Image analysis

Images were captured using AxioCam digital camera (Carl Zeiss) by switching the filter sets. In Adobe Photoshop CS4 (Adobe Systems, Inc., USA), the images were superimposed, and adjusted for brightness and contrast. Neuroanatomical description and nomenclature were adapted from the rat brain atlas of Paxinos and Watson [165]. For depicting the hypothalamic CART-immunoreactive fibers of ARC origin in the brain,

pituitary, and spinal cord as shown in Figures 2-4, schematics of the coronal sections of the respective regions were adapted from Paxinos and Watson [165] with minor modifications.

The innervations of hypothalamic CART immunoreactive fibers of ARC origin in brain, pituitary, and spinal cord of rat were visually scored [+ , low; ++, moderate; +++, high; –, absent] based on the relative density of double labelled fibers in each brain region (Table 1). The innervations were further semiquantified using colocalization tool of Image J [166]. The Manders' colocalization coefficients (MCC), M1 and M2 estimate fraction of one fluorophore overlapping another. The Manders' colocalization coefficient, M1 estimates fraction of red pixels (CART) overlapping green pixels (α -MSH), thereby representing the fraction of hypothalamic CART immunoreactive fibers originating from ARC (Table 1). The fraction of CART fibers other than ARC origin (M') was given by $1 - M1$ (Table 1). The M1 estimation in regions containing CART cell bodies did not represent the desired fraction as it is affected by the pixels of CART cell bodies in addition to that of CART fibers (Table 1).

Although the arbitrary scores and M1 help in distinguishing different regions for density of hypothalamic CART immunoreactive fibers of ARC origin, it was difficult to interpret subtle changes in the same regions (AVPe or MnPO) under a given experimental condition (estrous cycle or energy status). This might be due to the CART fibers from other brain regions contributing to the estimation of M1. Therefore, any changes in CART fibers of other brain regions will also be reflected in the M1, which makes the analysis of specifically the ARC CART fibers difficult. To distinguish the CART fibers of ARC origin from those of other brain regions, the total CART fibers of ARC origin was obtained by multiplying M1 with MGV where MGV is the mean gray value for red pixels, representing the total CART fibers in a given region. Pearson's correlation coefficient (PCC) was also calculated which gave the degree of association between intensities of two fluorophores in each pixel, and helped in quantifying colocalization. The total number of GnRH neurons and

the number of GnRH neurons contacted by CART fibers of ARC origin in the MnPO region during estrous cycle were counted and the percentage of GnRH neurons contacted by ARC CART axons were calculated, as described previously [167].

Statistical analysis

The sections from all the animals from the experiment (estrous cycle or energy states) were processed together for immunofluorescence to reduce the standard deviation (SD) between groups due to reagents, pipetting error etc. All the images were captured at same exposure time using constant microscopic settings. The data from all the animals in each group of an experiment was analyzed in Prism 7.02 software using Two-way ANOVA followed by Tukey's multiple comparisons test. A $P < 0.05$ was considered statistically significant. The values are represented as mean \pm SD.

RESULTS

Organization of CART-containing neurons co-expressing ER α in the hypothalamus

CART neurons were observed in the AVPe, PeV, PVN, SON, lateral hypothalamus, zona incerta, and DMN. Several neurons in the ARC showed intense CART immunoreactivity. A dense network of CART immunoreactive fibers were seen in the POA, PeV, PVN, DMN, lateral part of the hypothalamic ventromedial nucleus (VMNI), and ARC. Isolated CART fibers were seen in the SON. The ER α immunoreactive cells were observed in the AVPe and VMNI. Using double labeling immunofluorescence as described above, we explored the neuroanatomical organization of CART neurons co-expressing ER α . While the CART neurons in the AVPe contained weak ER α immunofluorescence, several CART neurons in the ARC contained distinct ER α immunoreactivity (Fig. 1). Approximately, 87 ± 1.2 % CART neurons in the ARC co-expressed ER α .

Effect of fasting and refeeding on cFos activation in ARC

In the normal fed animals, isolated cFos cells were seen in the ARC (Fig. 2A) but a significant increase ($P < 0.001$) in the number of cFos cells was apparent in the medial portion of the ARC following 65 h fasting (Fig. 2E). In the fasted rats refed for 2 h, a significant increase ($P < 0.001$) in cFos cells were observed in the lateral portion of the ARC (Fig. 2I). Isolated cells were observed in the medial portion of ARC after refeeding (Fig. 2I).

ER α -containing CART neurons in the hypothalamus are regulated by energy balance

Isolated cFos-expressing CART neurons were seen in the ARC of fed animals (Fig. 2A-C). Fasting for 65 h resulted in cFos activation in the medial part of the ARC (Fig. 2E), but none of the ARC CART neurons showed cFos during fasting (Fig. 2G, H). Refeeding of

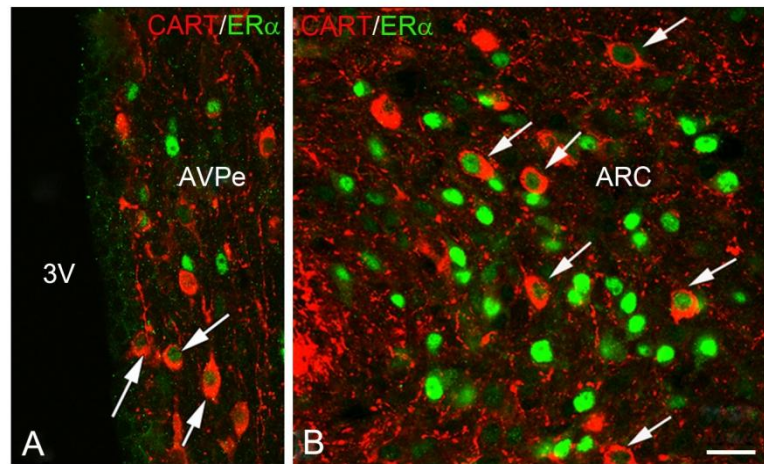


Figure 1: CART neurons in the preoptic area and hypothalamus of rat co-express estrogen receptor alpha ($ER\alpha$). Double-immunofluorescence photomicrographs showing presence of $ER\alpha$ (green) in CART neurons (red) in the anteroventral periventricular nucleus (AVPe, A) and hypothalamic arcuate nucleus (ARC, B). Double labelled neurons are shown with arrows. 3V, third ventricle. Scale bar = 25 μ m.

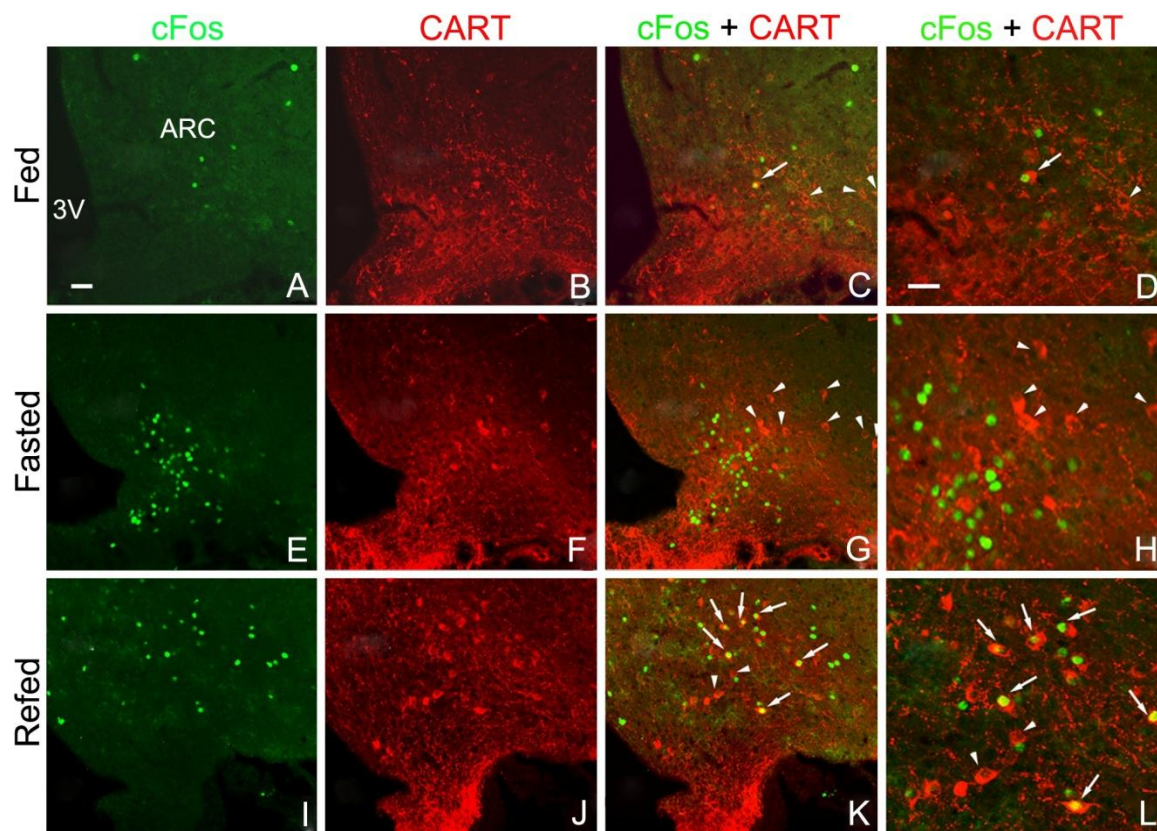


Figure 2: Energy status-dependent activation of hypothalamic neurons. Double-immunofluorescence photomicrographs of the coronal sections of the hypothalamic arcuate nucleus (ARC) of rat showing activation of cFos (green) in CART neurons (red). (A-D) *ad libitum* fed, (E-H) fasted for 65 h, and (I-L) fasted for 65 h and refed for 2 h. Note cFos activation in the medial ARC during fasting and in lateral ARC during refeeding. Refeeding activates cFos in CART neurons in lateral ARC (arrows). None of the CART neurons show cFos during fasting (arrowheads). 3V, third ventricle. Scale bar = 25 μ m.

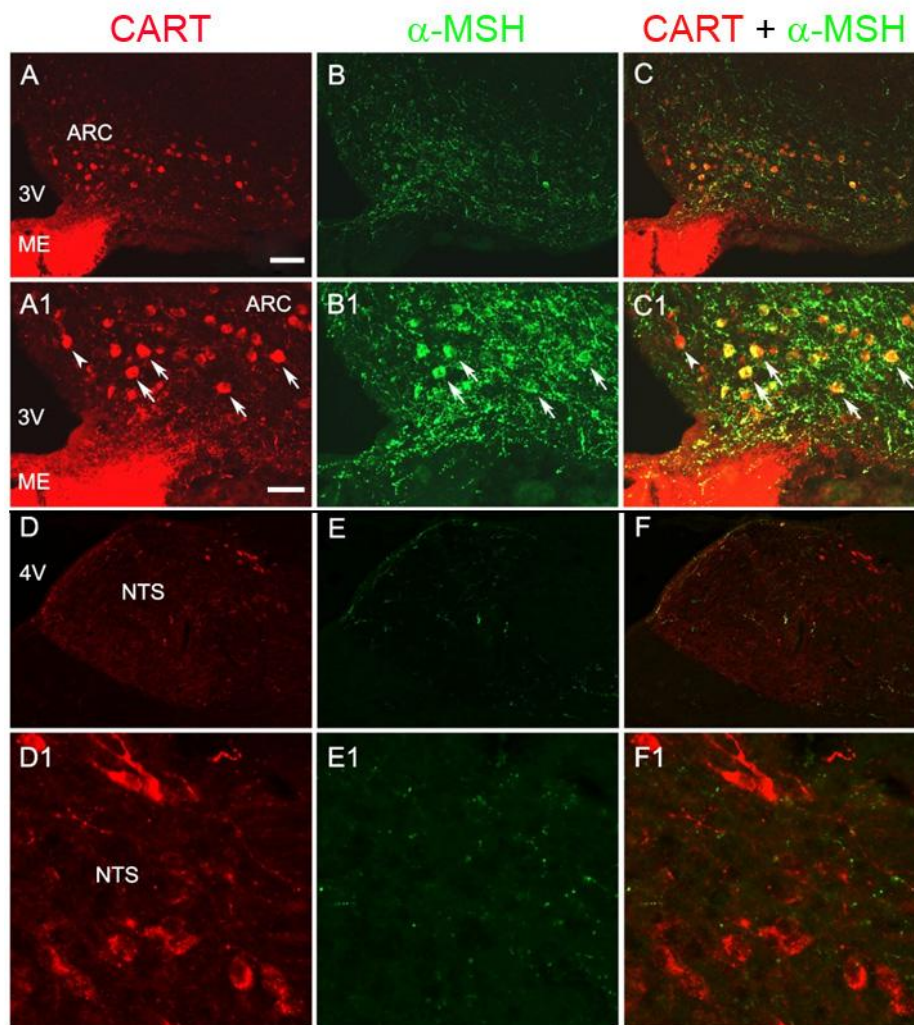


Figure 3: Co-localization of CART and α -MSH neurons in the rat brain. Double immunofluorescence photomicrographs are showing colocalization of CART and alpha-melanocyte stimulating hormone (α -MSH) in the neurons of the hypothalamic arcuate nucleus (ARC) (A-C, A1-C1, arrows). No colocalization of the CART and α -MSH is observed in the nucleus of the solitary tract (NTS) (D-F, D1-F1). Scale bar = 50 μ m (A-F) and 20 μ m (A1-F1).

fasting rats however showed cFos activation in the lateral ARC (Fig. 2I) and approximately 61 ± 1.7 % of the CART neurons in ARC contained cFos following refeeding (Fig. 2K, L). Compared to that in the fed (Fig. 2C, D) and fasted (Fig. 2G, H) rats, refeeding for 2 h induced cFos activation in a great majority of CART neurons in the ARC (Fig. 2K, L).

Organization of CART-immunoreactive fibers of ARC origin in the CNS

Colocalization of CART and α -MSH was observed in the ARC neurons (Fig. 3A-C, A1-C1). No colocalization of these two neuropeptides was seen in the neurons of NTS (Fig. 3D-F, D1-F1). The axons containing both the peptides would indicate its origin from ARC and not from other brain region, therefore serving as a useful tool to trace the projections of the ARC CART neurons in the brain. Using this approach, we have identified the projections of the CART neurons in the brain. Axons originated from the ARC CART neurons were observed in the forebrain (Fig. 4), midbrain (Fig. 5), hindbrain (Fig. 5), and spinal cord (Fig. 6). The semi-quantitative analysis of relative density of the innervation of ARC CART fibers in different regions of brain is given in Table 1.

In the forebrain, few double-labelled CART/ α -MSH immunoreactive fibers were observed in the olfactory bulb (OB, Fig. 4A), nucleus of the horizontal limb of the diagonal band (HDB, Fig. 4D), ventral pallidum (VP, Fig. 4E), vascular organ of the lamina terminalis (VOLT, Fig. 4G), amygdala (Fig. 4O), ARC (Fig. 4P), and posterior hypothalamic nucleus (PH, Fig. 4T). Moderate density of double labelled fibers was observed in the accumbens nucleus, shell (AcbSh, Fig. 4B), bed nucleus of the stria terminalis, medial division, anterior part (STMA, Fig. 4F), periventricular hypothalamic nucleus (Pe, Fig. 4K, L), PVN (Fig. 4M), anterior hypothalamic area (AH, Fig. 4N), and DMN (Fig. 4R, S). The regions including the medial septal nucleus (MS, Fig. 4C); MnPO (Fig. 4H); medial preoptic area (MPA, Fig. 4I),

and AVPe (Fig. 4J) were densely innervated by the CART/ α -MSH double labelled fibers. No double labelled fibers were seen in the ME (Fig. 4Q).

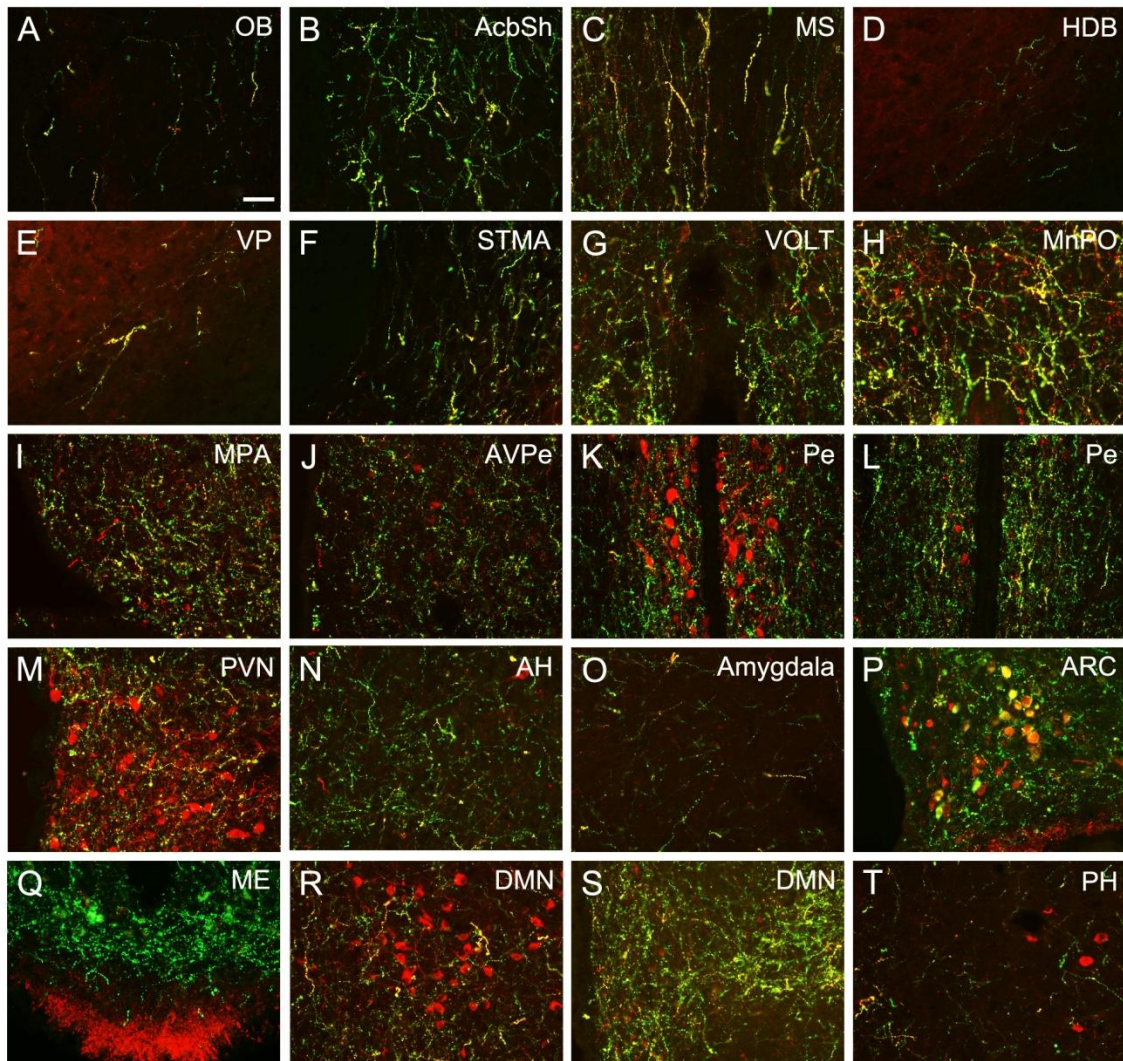


Figure 4: Organization of CART fibers of arcuate nucleus origin in the forebrain of rat. CART/ α -MSH double-labelled fibers (yellow) are seen in the olfactory bulb (OB, A), accumbens nucleus, shell (AcbSh, B), medial septal nucleus (MS, C), nucleus of the horizontal limb of the diagonal band (HDB, D), ventral pallidum (VP, E), bed nucleus of the stria terminalis, medial division, anterior part (STMA, F), vascular organ of the lamina terminalis (VOLT, G), median preoptic nucleus (MnPO, H), medial preoptic area (MPA, I), anteroventral periventricular nucleus (AVPe, J), periventricular hypothalamic nucleus (Pe, K, L), paraventricular hypothalamic nucleus (PVN, M), anterior hypothalamic area (AH, N), amygdala (O), arcuate hypothalamic nucleus (ARC, P), dorsomedial hypothalamic nucleus (DMN, R and S), and posterior hypothalamic nucleus (PH, T). No double-labelled fibers are seen in the medial eminence (ME, Q). Scale bar = 50 μ m.

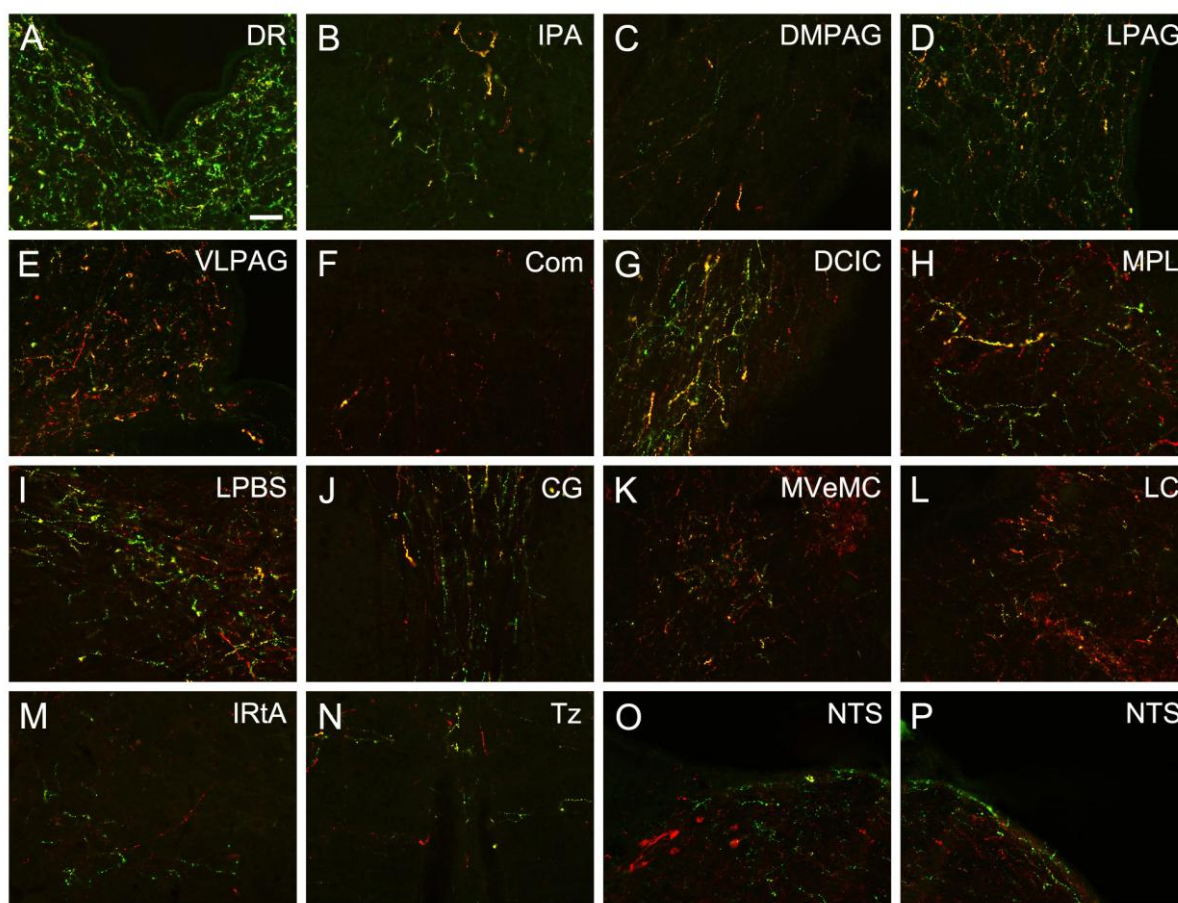


Figure 5: Organization of CART fibers of arcuate nucleus (ARC) origin in the midbrain and hindbrain of rat. The CART/ α -MSH double-labelled fibers (yellow) are seen in the dorsal raphe nucleus (DR, A), interpeduncular nucleus, apical subnucleus (IPA, B), dorsomedial periaqueductal gray (DMPAG, C), lateral periaqueductal gray (LPAG, D), ventrolateral periaqueductal gray (VLPAG, E), commissural nucleus of the inferior colliculus (Com, F), dorsal cortex of the inferior colliculus (DCIC, G), medial paralemniscial nucleus (MPL, H), lateral parabrachial nucleus, superior part (LPBS, I), central gray (CG, J), medial vestibular nucleus, magnocellular part (MVeMC, K), locus coeruleus (LC, L), intermediate reticular nucleus, alpha part (IRtA, M), nucleus of the trapezoid body (Tz, N), and nucleus of the solitary tract (NTS, O, P). Scale bar = 50 μ m.

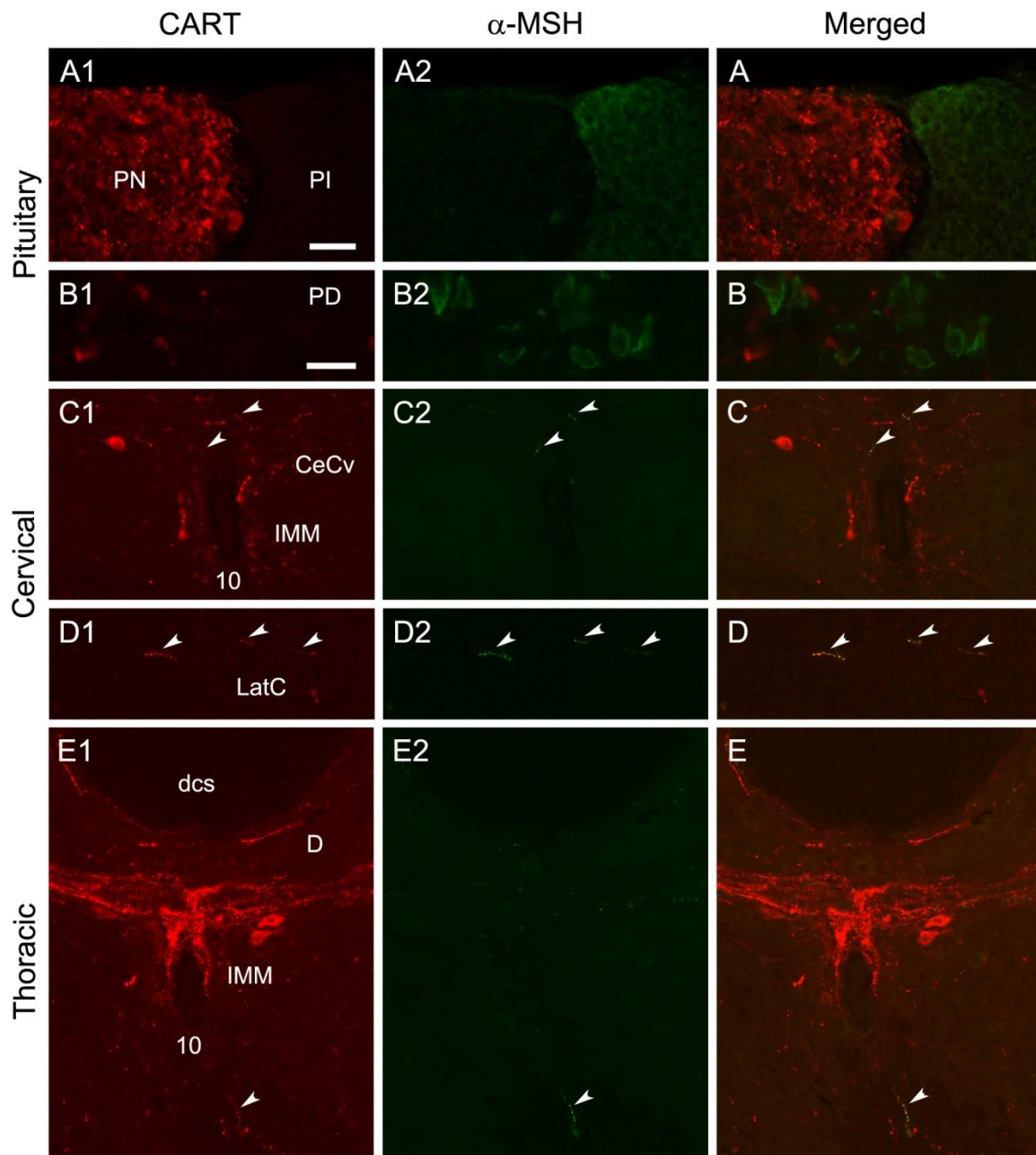


Figure 6: Organization of CART fibers of arcuate nucleus (ARC) origin in the pituitary gland and spinal cord of rat. CART/ α -MSH double-labelled fibers (yellow, arrowheads) are seen in the cervical (C, D) and thoracic (E) regions of the spinal cord. No double-labelled fibers are seen in the pituitary (A, B). Scale bar = 50 μ m (A1, A2, A, C1-E2, C-E) and 20 μ m (B1, B2, B).

Table 1: Semi-quantitative analysis of the CART/ α -MSH double labelled fibers in the forebrain, midbrain, hindbrain, spinal cord, and pituitary gland of rat

Areas of the brain	Fraction of CART fibers from arcuate nucleus (M1)	Fraction of CART fibers from brain regions other than arcuate nucleus (M'=1-M1)	Score based on density of CART fibers from arcuate nucleus**
Forebrain			
Olfactory bulb (OB)	0.722	0.278	+
Accumbens nucleus, shell (AcbSh)	0.929	0.071	++
Medial septal nucleus (MS)	0.796	0.204	+++
Nucleus of the horizontal limb of the diagonal band (HDB)	0.725	0.275	+
Ventral pallidum (VP)	0.832	0.168	+
Bed nucleus of the stria terminalis, medial division, anterior part (STMA)	0.935	0.065	++
Vascular organ of the lamina terminalis (VOLT)	0.697	0.303	+
Median preoptic nucleus (MnPO)	0.783	0.217	+++
Medial preoptic area (MPA)	0.709	0.291	+++
Anteroventral periventricular nucleus (AVPe)	0.741	0.259	+++
Periventricular hypothalamic nucleus (Pe)*	0.191*, 0.765	0.235	++
Paraventricular hypothalamic nucleus (PVN)*	0.295*	n/a	++
Anterior hypothalamic area (AH)	0.717	0.283	++
Amygdala	0.783	0.217	+
Hypothalamic arcuate nucleus (ARC)*	0.573*	n/a	+
Median eminence (ME)	0	1.000	-
Dorsomedial hypothalamic nucleus (DMN)*	0.319*, 0.832	0.168	++
Posterior hypothalamic nucleus (PH)*	0.390*	n/a	+
Midbrain			
Dorsal raphe nucleus (DR)	0.831	0.169	++
Interpeduncular nucleus, apical subnucleus (IPA)	0.804	0.196	+
Dorsomedial periaqueductal gray (DMPAG)	0.551	0.449	+
Lateral periaqueductal gray (LPAG)	0.559	0.441	++
Ventrolateral periaqueductal gray (VLPAG)	0.537	0.463	++
Commissural nucleus of the inferior colliculus (Com)	0.455	0.545	+
Dorsal cortex of the inferior colliculus (DCIC)	0.753	0.247	++
Medial paralemniscial nucleus (MPL)	0.565	0.435	+
Lateral parabrachial nucleus, superior part (LPBS)	0.695	0.305	++
Central gray (CG)	0.675	0.325	+

Hindbrain			
Medial vestibular nucleus, magnocellular part (MVeMC)	0.512	0.488	+
Locus coeruleus (LC)	0.577	0.423	+
Intermediate reticular nucleus, alpha part (IRtA)	0.240	0.760	+
Nucleus of the trapezoid body (Tz)	0.505	0.495	+
Nucleus of the solitary tract (NTS)*	0.167*, 0.296	0.704	+
Spinal cord			
Cervical	0.161	0.839	+
Thoracic	0.007	0.993	+
Lumbar	0.002	0.998	-
Sacral	0.000	1.000	-
Pituitary			
Pars distalis	0.000	1.000	-
Pars intermedia	n/a	n/a	-
Pars nervosa	n/a	n/a	-

*Regions containing CART cell bodies.

**Score based on density of CART fibers from arcuate nucleus: +, low; ++, moderate; +++, high; -, absent.

In the midbrain, few double-labelled CART/ α -MSH fibers were observed in the interpeduncular nucleus, apical subnucleus (IPA, Fig. 5B), dorsomedial periaqueductal gray (DMPAG, Fig. 5C), commissural nucleus of the inferior colliculus (Com, Fig. 5F), medial paralemniscial (MPL, Fig. 5H), and central gray (CG, Fig. 5J) nuclei. Moderate density of double labelled fibers was seen in the dorsal raphe nucleus (DR, Fig. 5A), and lateral (LPAG, Fig. 5D) and ventrolateral (VLPAG, Fig. 5E) subdivisions of periaqueductal gray, as well as in dorsal cortex of the inferior colliculus (DCIC, Fig. 5G) and lateral parabrachial nucleus, superior part (LPBS, Fig. 5I).

In the hindbrain, the isolated CART/ α -MSH double labelled fibers were observed in the medial vestibular nucleus, magnocellular part (MVeMC, Fig. 5K), locus coeruleus (LC, Fig. 5L), intermediate reticular nucleus, alpha part (IRtA, Fig. 5M), nucleus of the trapezoid body (Tz, Fig. 5N), and NTS (Fig. 5O, P).

No CART/ α -MSH double-labelled fibers were observed in the pituitary (Fig. 6A, B). While few double-labelled fibers were seen in the cervical (Fig. 6C, D) and thoracic (Fig. 6E) regions, no double labelled fibers were detected in the lumbar and sacral regions of the spinal cord.

Estrous cycle-related changes in GnRH-ir neurons and ARC CART fibers innervations in the POA

As compared to other brain regions, preoptic area was densely innervated by CART fibers of ARC origin (Table 1). Using triple immunofluorescence, the ARC CART fibers as well as CART fibers from other brain regions were seen in close association with GnRH neurons in the preoptic area (Fig. 7A-E). The CART/ α -MSH double labelled fibers were observed in AVPe (Fig. 8A-D) and MnPO (Fig. 8E-H) during all the four stages of the estrous cycle. The corresponding fluorograms of AVPe and MnPO are shown in

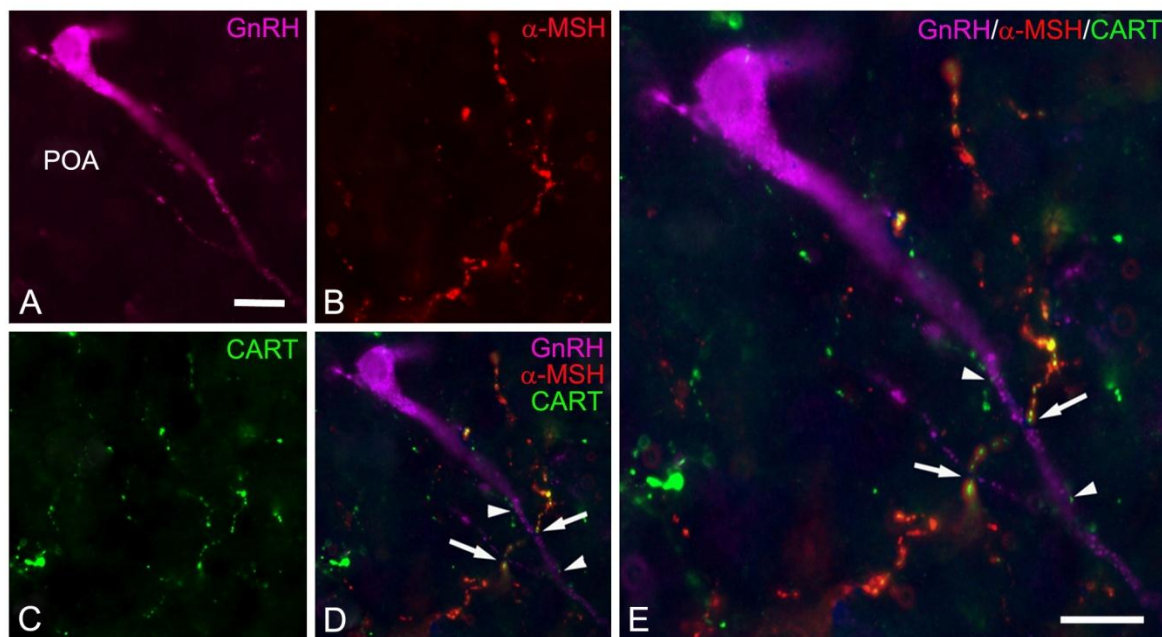


Figure 7: Association between GnRH neurons and CART axons in the median preoptic nucleus (MnPO). (A-E) Triple immunofluorescence photomicrographs of the preoptic region showing GnRH neurons (magenta) in the MnPO contacted by CART fibers originating from ARC (yellow, arrows) as well other brain regions (green, arrowheads). Scale bar = 25 μ m.

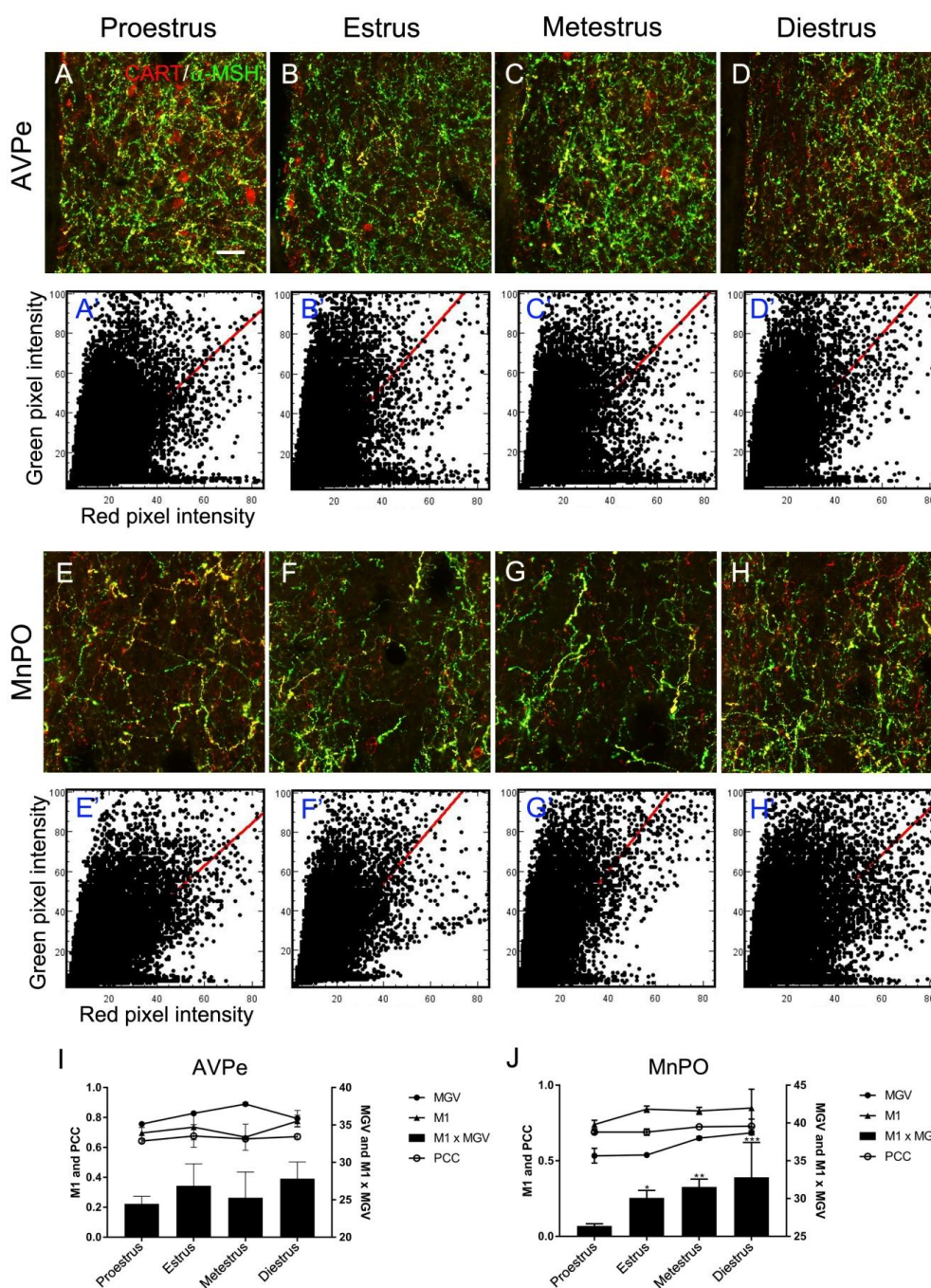


Figure 8: Arcuate nucleus CART fibers innervation in preoptic area show estrous cycle-related changes. Double immunofluorescence photomicrographs showing double-labelled CART/ α -MSH immunoreactive fibers (yellow) in the anteroventral periventricular nucleus (AVPe, A-D) and median preoptic nucleus (MnPO, E-H) during proestrus (A and E), estrus (B and F), metestrus (C and G), and diestrus (D and H) phases of the estrous cycle. The fluorograms showing changes in double labelled fibers during estrous cycle in AVPe (A'-D') and MnPO (E'-H'). Semiquantitative analysis of the double labelled fibers in AVPe (I) and MnPO (J) during estrous cycle. *, $P < 0.05$; **, $P < 0.01$; ***, $P < 0.001$. Scale bar = 40 μ m.

Figures 8A'-D' and 8E'-H', respectively. Compared to estrus ($P < 0.05$), metestrus ($P < 0.01$), and diestrus ($P < 0.001$), a significant decrease in CART/ α -MSH fibers innervations was observed in the MnPO during proestrus (Fig. 8J). Although similar pattern of reduction in double labelled fibers was observed in AVPe, the difference was non-significant (Fig. 8I). Using triple immunofluorescence, CART/ α -MSH fibers were observed in close apposition to MnPO-GnRH neurons during proestrus (Fig. 10A1-3, A), estrus (Fig. 10B1-3, B), metestrus (Fig. 10C1-3, C), and diestrus (Fig. 10D1-3, D) phases. Semi-quantitative analysis showed comparable number of MnPO-GnRH neurons during all the four stages of estrous cycle (Fig. 10F). Compared to proestrus, metestrus, and diestrus, a significant decrease ($P < 0.05$) in mean integrated density of MnPO-GnRH neurons was observed during estrus (Fig. 10E). In addition, a significant decrease ($P < 0.05$) in the percentage of MnPO-GnRH neurons contacting double-labelled fibers was observed during estrus compared to proestrus, metestrus, and diestrus (Fig. 10G) phases.

Energy states-related changes in GnRH neurons and ARC CART fibers innervations in the POA

CART/ α -MSH immunoreactive fibers were observed in AVPe (Fig. 9A-D) and MnPO (Fig. 9E-H) in POA of fed, fasted, and fasted rats refed for 4 and 8 h. The fluorograms showing changes in double labelled fibers of AVPe and MnPO of fed, fasted, and refed rats are shown in Figures 9A'-D' and 9E'-H', respectively. Compared to the double labelled fibers in AVPe and MnPO of refed rats for 4 h, a significant increase in CART/ α -MSH fibers innervations was observed in AVPe ($P < 0.01$) (Fig. 9I) and MnPO ($P < 0.001$) (Fig. 9J) of fasted animals. Using triple immunofluorescence, CART/ α -MSH fibers were observed in close apposition to MnPO-GnRH neurons in fed (Fig. 11A1-3, A), fasted (Fig. 11B1-3, B), and fasted animals refed for 4 (Fig. 11C1-3, C) and 8 (Fig. 11D1-3, D) h.

No significant difference in mean integrated density of MnPO-GnRH neurons was observed in fasted animals compared to the rats in fed and refeed groups (Fig. 11E).

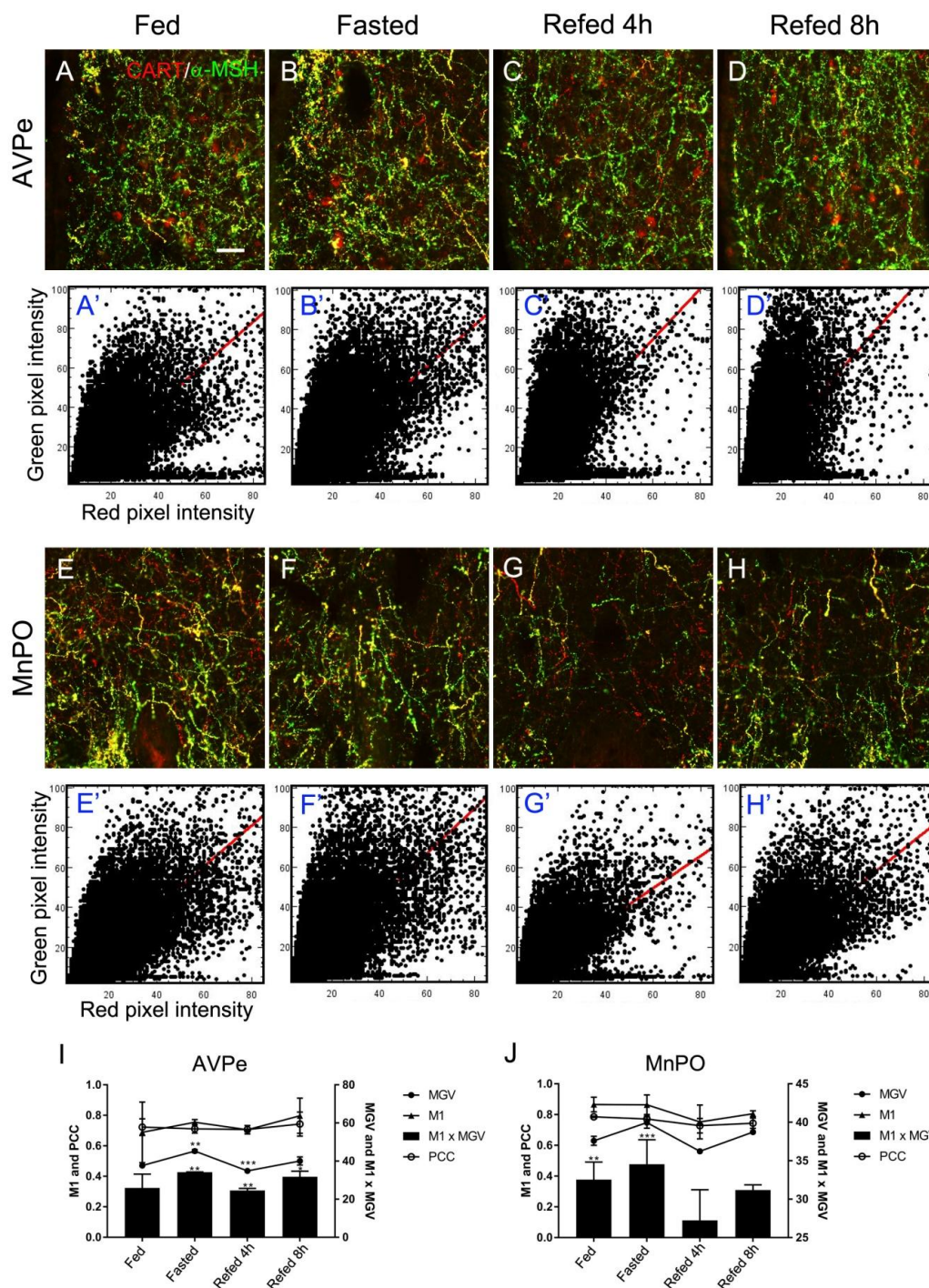


Figure 9: Arcuate nucleus (ARC) CART fibers innervation in preoptic area show energy status-related changes. Double immunofluorescence photomicrographs showing density of double labelled CART/ α -MSH fibers (yellow) in the anteroventral periventricular nucleus (AVPe, A-D) and median preoptic nucleus (MnPO, E-H) in the fed (A and E), fasted (B and F), and fasted rats refed for 4 (C and G) and 8 (D and H) h. The fluorograms showing changes in double labelled fibers during estrous cycle in AVPe (A'-D') and MnPO (E'-H'). Semiquantitative analysis of the double labelled fibers in AVPe (I) and MnPO (J) during different energy states. *, $P < 0.05$; **, $P < 0.01$; ***, $P < 0.001$. Scale bar = 40 μ m.

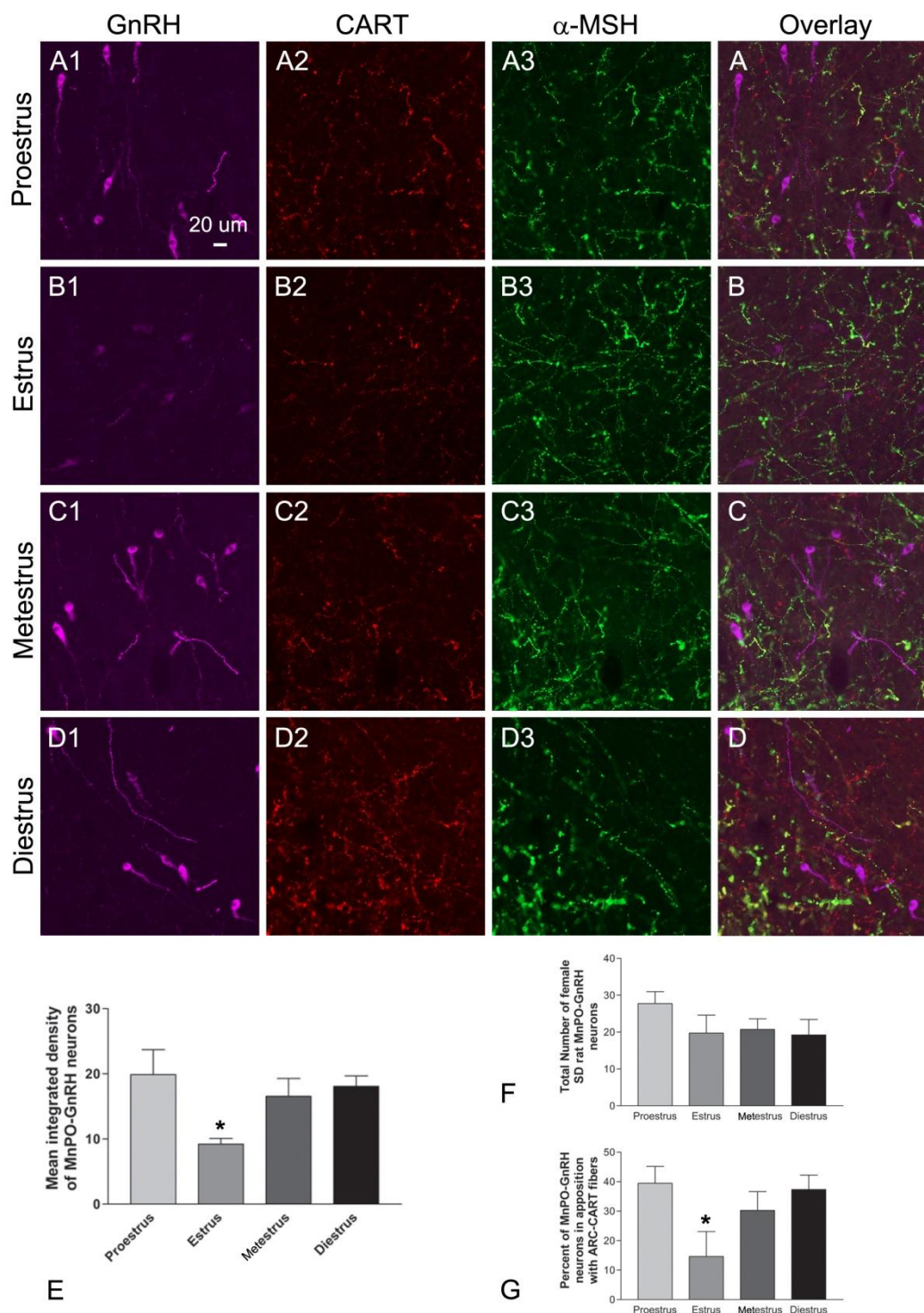
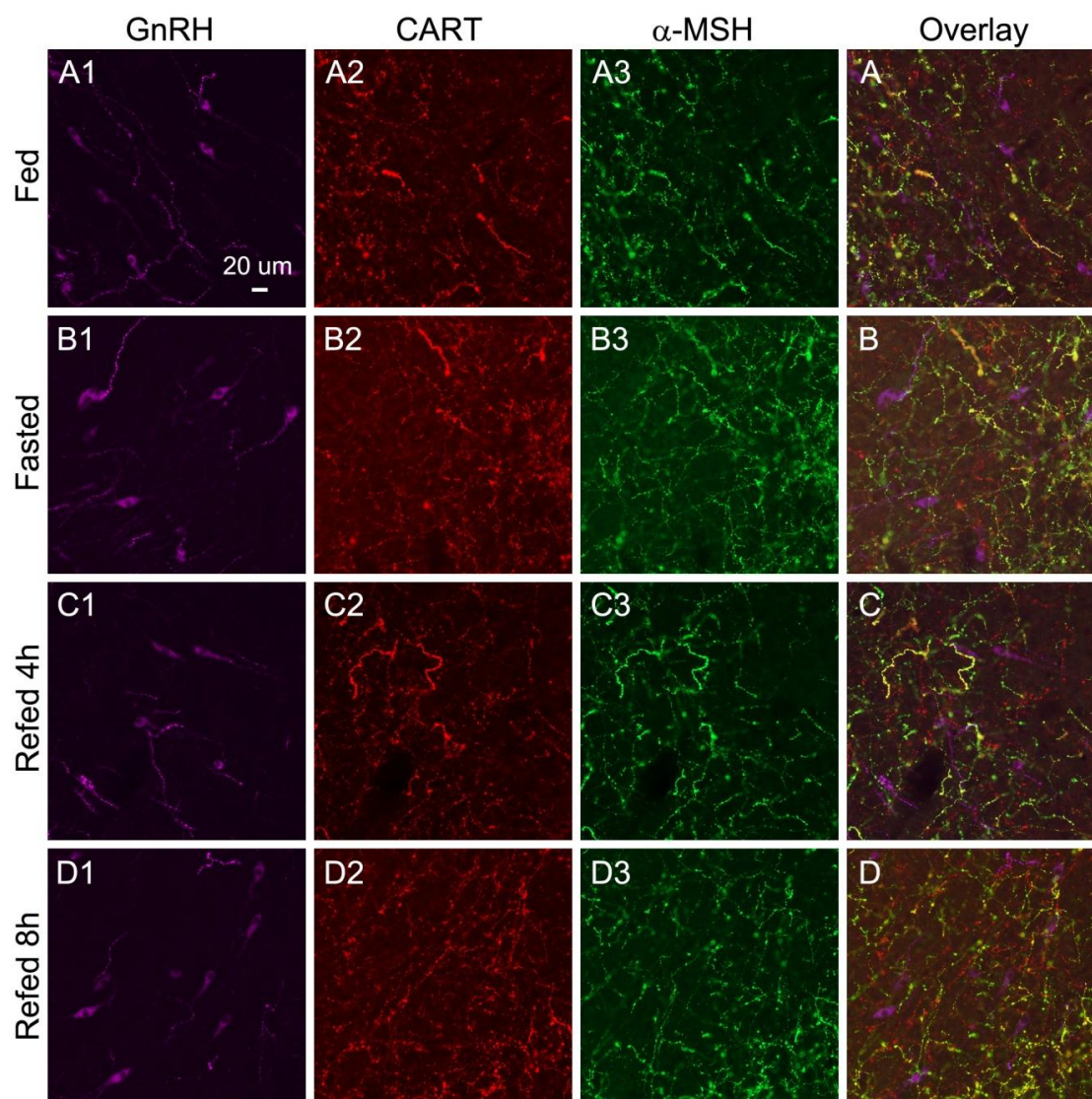


Figure 10: Arcuate nucleus (ARC) CART innervation of GnRH neurons in the median preoptic nucleus (MnPO) show estrous cycle-related changes. Triple immunofluorescence photomicrographs showing CART/ α -MSH double labelled fibers (yellow) closely associated with the MnPO GnRH neurons during proestrus (A1-3, A), estrus (B1-3, B), metestrus (C1-3, C), and diestrus (D1-3, D) phases. Semi-quantitative analysis of the mean integrated density of GnRH immunoreactivity in MnPO (E), total number of MnPO GnRH neurons (F), and percentage of MnPO GnRH neurons contacted by ARC CART fibers (G), during estrous cycle. *, $P < 0.05$. Scale bar = 20 μ m.



E

Figure 11: Arcuate nucleus (ARC) CART innervation of GnRH neurons in the median preoptic nucleus (MnPO) show energy status-related changes. Triple immunofluorescence photomicrographs showing CART/ α -MSH double labelled fibers (yellow) closely associated with the MnPO GnRH neurons in fed (A1-3, A), fasted (B1-3, B), and fasted rats refed for 4 (C1-3, C), and 8 (D1-3, D) h. Semi-quantitative analysis of the mean integrated density of GnRH immunoreactivity in MnPO (E) during fed, fasting, and refed states. Scale bar = 20 μ m.

DISCUSSION

GnRH neurons residing in the POA project to the external zone of the median eminence and secrete the neuropeptide into the portal circulation. GnRH *via* portal circulation is carried to the anterior pituitary gland and act and stimulates the LH and FSH secreting cells. These hormones regulate the gonadal function and reproduction. While a range of external and internal factors regulate the synthetic/secretory activity of GnRH neurons, the central regulation of these neurons is far more complex. In addition to the gonadal hormones and central factors, recent studies have underscored the importance of metabolic cues and energy status in the regulation of GnRH neuronal activity [168,169]. How these signals are transmitted to GnRH neurons is not well established. Fasting-induced glucoprivation, ICV insulin and 2-deoxyglucose treatments have been shown to alter GnRH neuronal activity. Zhang et al. [170] have demonstrated that the GnRH neurons are equipped with glucosensing mechanism. Although the GnRH neurons do not express ER α , the feedback signals from estradiol are conveyed to these neurons via other ER α expressing neuronal populations in the brain. Attempts have been made to find out whether such ER α -expressing neuronal populations which are linked to GnRH neurons serve as metabolic sensors in the brain [171,172]. True et al. [83] demonstrated that treatment with the anorectic neuropeptide, CART resulted in enhanced neuronal firing on GnRH neurons. The sources of CART innervation of GnRH neurons seem to originate from the hypothalamus. In the hypothalamic ARC, the feeding related CART neurons reside and the CART mRNA expression in ARC is modulated by changes in energy balance. Since ARC neurons express ER α and CART, we probed whether these neurons serve as substrate in the brain to link the neuronal pathways regulating reproduction and energy balance. We observed that the CART neurons in ARC are equipped with ER α and these neurons were activated in fasted animals refed for a short interval. The ARC CART neurons project to several different brain regions

with distinct innervation to POA contacting GnRH neurons. The CART/GnRH contacts showed changes with circulating levels of estradiol during estrous cycle. The CART fibers in the external zone of median eminence seem to originate from the PVN but the GnRH fibers in this region originate from the preoptic area [173,174]. Although CART as well as GnRH control LH and FSH secretion [52,175], and CART stimulate activity of GnRH neurons [176], these neuropeptidergic system might not interact at the level of median eminence. This is supported by the experiments showing no alterations in LH and FSH levels following central injections of CART [177]. The cultured LH cells however respond to CART treatment and resulted in inhibition of LH release [175]. Baranowska et al. (2003) suggested that CART may act directly on the pituitary cells to regulate LH secretion. Evidence from non-mammalian vertebrate also suggest role of CART as a regulator of LH secretion. In teleosts, CART expression in the pituitary LH cells showed reproduction phase dependent expression. CART is transiently expressed in LH cells only during the phase [178]. In the present study, this is for first time we demonstrate CART as common messenger in the neural pathways of energy balance and reproduction and ARC as a connecting link between these pathways.

Although various brain nuclei including the nucleus accumbens, lateral hypothalamus, paraventricular nucleus have been reported in the regulation of food intake [128], the ARC seems the major centre for the integration of central as well as peripheral cues of energy reserves. The primary neuronal populations involved in the direct sensing and processing of peripheral cues of energy reserves reside in this region [179]. The ARC neurons express ER α and mediate anorexigenic effects of estradiol [14,125]. We observed the expression of ER α in ARC CART neurons, and this is in agreement with the previous observation of presence of ER α in POMC neurons in ARC of ewe [180]. It is important to note that CART and POMC are co-expressed in ARC neurons [24]. We have also observed

ER α expression in AVPV CART neurons, which may contribute to the feedback effect of estradiol on GnRH neurons. It is important to note that the kisspeptin neurons of AVPV serve as target of estrogen positive feedback to induce GnRH/LH surge in female rats [181].

We observed energy status-dependent changes in cFos activation in ARC CART neurons. The metabolic control of GnRH neurons primarily involves NPY/AgRP and POMC/CART neuronal populations of the ARC [15]. By ICV route, CART peptide has been shown to decrease the food intake [23] and stimulates cFos expression in the feeding-related brain areas [147]. We have employed CART/MSH double immunofluorescence to find out the projections of ARC CART neurons in the CNS. This approach seems to be superior as compared to the neuronal tracing techniques. In the anterograde neuronal tracing, the tracer need to be injected or iontophoresed in the nucleus of interest to trace its projections. This needs further validation with retrograde neuronal tracing at multiple areas of projection of the neuronal group [182]. Injecting the tracer on either side of the brain in the nucleus of interest is challenging and involves extended surgery duration. Further, the injection site and its spread in the neighbouring regions vary from animal to animal. Employing the CART/MSH double immunofluorescence protocol seems to overcome these issues. Both CART and α -MSH are anorexigenic neuropeptides and the neurons synthesizing these neuropeptides resides in the lateral ARC [183]. Fasted rats refed for short interval showed pronounced activation of cFos in α -MSH [161] as well as CART (present study) neurons. Further, these neurons are known to express leptin and insulin receptors and are known to mediate the anorectic action to other brain regions [63]. Although previous studies have identified few brain regions including PVN and brainstem areas connected to the ARC neurons, anatomical evidence was not available. Our results suggest that projections of CART neurons from ARC may transmit energy status-related signals to the second order neurons in different brain regions. In addition to the anorectic role of ARC CART neurons, evidence suggests the

involvement of these neurons in the regulation of reproductive pathway in the brain [83]. While the GnRH neurons in the preoptic area are innervated by CART axons from ARC, CART peptide treatment increased neuronal firing in GnRH neurons [83]. We observed ER α in ARC CART neurons which suggest involvement of these neurons in estradiol feedback regulation of GnRH neuronal activity. Recently, using neuronal tracing connection between refeeding activated ARC neurons and central nucleus of amygdala (CeA) has been established [184]. Only a few refeeding-activated proopiomelanocortin (POMC) synthesizing neurons in ARC seem to project to CeA. Since CART and POMC are colocalized in ARC neurons, we anticipate similar projection pattern of the CART neurons to the CeA. Further, the ARC-CART neurons innervate the sympathetic preganglionic neurons in the thoracic spinal cord and its involvement in the leptin action has been suggested [156]. While tracing the ARC CART neurons projections in the rat brain, we observed dense innervations in the preoptic area compared to other brain regions. Further, these innervations were closely associated with GnRH neurons suggesting modulation of GnRH neurons by ARC CART neurons. Earlier studies have demonstrated that the CART axons from ARC and premammillary ventral nucleus innervate the POA GnRH neurons [20] and CART peptide treatment increases neuronal firing in GFP-GnRH neurons [83]. The ARC CART neurons may serve as yet another mediator of estradiol. While the ARC CART neurons express leptin receptors [61,148] and ER α , the POA GnRH neurons are devoid of these receptors [16]. The ARC neurons may therefore represent potential integrators of metabolic as well as reproductive signals in the regulation of GnRH neurons and CART in these neurons as common messenger in the neural pathways of energy balance and reproduction.

To further understand the role of ARC CART neurons in the regulation of POA GnRH neurons during reproductive cycle and metabolic states, we studied changes in the innervations of ARC CART neurons in two subdivisions of POA viz. MnPO and AVPV.

The MnPO contains GnRH cell bodies whereas AVPV is known to regulate GnRH neurons [181,185]. We have correlated these changes with alteration in the intensity of GnRH-ir neurons. Compared to the refed animals, fasting significantly increased ARC CART innervation in the MnPO and AVPe regions, supporting the possibility of suppression of CART release in POA under energy deficit condition. Berriman et al. [186] have observed metabolic fuel dependent changes in cFos-ir in GnRH neurons and suggested a decrease in GnRH secretion during food deprivation. The ARC CART innervations in MnPO region significantly decreases in proestrus rats compared to those in the other phases of the estrous cycle, which is expected if CART causes release of GnRH. We presume that the release of CART peptide from the axons may trigger GnRH release and therefore the GnRH-ir intensity was reduced. These results are supported by previous findings showing the expression of cFos in GnRH cells contacted by CART axons in the afternoon of proestrus [20] and increased GnRH activity in cycling female rats following CART treatment [21,26]. We did not observe significant changes in the number of MnPO GnRH neurons during estrous cycle. While few earlier studies showed comparable number of GnRH mRNA-expressing neurons in POA of rat throughout the estrous cycle [185], more number of LHRH-ir cell bodies was seen in POA during proestrus compared to estrus phase [187]. These discrepancies might be due to difference in timing of experimentation during proestrus. Reduced number of GnRH mRNA-expressing cells was observed at 1400-1600 h, increase significantly at 1800 h (the time of the LH surge), and gradually return to basal levels at 2200 h during proestrus [188]. However, during other stages of the estrous cycle the GnRH mRNA expressions remained unaltered [188]. In addition, two peaks of GnRH expression were also observed during estrous cycle [189]. The GnRH mRNA level increased at 1100 h during proestrus, rapidly decreased with a nadir at 1600 h, and again increased at 1100 h during estrus [189]. We speculate that the peak of GnRH mRNA in morning of proestrus might be due to the rise in

circulating estradiol in this phase of the estrous cycle. The subcutaneous implantation of estradiol-containing silastic tubing in the ovariectomized rats have been shown to increase hypothalamic GnRH mRNA levels [189]. We have observed a significant decrease both in the percentage of MnPO GnRH neurons contacted by ARC CART fibers and intensity of MnPO GnRH neurons in estrus rats compared to those in other phases of the estrous cycle. Estradiol levels remained lowest during estrus compared to proestrus, metestrus, and diestrus [124] and this might be a reason of reduced CART axons contacts on GnRH neurons during estrus. Moreover, reduced GnRH immunoreactivity has been reported in the morning of estrus suggesting a prior depletion [5]. The major molecular component of transient outward A-type currents [I(A)] in MPOA GnRH neurons are Kv4.3 channels, and its expression showed reduction during estrus phase compared to diestrus/proestrus phases in rats [190]. In addition, GnRH also seems to regulate its own activity. For example, an increase in GnRH mRNA levels was observed in response to GnRH hypersecretion during LH surge [188] and a predominant excitatory influence on GnRH neurons caused by GnRH in adult male and female mice has also been demonstrated [191]. The mean firing rate of fluorescently tagged GnRH neurons in brain slices from proestrous mice was higher compared to that from diestrous mice [192].

CHAPTER 2

TRANSIENT RECEPTOR POTENTIAL VANILLOID 1-6 (TRPV1-6) GENE EXPRESSION IN THE MOUSE BRAIN DURING ESTROUS CYCLE

S. Kumar, O. Singh, U. Singh, and P.S. Singru. Transient receptor potential vanilloid 1-6 (TRPV1-6) gene expression in the mouse brain during estrous cycle (under review).

INTRODUCTION

The transient receptor potential (TRP) ion channels are integral membrane proteins, serve as cationic channels, and play a role in cellular functions [193]. These ion channels are polymodal in nature and gated by voltage, temperature, osmolality, vanilloids, and phospholipids [194], and regulate cellular signalling and a range of physiological processes [195–197]. While the TRP ion channels have been suggested as putative targets of steroids [198], analysis of the human, mouse, and rat genomes suggests the presence of steroid response elements in the promoter regions of TRP genes [34,199,200]. Among TRP superfamily, the importance of TRPV subfamily of ion channels in the neural and neuroendocrine regulation has been explored [159,201–203]. The interaction between TRPV and steroid hormone appears to be a crucial regulator of the activity of these ions channels in brain and peripheral tissues. While estrogen and its precursors have been suggested to bind with the same hydrophobic pocket of TRPV1, 17 β -estradiol activate this ion channel [204]. In the absence of estrogen TRPV1 does not contribute to the normal mechanosensation in the cervix [205]. In addition to TRPV1, other members of TRPV subfamily have also been shown to be regulated by estradiol. Weber et al. [34] have demonstrated the presence of a putative estrogen response element in the promoter sequence of TRPV6 gene. Estrogen upregulate expression of TRPV5 in the kidney and TRPV6 in duodenal tissue [140,141]. Changes in expression of uterine TRPV6 mRNA were studied during estrous cycle and pregnancy in mice [206]. While the increase in TRPV6 mRNA expression was observed in estrus, its expression during pregnancy showed two peaks, mid pregnancy and the other at birth [206]. In immature mice, estradiol but not progesterone treatment induced TRPV6 mRNA expression in the uterus [206]. Estradiol upregulate expression of renal TRPV5 [140,207], duodenal TRPV5 and TRPV6 [141], and endometrial TRPV6 [208] expression. TRPV6 mediated Ca²⁺ entry/signalling in T84 colonic cells is 17 β -estradiol sensitive [209].

The effect of estradiol on TRPV5 and TRPV6 appears to be mediated *via* estrogen receptors [210]. Reduction in intestinal TRPV6 mRNA expression was observed in the ER α knockout but not in the ER β knockout mice [211]. Estradiol seem to interact with TRPV6 *via* estrogen receptors since TRPV6 mRNA expression in the uterus and placenta of mice was reduced by treatment with estrogen receptor antagonist [212].

Evidences show wide organization of TRPV1-6-expressing elements in the brain [33,159,201–203,213–216]. The sensory neurons, and neurons as well as glial cells in the brain are equipped with different TRPV ion channels [33,159,201–203,213,215–217]. The TRPV-steroid hormone interaction has also been observed in the sensory neurons [218] and brain [159,201], and the ion channel expression is modulated by estradiol. Estrogen receptors are widely expressed in the brain [219–222] and the estrogen receptor activity in mouse brain is influenced by estrous cycle [223]. While TRPV1 expression in the amygdala, prefrontal cortex, and thalamus is estradiol independent, hippocampal TRPV1 expression is regulated by estradiol [224]. The TRPV6-expressing neurons in the hypothalamic arcuate nucleus in mice co-express ER α [201], and the expression of TRPV5/TRPV6 in the hypothalamus showed estrous cycle-dependent changes [159,201]. In addition to CNS, 17 β -estradiol also interacts with TRPV ion channels in the sensory neurons. While the hormone enhances the currents and TRPV1 expression in dorsal root ganglia (DRG) neurons [225], TRPV1 expression in these neurons was inhibited by non-classical estrogen-signalling pathway [226]. Estradiol *via* estrogen receptors increases the expression of TRPV1 in uterine cervical afferent as well as DRG neurons [227].

In this background, the present study was aimed at finding out whether TRPV1-6 ion channels serve as direct targets of estradiol and changes in circulating levels of estradiol during estrous cycle modulates their gene expression in the brain. Champion ChiP Transcription Factor Search Portal and Dragon ERE Finder v 3.0 [228] are well established

bioinformatic tools to identify the putative estrogen binding sites in the genes [229]. Using these tools, we have determined if the promoter regions of TRPV1-6 genes contain estrogen response elements (ERE). Next, we have studied whether the TRPV1-6 mRNA expression in the brain of mice show correlation with estrous cycle. Different brain regions, known to express estrogen receptors, were isolated from the mice during each stage of estrous cycle and processed for qRT-PCR analysis using TRPV1-6 specific primers. We have also explored the relative expression of TRPV1-6 mRNA in different brain regions of male mice.

MATERIALS AND METHODS

Animals

Adult, female and male BALB/c mice [25-30 g body weight (BW)] were housed under standard temperature and humidity of the animal house facility at NISER, Bhubaneswar, India and given *ad libitum* food and water. All the experimental procedures employed in this study were approved by the Institutional Animal Ethical Committee (IAEC), NISER, Bhubaneswar, under the Committee for the Purpose of Control and Supervision of Experiments for Animals (CPCSEA), New Delhi, India.

Assessment of the estrous cycle

Estrous cycle in mice was assessed as previously described [201,230]. In brief, the vaginal smears were collected on slides and observed under light microscope. The cell types present in the vaginal smears during the four different stages of the cycle were identified (Proestrus: nucleated epithelial cells; Estrus: cornified cells; Metestrus: mixture of leukocytes, nucleated epithelial and cornified cells; Diestrus: predominant leukocytes in diestrus). Based on the cell types present in the smear, the mice in each stage of the estrous cycle were identified.

Tissue collection for quantitative real-time polymerase chain reaction (qRT-PCR)

Mice showing regular estrous cycle were used in further experiments. Three mice per stage of the estrous cycle, and three male mice were anesthetized with an intraperitoneal (i.p.) injection of a mixture containing ketamine (Neon Laboratories Ltd., Mumbai, India; 80 mg/kg BW) and xylazine (Stanex Drugs and Chemicals Pvt. Ltd., Hyderabad, India; 10 mg/kg BW). The brains were isolated, frozen on dry-ice. Using a sterile stainless steel

blade, the olfactory bulb, cortex, hypothalamus, hippocampus, brainstem and cerebellum were isolated and stored at - 80 °C.

Total RNA isolation and qRT-PCR

The tissues were homogenized in 1 ml QIAzol lysis reagent using TissueLyser (Qiagen) at 50 Hz for 2 mins. Total RNA were isolated from each brain region of each animal using RNeasy Lipid Tissue Mini Kit (Qiagen). The RNA was quantified in NanoDrop 2000 Spectrophotometer (Thermo Scientific). One µg of the total RNA from each tissue were reverse transcribed into cDNA using QuantiTect Reverse Transcription Kit (Qiagen). qRT-PCR was performed as described earlier [159]. Briefly, 2 µl of the cDNA from each brain regions were amplified in 7500 Real Time PCR System (Applied Biosystems) using KAPA SYBR Fast qPCR master mix (2X) (KAPA Biosystems) along with the TRPV primers. The details of primers used for relative quantification of TRPV1-6 in the mouse brain are given in Table 1. The specificity of the primers and amplification of single correct sized fragment was confirmed by running the amplified amplicons along with 100 bp DNA ladder (Gene Ruler, Cat. # SM0243, Thermo Scientific) on 1 % agarose gel. The DNA was eluted using QIAquick gel extraction kit (Cat. # 28704, Qiagen) and sequenced at DNA sequencing facility (Institute of Life Sciences, Bhubaneswar, India). The relative expressions of TRPV1-6 mRNA were normalized by HPRT mRNA (endogenous control) and represented as relative C_T values (C_T of TRPV/ C_T of HPRT), as previously described [231].

Table 1: Quantitative real-time PCR primer sequences for mouse TRPVs (target genes) and HPRT (endogenous control gene).

Target gene	Primer	Primer sequence (5'--->3')	Amplicon length (bp)
TRPV1	F	CAAACCTCCACCCCACACTGA	101
	R	AGGCCAAGACCCCAATCTTC	
TRPV2	F	GTTTGACCGTGACCGACTCT	123
	R	GAGCCTTCTGTGTATGCCGA	
TRPV3	F	GCCCCTCATGGGCAAAGAA	100
	R	GTGTGCACTCTTCTTGGTGGG	
TRPV4	F	ACTGGAACCAGAACTTGGGC	111
	R	AGGACCAACGATCCCTACGAA	
TRPV5	F	CTTACGGGTTGAACACCACCA	163
	R	TTGCAGAACCACAGAGCCTCTA	
TRPV6	F	GGGGTTAATACTCTGCCTATGG	191
	R	GCACCTCACATCCTTCAAACCT	
HPRT	F	TTATCAGACTGAAGAGCTACTGTAATGATC	127
	R	TTACCAGTGTC AATTATATCTTCAACAATC	

Bioinformatics analysis of TRPV1-6 genes for putative estrogen response elements

The promoter sequences of mouse TRPV1-6 genes from -3000 to +1000 bp relative to transcription start site (TSS) were obtained using EPDnew Mouse version 002 [232]. These promoter sequences were further analyzed for putative estrogen response element (ERE) patterns at the sensitivity of 87% using Dragon ERE Finder version 3.0 [228].

The promoter sequences of mouse TRPV1-6 genes were further analyzed using Champion ChiP Transcription Factor Search Portal for ER α binding site. The Champion ChiP Transcription Factor Search Portal is based on SABiosciences' proprietary database known as DECipherment Of DNA Elements (DECODE).

Statistical analysis

Three biological replicates per group were used. Each biological replicate was further tested thrice ($n = 3$, three technical replicates) to obtain C_T value. Any outlier in technical replicates was omitted by the 7500 Real Time PCR System software (Applied Biosystems). Expression of TRPV1-6 genes in different regions of the brain is represented as mean C_T value (mean of technical replicates). Two close mean C_T values for each TRPV gene/brain region/group ($N = 2$, two biological replicates) were analysed using GraphPad Prism (GraphPad Software Inc., USA) using Two-way ANOVA followed by Tukey's multiple comparison test. $P < 0.05$ was considered statistically significant.

RESULTS

TRPV1-6 mRNA expression in the mouse brain

Using qRT-PCR, a single band of appropriate sized amplicon for HPRT as well as each member of the TRPV subfamily viz. TRPV1, TRPV2, TRPV3, TRPV4, TRPV5 and TRPV6, was observed in different compartments (olfactory bulb, cortex, hypothalamus, hippocampus, brainstem, and cerebellum) of the male mouse brain (Fig. 1). Sequencing of TRPV1-6 amplicons followed by *Mus musculus* Nucleotide BLAST analysis confirmed the amplification of correct gene using respective set of primers (sequencing data not shown).

Putative functional ERE patterns in the promoter region of mouse TRPV1-6 genes

Analysis of the promoter sequences of mouse TRPV1-6 genes using Champion ChiP Transcription Factor Search Portal detected ER α binding sites in the promoter regions of TRPV1, TRPV3, TRPV5 and TRPV6 genes (Table 2). While no ER α binding sites were detected in the promoter regions of TRPV2 and TRPV4 genes using Champion ChiP Transcription Factor Search Portal, screening with the Dragon ERE Finder 3.0 showed the presence of putative functional ERE patterns in the promoter regions of TRPV1-6 genes (Table 3).

TRPV1-6 mRNA levels in the mouse brain during estrous cycle

The TRPV1-6 mRNA expression in the brain during different stages of the estrous cycle in mice is shown in Figures 2-9. The expression of each ion channel in different regions of the mice brain (olfactory bulb, cortex, hypothalamus, hippocampus, brainstem, and

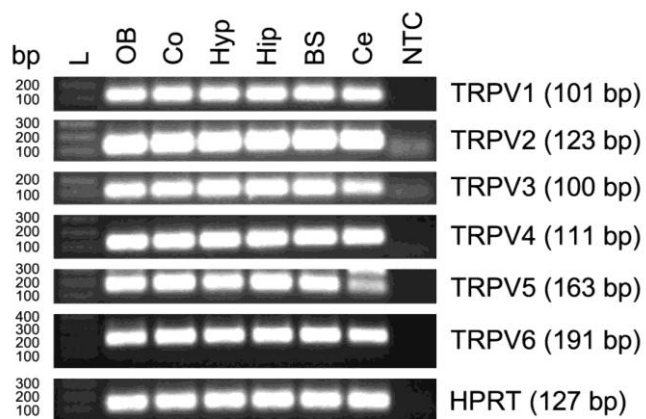


Figure 1: TRPV1-6 mRNA expression in the mouse brain. The bands represent the qRT-PCR products. L, DNA ladder; OB, olfactory bulb; Co, cortex; Hyp, hypothalamus; Hip, hippocampus; BS, brainstem; Ce, cerebellum; NTC, no template control; bp, basepair.

Table 2: ER- α binding sites in the promoter region of mouse TRPV1-6 genes analysed using Champion ChiP Transcription Factor Search Portal. The Champion ChiP Transcription Factor Search Portal is based on SABiosciences' proprietary database known as DECODE (DECipherment Of DNA Elements).

Gene	Binding Position	Strand	Binding Sequence
TRPV1	chr11: 73036440-73036458	+	CCTGGGCCCATGTGACCCGG
TRPV2	no binding site		
TRPV3	chr11: 73068349-73068367	+	CAAGCGCACCCCTGAGCTTC
TRPV4	no binding site		
TRPV5	chr6: 41625403-41625421	+	GCAGTGCAGTCTGACCTGG
TRPV6	chr6: 41576999-41577017	+	GTAGTGCAGTCTGACCTGG

Table 3: Putative functional estrogen response element (ERE) patterns in the promoter region of mouse TRPV1-6 genes analysed using Dragon ERE Finder version 3.0. EPDnew Mouse version 002 was used to get promoter sequence from -3000 to +1000 bp relative to TSS. These promoters were further analysed for putative ERE patterns.

Gene	Promoter ID	Expected ERE sensitivity: 87 %	
		Strand	ERE Pattern
TRPV1	FP013256 Trpv1_1 :+U EU:NC; range -3000 to 1000	+	AA-GGGCA-GCC-CAGCC-TC
TRPV2	FP013052 Trpv2_1 :+U EU:NC; range -3000 to 1000 FP013053 Trpv2_2 :+U EU:NC; range -3000 to 1000	+	No ERE pattern GT-GGTCC-TGA-TGATC-AG
TRPV3	FP013257 Trpv3_1 :+U EU:NC; range -3000 to 1000	+	GT-GGTGG-GTG-TGGCC-TG
		-	CT-GATCA-CTA-CAACC-TG
TRPV4	FP006010 Trpv4_1 :+U EU:NC; range -3000 to 1000	+	AA-GAACA-AGT-CAGCC-TC
		+	CG-GGTGG-GCG-GGACC-CC
		-	TG-GGTGG-CCG-TGGTC-TC
TRPV5	FP006756 Trpv5_1 :+U EU:NC; range -3000 to 1000	+	CA-AGTCT-GTC-TGACT-CA
TRPV6	FP006755 Trpv6_1 :+U EU:NC; range -3000 to 1000	+	CA-GGGCT-GTA-TGGCC-TG
		+	TA-GCACA-GGC-TGCCC-TC
		-	CC-AGTCC-CCC-TAGCC-TG

cerebellum), and the changes in their mRNA levels in each of these brain regions are described below.

TRPV1

Compared to metestrus and diestrus phases, significantly lower level of TRPV1 mRNA expression was observed in the olfactory bulb (Fig. 2A), cortex (Fig. 2B), hypothalamus (Fig. 2C), hippocampus (Fig. 3A), brainstem (Fig. 3B), and cerebellum (Fig. 3C) during proestrus (Figs. 4A, 5A). Except in the hypothalamus (Fig. 2C) and olfactory bulb (Fig. 2A), similar changes in TRPV1 mRNA expression levels were also observed in other brain regions of mice in estrus compared to those in metestrus and diestrus (Figs. 2B, 3A-C, 4A, 5A). In the olfactory bulb (Fig. 2A) and hypothalamus (Fig. 2C), significantly lower levels of TRPV1 mRNA were detected during proestrus as compared to that in estrus (Figs. 4A, 5A).

TRPV2

Compared to estrus, metestrus, and diestrus phases, significantly higher level of TRPV2 mRNA was observed in the olfactory bulb (Fig. 2D), cortex (Fig. 2E), hypothalamus (Fig. 2F), hippocampus (Fig. 3D), brainstem (Fig. 3E), and cerebellum (Fig. 3F) during proestrus phase (Figs. 4B, 5B). In the cerebellum (Fig. 3F), compared to estrus phase, a significant decrease in TRPV2 mRNA levels was observed during diestrus phase (Figs. 4B, 5B).

TRPV3

Compared to metestrus, significant decrease in TRPV3 mRNA level was observed in the cortex (Fig. 2H), hypothalamus (Fig. 2I), brainstem (Fig. 3H), and cerebellum (Fig. 3I)

during estrus (Figs. 4C, 5C). Higher TRPV3 mRNA expression was seen in the hypothalamus (Fig. 2I) and hippocampus (Fig. 3G) during diestrus compared to estrus (Figs. 4C, 5C). During proestrus, the TRPV3 mRNA level in all the brain regions was comparable ($P>0.05$) to that observed during estrus, metestrus, and diestrus phases.

TRPV4

Compared to estrus, higher TRPV4 mRNA level was detected in the olfactory bulb (Fig. 2J), cortex (Fig. 2K), hypothalamus (Fig. 2L), and brainstem (Fig. 3K) of mice in proestrus (Figs. 4D, 5D). Compared to metestrus and diestrus phases, significantly higher expression of TRPV4 mRNA was observed in the hypothalamic tissue (Fig. 2L) of mice in proestrus (Figs. 4D, 5D). Significantly higher expression of TRPV4 was detected in the hippocampus (Fig. 3J) of mice in proestrus as compared to that in diestrus phase (Figs. 4D, 5D).

TRPV5

TRPV5 mRNA levels in the olfactory bulb (Fig. 2M), cortex (Fig. 2N), and brainstem (Fig. 3N) were significantly reduced during proestrus compared to estrus, metestrus, and diestrus phases (Figs. 4E, 5E). A significant decrease in TRPV5 mRNA expression was observed in the hypothalamus (Fig. 2O), hippocampus (Fig. 3M) and cerebellum (Fig. 3O) of mice in proestrus and estrus compared to that in the metestrus and diestrus phases (Figs. 4E, 5E).

TRPV6

Compared to estrus, metestrus, and diestrus phases, significantly higher TRPV6 mRNA level was detected in the olfactory bulb (Fig. 2P), cortex (Fig. 2Q), hypothalamus

(Fig. 2R), hippocampus (Fig. 3P), brainstem (Fig. 3Q), and cerebellum (Fig. 3R) of mice in proestrus (Figs. 4F, 5F).

Estrous cycle-related changes in TRPV1-6 mRNA expression in the olfactory bulb

The changes in TRPV1-6 mRNA expression in the olfactory bulb during estrus cycle are shown in Figures 6A-D, 8A, and 9A. In the olfactory bulb, a significant increase in TRPV1 mRNA levels was observed in the estrus compared to the proestrus phase. TRPV1 mRNA level in the olfactory bulb of mice in the estrus, metestrus, and diestrus phases was comparable. Similar to TRPV1, the expression of TRPV5 mRNA in the olfactory bulbs during estrous cycle also showed similar pattern. TRPV2 mRNA was abundantly expressed in the olfactory bulbs of mice in proestrus but reduced levels were seen in the tissues collected during estrus, metestrus, and diestrus phases. During proestrus, abundant TRPV2 and least TRPV5 mRNA expression were observed in the olfactory bulb. TRPV1 mRNA was significantly lower than TRPV2-4 and TRPV6 mRNAs, TRPV2 mRNA was significantly higher than TRPV3-6, TRPV3 mRNA significantly lower than TRPV4 and significantly higher than TRPV5, TRPV5 mRNA was significantly lower than TRPV4 and TRPV6 in olfactory bulbs during proestrus. During estrus TRPV6 mRNA level was significantly lower than the mRNA levels of TRPV1 and TRPV5. The TRPV2 mRNA level was significantly higher than TRPV3-6 mRNA levels. The TRPV6 mRNA level was also significantly reduced compared to those of TRPV1-5 during metestrus and TRPV1-3 and TRPV5 during diestrus.

Estrous cycle-related changes in TRPV1-6 mRNA expression in the cortex

The changes in TRPV1-6 mRNA expression in the cortex during estrus cycle are shown in Figures 6F-I, 8B, and 9B. During proestrus, highest level of TRPV2 and lowest

level of TRPV1 mRNA were detected in the cortex. Compared to TRPV2-4 and TRPV6, significantly lower level of TRPV1 mRNA was observed in the cortex during proestrus. Cortical TRPV1 and TRPV5 mRNA levels were comparable during proestrus. In the cortex of mice during proestrus, compared to the TRPV1 and TRPV3-6 mRNA levels, significantly higher TRPV2 mRNA level was observed. TRPV3 mRNA level detected in the cortex of mice in proestrus was significantly lower than TRPV4 and TRPV6, but higher than TRPV5 mRNA level. TRPV5 mRNA levels were significantly lower than TRPV4 and TRPV6 in cortex of proestrus mice. During estrus, as compared to other TRPV mRNA, significantly higher level of TRPV2 mRNA levels was detected in cortex. During metestrus and diestrus, as compared to TRPV4 and TRPV6, higher level of TRPV2 mRNA was observed in the cortex. The TRPV5 mRNA level was significantly higher than TRPV6 in the cortex of mice in metestrus.

Estrous cycle-related changes in TRPV1-6 mRNA expression in the hypothalamus

The changes in TRPV1-6 mRNA expression in the hypothalamus during estrus cycle are shown in Figures 6K-N, 8C, and 9C. Highest level of TRPV2 and lowest TRPV5 mRNA levels were observed in the hypothalamus of mice during proestrus. During this phase of estrous cycle, compared to levels of TRPV2, TRPV4, and TRPV6 mRNA, significantly lower level of TRPV1 mRNA was detected in the hypothalamus. While TRPV2 mRNA level was significantly higher than TRPV3-6, the TRPV3 level was lower than TRPV4 but higher than TRPV5. The TRPV5 mRNA level was significantly lower than those of TRPV4 and TRPV6. During estrus, TRPV1 level was significantly higher than TRPV3, TRPV5, and TRPV6; TRPV2 levels were significantly higher than TRPV3-6, and TRPV4 levels were significantly higher than TRPV6. The TRPV6 mRNA level was significantly lower than TRPV1-5 during metestrus and diestrus.

Estrous cycle-related changes in TRPV1-6 mRNA expression in the hippocampus

The changes in TRPV1-6 mRNA expression in the hippocampus during estrous cycle are shown in Figures 7A-D, 8D, and 9D. Hippocampal levels of TRPV2 mRNA level was highest and that of TRPV5 lowest during proestrus. During this phase, the TRPV1 mRNA level was significantly lower than TRPV2-4 and TRPV6. The TRPV2 mRNA level was significantly higher than TRPV3-6. The TRPV3 mRNA level was significantly lower than those of TRPV4 and TRPV6, and significantly higher than that of TRPV5. The TRPV5 mRNA level was significantly lower than the mRNA levels of TRPV4 and TRPV6. During estrus, TRPV1 mRNA level was significantly lower than those of TRPV2 and TRPV4. The TRPV2 mRNA level was significantly higher than the levels of TRPV3, TRPV5, and TRPV6 mRNA. Compared to TRPV3, TRPV5, and TRPV6, higher level of TRPV4 mRNA was observed. During metestrus, TRPV6 level was significantly lower than the mRNA levels of other TRPV ion channels. The hippocampal TRPV6 mRNA level was significantly lower than TRPV1-3 during diestrus.

Estrous cycle-related changes in TRPV1-6 mRNA expression in the brainstem

The changes in TRPV1-6 mRNA expression in the brainstem during estrus cycle are shown in Figures 7F-I, 8E, and 9E. During proestrus, highest TRPV2 and lowest TRPV5 mRNA levels were observed in the brainstem. While the TRPV1 levels were significantly lower than TRPV2, TRPV4, and TRPV6, the TRPV2 mRNA level was significantly higher than those of TRPV3-6. Compared to TRPV4 and TRPV6, lower level of TRPV3 mRNA was observed. The TRPV3 mRNA levels were higher than that of TRPV5. Compared to TRPV4 and TRPV6 mRNA levels, significantly lower level of TRPV5 mRNA was observed. During estrus, the TRPV2 mRNA level was significantly higher than those of TRPV1, TRPV3, TRPV5, and TRPV6; and TRPV6 mRNA level was significantly lower than that of

TRPV4. The brainstem TRPV6 mRNA level was significantly lower than TRPV1-5 mRNA levels during metestrus and diestrus phases.

Estrous cycle-related changes in TRPV1-6 mRNA expression in the cerebellum

The changes in TRPV1-6 mRNA expression in the cerebellum during estrus cycle are shown in Figures 7K-N, 8F, and 9F. During proestrus, while TRPV2 was highly expressed, lowest level of TRPV5 mRNA was seen in the cerebellum. The TRPV1 mRNA level was significantly lower than those of TRPV2, TRPV4, and TRPV6. The TRPV2 mRNA level was significantly higher than those of TRPV3-6. The TRPV3 mRNA level was significantly lower than those of TRPV4 and TRPV6, but significantly higher than that of TRPV5. The TRPV5 mRNA level was significantly lower than those of TRPV4 and TRPV6. During estrus, the TRPV1 mRNA was significantly lower than TRPV2 and TRPV4. The TRPV2 expression was significantly higher than those of TRPV3-6. The expression of TRPV4 was significantly higher than those of TRPV3, TRPV5, and TRPV6. During metestrus, the TRPV2 mRNA levels were significantly higher than those of TRPV3, TRPV4, and TRPV6; and TRPV6 mRNA levels were significantly lower than those of TRPV1 and TRPV3-5. During diestrus, compared to the mRNA levels of TRPV1, TRPV2, TRPV4 and TRPV5, significantly lower level of TRPV6 mRNA was observed in the cerebellum. During this stage, compared to the TRPV3, the TRPV2 mRNA levels remained significantly elevated.

TRPV1-6 mRNA levels in different regions of the brain of male mice

TRPV1-6 mRNA levels in the olfactory bulb, cortex, hypothalamus, hippocampus, brainstem, and cerebellum of male mice are shown in Figures 2-9. A comparable level of TRPV1-6 mRNA was observed in the olfactory bulbs of male mice (Figs. 6E, 8A, 9A).

TRPV2 mRNA level was significantly higher as compared to TRPV5 and TRPV6 in the cortex of male mice (Figs. 6J, 8B, 9B). In the hypothalamus, the TRPV6 mRNA level was significantly lower than TRPV2, TRPV3, and TRPV4 whereas the TRPV5 mRNA level was significantly lower than TRPV2 (Figs. 6O, 8C, 9C). In the hippocampus, while the TRPV4 mRNA level was significantly higher than TRPV1, the TRPV5 level was significantly lower than TRPV2 and TRPV4 (Figs. 7E, 8D, 9D). In the brainstem, compared to TRPV2, significantly lower level of the TRPV5 mRNA was observed (Figs. 7J, 8E, 9E). Cerebellar TRPV6 mRNA level was significantly lower than TRPV1-4 whereas TRPV5 level was significantly lower than TRPV2 (Figs. 7O, 8F, 9F). Except hippocampal TRPV4 mRNA (Figs. 3J, 4D, 5D) and the TRPV6 expression in the olfactory bulb (Figs. 2P, 4F, 5F), hippocampus (Figs. 3P, 4F, 5F) and brainstem (Figs. 3Q, 4F, 5F), the mRNA levels of TRPV in various brain compartments of male mice were comparable to that of female mice during metestrus and diestrus (Figs. 2-9).

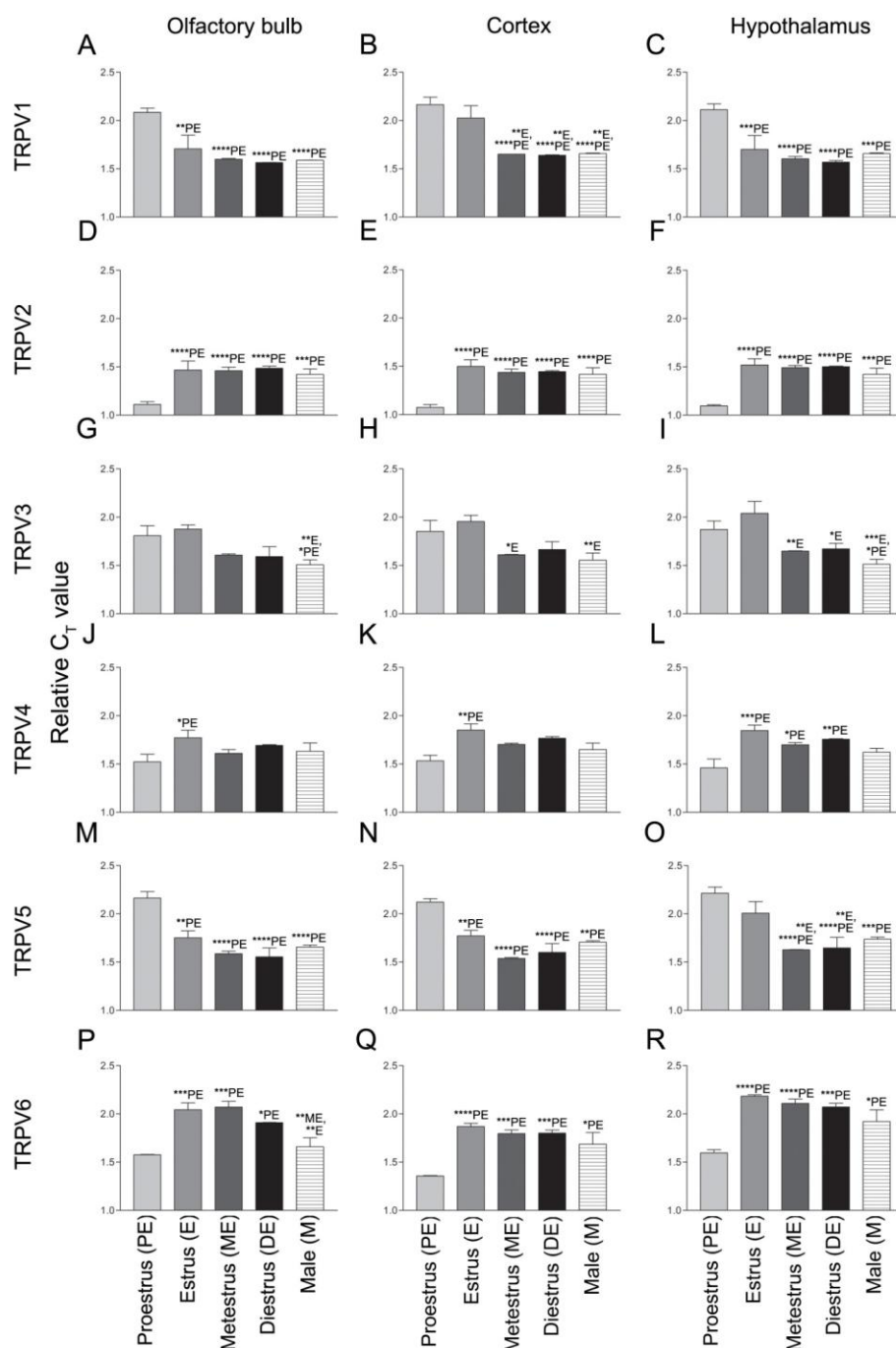


Figure 2: Estrous cycle-related changes in TRPV1-6 mRNA expression in the olfactory bulb, cortex, and hypothalamus of mice. Changes in TRPV1 (A-C), TRPV2 (D-F), TRPV3 (G-I), TRPV4 (J-L), TRPV5 (M-O), and TRPV6 (P-R) mRNA levels in the olfactory bulb (A, D, G, J, M, P), cortex (B, E, H, K, N, Q), and hypothalamus (C, F, I, L, O, R) of mice during proestrus, estrus, metestrus, and diestrus stages of the estrous cycle, and in male mice. The relative C_T values are represented as mean \pm SD. The statistical comparison is represented above each bar [* , P<0.05; ** , P<0.01; *** , P<0.001; **** , P<0.0001 compared to the proestrus (PE), estrus (E), metestrus (ME), diestrus (DE) or male mice (M)]

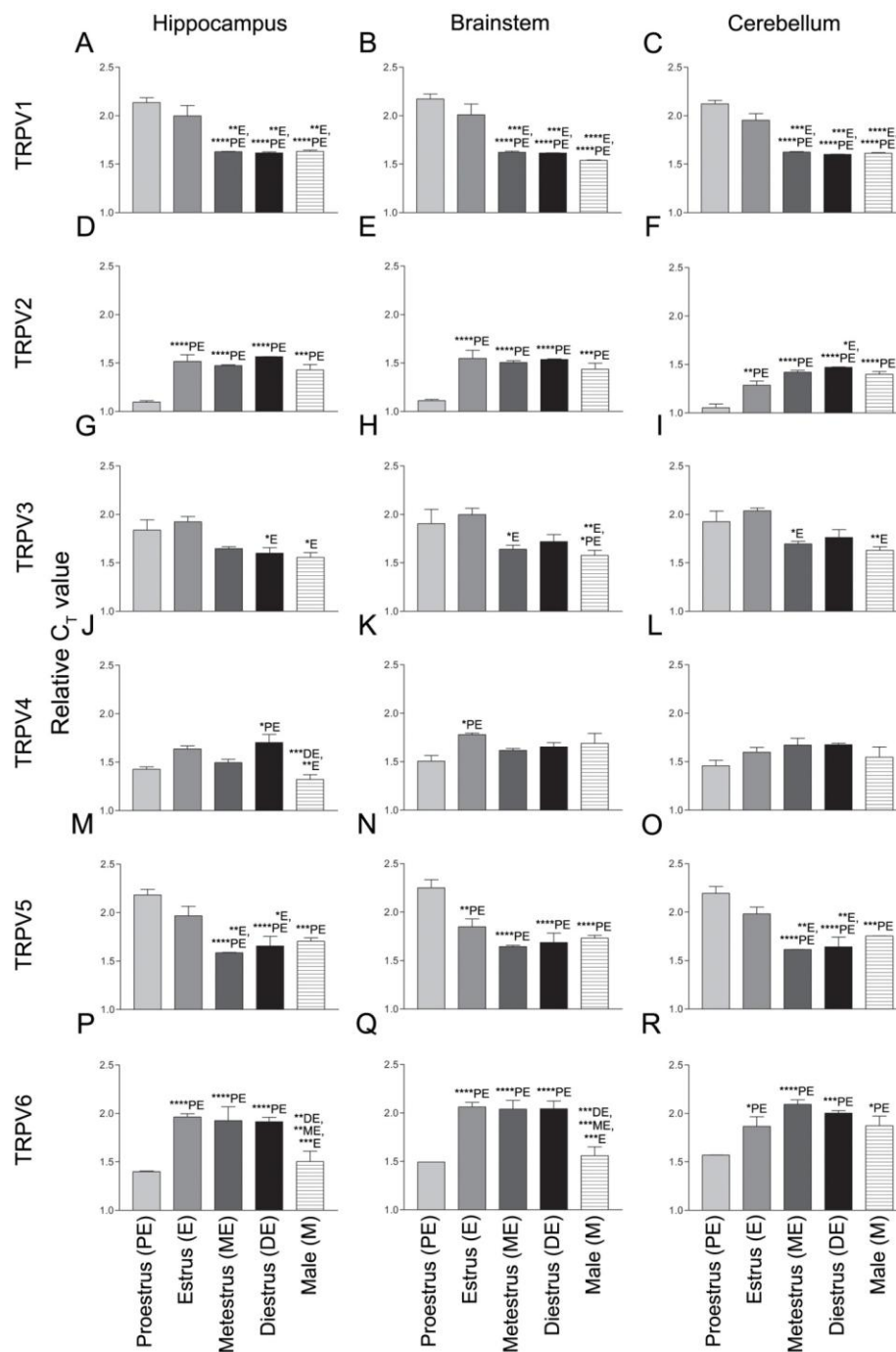


Figure 3: Estrous cycle-related changes in TRPV1-6 mRNA expression in the hippocampus, brainstem, and cerebellum of mice. Changes in TRPV1 (A-C), TRPV2 (D-F), TRPV3 (G-I), TRPV4 (J-L), TRPV5 (M-O), and TRPV6 (P-R) mRNA levels in the hippocampus (A, D, G, J, M, P), brainstem (B, E, H, K, N, Q), and cerebellum (C, F, I, L, O, R) of mice during proestrus, estrus, metestrus, and diestrus stages of the estrous cycle, and in male mice. The relative C_T values are represented as mean \pm SD. The statistical comparison is represented above each bar [* , $P < 0.05$; ** , $P < 0.01$; *** , $P < 0.001$; **** , $P < 0.0001$ compared to the proestrus (PE), estrus (E), metestrus (ME), diestrus (DE) or male mice (M)].

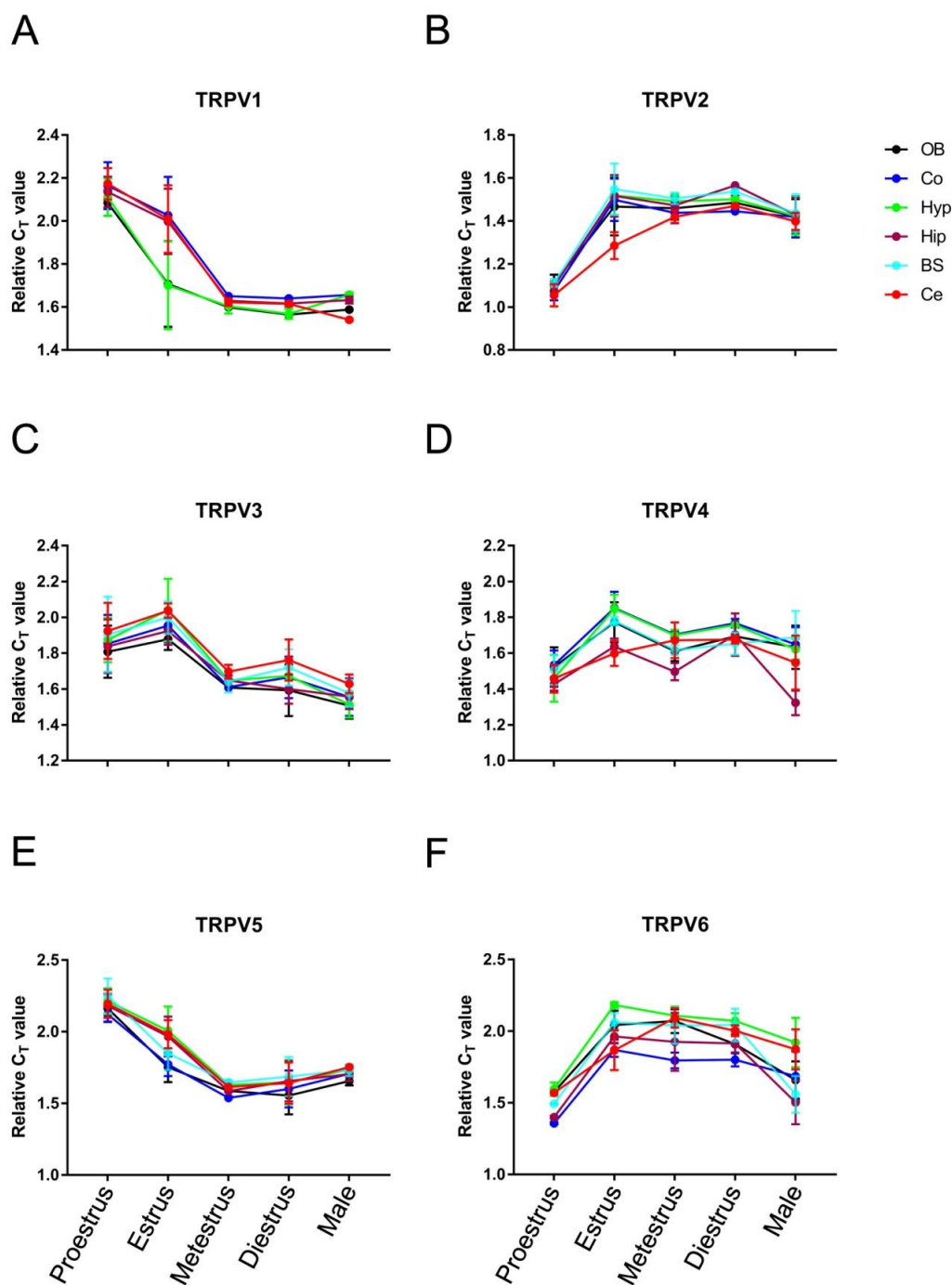


Figure 4: Representation of estrous cycle-related changes in TRPV1-6 mRNA levels in different brain regions of mice. Representation of overall changes in TRPV1 (A), TRPV2 (B), TRPV3 (C), TRPV4 (D), TRPV5 (E), and TRPV6 (F) mRNA levels in the olfactory bulb (OB), cortex (Co), hypothalamus (Hyp), hippocampus (Hip), brainstem (BS), and cerebellum (Ce) of mice during proestrus, estrus, metestrus, and diestrus stages of the estrous cycle, and in male mice. The relative C_T values are represented as mean \pm SD.

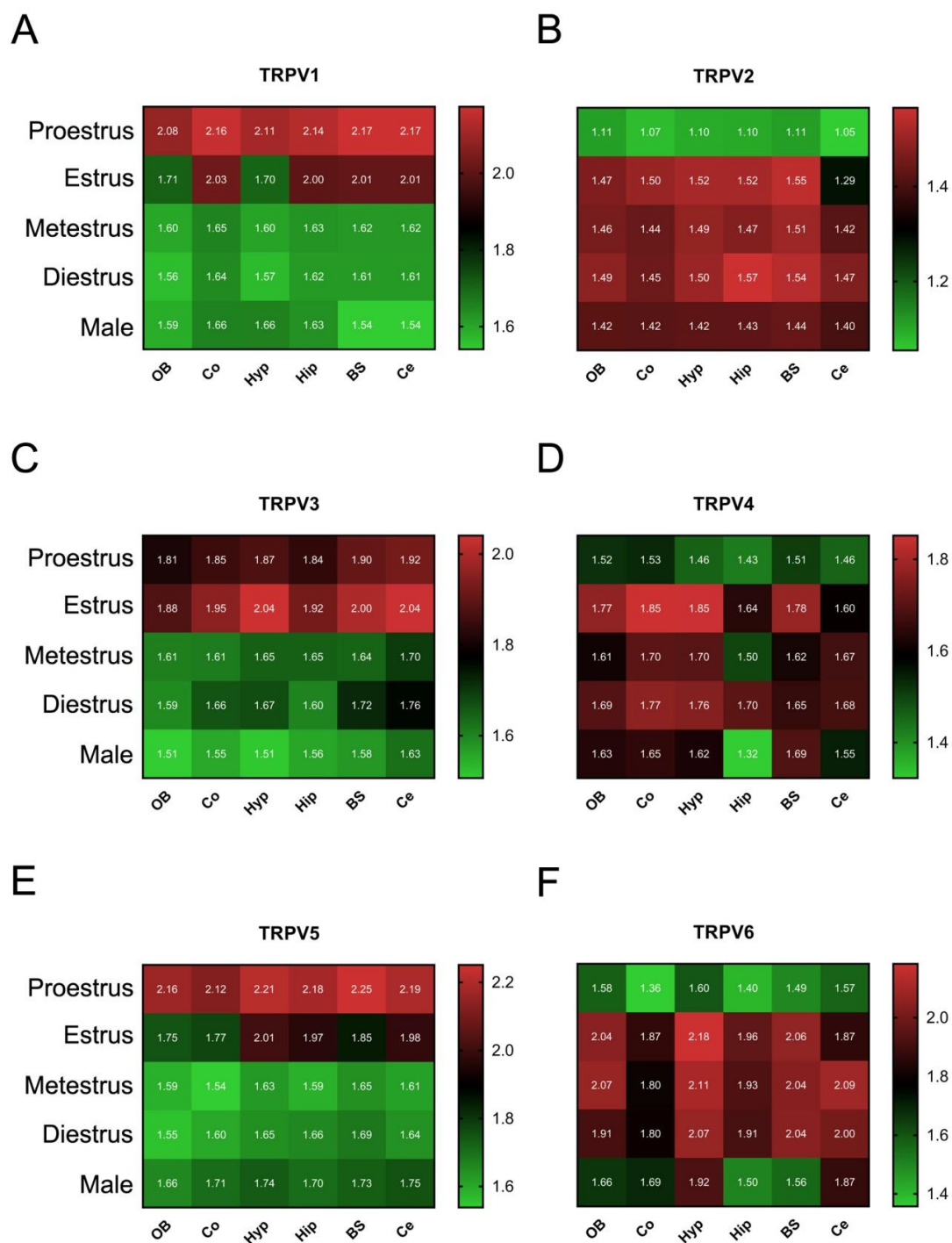


Figure 5: Heat maps showing estrous cycle-related changes in TRPV1-6 mRNA levels in the olfactory bulb, cortex, hypothalamus, hippocampus, brainstem, and cerebellum of mice. Heat maps showing mRNA levels of TRPV1 (A), TRPV2 (B), TRPV3 (C), TRPV4 (D), TRPV5 (E), and TRPV6 (F) in the olfactory bulb (OB), cortex (Co), hypothalamus (Hyp), hippocampus (Hip), brainstem (BS), and cerebellum (Ce) of mice during proestrus, estrus, metestrus, and diestrus stages of the estrous cycle, and in male mice. The relative C_T values are represented as mean.

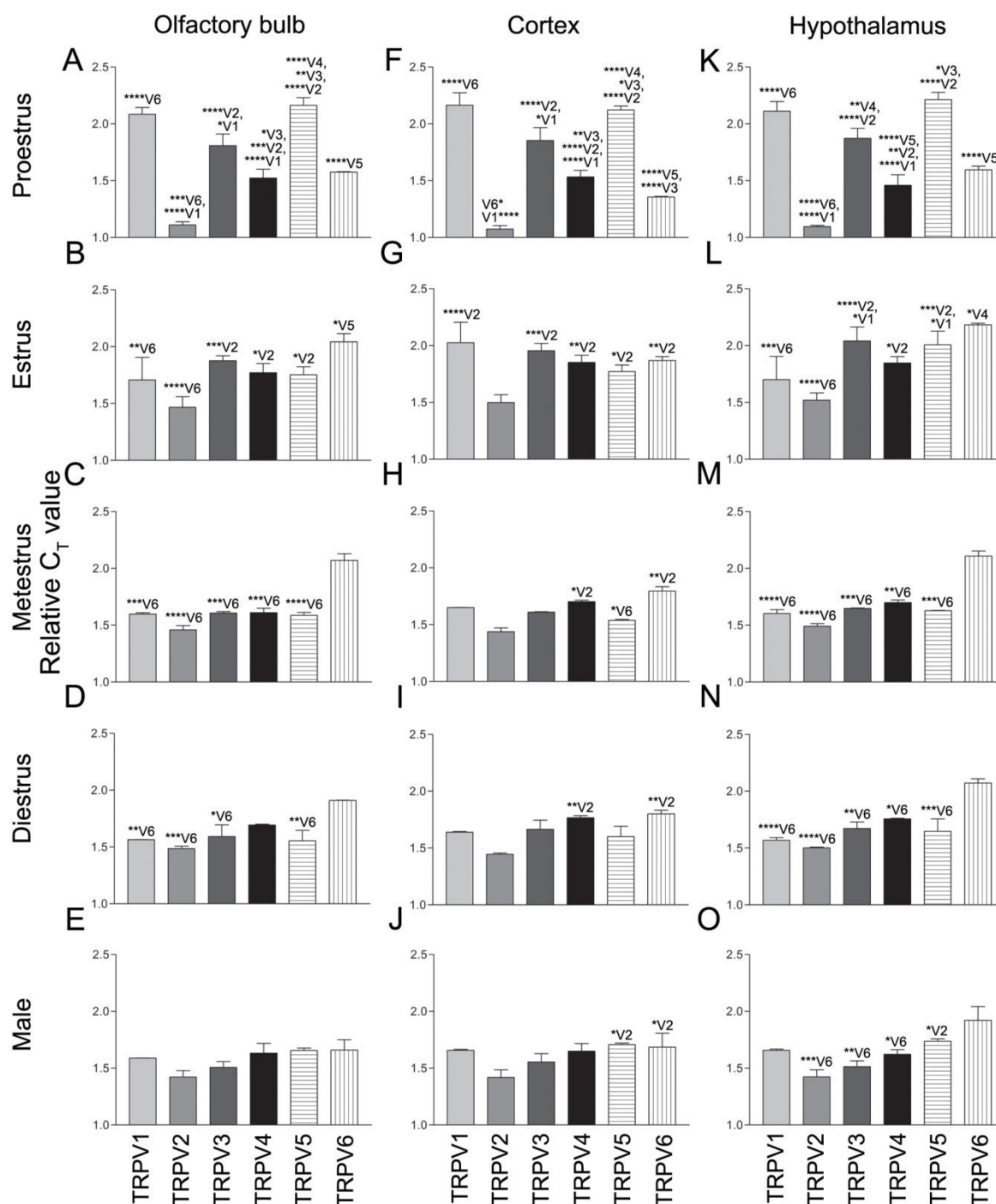


Figure 6: Estrous cycle-related changes in TRPV1-6 mRNA expression in the olfactory bulb, cortex, and hypothalamus of mice. TRPV1-6 mRNA expression in the olfactory bulb (A-E), cortex (F-J), and hypothalamus (K-O) of mice during proestrus (A, F, K), estrus (B, G, L), metestrus (C, H, M), and diestrus (D, I, N) stages of the estrous cycle, and in male mice (E, J, O). The relative C_T values are represented as mean \pm SD. The statistical comparison is represented above each bar [* , P<0.05; ** , P<0.01; *** , P<0.001; **** , P<0.0001 compared to TRPV1-6 (V1-V6)].

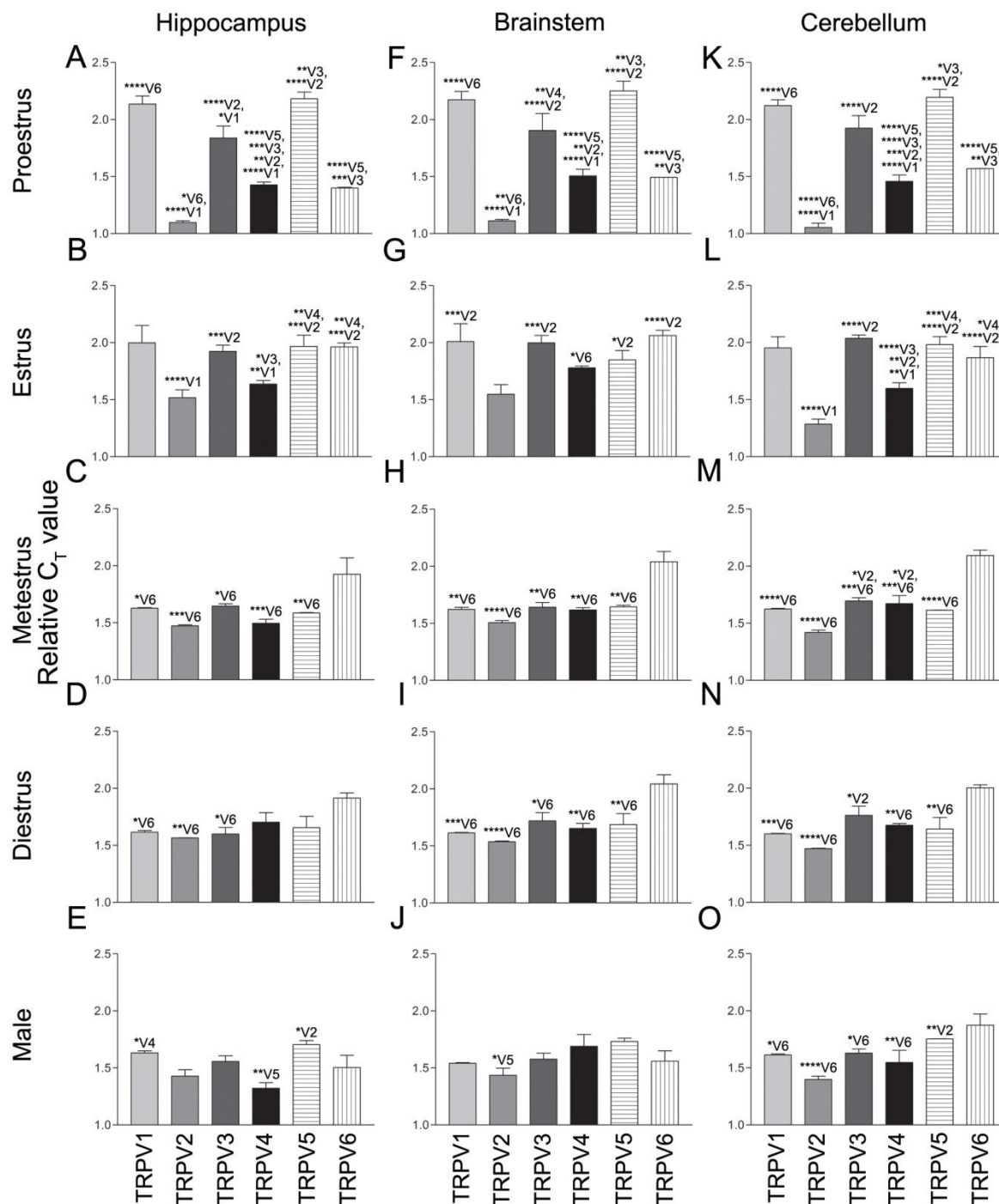


Figure 7: Estrous cycle-related changes in TRPV1-6 mRNA expression in the hippocampus, brainstem, and cerebellum of mice. TRPV1-6 mRNA expression in the hippocampus (A-E), brainstem (F-J), and cerebellum (K-O) of mice during proestrus (A, F, K), estrus (B, G, L), metestrus (C, H, M), and diestrus (D, I, N) stages of the estrous cycle, and in male mice (E, J, O). The relative C_T values are represented as mean \pm SD. The statistical comparison is represented above each bar [* , P<0.05; ** , P<0.01; *** , P<0.001; **** , P<0.0001 compared to TRPV1-6 (V1-V6)].

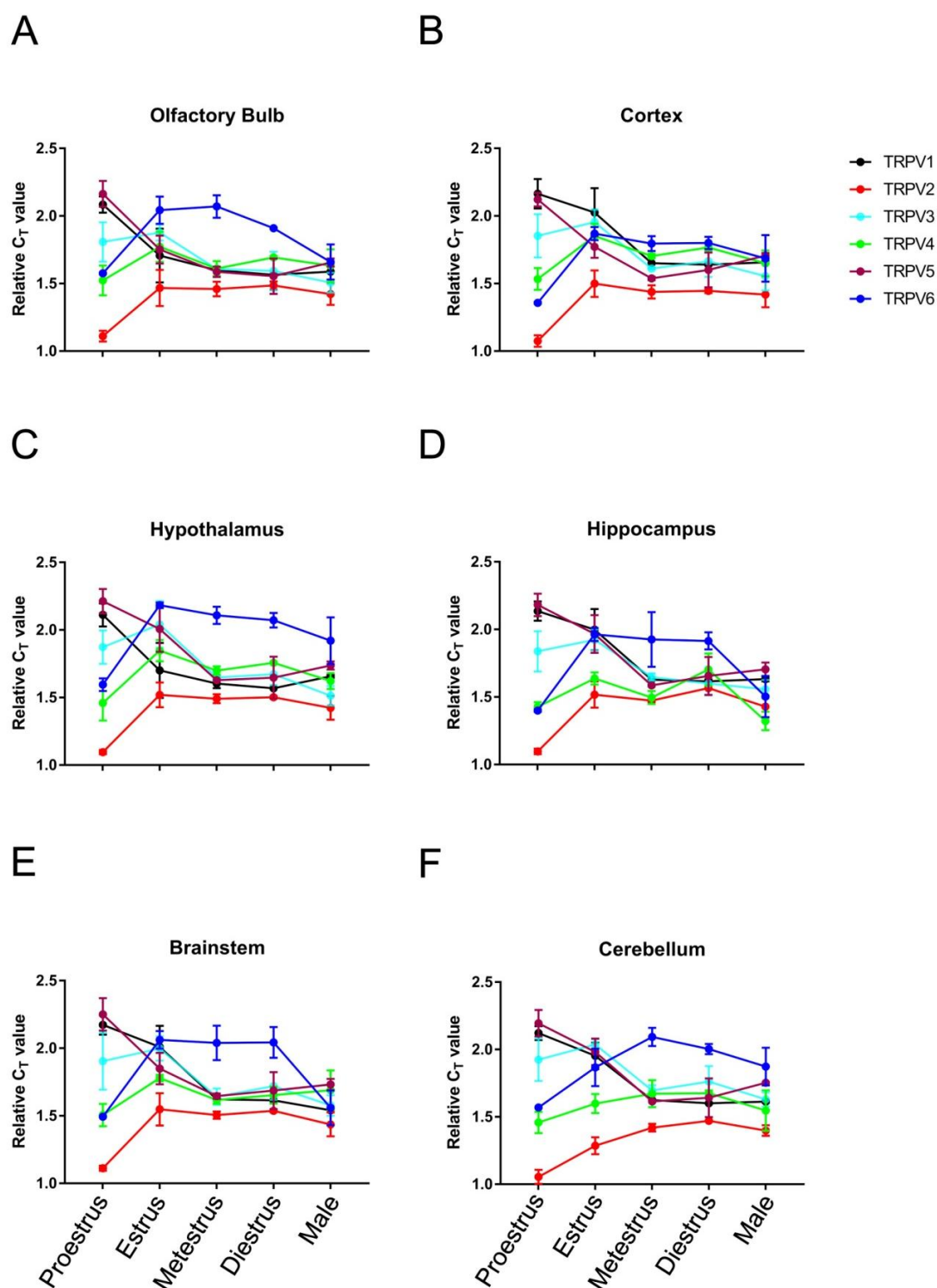


Figure 8: Representation of estrous cycle-related changes in TRPV1-6 mRNA levels in different brain regions of mice. Representation of overall changes in TRPV1-6 mRNA expression in the olfactory bulb (A), cortex (B), hypothalamus (C), hippocampus (D), brainstem (E), and cerebellum (F) of mice during proestrus, estrus, metestrus, and diestrus stages of the estrous cycle, and in male mice. The relative C_T values are represented as mean \pm SD.

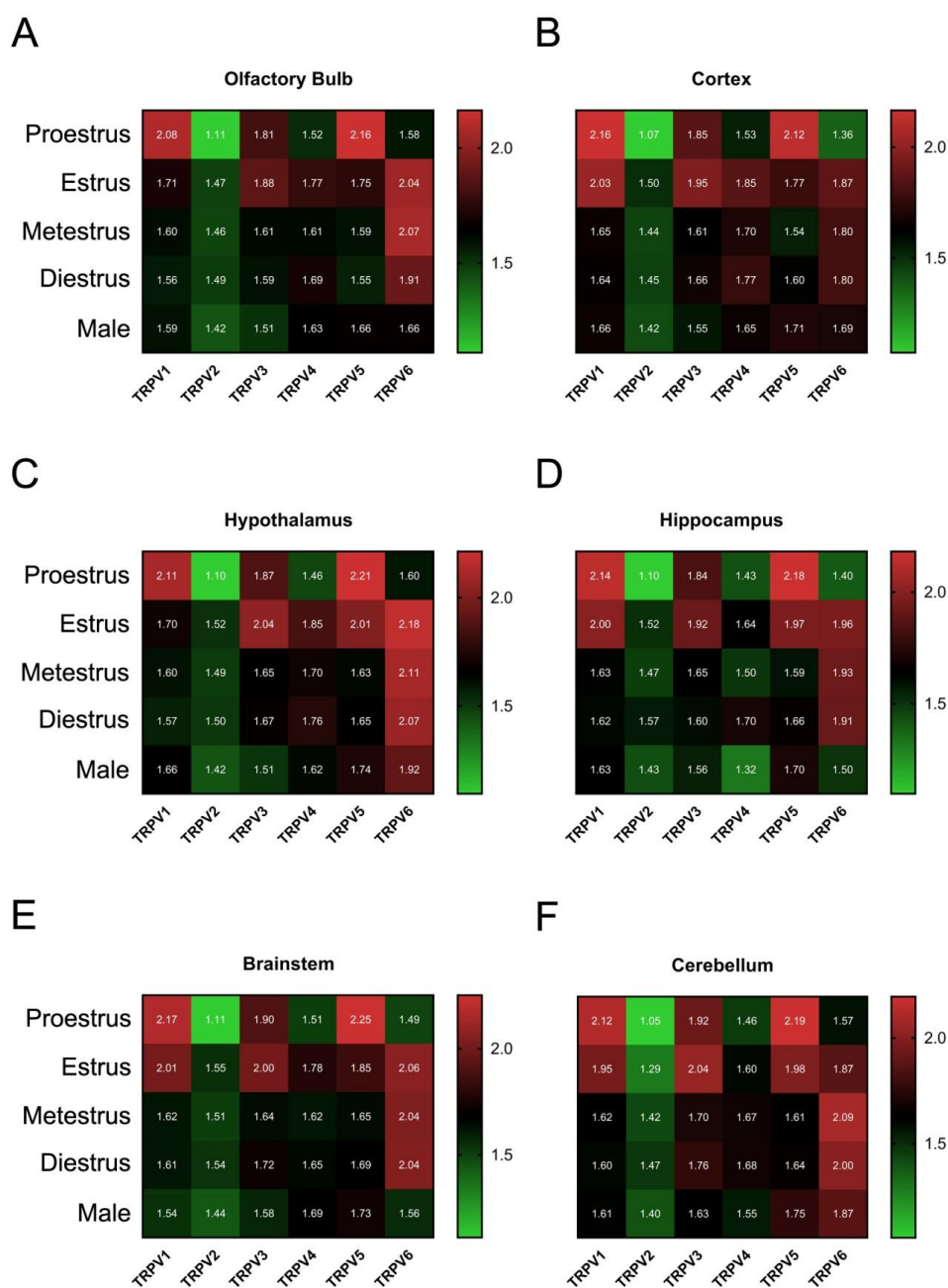


Figure 9: Heat maps showing estrous cycle-related changes in TRPV1-6 mRNA levels in the olfactory bulb, cortex, hypothalamus, hippocampus, brainstem, and cerebellum of mice. Heat maps showing mRNA levels of TRPV1-6 in the olfactory bulb (A), cortex (B), hypothalamus (C), hippocampus (D), brainstem (E), and cerebellum (F) of mice during proestrus, estrus, metestrus, and diestrus stages of the estrous cycle, and in male mice. The relative C_T values are represented as mean.

DISCUSSION

TRPV subfamily of ion channels has emerged as novel cationic channels. These ion channels are gated by a range of external as well as internal stimuli, expressed in the peripheral tissues as well as sensory neurons, and have been suggested to control a range of cellular and physiological processes. Recent evidences have demonstrated the presence of TRPV ion channels in the brain. TRPV1 mRNA was observed in the brain [231,233] and neurons expressing TRPV1 were seen in the olfactory bulb, hypothalamus, hippocampus, midbrain, brainstem, and cerebellum [213,234–237]. TRPV2-ir neurons reside in the cerebral cortex, preoptic region, hypothalamus, and hindbrain [202,235]. The presence of TRPV3-equipped neurons has been described in the cerebral cortex, midbrain, and brainstem [215,238]. The neurons as well as astrocytes in the brain have been shown to express TRPV4 [239–241] and TRPV5 [159]. The TRPV4-expressing cell bodies were observed in the cerebral cortex, hippocampus, thalamus, preoptic area, hypothalamus and cerebellum [240,241]. Wide organization of TRPV5- and TRPV6-immunoreactive neurons was seen in the brain including olfactory bulb, hypothalamus, hippocampus, cortex, midbrain, brainstem and cerebellum [159,201]. Activity of TRPV1, TRPV5 and TRPV6 in the sensory neurons, peripheral tissues, and brain seem to be modulated by circulating levels of estradiol during estrous cycle. While the present study is in agreement with the reports showing presence of TRPV1-6 ion channel expression in different brain compartments, changes in the expression of these ion channels in each brain region during estrous cycle suggest that circulating levels of estradiol may regulate neuronal function by differentially modulating the expression of TRPV ion channels.

Using Champion ChiP Transcription Factor Search Portal as well as Dragon ERE Finder version 3.0 [228], we found the putative estrogen binding sites in the promoter region of TRPV1-6 genes. The Champion ChiP Transcription Factor Search Portal is a widely used

bioinformatics tool to identify the putative binding sites of the transcription factors in the gene of interest. Using ChIP search portal, no putative ER α binding sites were detected in the promoter regions of TRPV2 and TRPV4 genes, but the promoter sequences of TRPV1, TRPV3, TRPV5 and TRPV6 genes showed ER α binding domains. For further validation, we have employed Dragon ERE Finder tool. This program has been developed to identify putative estrogen receptor elements in the genes of interest [228] and has used to identify the candidate estrogen responsive genes [229]. Application of this tool revealed the presence of putative ERE pattern in the promoters of TRPV1-6 genes. We suggest that the circulating levels of estradiol by interacting with specific estrogen receptors may directly influence the expression and activity of TRPV channels in the brain.

The olfactory bulb, cortex, hypothalamus, hippocampus, brainstem, and cerebellum are known to express estrogen receptors [219–221]. Expression of ER α as well as ER β mRNA have been described in different brain regions of adult male mice [ER α : hypothalamus > brainstem > cerebral cortex > hippocampus > olfactory areas > cerebellum; and ER β : hypothalamus > brainstem > cerebral cortex > olfactory areas > hippocampus] [219]. The 3D spatial gene expression data from the Allen Brain Atlas showed the mRNA expression of ER α and ER β throughout the mouse brain [ER- α : hypothalamus > olfactory areas > brainstem > cerebellum = hippocampus = cortex, and ER- β : hypothalamus > olfactory areas > brainstem = hippocampus = cortex > cerebellum] [220]. The expressions of TRPV1-6 mRNA in these regions of the mouse brain suggest that estradiol may regulate neuronal function in these brain regions by modulating TRPV ion channels.

We have observed decreased TRPV1 mRNA expression during proestrus and estrus phases when estradiol levels remain high. Although estradiol is known to interact with TRPV1 in CNS as well as DRG neurons, the role of hormone in the regulation of TRPV1 expression is still not clear. TRPV1 expression in the amygdala, prefrontal cortex, and

thalamus seems estradiol independent whereas hippocampal TRPV1 expression is modulated by estradiol [224]. In DRG neurons, estradiol increases the currents and TRPV1 expression [225]. Xu et al. (2008) suggested that the expression of TRPV1 expression in sensory neurons was inhibited by non-classical estrogen-signalling pathway [226]. In addition, estradiol *via* estrogen receptors has been shown to increase the expression of TRPV1 in uterine cervical afferent as well as DRG neurons [227].

In the olfactory bulb, cortex, hypothalamus, hippocampus, brainstem, and cerebellum, lower levels of TRPV5 mRNA were observed during the proestrus phase as compared to its expression levels in the metestrus and diestrus. The TRPV5 mRNA levels in the hypothalamus, hippocampus, and cerebellum of mouse in estrus were comparable to those in proestrus. Recently, reduced TRPV5 immunoreactivity has been shown in the astrocytes of arcuate nucleus during proestrus and estrus, as compared to those in the metestrus and diestrus [159]. Further, the percentage of TRPV5-equipped CART neurons in the arcuate nucleus were reduced during proestrus as compared to those in estrus, metestrus, and diestrus [159]. TRPV5 and TRPV6 seem to serve as potential mediator of estradiol signalling in the brain, and TRPV5 and TRPV6 mRNA levels in the brain appears to be regulated in opposite manner during estrous cycle. The TRPV5 and TRPV6 immunoreactive cells in the arcuate nucleus co-express ER α [159,201] and estradiol treatment up-regulate renal TRPV5 and Ca²⁺ reabsorption [140,141,207]. The regulation of TRPV5 ion channel by estradiol seems to be mediated *via* estrogen receptors [210]. Compared to estrus, metestrus, and diestrus, an increase in TRPV6 mRNA level was observed in the olfactory bulb, cortex, hypothalamus, hippocampus, brainstem, and cerebellum during proestrus. Recently, we have shown a rise in TRPV6 protein levels in the hypothalamic tissue of mouse during proestrus and estrus as compared to that in metestrus and diestrus [201]. Evidences suggest potential role of estradiol in the regulation of TRPV6.

The presence of a putative ERE has been demonstrated in the promoter sequence of TRPV6 [34]. While the expression of TRPV6 in the duodenum of mouse remained unaltered by estrogen treatment [34], a significant increase in the expression of TRPV6 was observed in the duodenum of rats as well mice following estradiol treatment [141]. In contrast to duodenum, the renal TRPV6 level remained unaffected by treatment with estradiol in combination with progesterone [242]. The intestinal TRPV6 mRNA expression was reduced in ER α KO mice but not in ER β KO mice [211]. TRPV6 expression in mice seem to be mediated via estrogen receptors since it was blocked by ICI 182, 780 (anti-estrogen) treatment [212]. Estradiol treatment results in significant increase in TRPV6 mRNA expression in the gilt endometrial explants and Ishikawa cell line [208,243].

In addition to estradiol, other steroid hormones have also been shown to modulate the activity of TRPV ion channels. Glucocorticoid-induced transient increase in miniature excitatory postsynaptic currents in the feeding-related, preautonomic PVN neurons seem to be mediated via TRPV1 and TRPV4 [244]. In isolated DRG neurons, treatment with pregnenolone sulphate and dehydroepiandrosterone has resulted in inhibition of the capsaicin-induced ionic currents [245,246]. Although the present study describes the changes in the expression pattern of TRPV channels in the brain in response to circulating estradiol levels, it is not clear how the hormone in a given region of brain influences the expression of TRPV1-6 differently. We propose that estradiol and other steroid hormones by regulating TRPV expression in different brain regions may modulate neuronal function, plasticity, and behaviour.

CHAPTER 3

TRANSIENT RECEPTOR POTENTIAL VANILLOID 5 (TRPV5), A HIGHLY Ca^{2+} -SELECTIVE TRP CHANNEL IS WIDELY DISTRIBUTED IN THE BRAIN AND MAY SERVE AS POTENTIAL MODULATOR OF ARCUATE NUCLEUS CART NEURONS

Kumar S, Singh U, Goswami C, Singru PS. (2017). Transient receptor potential vanilloid 5 (TRPV5), a highly Ca^{2+} -selective TRP channel in the rat brain: relevance to neuroendocrine regulation. *Journal of Neuroendocrinology* 29, 4, DOI: 10.1111/jne.12466

INTRODUCTION

Transient receptor potential vanilloid (TRPV) subfamily constitutes a group of ion channels gated by vanilloid compounds, temperature, osmotic and pH changes, certain lipophilic agents, and steroid hormones [137]. The TRPV subfamily consists of six members *viz.*, TRPV1-6 [214]. While TRPV1-4 are non-selective cation channels and known as ‘Thermo TRPs’ as these respond to temperature changes [247], TRPV5 and TRPV6 are highly selective for Ca^{2+} , but are temperature insensitive [248].

Reports underscoring the importance of TRPV channels in neural and neuroendocrine regulation are emerging [31,33,249]. While gene expression studies suggest the presence of TRPV mRNA in the brain tissue [216], neuroanatomical organization of TRPV neurons has also been explored using immunohistochemistry and *in situ* hybridization histochemistry (Table 1). Presence of TRPV1, TRPV2 and TRPV4 has been demonstrated in the PVN and SON nuclei [202,203,213,250]. The oxytocin and vasopressin neurons in these nuclei express thermosensitive TRPVs and these channels seem to play important regulatory functions [202,203,250,251]. In addition to the neuronal expression, presence of TRPV channels was also observed in the astrocytes [252]. While TRPV4-mediated Ca^{2+} oscillations were observed in the astrocytic endfeet processes [253], TRPV1 agonist was found to stimulate cFos expression in the astrocytes [254].

TRPV5 and TRPV6 are unique members of the TRP superfamily. These are highly selective for Ca^{2+} ($P_{\text{Ca}}/P_{\text{Na}} > 100$) [248,255]. Although they share a high degree of homology, TRPV5 and TRPV6 are distinct epithelial Ca^{2+} channels [256]. While their presence and role in the kidney and gastrointestinal tract has been extensively studied [257,258], the information with reference to brain is much limited. Using RT-PCR analysis, TRPV5 mRNA expression was observed in the human brain tissue [258], while the presence of TRPV5 as well as TRPV6 was demonstrated in the mouse brain [257]. Recently,

organization of TRPV6-immunoreactive elements in the mouse brain has been described [201] but the relevant information about TRPV5 in the brain (Table 1) and its significance remains elusive.

Confluent lines of evidences suggest that TRPV5 may be a novel player in neuroendocrine regulation. TRPV5 gene has vitamin D (VD) response element in its promoter [34] and 1, 25-dihydroxyvitamin D₃ up regulate TRPV5 expression in the kidney [258–260]. Both, VD receptors (VDR) [261] as well as binding protein (DBP) are abundantly expressed in the hypothalamus [262]. While the oxytocin neurons contain VDR [261], vasopressin neurons express DBP [262], suggesting involvement of VD in the regulation of these neurons *via* TRPV5. In this background, we wanted to test the role of TRPV5 in neuroendocrine regulation. Since there is no information on the neuroanatomical organization of TRPV5, we first focused on the distribution of TRPV5-immunoreactive elements in the rat brain using immunofluorescence method. While TRPV5 cells were widely noticed in the brain, discrete groups of cells were seen in the hypothalamus. We employed double immunofluorescence to determine if oxytocin and vasopressin neurons in the hypothalamus co-express TRPV5. Double immunofluorescence for glial fibrillary acidic protein (GFAP) and vimentin was used to find out whether astrocytes and tanycytes in the mediobasal hypothalamus express TRPV5. Recent evidence underscores the importance of 17 β -estradiol as potential regulator of TRPV5. The hormone up-regulates TRPV5 mRNA expression in the kidney [140], and *via* TRPV5, it seem to modulate influx of Ca²⁺ in several cells and estrogen receptors (ER) in osteoclasts [210]. While neurons, as well as astrocytes, in the ARC express ER [263,264], the nucleus serves as an important site for estrogen feedback [172]. CART is a novel neuropeptide enriched in the ARC neurons and seems to play an important role in neuroendocrine regulation [22]. CART and POMC are co-localized in the ARC neurons [22] and POMC neurons express ER α [180]. CART neurons in the ARC

have been shown to innervate GnRH neurons in the POA including the AVPe and MnPO [20,83], CART treatment regulate GnRH neuronal activity in POA [83], and these neurons respond to ovariectomy and estradiol treatment [265]. Double immunofluorescence was employed to study if CART neurons and astrocytes in the ARC express TRPV5. To determine whether ARC CART neurons equipped with TRPV5 project to the preoptic area, retrograde neuronal tracer, cholera toxin- β subunit (CtB) was iontophoresced into the AVPe and MnPO, and using triple immunofluorescence the TRPV5-expressing CART neurons accumulating CtB were identified in ARC. Finally, we have studied whether the channel protein expression in these cells show estrous cycle-related changes.

Table 1: Organization of TRPV-expressing neurons in different areas of the brain

TRPV Subfamily	TRPV1	TRPV2	TRPV3	TRPV4	TRPV5	TRPV6
Areas of the brain	Cerebral cortex, olfactory bulb, hippocampus, basal ganglia, amygdala, thalamus, paraventricular thalamic nucleus, median preoptic nucleus (MnPO), hypothalamic paraventricular (PVN), supraoptic (SON), dorsomedial (DMN), and arcuate (ARC) nuclei, lateral hypothalamus, anterior hypothalamic nucleus, suprachiasmatic nucleus (SCN), subfornical organ (SFO), organum vasculosum of lamina terminalis (OVLT), Cerebellar Purkinje cells, periaqueductal grey, intrafascicular, trigeminal and parabrachial nuclei, hypoglossal nucleus, locus coeruleus (LC), area postrema (AP), dorsal motor nucleus of vagus (DMV), nucleus of the solitary tract (NTS). [33,213,233,235–237,266–268]	Cerebral cortex, PVN, SCN, SON, lateral hypothalamus, MnPO, OVLT, SFO, ARC, globus pallidus, raphae magnus and pallidus, LC, inferior olive, hypoglossal nucleus, nucleus ambiguous, rostral division of the ventrolateral medulla, lateral tegmental and pontine nucleus, AP, NTS, nucleus ambiguus, trigeminal motor nucleus. [33,202,203,235, 250,269]	Cerebral cortex, thalamus, hippocampus, striatum, ventral tegmental area, substantia nigra, hypoglossal nucleus, medial NTS. [33,215,216,270]	Optic chiasm, Cortex, hippocampus, thalamus, basal ganglia, circumventricular organ, medial preoptic area (MPA), MnPO, SON, cerebellum. [33,202,240,271,272]	No information is available.	OB, Ventral pallidum, Piriform cortex, amygdala, hippocampus, Nucleus of the horizontal limb of the diagonal band (HDB), OVLT, medial and lateral preoptic area, septohypothalamic, SON, DMN, ARC, nuclei, anterior hypothalamic area, Peduncular part of lateral hypothalamus, subincertal nucleus, zona incerta, SFO, raphe pallidus, A11 dopamine cells, periolivary nucleus, nucleus of trapezoid body, Ventral cochlear nucleus, Cerebellar Purkinje cells. [201]

MATERIALS AND METHODS

Animals

Adult, female, Sprague-Dawley rats (220-250 g) were maintained under 12 h light:12 h darkness cycle and the standard temperature and humidity of the animal facility. Food and water was provided *ad libitum*. All the experimental protocols were reviewed and approved by the Institutional Animal Ethical Committee (IAEC) at the National Institute of Science Education and Research (NISER), Bhubaneswar, under the Committee for the Purpose of Control and Supervision of Experiments for Animals (CPCSEA), New Delhi, India.

Quantitative real-time PCR (qRT-PCR) analysis

Rats (n = 3) were anaesthetized with intraperitoneal injection of a mixture containing ketamine [Neon Laboratories Ltd., Mumbai, India; 90 mg/kg body weight (BW)] and xylazine (Stanex Drugs and Chemicals Pvt. Ltd., Hyderabad, India; 10 mg/kg BW). Brains were rapidly dissected out and frozen on dry ice. Each brain was mounted on a cryostat and regions including the olfactory bulb, cortex, hippocampus, hypothalamus, midbrain, brainstem and cerebellum were micro-dissected out using sterile stainless steel blade. Total RNA was extracted from each tissue using TRIzol[®] Reagent (Ambion) as per manufacturer's instructions. The purity of the isolated RNA was detected using 1% agarose gel and estimated in a NanoDrop 2000 spectrophotometer (Thermo Scientific). Using high-capacity cDNA reverse transcription kit (Applied Biosystems), 2 µg of the RNA was reverse-transcribed to obtain cDNA. Diluted cDNA samples were used for qRT-PCR. The KAPA SYBR Fast qPCR master mix (2X) (KAPA Biosystems) along with the primers (200 nM) for rat TRPV5: *forward primer* 5'-CTTACGGGTTGAACACCACCA-3' and *reverse primer* 5'-TTGCAGAACCACAGAGCCTCTA-3' [140] and rat Hprt1: *forward primer* 5'-

ATGCTGAAGATTTGGAAAAGGTG-3' and reverse primer 5'-ACACAGAGGGCCACAATG-3' (designed using IDT-RealTime PCR tool, NM_012583.2), TRPV5 and Hprt1 cDNAs, respectively were amplified in 7500 Real Time PCR System (Applied Biosystems). Relative abundance of TRPV5 mRNA was obtained by comparing its C_T values with that of Hprt1 gene, as previously described [231]. The qRT-PCR amplified products were finally run on 1.7% agarose gel to confirm size of the amplified products.

Tissue processing

Animals were deeply anaesthetized with intraperitoneal injections of ketamine (90 mg/kg BW) and xylazine (10 mg/kg BW) and perfused transcardially with phosphate buffered saline (PBS, pH 7.4) followed by 100 ml 4% paraformaldehyde in phosphate buffer (PB, pH 7.4). The brains were removed from the calvarium, post-fixed in the same fixative and cryoprotected in 25% sucrose solution in PBS. Serial 25 µm thick coronal sections through the rostro-caudal extent of the brain and spinal cord were cut on a cryostat (Leica CM3050 S, Leica Microsystems, Nussloch GmbH, Germany) and free-floating sections were obtained. Sections were collected in PBS, transferred to the antifreeze solution (30% ethylene glycol and 25% glycerol in 0.05 M PB), and stored at -20 °C until processed further.

Immunofluorescence

Details of the antisera and their dilutions used for localization of TRPV5 in the brain and spinal cord, and the phenotypic characterization of TRPV5-expressing cells are given in Appendix 1. Sections were processed for immunofluorescence as previously described [167]. Application of TRPV5 antiserum at 1:1000 and 1:2500 dilutions followed by Alexa Fluor 488-conjugated anti-rabbit IgG (1:500) produced weak immunofluorescence. Tyramide amplification protocol was therefore employed for signal amplification. In brief, a set of free

floating brain sections from each rat (n = 6) were treated with 0.5% Triton X-100 in PBS followed by 3% normal horse serum in PBS, and incubated in rabbit polyclonal TRPV5 antiserum at 1:1000 dilution overnight at 4 °C. Following incubation in TRPV5 antiserum, sections were rinsed in PBS and incubated in biotinylated goat anti-rabbit IgG (Vector Laboratories, 1:400) followed by streptavidin-peroxidase (ABC, 1:1000). The immunoreaction was amplified using Tyramide Signal Amplification kit as per manufacturer's instructions (New England Nuclear Life Science Products, USA). Sections were incubated in DTAF-avidin (1:300, Jackson ImmunoResearch) for 2 h, rinsed in Tris buffer (pH 7.6), and mounted with Vectashield mounting medium containing DAPI (Vector).

Double immunofluorescence

For phenotypic characterization of TRPV5-immunoreactive cells, sets of alternate sections through the rostro-caudal extent of hypothalamus from each animal (n = 12) were incubated separately in a mixture of rabbit TRPV5 antiserum and either mouse monoclonal oxytocin, vasopressin, CART, vimentin, or GFAP antibodies (Appendix 1) overnight at 4 °C. Following rinsing in PBS, TRPV5 signal was amplified as described above. For visualization of oxytocin, vasopressin, CART, vimentin and GFAP, sections were incubated in Alexa Fluor 594-conjugated anti-mouse IgG (Life Technologies, 1:500) for 2 h at room temperature. In addition, few sections through the ARC region were incubated in rabbit anti-estrogen receptor alpha (ER α) antiserum followed by incubation in Alexa Fluor 594-conjugated anti-rabbit IgG (Life Technologies, 1:500). Sections were rinsed in PBS and incubated in rabbit TRPV5 antiserum followed by tyramide amplification as described above.

To study the estrous cycle-related change in TRPV5-immunoreactivity in the ARC, coronal sections through this nucleus were processed for double immunofluorescence labeling using mouse anti-CART antibody and rabbit anti-TRPV5 antiserum. Sections were

incubated in Alexa Fluor 594-conjugated goat anti-mouse IgG (Life technologies, 1:500) for visualization of CART. Tyramide amplification protocol was employed for TRPV5 as described above. After rinsing in Tris buffer, sections were mounted on glass slides and coverslipped with Vectashield mounting medium.

Images were captured using AxioCam digital camera (Carl Zeiss) by switching the filter sets. In Adobe Photoshop CS4 (Adobe Systems, Inc., USA), the images were superimposed, and adjusted for the brightness and contrast. In addition, the sections were also analyzed under laser-scanning confocal microscope (LSM780, Carl Zeiss, Germany). Immunofluorescence signal was detected at excitation/emission wavelengths of 495/517 nm (DTAF, green), 590/619 nm (Alexa Fluor 594, red), and 358/463 nm (DAPI, blue). Association between TRPV5 and oxytocin or vasopressin in the PVN, SON, ANS and SOR was analyzed under a fluorescence microscope and images were captured. Using a 63x oil objective, serial optical sections through the hypothalamus and cortex were obtained to explore the association between TRPV5 and oxytocin, vasopressin, CART, GFAP or vimentin-immunoreactive elements. The series of optical slices from each region were merged using LSM software. The images were opened using Adobe Photoshop CS4, adjusted for brightness and contrast, and panels were prepared. Sections of the ARC doubled labeled with TRPV5 and ER α were observed to find out if the ER α expressing cells in the ARC co-express TRPV5.

Neuroanatomical description, nomenclature, and schematic of the coronal sections of the brain to depict TRPV5-immunoreactive neurons as shown in Fig. 5 was adapted from the rat brain atlas of Paxinos and Watson [165] with minor modifications.

Estrous cycle-dependent changes in TRPV5-immunoreactivity in the arcuate nucleus (ARC)

The stages of estrous cycle were determined by vaginal smear cytology: predominant nucleated epithelial cells in proestrus; cornified epithelial cells in estrus; mixture of leukocytes, nucleated epithelial cells and cornified cells in metestrus; and predominant leukocytes in diestrus [160]. Rats (n = 3) in each stage of the estrous cycle were anaesthetized with intraperitoneal injection of a mixture containing ketamine (90 mg/kg BW) and xylazine (10 mg/kg BW), perfused, brains sectioned on a cryostat and processed for double immunofluorescence labeling as described above.

Retrograde neuronal tracing

In rats, the CART neurons of ARC are known to project to MnPO and AVPV in POA [20]. To find out if these neurons are equipped with TRPV5, retrograde neuronal tracing was employed, as described previously [20,215] with minor modifications. Adult, female, Sprague Dawley rats (200–250 g) were anesthetized with an i.p. injection of mixture containing Ketamine and Xylazine (Ketamine: 75 mg/kg and Xylazine: 10 mg/kg body weight) and placed into a stereotaxic apparatus (Leica). The retrograde neuronal tracer CtB (Cat. # 104, List Biological Laboratories, Inc.) was iontophoresed (Stoelting Co.) using 6 μ A positive current for 10 min through a glass micropipette (tip diameter: 15-20 μ m) in the MnPO and AVPe under stereotaxic coordinates [coordinates for MnPO from bregma: -0.26 mm anterior-posterior, 0.07 mm lateral to the midline, and 7.77 mm dorso-ventral; coordinates for AVPe from bregma: 0.30 mm anterior-posterior, 0.17 mm lateral to the midline, and 8.59 mm dorso-ventral] [165]. After 10 days, the rats were anesthetized and perfused transcardially; the brains were dissected out and post-fixed in 4% paraformaldehyde, and immersed overnight in 25% sucrose solution in PBS. Coronal sections (25 μ m thick) containing the POA and ARC were collected in PBS. The sites of CtB injection were detected by incubating the sections in goat anti-CtB (1:2000) followed by incubation in

AlexaFluor 594-conjugated donkey anti-sheep IgG, (Life technologies, 1: 1000). The rostro-caudal series of sections containing ARC were subjected to sequential triple immunofluorescence using goat anti-CtB (1:5000) and rabbit anti-TRPV5 (Alomone, 1:1000). The TRPV5 signal was amplified using BT and visualized using DTAF-avidin (1:300) and CtB cells in ARC were detected using AlexaFluor594-anti-goat IgG (1:1000). The sections were rinsed in PBS several times in PBS and incubated in rabbit anti-CART (55-102) (1:5000) followed by incubation in DyLight649-conjugated donkey anti-rabbit IgG (BioLegend, 1:1000 dilution). To ensure that the secondary antibody used for detecting CART neurons in ARC are not binding to the TRPV5 labelled neurons, few TRPV5-labelled sections of ARC were incubated in DyLight 649-conjugated donkey anti-rabbit IgG. No DyLight649 immunofluorescence was seen in TRPV5 labelled neurons.

Image analysis

Qualitative analysis of the number of TRPV5-immunoreactive neurons and fibers/terminal fields in the brain was performed as described earlier [273]. Briefly, sections were visualized under a fluorescence microscope. The relative abundance of the TRPV5-immunoreactive cells and fibers/terminals was estimated by observing the immunolabelled sections under the microscope and analyzed using a qualitative scale [+ , few; ++, moderate; +++, high; -, negative]. The analysis is given in Table 2.

To determine the percentage of TRPV5-expressing oxytocin and vasopressin neurons in the PVN, SON, ANS, and SOR, six sections through the rostro-caudal extent of these nuclei [SON: -0.80 mm to -1.88; PVN: -1.80 to -2.12; SOR: -2.12 to 3.14 mm, relative to bregma [165]] from each animal were analyzed under an AxioImager M2 fluorescence microscope. While switching the filter sets, green for TRPV5 and red for oxytocin or vasopressin, the double-labelled neurons on either side of the brain were identified, counted,

and percentages determined for each animal. Percentage of double-labeled cells from each animal was pooled and mean \pm SEM was calculated. The analysis of neurons double labeled for TRPV5 and oxytocin or vasopressin in the PVN, SON, ANS and SOR is given in Table 4.

To determine the estrous cycle-related changes in the TRPV5-expressing CART neurons of the ARC, total number of CART neurons and CART neurons expressing TRPV5 in this nucleus [from bregma: -2.56 to 3.30 mm [165]] were counted in each animal, percentages were determined, and mean \pm SEM calculated. To study the estrous cycle-related changes in TRPV5-expressing astrocytes of the ARC, relative quantitative analysis of the intensity of TRPV5-immunoreactivity in the astrocytes of ARC was determined as described earlier [167] with minor modifications. Briefly, the image analysis system consisted of an AxioImager M2 fluorescence microscope equipped with a CCD camera. Slides were coded for the observer blind to the experiment. TRPV5-expressing astrocytes were analysed throughout the rostro-caudal extent of the ARC of each animal while keeping the fluorescence intensity and exposure time unaltered. For measuring the pixel intensity of TRPV5-immunoreactivity, eight sections encompassing the rostro-caudal extent of ARC from either side of the brain of each animal were analysed. The images of ARC were captured and TRPV5-immunofluorescence intensity values within the area of imaged section were determined using Zen 2011 software (Carl Zeiss). The background intensity values of the non-immunoreactive area and TRPV5-immunoreactive neurons in the ARC were subtracted from the total intensity. The data from all the animals in each stage of the estrous cycle was pooled separately and mean \pm SEM calculated. The changes in percentage of TRPV5/CART double labeled neurons and TRPV5-immunoreactivity in astrocytes in the ARC during different phases of estrous cycle were statistically analysed.

Specificity of the antisera

CART, GFAP, oxytocin, vasopressin, ER α , and vimentin antibodies have already been used in previous studies for localization of respective antigens in rat brain [134,162,274–278]. We have characterized the specificity of TRPV5 antiserum in further detail. Affinity purified TRPV5 antiserum (Alomone Labs and Sigma) was raised against a synthetic peptide [C-GLNLSEGDGEEVYHF], corresponding to the amino acid residues 715-729 of human TRPV5. TRPV5 protein sequences of human (NP 062815.2) and rat (NP 446239.2) were aligned and analyzed using CLUSTAL Omega. In addition, another TRPV5 antiserum (Cat. # ab77351, abcam, USA; 1:2000) was also used to compare the immunostaining pattern. Sections were incubated in the diluted antiserum and antiserum preadsorbed with the control peptide (1:1) for 24 h. To determine whether the antiserum recognizes TRPV5, Western blot analysis of the rat hypothalamus, cerebellum, and kidney was performed as described below.

Western blot analysis

Rats were anaesthetized with intraperitoneal injection of a mixture containing ketamine (90 mg/kg BW) and xylazine (10 mg/kg BW), and decapitated, brains dissected out, and frozen on dry ice. Western blot analysis was performed as described earlier [167]. Tissue blocks containing hypothalamus, cerebellum, and kidney were isolated and homogenized in 10 mM Tris-HCl (pH 8.0) lysis buffer containing 1% protease inhibitor cocktail (Sigma). The homogenate was centrifuged at 4 °C at 14000 rpm for 30 min and the supernatant was used for SDS-PAGE analysis. Protein concentration was estimated using Bradford reagent (Sigma) and 60 μ g of the protein along with the protein marker (Fermentas) were run in 9 % SDS-PAGE in the adjacent lane. Separated protein bands in the gel were transferred to the Immobilon®-P Polyvinylidene difluoride membrane (PVDF, Sigma) using wet transfer (BioRad). The blot was blocked in 3% bovine serum albumin (HIMEDIA,

India) solution for 1 h and incubated in rabbit anti-TRPV5 antiserum (1:5000) for 1 h at room temperature. In addition, the TRPV5 antiserum was preadsorbed with the control peptide (1:1) for 24 h and the blot was incubated with the preadsorbed antiserum. After washing in TBST buffer, the blots were incubated in goat anti-rabbit horseradish peroxidase-conjugated antibody (1:10000; Cell Signaling) for 1 h at room temperature. The signal was visualized using enhanced chemiluminescence method (ECL, Amersham) and detected in Gel Doc system (BioRad).

To further validate the specificity of the TRPV5 antiserum, *Trpv5* gene was cloned into a vector and using transfection the gene was expressed in HEK293T cells. The transfected cells were processed for TRPV5 immunofluorescence. In addition, a knockdown protocol using siRNA was employed. Details of these experiments are given below.

Cell culture and *in vitro* transfection

HEK293T cells were grown in Dulbecco's Modified Eagle's Medium (DMEM, HiMedia) supplemented with 2 mM GlutaMAX-I (Life Technologies), 10% fetal bovine serum (FBS, HiMedia), and 100 U/ml Penicillin/100 µg/ml Streptomycin (HiMedia) at 37 °C in a humidified environment with 5% CO₂ in air. The HEK293T cells were used for transfection only after the third passage. The cells were treated with 0.25% Trypsin (Gibco, Life Technologies) for 2 min at 37 °C, allowed to grow for 24 h, and processed for transfection.

HEK293T cells were transfected with 500 ng of either the shuttle vector (pLenti-C-mGFP-P2A-Puro, Lenti vector with C-terminal mGFP tag, and P2A-Puro, OriGene Technologies Inc, USA, Cat. # PS100093) or rat *Trpv5* plasmid (Lenti ORF clone of *Trpv5*-mGFP-tagged ORF, Accession No. NM_053787, OriGene Technologies Inc., Cat. # RR208885L4) using lipofectamine 3000 reagent (Invitrogen), as per the instructions of the

manufacturer. Cells treated with lipofectamine 3000 without DNA served as control. The efficiency of transfection was accessed by expression of GFP. Forty-eight hours after transfection, the cells on the coverslips were fixed with 4 % paraformaldehyde in PBS and processed for TRPV5 immunofluorescence. The coverslips were incubated in rabbit anti-TRPV5 antiserum (Alomone, 1:1000) for 3 h at room temperature followed by incubation in AlexaFluor594-conjugated donkey anti-rabbit IgG (1:1000) for 1 h. The untransfected cells were also incubated in Alexa Fluor 594-conjugated donkey anti-rabbit IgG antiserum (1:1000) to guard against the possibility of any non-specific binding by the secondary antibody. The coverslips were rinsed in PBS and mounted using Vectashield mounting medium containing DAPI, observed under a fluorescence microscope, and images were captured using AxioCam digital camera by switching the filter sets. The captured images were superimposed and adjusted for the brightness and contrast in Adobe Photoshop CS4 (Adobe Systems, Inc., USA).

Knockdown of TRPV5 in the rat brain and pituicytes

The Accell rat TRPV5 siRNA–SMARTpool (GE Dharmacon) was used to knockdown TRPV5 in the rat brain and pituicytes. The TRPV5 siRNA targets the following sequences: CUAACAUCUCCAUUUAUG (ORF), CGAUUAGGUUUUAUUUUCU (3'UTR), GUAUGUACCUUAUAAGUUC (3'UTR), and CUA AUGUACUUUAUAAUUG (3'UTR). The DyLight547-labeled non-target siRNA was used for the assessment of siRNA uptake by the cells. While the GAPDH siRNA served as positive control, the non-targeting siRNA was used as a negative control (control siRNA). The siRNAs were resuspended in 1X siRNA buffer and the delivery media was used for further dilutions. The vehicle-treated control animals or cells received equivalent volume of 1X siRNA buffer in the delivery media. The vehicle or siRNA were delivered through the following two routes.

A. Intracerebroventricular (ICV) administration:

Rats were anaesthetized with intraperitoneal injection of a mixture containing ketamine (90 mg/kg BW) and xylazine (10 mg/kg BW), and guide cannula (PlasticOnes, USA) was stereotaxically placed in the right lateral ventricle using coordinates [AP -0.8 mm, ML -1.4 mm, DV -3.5 mm from bregma] [165] and secured using screws and dental cement. Seven days following surgery, experiments were performed. In the freely moving rat, through an internal cannula, either vehicle, DyLight547-conjugated non-target siRNA, non-target siRNA, GAPDH siRNA or TRPV5 siRNA (5 µg/rat) in 5 µl of siRNA delivery media was administered in the lateral ventricle at a rate of 0.5 µl/min (n = 3/treatment group), as describe earlier [279]. Four days following injections, animals were sacrificed, and brains were collected and processed for TRPV5 immunofluorescence or western blot analysis, as given below. The effect of control non-target siRNA, vehicle, and TRPV5 siRNA treatments on TRPV5-immunoreactivity in the hypothalamic SOR and cerebellar Purkinje neurons was determined using relative quantitative analysis, as described above in the image analysis. The data from all the animals in each group was statistically analyzed.

The hypothalamic and cerebellar tissues from the control non-target siRNA, vehicle, and TRPV5 siRNA-treated rats were excised from the brain. The tissues were homogenized in 10 mM Tris-Cl, pH 8.0 buffer in the presence of HaltTM protease inhibitor cocktail (Thermo Scientific) followed by centrifugation. The supernatant collected and the total protein was estimated using Bradford reagent (Sigma). The protein (60 µg) from each test sample was resolved on 9% SDS-PAGE and transferred to PVDF membrane using wet-transfer (Bio-Rad). The blots were incubated with either mouse monoclonal anti-GAPDH (Abgenex; dilution 1:8000), and rabbit monoclonal anti-β-Actin (Cell Signaling; dilution 1:8000) antibodies, or rabbit polyclonal TRPV5 antiserum (Alomone; 1:5000) followed by incubation in respective HRP-conjugated secondary antibodies (Cell Signaling; dilution

1:10000). The signal was detected using Chemiluminescent HRP substrate (Millipore). The band intensities were analyzed using Quantity One software. The percent intensity of the target proteins (TRPV5 or GAPDH) relative to the loading controls (GAPDH or β -Actin) were determined for each treatment groups and represented as mean \pm SD. The data was statistically analysed.

B. Delivery of Accell siRNA in rat pituicytes primary cells:

Pituicytes were obtained from the rat pituitary glands as described previously [280]. Rats were anaesthetized with intraperitoneal injection of a mixture containing ketamine (90 mg/kg BW) and xylazine (10 mg/kg BW); pituitaries were dissected out, kept in fresh ice-cold Hanks' balanced salt solution (HBSS), and rinsed in 0.1 M PBS, pH 7.4. The anterior and intermediate lobes of the pituitary were separated, pars nervosa was isolated, gently triturated in growth plating media [281] and passed through the cell strainer (40 μ m). The suspension was centrifuged at 1000 rpm for 5 min and the pellet was resuspended in growth plating media. Approximately 2×10^5 cells per well were plated on poly-d lysine coated cover slips and were allowed to adhere in the incubator for 2 days with constant supply of 95% O₂ and 5% CO₂ at 37 °C. The cells were rinsed in Accell siRNA delivery media supplemented with B-27 followed by 1 h incubation in the same media. After 1 h, vehicle or 1 μ M DyLight547-conjugated non-target siRNA, non-target siRNA, or TRPV5 siRNA was added in the delivery media supplemented with B-27. Four days after the treatment, the cells were fixed in 4 % paraformaldehyde and processed for GFAP or TRPV5 immunofluorescence. All the conditions including chemicals, dilution, treatment time, and exposure time for capturing the images were kept constant to minimize the errors.

Statistical analysis

The data analysis was performed using Prism 4 software (GraphPad Software Inc., La Jolla, CA). The estrous cycle-related changes in TRPV5-expressing CART neurons and TRPV5-immunoreactivity in ARC; the effect of control non-target siRNA, vehicle, and TRPV5 siRNA treatments on TRPV5-immunoreactivity in the hypothalamic SOR and cerebellar Purkinje neurons, and TRPV5 and GAPDH protein expression were analysed using one-way analysis of variance (ANOVA) followed by Bonferroni's multiple comparison test. A $P < 0.05$ was considered statistically significant.

Table 2: Distribution of TRPV5-immunoreactive neuronal cell bodies and fibers/terminals in rat brain

Areas of the brain	Cell bodies	Fibers/terminals
Cerebral cortex		
Piriform cortex	+++	+
Retrosplenial dysgranular cortex	++	+
Primary motor (M1 and M2) cortex	++	+
Somatosensory cortex	+	+
Hippocampus		
Field CA1	+	++
Field CA3	+	++
Hypothalamus		
Paraventricular nucleus (PVN)	++	-
Supraoptic nucleus (SON)	+++	++
Accessory neurosecretory nuclei (ANS)	++	-
Arcuate nucleus (ARC)	++	++
Supraoptic nucleus, retrochiasmatic part (SOR)	+++	++
Medial tuberal nucleus (MTu)	++	+
Cerebellum		
Purkinje cell layer (PCL)	+++	-
Molecular layer (ML)	-	+++
Midbrain and brainstem		
Substantia nigra, reticular part (SNR)	++	+
Ventral tegmental area (VTA)	++	+
C1/A1 region	+	-
Trapezoid nucleus	+++	-

Number of cell bodies and fibers/terminals: +, few; ++, moderate; +++, high; -, negative

RESULTS

TRPV5 mRNA expression in the brain

qRT-PCR showed a single band of desired amplicon length for TRPV5 (163 bp) as well as endogenous control gene *Hprt1* (118 bp) (Fig. 1A). The relative TRPV5 mRNA abundance in various regions of the rat brain is shown in Fig. 1B. Highest TRPV5 mRNA expression was observed in the hippocampus, midbrain, and brainstem, followed by cortex, cerebellum and hypothalamus.

Specificity of the TRPV5 antiserum

Alignment of the human and rat TRPV5 sequences showed high degree of similarity (Fig. 2A). The fifteen amino acids (715-729) human TRPV5 peptide sequence against which the antiserum # 1 was raised showed 73.3 % sequence similarity with the rat TRPV5 (Fig. 2A). Using this antiserum, TRPV5 immunoreactive neurons were seen in the retrochiasmatic part of the hypothalamic supraoptic nucleus (SOR) (Fig. 2B) and other brain regions. The antiserum # 2 was raised against twelve amino acids (697-708) human TRPV5 peptide sequence. It showed 91.66 % sequence similarity with the rat TRPV5 (Fig. 2A). Application of this antiserum on the sections of the brain resulted in immunostaining pattern similar to antiserum # 1 (Fig. 2C). Incubation of the hypothalamic sections with preadsorbed TRPV5 antiserum resulted in a complete loss of TRPV5-immunoreactivity in SOR (Fig. 2D) as well as other areas of the brain. Using Western blot analysis, a prominent band at 65-68 kDa was consistently observed in tissue homogenate of the hypothalamus, cerebellum, and kidney (Fig. 2E). Application of TRPV5 antiserum preadsorbed with the control peptide resulted in absence of the TRPV5-immunoreactive bands (Fig. 2E).

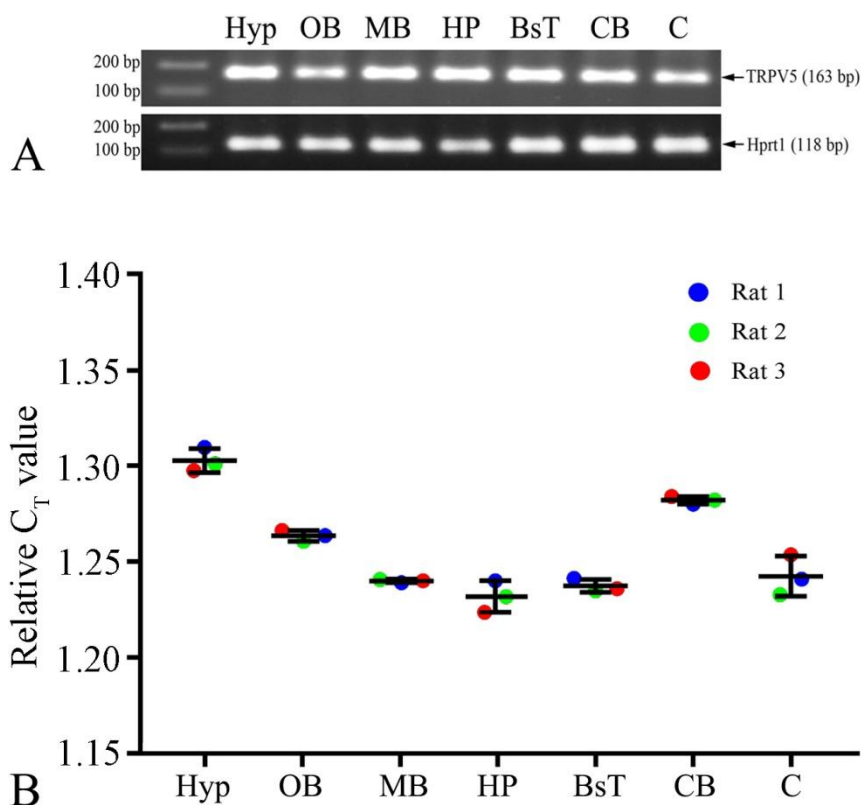


Figure 1: TRPV5 mRNA expression in the rat brain. (A) qRT-PCR analysis of the TRPV5 mRNA expression in different regions of the rat brain. (B) The relative abundance of TRPV5 mRNA in different brain regions was obtained by comparing its C_T values with that of Hprt1 gene in the respective region of the brain. BsT, brainstem; C, cortex; CB, cerebellum; HP, hippocampus; Hyp, hypothalamus; MB, midbrain; OB, olfactory bulb.

The TRPV5 immunoreactivity in the primary rat pituicytes and brain responded to the TRPV5 siRNA treatment. While no immunoreactivity was observed in pituicytes in the absence of GFAP (Fig. 3A) or TRPV5 (Fig. 3C) antisera, application of these antisera resulted in labeling of the pituicytes (Fig. 3B, D). No labeling was observed in the pituicytes treated with vehicle (Fig. 3E), whereas DyLight547-conjugated non-target siRNA was detected in the pituicytes (Fig. 3F). While intense TRPV5 immunofluorescence was observed in the pituicytes treated with non-target siRNA, serving as control (Fig. 3G), TRPV5 siRNA treatment resulted in a drastic reduction in TRPV5 immunoreactivity in the pituicytes (Fig. 3H). Following icv administration, the DyLight547-conjugated non-target siRNA were detected in the neurons in different regions of the brain including the Purkinje cells of the cerebellum (Fig. 3I, i) as well as the neurons of SOR (Fig. 3M). TRPV5-immunoreactivity was observed in the Purkinje (Fig. 3J, j, K, k) and SOR (Fig. 3N, O) neurons of the control non-target siRNA- (Fig. 3J, j, N) as well as vehicle- (Fig. 3K, k, O) treated animals. Compared to the control non-target siRNA- and vehicle-treated animals, a significant reduction in TRPV5-immunoreactivity in the Purkinje ($P < 0.001$) as well as hypothalamic SOR ($P < 0.01$) neurons (Fig. 3L, l, P, Q) was observed in the animals treated with TRPV5 siRNA. Using Western blot analysis, a significant reduction ($P < 0.01$) in GAPDH level in the hypothalamus and cerebellum was apparent following the treatment with GAPDH siRNA (Fig. 3R). Treatment with TRPV5 siRNA resulted in a significant reduction ($P < 0.001$) of the ~65-68 kDa TRPV5-immunoreactive band in the hypothalamus and cerebellum (Fig. 3S).

While no GFP expression was seen in untransfected HEK293T cells (Fig. 4A-C, M-O), cells transfected with shuttle vector expressed GFP (Fig. 4D-F). Transfection of HEK293 cells with GFP-ratTrpv5 resulted in expression of TRPV5 in these cells (Fig. 4G-I). Application of TRPV5 immunofluorescence resulted in labeling of the GFP-TRPV5-

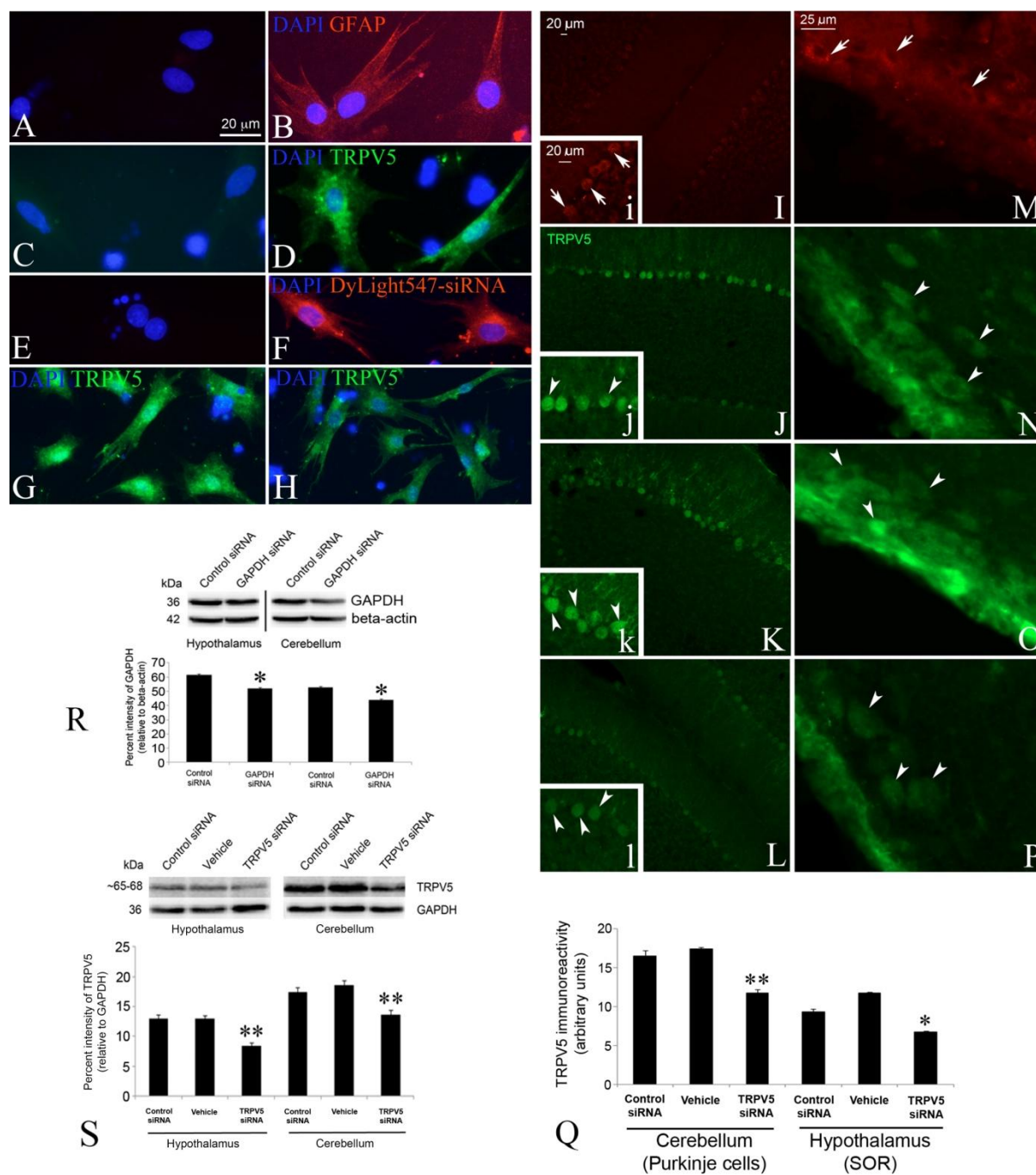


Figure 3: Specificity of TRPV5 antiserum using TRPV5 siRNA approach. Specificity of the TRPV5 antiserum in rat (A-H) primary pituitary cells and (I-S) brain following siRNA treatment. The pituitary cells were treated with TRPV5 siRNA in vitro as well as administered intracerebroventricularly (icv). The pituitary cells from rat pituitary without (A) GFAP or (C) TRPV5 antiserum and with (B) GFAP or (D) TRPV5 antiserum. Note the GFAP and TRPV5 immunofluorescence in pituitary cells. The pituitary cells treated with (E) vehicle and (F) DyLight547-conjugated siRNA. The pituitary cells show uptake of siRNA (F). Compared to (G) non-target siRNA, note a drastic reduction in TRPV5-immunofluorescence in the pituitary cells (H) treated with TRPV5 siRNA. Following icv DyLight547-conjugated non-target siRNA, immunofluorescence (arrows) is seen in the (I, i) cerebellar Purkinje cells and (M)

retrochiasmatic part of the supraoptic nucleus (SOR). TRPV5 immunofluorescence (arrowheads) in the (j, J, k, K, l, L) purkinje cells and (N, O, P) SOR following treatments with (J, j, N) non-target siRNA control, (K, k, O) vehicle control, and (L, l, P) TRPV5 siRNA. Note a drastic reduction in TRPV5 immunoreactivity in purkinje and SOR neurons following TRPV5 siRNA treatment (L, l, P). Semiquantitative image analysis of the TRPV5-immunoreactivity in the hypothalamic SOR and cerebellar purkinje neurons (Q). Note a significant reduction in TRPV5-immunoreactivity following TRPV5 siRNA treatment. Effect of siRNA treatment on protein expression in the brain (R and S). Treatment with GAPDH siRNA shows significant reduction in its protein expression (R), serving as control. Treatment with TRPV5 siRNA (S) significantly reduces the intensity of the ~65-68 kDa TRPV5-immunoreactive band. *, $P < 0.01$; **, $P < 0.001$. Scale bar = 20 μm A-L and 25 μm in M-P.

expressing cells (Fig. 4I) but not in the untransfected cells (Fig. 4C) as well as cells transfected with shuttle vector (Fig. 4F). Application of TRPV6 immunofluorescence in GFP-mouse *Trpv6* transfected HEK293T cells resulted in labeling of the GFP-TRPV6-expressing cells (Fig. 4P-R) but not in the GFP-rat *Trpv5* transfected cells (Fig. 4J-L) and vice versa (Fig. 4S-U).

Organization of TRPV5-immunoreactive elements in the brain

TRPV5-immunoreactivity was observed in the neurons as well as glial cells in the brain. The organization of TRPV5-immunoreactive neurons in the brain and hypothalamus is schematically represented in Fig. 5. The relative density of TRPV5-immunoreactive neurons and fibers/terminals in different regions of the brain is summarized in Table 2. Distinct TRPV5 labelled neurons were observed in the CA1 and CA3 regions of the hippocampus (Figs. 5B-D and 6A, B) and piriform cortex (Figs. 5A-D and 6C). TRPV5-immunoreactive cells were seen in the retrosplenial agranular, primary motor (M1 and M2), and somatosensory (Fig. 5A-D and F) cortices. The cells were organized in distinct layers (I and IV) of the cerebral cortex (Fig. 6D, E). In addition, TRPV5 labeling was observed in the cortical cells located below the amygdala (Fig. 6F).

Diagrammatic representation of the TRPV5-immunoreactive elements in the hypothalamus is shown in Fig. 5A-D. TRPV5 immunofluorescence was observed in the neurons of the PVN (Figs. 5B and 7A), SON (Figs. 5A, B and 7B), accessory neurosecretory nuclei (ANS) (Figs. 5B and 7C), retrochiasmatic area of the SON (SOR) (Figs. 5C-E and 7D), medial tuberal nucleus (MTu) (Figs. 5D, E and 7E), and ARC (Figs. 5C-E and 7F). In PVN, the TRPV5-immunoreactive cells were seen in the magnocellular and ventral parvocellular subdivisions. While weak TRPV5 immunofluorescence was seen in PVN neurons, moderate labeling was observed in neurons of the SON (Fig. 7A, B). Compared to

the PVN and SON, intense TRPV5 immunofluorescence was observed in neurons of the SOR (Fig. 7D). In the above described hypothalamic nuclei, TRPV5-immunoreactivity was restricted to the cell bodies of the neurons whereas isolated TRPV5-immunoreactive fibers were seen in the SOR (Fig. 7Dd). In the median eminence, TRPV5-immunoreactivity was restricted to the cells in the internal zone and processes in the external zone (Fig. 7G). In the midbrain, neurons in the reticular part of the substantia nigra (SNR) (Figs. 5F and 7H), and ventral tegmental area (VTA) (Figs. 5F and 7I) were moderately TRPV5-immunoreactive. TRPV5-immunoreactive neurons were seen in the C1/A1 region (Figs. 5G and 7J) and nucleus of the trapezoid body (Figs. 5G and 7K) in the brainstem. In the cerebellum, Purkinje cells in the purkinje cell layer and fibers in the molecular layer were TRPV5-immunoreactive (Figs. 5G, H and 7L, M).

In addition, TRPV5-immunoreactivity was also observed in the glial cells in the cortical layer I (Fig. 6D, E). In the mediobasal hypothalamus, tanycytes lining the wall of third ventricle were TRPV5-immunoreactive (Fig. 5E and 8A, B). Glial cells in the ARC (Fig. 8C), inferior olive dorsal nucleus (IOD) in the brainstem (Fig. 8D), and spinal cord also showed TRPV5-immunostaining. Moderate TRPV5 immunofluorescence was observed in cells of the choroid plexus (Fig. 8E). TRPV5-immunoreactivity was observed along the blood vessels in cortex (Fig. 8F) and in the Pia mater (Fig. 8G). Few TRPV5-immunoreactive cells were also detected in close association with the blood vessels (Fig. 8F).

Phenotypic characterization of TRPV5-immunoreactive cells

In the cortex, GFAP-labelled astrocytes and their processes showed TRPV5 immunofluorescence (Fig. 9A-F). TRPV5-immunoreactive astrocytic endfeet-like processes were closely associated with the blood vessels in the cortex (Fig. 9G-L). TRPV5-immunoreactivity was more intense in the cell bodies (Fig. 9J-L) and end-feet processes of

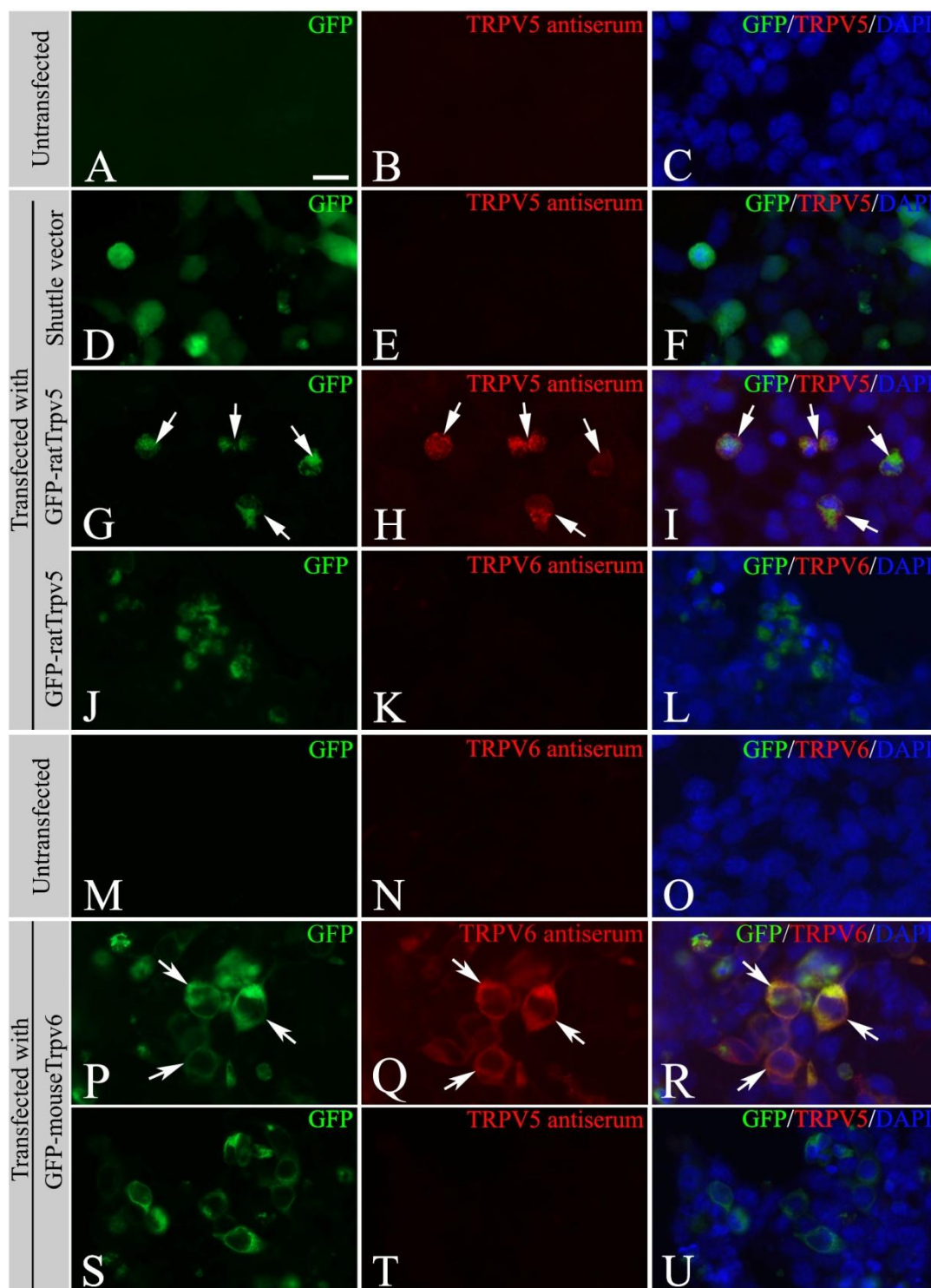


Figure 4: Specificity of TRPV5/6 antisera using transfection protocol. Fluorescence photomicrographs showing HEK293T cells (A-C, M-O) untransfected, and transfected with (D-F) shuttle vector, (G-L) GFP-ratTrpv5 cloned vector or (P-U) GFP-mouse Trpv6 cloned vector. No TRPV5/6 immunofluorescence is seen in untransfected cells or cells transfected with shuttle vector. TRPV5/6 immunofluorescence is observed in cells expressing GFP-Trpv5/GFP-Trpv6. Scale bar = 20 μ m.

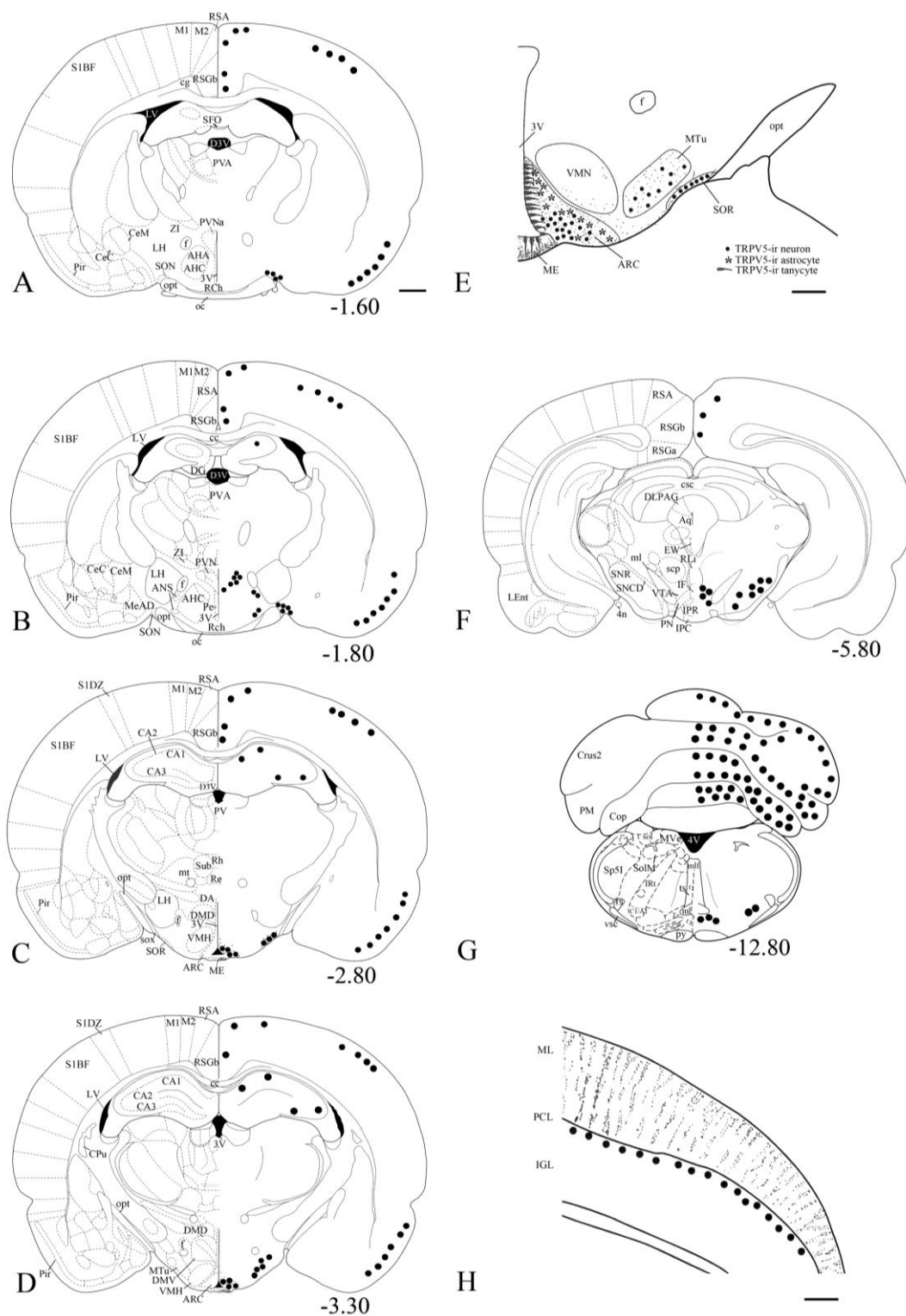


Figure 5: Schematics showing the organization of TRPV5-immunoreactive elements in the rat brain. Schematic drawings of the rostro-caudal series of the coronal sections (A-H) of rat brain adapted from Paxinos and Watson (38) [A: -1.6, B: -1.8, C: -2.80, D: -3.30, F: -5.80, and G: -12.80 relative to bregma] showing the cytoarchitectonic areas on left and TRPV5-immunoreactive neurons (closed circles) on the right. Enlarged view of the (E) hypothalamus and (H) cerebellum showing TRPV-5 immunoreactive cells, fibers and terminals. Scale bar = 1 mm in A-D, F and G, and 500 μ m in E and H.

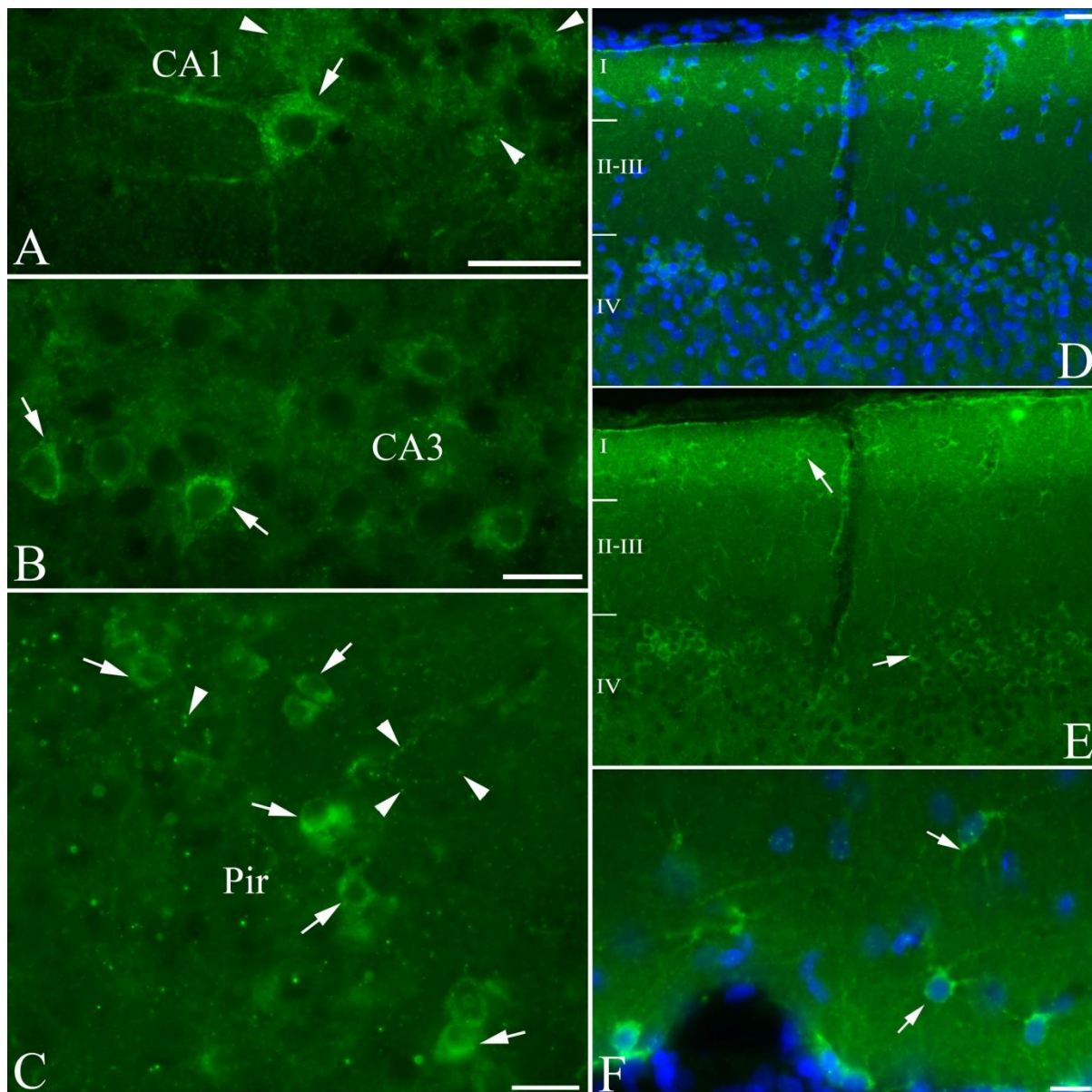


Figure 6: Organization of TRPV5-immunoreactive elements in the hippocampus and cortex. Photomicrographs showing the TRPV5-immunoreactive cells (arrows) and terminals (arrowheads) in (A) CA1 and (B) CA3 areas of the hippocampus, and (C) piriform cortex (Pir). Sections of the cortex counterstained with DAPI (blue) showing TRPV5-labeled cells (arrows) in (D-E) different layers of the cerebral cortex and (F) below the amygdala. Scale bar = 15 μ m.

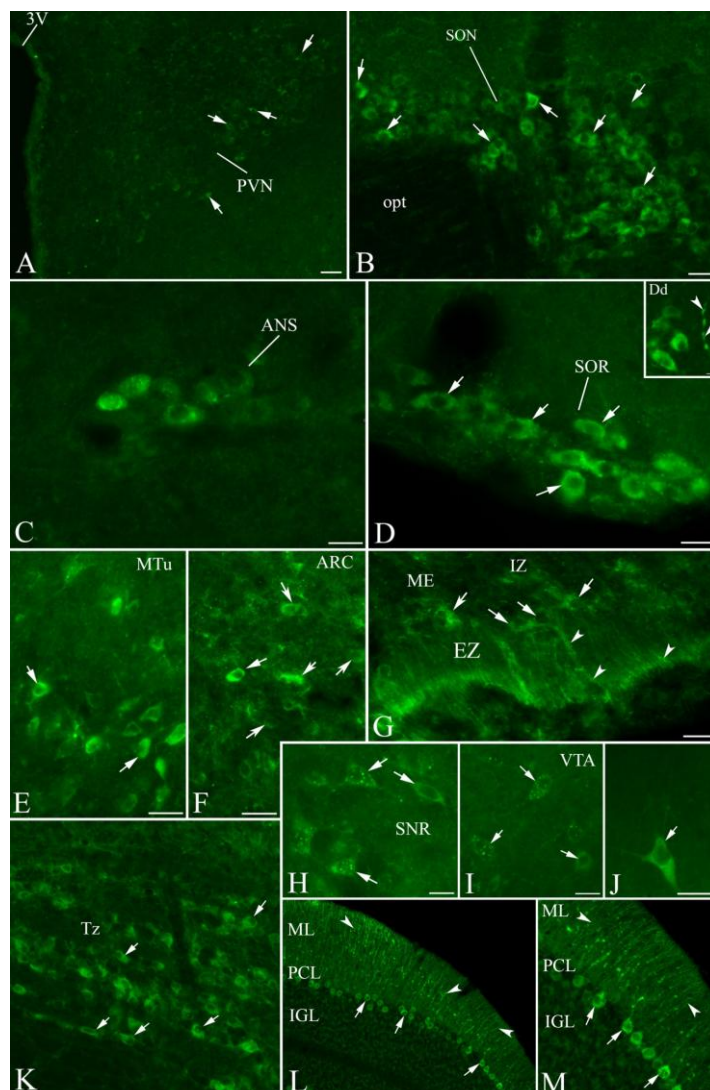


Figure 7: Organization of TRPV5-immunoreactive elements in the hypothalamus, midbrain, brainstem, and cerebellum. TRPV5-immunoreactive neurons (arrows) are seen in the hypothalamic (A) paraventricular nucleus (PVN), (B) supraoptic nucleus (SON), (C) accessory neurosecretory nuclei (ANS), (D) retrochiasmatic area of the SON (SOR), (E) medial tuberal nucleus (MTu), and (F) arcuate nucleus (ARC). (Dd) isolated TRPV5-immunoreactive fiber (arrowheads) is also seen in the SOR. (G) TRPV5 immunofluorescence is seen in the cells (arrows) of internal zone (IZ) of the median eminence (ME). TRPV5 labeled processes (arrowheads) are seen in the external zone (EZ) of the ME. In midbrain, TRPV5 labeled neurons (arrows) are seen in the (H) substantia nigra, reticular part (SNR) and (I) ventral tegmental area (VTA). In the brainstem, TRPV5 cells (arrows) are seen in the (J) C1/A1 region and (K) nucleus of the trapezoid body (Tz). In the cerebellum, (L, M) purkinje neurons (arrows) in the purkinje cell layer (PCL) and fibers (arrowheads) in the molecular layer (ML) with TRPV5-immunofluorescence are seen. Arrowheads indicate TRPV5-immunoreactive terminals. IGL, internal granule cell layer. opt, tract; 3V, third ventricle. Scale bar = 100 μ m in A; 25 μ m in B-J; 15 μ m in Dd; 10 μ m in K; and 25 μ m in L, M.

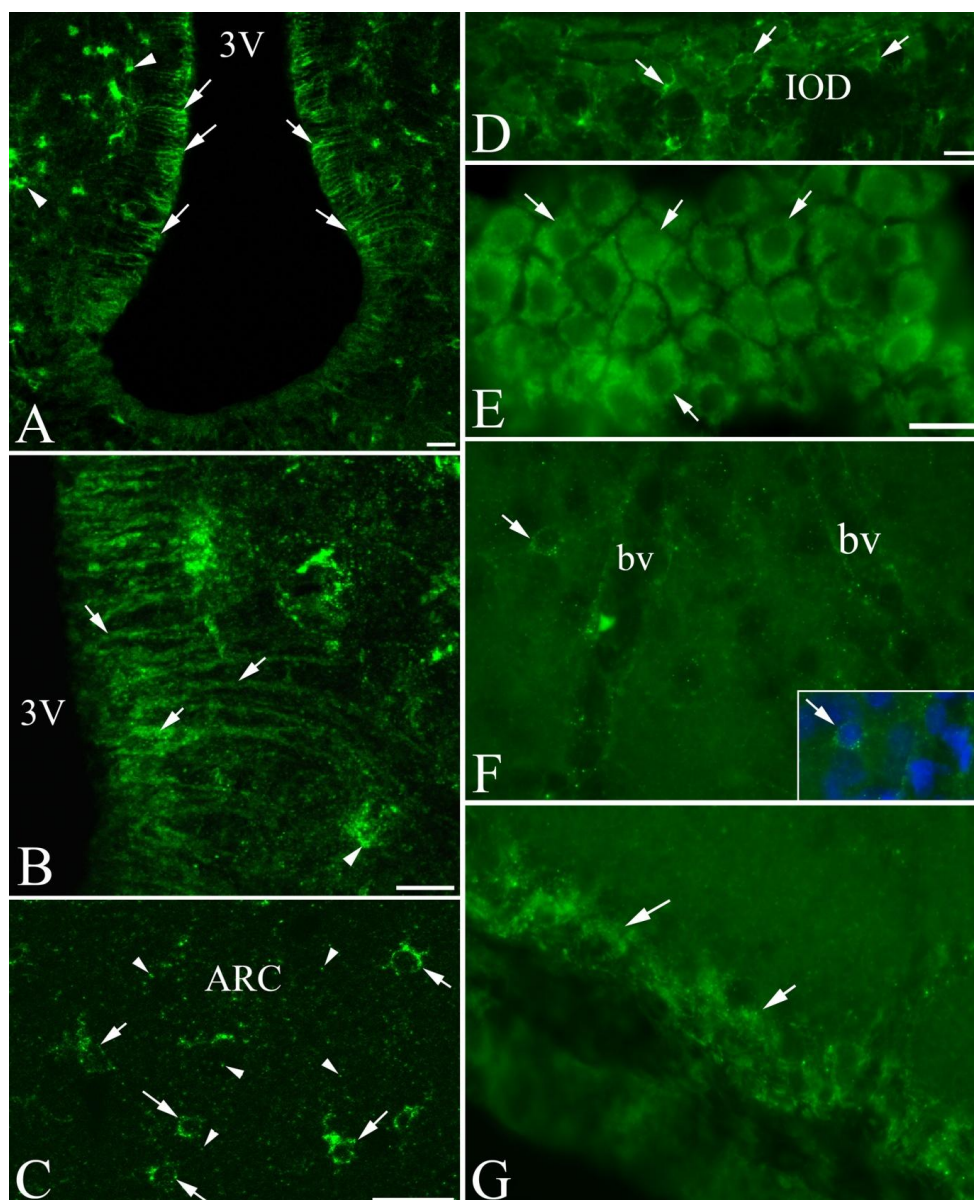


Figure 8: TRPV5-immunoreactive elements in the arcuate nucleus, brainstem, choroid plexus, around the brain blood vessel, and Pia mater. Photomicrographs showing TRPV5 immunofluorescence in the (A-C) mediobasal hypothalamus, (D) brainstem, (E) cells of the choroid plexus, (F) around the brain blood vessel (bv), and (G) Pia mater. (A, B) TRPV5-immunoreactivity is seen in tanycytes (arrows) and glial cells (arrowheads) in the mediobasal hypothalamus. Distinct TRPV5-immunoreactive glial cells (arrows) are seen in the (C) arcuate nucleus (ARC) and (D) inferior olive, dorsal nucleus (IOD) in the brainstem. (C) TRPV5 terminals (arrowheads) are seen in the ARC. (F) Isolated TRPV5-immunoreactive cell (arrow in F and also shown with DAPI in inset) is seen near the bv in the cortex. (A-C) confocal and (D-G) fluorescence photomicrographs. 3V, third ventricle. Scale bar = 25 μm in A, C and D-G; 10 μm in B.

the astrocytes (Fig. 9M-O). The vimentin-immunoreactive tanycytes lining the wall of third ventricle in the mediobasal hypothalamus were TRPV5-immunoreactive. In the hypothalamus, vasopressin and oxytocin neurons in the PVN, SON, ANS and SOR seem to be equipped with TRPV5 (Figs. 10 and 11; Table 3). Compared to oxytocin neurons, a vast majority of the vasopressin neurons in the PVN (Figs. 10A-C, M and 11A-C, M), ANS (Figs. 10G-I, O and 11G-I, O), and SON (Figs. 10D-F, N and 11D-F, N) were co-labelled with TRPV5 antiserum. In the SOR, $86.5 \pm 1.74\%$ oxytocin (Fig. 11J-L, P) and all vasopressin (Fig. 10J-L, P) neurons were TRPV5-immunoreactive.

TRPV5-immunoreactivity in the ARC shows estrous cycle-dependent changes

In the ARC, while both glial cells and neurons were TRPV5-immunoreactive (Fig. 12A-C), cells co-expressing ER α and TRPV5 were also seen. Application of TRPV5 and GFAP double immunofluorescence resulted in the labeling of TRPV5-expressing astrocytes in the ARC (Fig. 12A-F). Majority of CART neurons in the ARC also showed TRPV5-immunoreactivity (Fig. 12G-I). As described previously [20], iontophoretic injection of CtB in AVPV and MnPO, resulted in retrograde accumulation of CtB in ARC neurons (Fig. 12J, N). The CtB/CART neurons in ARC also contained TRPV5-immunoreactivity (Fig. 12J-Q). The CART neurons and astrocytes in ARC equipped with TRPV5 showed estrous cycle-related changes (Fig. 12R-U). Compared to proestrus phase, TRPV5-immunoreactivity in the astrocytes showed a significant increase during metestrus phases ($P < 0.05$). Further increase in TRPV5-immunoreactivity was observed in diestrus phase compared to proestrus, estrus, and metestrus phases ($P < 0.001$) (Fig. 12R-V). The percentage of CART/TRPV5 double-labelled neurons in the ARC, however, was significantly higher ($P < 0.001$) in the estrus, metestrus, and diestrus phases, compared to those in the proestrus phase (Fig. 12W).

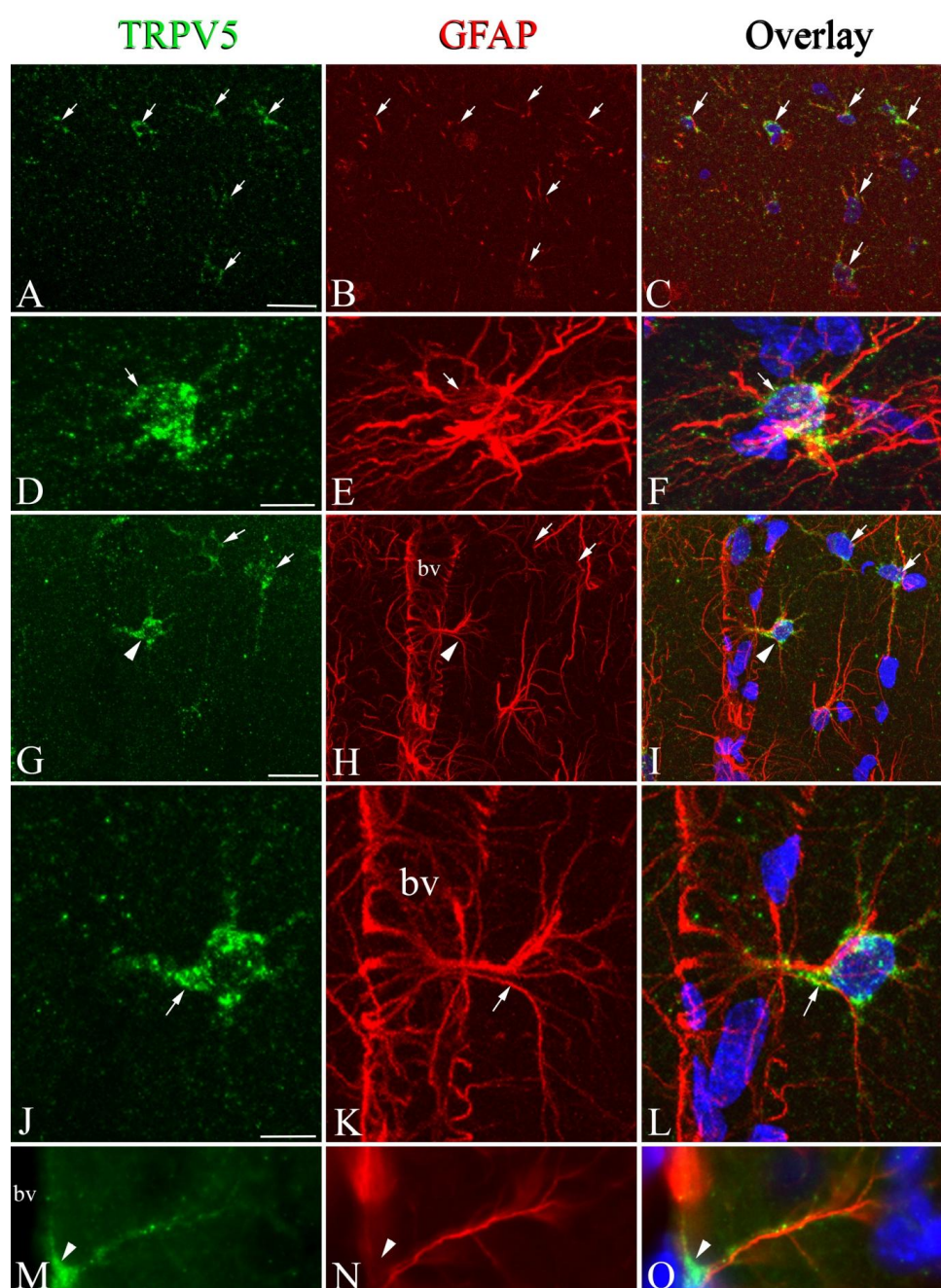


Figure 9: TRPV5-immunoreactive astrocytes in the cerebral cortex. Confocal photomicrographs of the coronal sections through the cerebral cortex showing (A-C) TRPV5 immunoreactivity (green) on GFAP labelled astrocytes (red). Astrocytes showing TRPV5 immunofluorescence (arrows) are seen. (D-F) Magnified view of an astrocyte equipped with TRPV5-immunoreactivity (arrow). (G-I) TRPV5-immunoreactive astrocytes (arrows) are seen around the brain blood vessel (bv). An astrocyte equipped with TRPV5 is associated with bv (arrowhead in G-I). TRPV5-labeled astrocyte in (G-I) is shown at higher magnification in (J-L, arrow). (M-O) TRPV5-immunoreactive endfeet-like process of the astrocyte in close association with the bv (arrowhead). Scale bar = 25 μm in A-C and G-I; 10 μm in D-F and J-O.

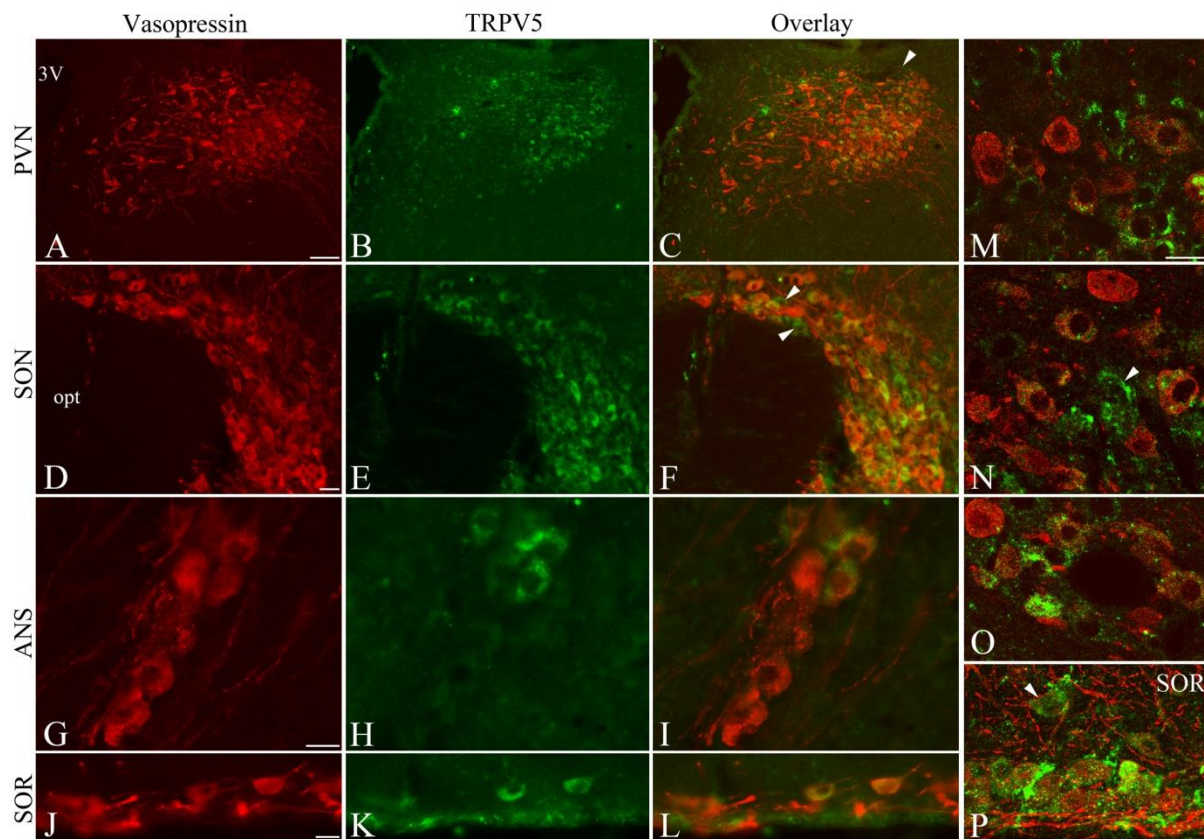


Figure 10: Hypothalamic vasopressin neurons are equipped with TRPV5. Fluorescence (A-L) and Confocal (M-P) photomicrographs showing association between vasopressin (red) and TRPV5 (green) in the hypothalamic paraventricular nucleus (PVN, A-C and M), supraoptic nucleus (SON, D-F and N), accessory neurosecretory nuclei (ANS, G-I and O), and retrochiasmatic part of the SON (SOR, J-L and P). Note the presence of TRPV5 on vasopressin neurons in each of these nuclei. Isolated TRPV5 neurons are also seen (arrowheads). opt, optic tract; 3V, third ventricle. Scale bar = 100 μ m in A-C and 25 μ m in D-P.

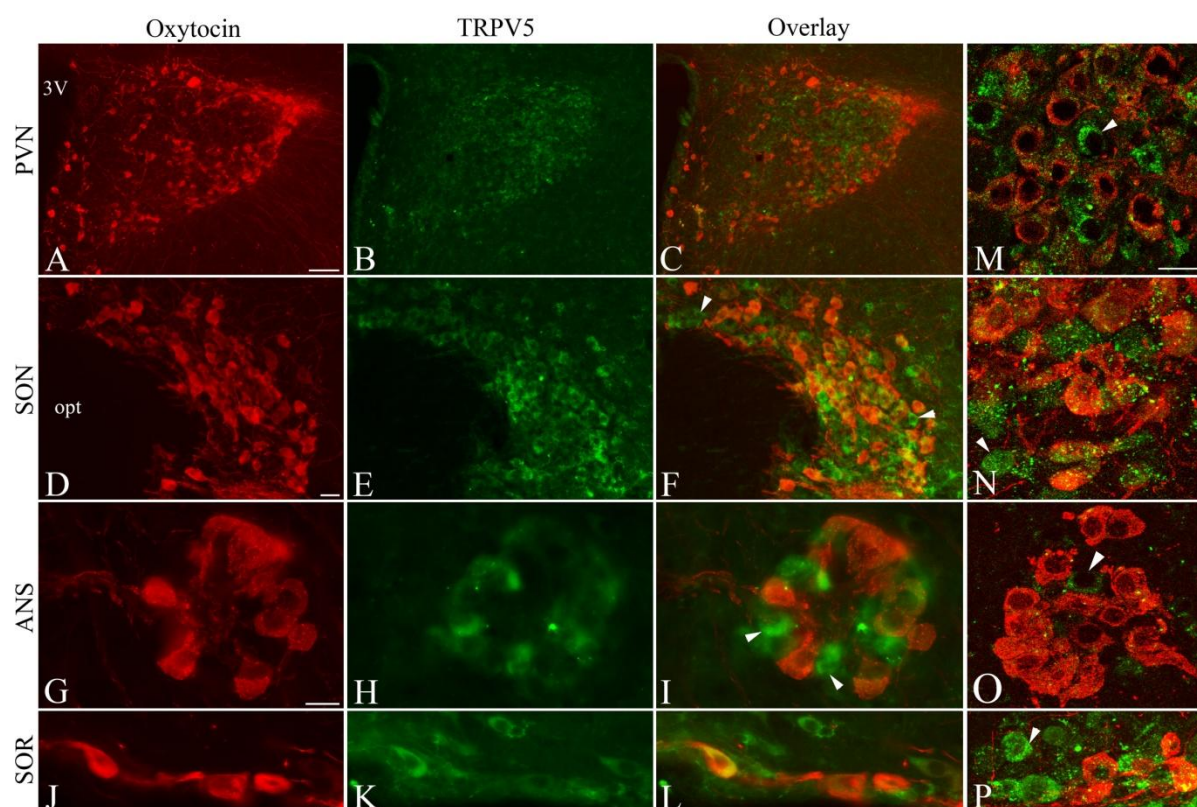


Figure 11: Hypothalamic oxytocin neurons co-express TRPV5. Fluorescence (A-L) and Confocal (M-P) photomicrographs showing association between oxytocin (red) and TRPV5 (green) in the hypothalamic paraventricular nucleus (PVN, A-C and M), supraoptic nucleus (SON, D-F and N), accessory neurosecretory nuclei (ANS, G-I and O), and retrochiasmatic part of the SON (SOR, J-L and P). Note the presence of TRPV5 on oxytocin neurons in each of these nuclei. Isolated TRPV5 neurons are also seen (arrowheads). opt, optic tract; 3V, third ventricle. Scale bar = 100 μ m in A-C and 25 μ m in D-P.

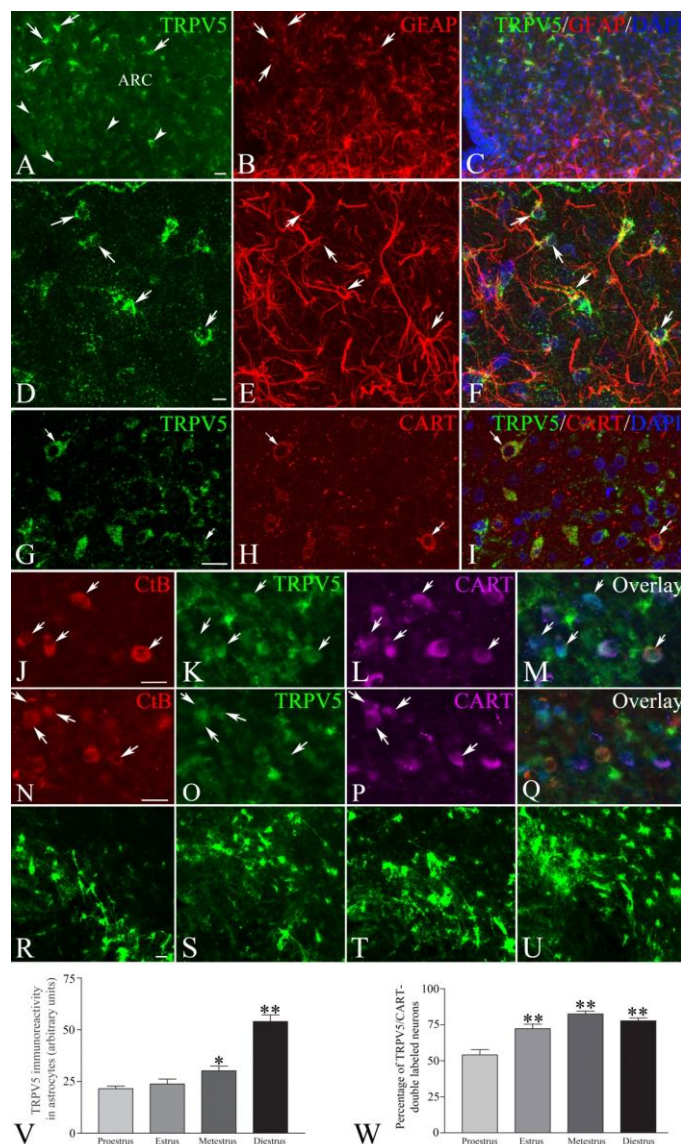


Figure 12: TRPV5-immunoreactivity in the arcuate nucleus shows estrous cycle-related changes. Immunofluorescence (A-C) and confocal (D-I) photomicrographs of the coronal sections through mediobasal hypothalamus of rat showing TRPV5-immunofluorescence (green) on (A-F) astrocytes (arrows in A-C) and neurons (arrowheads in A). (G-I) CART neurons in the arcuate nucleus (ARC) show TRPV5 immunofluorescence (arrows). (J-Q) CART neurons (magenta) in ARC equipped with TRPV5 (green) showing retrograde accumulation of cholera toxin beta subunit (red) injected in either (J-M) median preoptic nucleus (MnPO) or (N-Q) anteroventral periventricular nucleus (AVPe). Note CtB/TRPV5/CART the triple labeled neurons in ARC (arrows). TRPV5-immunoreactivity in the ARC during (R) proestrus, (S) estrus, (T) metestrus, and (U) diestrus phases of the estrus cycle. Semiquantitative image analysis of the (V) TRPV5-immunoreactivity in astrocytes and (W) percentage of CART neurons expressing TRPV5, in the ARC during estrous cycle. (V) *, $P < 0.05$ compared to proestrus phase and **, $P < 0.001$ compared with proestrus, estrus, and metestrus phases. (W) **, $P < 0.001$ compared to proestrus phase. Scale bar = 25 μm in A-C and R-U, 10 μm in D-Q.

Table 3: Semi-quantitative analysis of the percentage of hypothalamic oxytocin and vasopressin neurons co-expressing TRPV5

Neuropeptides	PVN	SON	ANS	SOR
Vasopressin	50.73 ± 3.82	75.91 ± 2.34	49.12 ± 4.28	100%
Oxytocin	6.88 ± 1.21	63.34 ± 5.69	20.40 ± 4.14	86.5 ± 1.74%

DISCUSSION

Using qRT-PCR, presence of TRPV5 mRNA expression has been demonstrated in the brain of mouse [257]. On the similar lines, we investigated the TRPV5 mRNA expression and neuroanatomical organization of the channel proteins expressing elements in different brain compartments of rat. TRPV5 immunoreactivity was noticed in the neurons as well as glia in several areas, hypothalamus being most conspicuous. Distinct TRPV5-immunoreactivity was noticed in the neuroendocrine neurons of the PVN, SON, and SOR. Oxytocin and vasopressin neurons in these nuclei, tanycytes in the medio-basal hypothalamus, and astrocytes along with their end-feet like processes associated with blood vessels seem equipped with TRPV5. Presence of TRPV5 on oxytocin and vasopressin neurons and the estrous-cycle dependent changes in the TRPV5-immunoreactivity in the ARC, suggests the neuroendocrine salience of TRPV5. To our knowledge, this is also the first report describing neuroanatomical organization of TRPV5, a highly Ca^{2+} -selective TRP channel-expressing elements in the brain. The importance of thermosensitive TRPV-channels *viz.*, TRPV1, TRPV2, and TRPV4 in the neuroendocrine regulation has been suggested [33,202,203,282]. TRPV5 and TRPV6 are known as highly Ca^{2+} selective TRP channels. Recently, we have demonstrated the neuroanatomical organization of TRPV6 in mouse brain [201]. While TRPV6-expressing elements were widely organized in the brain, hypothalamic neurons were equipped with this ion channel. The TRPV6 protein expression in ARC showed estrous cycle dependent changes.

The TRPV5 antiserum used in the present study was raised against fifteen amino acids human TRPV5 sequence, which shares 73% similarity with rat TRPV5. The specificity of the TRPV5 antiserum in rat brain was further validated by preadsorption of the antiserum with control peptide. Antisera from two different sources showed comparable immunoreactivity pattern in the brain. The specificity of the TRPV5 antiserum was further

validated using siRNA treatment and transfection protocols. The TRPV5-immunoreactivity in the rat pituicytes, hypothalamic SOR, and cerebellar purkinje neurons responded to TRPV5 siRNA treatment with a reduction in TRPV5-immunoreactivity, suggesting the specificity of the antiserum. In the hypothalamic and cerebellar tissue, treatment with TRPV5 siRNA resulted in a significant reduction ($P < 0.001$) in the TRPV5-ir band. We believe that the siRNA may block the further synthesis of the channel proteins but not affect the protein already synthesized. The TRPV5 antiserum used in the present study has previously been used to localize TRPV5 in the kidney [283]. The kidney tissue therefore served as positive control. The Western blot analysis of the hypothalamus, cerebellum, and kidney yielded similar results, and one prominent band at 65-68 kDa was consistently observed. Previously, while the application of TRPV5 antiserum revealed two bands in the human retinal pigment epithelium [284], TRPV5-immunoreactive bands of varying sizes were observed in the membrane extracts and soluble fractions of the human parathyroid gland [285]. These authors observed a prominent band at around 75-80 kDa but additional weaker bands at ~135, 110, and 47-60 kDa were also seen. The band sizes ranging between 85–100 kDa were also observed in the lysates of cells expressing recombinant TRPV5 and presence of mature glycosylated TRPV5 protein was suggested [286]. Multiple bands of TRPV5 have also been observed previously [287,288]. More than one band might represent two types of post-translational modifications or two levels of glycosylation [287]. The Western blot analysis of the *Xenopus laevis* oocyte homogenate showed three TRPV5 bands, which represents the core-glycosylated, complexly-glycosylated, and unglycosylated forms [289]. While one band was observed between 75 and 100 kDa, other two bands were seen below 75 kDa [289]. In the present study, the 65-68 kDa TRPV5-immunoreactive band responded to TRPV5 siRNA treatment and might represent the core TRPV5 band. Presence of TRPV5-ir band below the predicted molecular weight of TRPV5 is not surprising since in previous

studies application of a specific TRPV5 antiserum was unable to detect a band of appropriate molecular weight [290]. Western blot analysis of the HEK293 cells transfected with TRPV5 [291] and *N*-glycosylation-deficient mutant TRPV5^{N358Q} [292] showed a TRPV5-ir band of less than 75 kDa. Our observation of the 65-68 kDa TRPV5-ir band is in agreement with these reports. The HEK293T cells were transfected with GFP-ratTrpv5 vector and the transfected cells showed TRPV5 immunofluorescence, suggesting the specificity of TRPV5 antiserum. Application of qRT-PCR technique revealed TRPV5 mRNA expression in the olfactory bulb, cortex, hypothalamus, hippocampus, midbrain, brainstem, and cerebellum. However, in some discrete areas like hypothalamus, cerebellum and hippocampus, dissimilar expression pattern across qRT-PCR and immunofluorescence preparations were encountered. While the present study clearly demonstrates the presence of TRPV5 in various regions of the brain, the lack of correspondence might be due to the difference in the expression levels of transcript and channel protein.

Although TRPV5 cells were widely distributed in the brain, a discrete organizational pattern was observed in the hypothalamus. TRPV5-immunoreactive cell bodies were detected in the PVN, SON, ANS and SOR. However, with the exception of some isolated fibers in the SOR, no immunoreactive fibers were observed in the hypothalamus. Among the different immunoreactive groups in the hypothalamus, the neurons in the SOR showed maximum immunoreactivity. Both SON and SOR share similarities including the presence of oxytocin and vasopressin neurons and are the part of the neuroendocrine effector systems. These regions show activation following exposure to 38.5 °C [293]. TRPV channels seem novel component of the regulatory system controlling neuroendocrine neurons. The neurons in SON express N-terminal variant of TRPV1 and this variant seem essential for osmosensory transduction in vasopressin neurons [251]. Evidence suggests that the deletion of TRPV1 results in loss of the intrinsic response of vasopressin neurons to hyperosmotic challenge

[251]. Importance of TRPV2 in the regulation of vasopressin as well as oxytocin neurons has been suggested [203]. In view of the neuroendocrine importance of TRPV [33,203,282] and high Ca^{2+} selectivity of TRPV5, we speculate that the regulation of oxytocin and vasopressin neurons in the PVN, SON, ANS, and SOR might be mediated by TRPV5. The neuroendocrine significance of TRPV ion channels may further be supported by occurrence of TRPV6 in the neuroendocrine neurons in hypothalamus and modulation of TRPV6 protein expression in the mediobasal hypothalamus during estrous cycle [201]. We suggest that TRPV5 and TRPV6 may serve as crucial regulators of the neuroendocrine pathways in the brain. In the midbrain, TRPV5 cells were observed in the VTA and SN. While presence of TRPV3 has been demonstrated in the SN of rat, the neurons showed increased firing following exposure to 39 °C [294]. Both VTA and SN contain dopamine neurons and control reward and motor movements, respectively [295]. We suggest that the dopamine neurons in VTA and SN might be equipped with TRPV5. Neurons in C1/A1 area, nucleus of the trapezoid body in the brainstem, and Purkinje neurons in the cerebellum were equipped with TRPV5 and role of these channels in the regulation of these neurons is suggested. In the cortex, astrocytes showed TRPV5 immunofluorescence and were associated with the blood vessels. Both, expression of TRPV channels on the astrocytes [252,296,297] as well as their importance in the regulation of Ca^{2+} dynamics has been demonstrated [253]. In view of the higher Ca^{2+} selectivity, presence of TRPV5 on astrocytes in close association with blood vessels may play role in regulation of cerebrovasculature and sensing of blood-borne molecules.

ARC contains neurons that synthesize neuropeptide Y/agouti-related peptide, and other subpopulation producing CART/proopiomelanocortin [22]. While the importance of the ARC CART neurons in food intake and energy balance is well established, recent evidence suggest role of this subpopulation in the regulation of GnRH neurons and

reproduction [83]. CART neurons of ARC innervate GnRH neurons in POA, CART peptide treatment increases neuronal firing in GnRH neurons [83], and the CART neurons respond to ovariectomy and estradiol treatment [265]. Using retrograde neuronal tracing, CART neurons in the ARC have been shown to project to the MnPO and AVPe regions in POA [20]. We observed that the ARC CART neurons projecting to AVPe and MnPO co-express TRPV5, suggesting role of these ion channels in the modulation of CART-GnRH pathway. In the ARC of ewes, orphanin FQ neurons co-express POMC and these neurons showed presence of ER α [180]. Since POMC and CART are colocalized in the ARC [24], possibility exists that CART neurons of the ARC also express ER α . There seems an inverse relationship between estradiol and ER expression in the ARC. In ovariectomized rats, estradiol treatment resulted in 64% reduction in the ER mRNA in the ARC [122]. Majority of the dopaminergic neurons in the ARC express ER α during diestrus phase but showed significant reduction during proestrus phase [123], when plasma estradiol levels remain high [124]. As compared to proestrus phase, we observed a significant increase in the percentage of CART neurons expressing TRPV5 in the estrus, metestrus, and diestrus phases. It is interesting to note that estradiol treatment modulates TRPV5 expression in the kidney [140] and intracellular Ca²⁺ *via* TRPV5 in the cortical collecting duct cells of rat [207]. We suggest that *via* ER α the changes in circulating estradiol levels may modulate recruitment of TRPV5 channels on CART neurons of ARC during estrous cycle. A significant increase in TRPV5-immunoreactivity in the astrocytes of ARC was observed during the metestrus and diestrus phases. The role of estradiol in the regulation of astrocytes in the ARC *via* TRPV5 seems valid since astrocytes in this nucleus express ER α [263]. While we suggest a role of TRPV5 ion channels in the regulation of ARC neurons, further studies are essential to determine the significance of TRPV5 ion channels in the ARC and their relevance to reproduction. It is interesting to note that the TRPV6 protein expression in mediobasal hypothalamus showed

estrous cycle-dependent changes, with higher expression during proestrus [201]. We suggest that TRPV5 and TRPV6 in the hypothalamus might be regulated by circulating estradiol levels in opposite manner.

In summary, TRPV5 is expressed in several discrete nuclei as well as glial cells in the brain. While TRPV channels play an important role in neural regulation, activity of these ion channels in neurons modulate signaling cascade by increasing or decreasing intracellular Ca^{2+} levels [33]. In view of this and high Ca^{2+} -selectivity feature of TRPV5, discrete organization of these channel protein-expressing cells in the hypothalamus, regulation by circulating levels of estradiol, and co-expression on CART, oxytocin, and vasopressin neurons in the hypothalamus, we suggest that TRPV5 may play a role in neuroendocrine regulation. The present observations will set basis for future studies exploring significance of TRPV5 in the brain.

CHAPTER 4

ORGANIZATION OF TRANSIENT RECEPTOR POTENTIAL VANILLOID 6 (TRPV6)-EQUIPPED ELEMENTS IN THE BRAIN, ESTROUS CYCLE-RELATED CHANGES IN THE HYPOTHALAMUS, AND ROLE IN REGULATION OF ARCUATE NUCLEUS NEURONS

Kumar S, Singh U, Singh O, Goswami C, Singru PS. (2017). Transient receptor potential vanilloid 6 (TRPV6) in the mouse brain: Distribution and estrous cycle-related changes in the hypothalamus. *Neuroscience* 344: 204-216.

INTRODUCTION

Transient receptor potential vanilloid (TRPV) are cation channels gated by a range of stimuli including heat, mechanical stretch, osmotic pressure, and steroid hormones [33,214,298]. TRPV subfamily consists of six members viz., TRPV1-6 [137]. TRPV1-4 are thermosensitive, non-selective cationic channels and suggested to play a role in neural regulation. Although the distribution and functional significance of TRPV1-4 in the brain has been explored [33,202,203,213,215–217,235,269,271,272], relevant information about TRPV5 and TRPV6 is not available. TRPV5 and TRPV6 draws attention as they have been identified as unique members of the TRP superfamily and are distinct from other members of TRPV subfamily [299]. They are close homologs, highly selective for Ca^{2+} (permeability ratio $P_{\text{Ca}}/P_{\text{Na}} > 100$) [298–300], but does not seem responsive to temperature. Although only TRPV6-like gene was observed in fish and birds, both TRPV5 and TRPV6 are present in mammals [299]. Due to gene duplication, TRPV5 might have been produced from TRPV6 during evolution [299]. TRPV6 has been suggested to serve as Ca^{2+} entry channel for the transcellular Ca^{2+} transport pathway [299] and TRPV6 knockout mice showed phenotypes associated with impaired Ca^{2+} homeostasis [301–303]. While the studies exploring presence and role of TRPV5 and TRPV6 were mostly focussed on peripheral tissues including kidney, gastro-intestinal tract, uterus, and placenta [257,299], RT-PCR analysis demonstrated the presence of TRPV5 and TRPV6 mRNA in the mouse brain [257]. Although higher TRPV6 mRNA expression was observed in the mouse brain compared to TRPV5 [257], the lack of information on neuroanatomy of neural elements expressing these ion channels has posed a major impediment in understanding its functional significance in the brain.

Using the TRPV6 specific antiserum, we explored the neuroanatomical organization of TRPV6-immunoreactive elements in the brain of mouse. Estradiol seems to

be a potential regulator of TRPV6 in the peripheral tissues. Increase in TRPV6 mRNA expression was observed in the uterus of rodents during pregnancy and estrus phase of estrous cycle [206,212]. In immature mice, estradiol-induced increase in TRPV6 mRNA expression in the uterus was attenuated by pre-treatment with estrogen receptor antagonist [206]. While the duodenal TRPV6 expression was increased by estradiol treatment in ovariectomized rats, 55% reduction in TRPV6 was observed in estrogen receptor alpha (ER α) knockout mice [141]. Presence of estrogen response element has been described in promoter region of mouse TRPV6 gene [34] and regulation of TRPV6 by estrogen *via* ER α -dependent pathway has been suggested [206]. The mediobasal hypothalamus (MBH) serve as the primary site for feedback effect of estradiol [304]. In MBH, neurons in the hypothalamic arcuate nucleus (ARC) express ER α [305,306] and these neurons mediate negative feedback effect of estrogen on gonadotropin secretion [307]. Double immunofluorescence was employed to find out if TRPV6-immunoreactive cells in ARC co-express ER α . Using Western blot analysis, changes if any in the TRPV6 protein expression in the MBH during different phases of the estrous cycle were studied.

MATERIALS AND METHODS

Animals

Adult, male and female, BALB/c mice [25-30 g body weight (BW)] were used in the study. Mice were maintained under standard environment of the animal facility. Food and water were provided *ad libitum*. All the experimental protocols were reviewed and approved by the Institutional Animal Ethical Committee (IAEC) at the National Institute of Science Education and Research (NISER), Bhubaneswar, under the Committee for the Purpose of Control and Supervision of Experiments for Animals (CPCSEA), New Delhi, India.

Tissue processing

Mice were deeply anaesthetized with intraperitoneal (i.p.) injection of a mixture containing ketamine [Neon Laboratories Ltd., Mumbai, India; 80 mg/kg body weight (BW)] and xylazine (Stanex Drugs and Chemicals Pvt. Ltd., Hyderabad, India; 10 mg/kg BW). The animals were perfused transcardially with ice-cold phosphate buffered saline (PBS, pH 7.4) followed by 60 ml 4% paraformaldehyde in phosphate buffer (PB, pH 7.4). The brains were removed, post-fixed in 4% paraformaldehyde and cryoprotected in 25% sucrose solution in PBS. Serial 25 µm thick coronal sections through the rostro-caudal extent of the brain were cut on a cryostat (Leica CM3050 S, Leica Microsystems, Nussloch GmbH, Germany) and four sets of free floating sections were collected in PBS. The sections were kept in the anti-freezing solution for 4 h at room temperature and stored at -20 °C until processed further. For specificity controls, dorsal root ganglia (DRG) of rat and kidney tissues of mice were isolated, postfixed, and sectioned on the cryostat. The sections were collected on the poly-L-lysine coated slides and stored at -20 °C.

Immunofluorescence/immunohistochemistry

One set of sections from each mice ($n = 5$) was processed for TRPV6 immunofluorescence. Sections were immersed in 0.5% Triton X-100 in PBS for 20 min to improve antibody penetration and incubated in blocking solution (3% normal horse serum, 0.1% Triton X-100, 0.08% sodium azide) for 30 min. Sections were incubated in rabbit polyclonal TRPV6 antiserum (Alomone Labs., Jerusalem, Israel; Cat. # ACC-036) at 1:1000 dilution for 24 h at 4 °C. Following rinsing in PBS, sections were incubated in biotinylated goat anti-rabbit IgG (Jackson Immunoresearch, West Grove, USA; 1:400) and later in streptavidin-peroxidase (ABC, 1:1000, Vector Laboratories, Burlingame, USA). Sections were processed for biotinylated tyramide amplification as per the instructions of the manufacturer (NEN Life Sciences, Boston, MA), rinsed in PBS and incubated in DTAF-avidin (1:300, Jackson ImmunoResearch) for 4 h at room temperature.

To determine whether TRPV6 labelled neurons in the ARC co-express ER α / CART/ NPY sections containing ARC were processed for double immunofluorescence. Sections were processed for TRPV6 immunofluorescence as mentioned above. Sections were further rinsed several times in PBS, treated with blocking solution for 30 min, and incubated in rabbit polyclonal ER α / rabbit polyclonal CART/ sheep polyclonal NPY antisera for 24 h at 4 °C. Sections were rinsed in PBS, and incubated in Alexa Fluor-594-conjugated anti-rabbit/ anti-sheep IgG (Invitrogen, 1:1000).

To find out if TRPV6 equipped CART neurons of ARC innervate preoptic area, rostro-caudal series of sections containing ARC from rat brains of retrograde neuronal tracer in MnPO and AVPe regions as described in Chapter 3 (Material and method section, Retrograde neuronal tracing paragraph) were employed for sequential triple immunofluorescence using goat anti-CtB (1:5000) and rabbit anti-TRPV6 (Alomone, 1:1000). The TRPV6 signal was amplified using BT and visualized using DTAF-avidin

(1:300) and CtB cells in ARC were detected using AlexaFluor594-anti-goat IgG (1:1000). The sections were rinsed in PBS several times and incubated in rabbit anti-CART (55-102) (1:5000) followed by incubation in DyLight649-conjugated donkey anti-rabbit IgG (BioLegend, 1:1000 dilution).

Sections of the DRG, kidney and cerebellum were processed for immunohistochemistry as previously described [308]. Sections were treated with 0.5% Triton X-100 in PBS followed by 3% normal horse serum in PBS, and incubated in TRPV6 antiserum (1:1000) for 24 h at 4 °C. Sections were rinsed in PBS and incubated in biotinylated goat anti-rabbit IgG (Vector Laboratories, Burlingame, USA, 1:400) for 2 h followed by streptavidin-peroxidase (ABC, Vector, 1:100) for 2 h. Following rinsing in PBS and Tris buffer (pH 7.6), sections were incubated in 0.025% diaminobenzidine containing 0.0036% H₂O₂ in 0.05 M Tris buffer pH 7.6 for 5 min. All the sections/slides were rinsed in PBS, mounted on glass slides, and coverslipped with Vectashield mounting medium.

All the fluorescently labelled sections were observed under AxioImager M2 fluorescence microscope (Carl Zeiss, Germany).

Neuroanatomical description, nomenclature, and schematics showing the distribution of TRPV6 cells and fibers in the mouse brain were adopted from the mouse brain atlas [309]. Description of the relative intensity and density of TRPV6 cells and fibers in the mouse brain is given in Table 1.

Specificity of TRPV6 antiserum

Details of the antisera and their dilutions used for localization of TRPV6 in the mouse brain, and the phenotypic characterization of TRPV6-expressing cells are given in Appendix 1. The specificity of TRPV6 antiserum has already been established [310,311].

Using Western blot analysis, the antiserum has been shown to recognize TRPV6 in prostate carcinoma cell line (LNCaP) endogenously expressing the ion channels [311]. In human embryonic kidney (HEK) cells transfected with TRPV6-YFP, specificity of the antiserum has been demonstrated using immunofluorescence and Western blot [310]. The specificity of the antiserum to recognize mouse TRPV6 has also been established [312,313]. The affinity purified TRPV6 antiserum was raised against a synthetic peptide (NRGLEDGESWEYQI), corresponding to the amino acid residues 712-725 of C-terminus end of human TRPV6. The human and mouse TRPV6 sequences were aligned using CLUSTAL-OMEGA. The sections of the brain were incubated in diluted TRPV6 antiserum. The diluted antiserum was preadsorbed with the control peptide (Alomone Labs) at 1:1 ratio for 24 h and applied on the sections of the brain. Using this antiserum, the manufacturer has demonstrated TRPV6 immunofluorescence in the sensory neurons of DRG (Alomone Labs) and presence of TRPV6 has been demonstrated in the mouse kidney [257]. DRG and kidney tissues therefore served as positive controls. To determine whether the antiserum recognizes TRPV6 in the mouse brain, western blot analysis of the mouse hypothalamus was performed as described below.

Total RNA isolation and RT-PCR

Adult, female, mice were anesthetized with an i.p. injection of a mixture containing ketamine (80 mg/kg BW) and xylazine (10 mg/kg BW), brains were dissected out, quickly frozen in dry ice, cut on a cryostat, and a block of tissue containing the hypothalamus was isolated. Total RNA was isolated from mouse hypothalamus using TRIzol[®] Reagent (Ambion) and quantified using NanoDrop 2000 Spectrophotometer (Thermo Scientific) and then stored in -80°C. The cDNA was synthesized using high-capacity cDNA reverse transcription kit (Applied Biosystems). TRPV6 cDNA was PCR amplified using total cDNA

(0.5 μ l) as template, mouse TRPV6 gene specific primers (forward primer: 5'-GGGGTTAATACTCTGCCTATGG-3', and reverse primer: 5'-GCACCTCACATCCTTCAAACCTT-3'; [231] and the Phusion High-Fidelity PCR kit (Cat. # E0553S, BioLabs). The PCR product along with Gene Ruler 100 bp DNA ladder (Gene Ruler, Cat. No. SM0243, Thermo Scientific) was electrophoresed on 1.7% agarose gel and visualized in the Gel Doc (Bio-Rad).

Estrous cycle-related changes in TRPV6 in the mediobasal hypothalamus

Adult, female mice were employed to study the estrous cycle-related changes in TRPV6 in the mediobasal hypothalamus (MBH). Animals were handled every morning 8:00-9:00 am for a week prior to experiment to reduce the handling-related stress. The estrous cycle was assessed by vaginal smear cytology: predominant nucleated epithelial cells in proestrus; cornified cells in estrus; mixture of leukocytes, nucleated epithelial cells and cornified cells in metestrus; and predominant leukocytes in diestrus [230]. Vaginal smears were collected over glass slides between 8:00-9:00 am everyday by flushing vagina gently with 10 μ l 0.01 M PBS, pH 7.4 using pipette after cleaning the vagina with PBS-soaked cotton balls. The unstained slides having vaginal smears (flush) were observed under light microscope with a 10X objective. Three mice per stage of estrous cycle were anesthetized with i.p. injection of a mixture containing ketamine (80 mg/kg BW) and xylazine (10 mg/kg BW), brains were dissected out, frozen on dry ice, and stored at - 80 °C until processed further. MBH was isolated from each brain and further processed for Western blot analysis as described below.

Western blot analysis

To determine the specificity of the TRPV6 antiserum and study the estrous cycle-related changes in TRPV6 expression in MBH, Western blot analysis was performed. Mice were anaesthetised with i.p. injection of a mixture containing ketamine (80 mg/kg BW) and xylazine (10 mg/kg BW) and decapitated; brain was dissected out, and frozen on dry ice. Using cryostat, a tissue block containing the hypothalamus was isolated from each animal, lysed in 10 mM Tris-Cl, pH 8.0 buffer in the presence of HaltTM protease inhibitor cocktail (Thermo Scientific) in a tissue lyser (Qiagen) and centrifuged at 4°C for 30 min (Laura Giusti, J cell Mol Med., 2014). The supernatant was collected and total protein was estimated using Bradford reagent (Sigma). The protein sample along with protein marker (Fermentas, Cat# SM0671) in adjacent lane was electrophoresed using minigel apparatus (BioRad). Similarly, 40 µg of the protein isolated from mediobasal hypothalamic tissue from mouse in each phase of the estrous cycle, was resolved on 9 % SDS-PAGE. Proteins were transferred to Immobilon®-P Polyvinylidene Difluoride membrane (PVDF, Sigma) using wet-transfer system (Biorad). The blots were incubated with mouse monoclonal GAPDH antibody (Abgenx, 100 ng/ml) and rabbit polyclonal TRPV6 antiserum (Alomone, 50 ng/ml) followed by goat anti-mouse and anti-rabbit horseradish peroxidase-conjugated antibodies (Cell Signaling, 1:10000), respectively. The signal was detected in ChemiDoc (Biorad) using Chemiluminescent HRP substrate (Millipore). The band intensities were measured using Quantity One software. The percentage intensity of TRPV6 protein relative to GAPDH (loading control) was calculated. The values were represented as mean ± SEM.

Statistical analysis

Changes in TRPV6 protein expression in MBH during estrous cycle (3 mice per phase of the estrous cycle) was analysed in GraphPad Prism using One-way ANOVA

followed by Bonferroni's Multiple Comparison Test. $P < 0.05$ was considered statistically significant.

RESULTS

Specificity of TRPV6 antiserum

CLUSTAL-OMEGA analysis of the human and mouse TRPV6 showed a high degree of similarity (Fig. 1A). The fourteen amino acid human TRPV6 peptide against which the antiserum was raised has 92.9% sequence identity with mouse TRPV6 (Fig. 1A). Application of TRPV6 antiserum on sections of the mouse brain resulted in labelling of neurons in the SON (Fig. 1B) and other brain regions. No immunoreactivity was observed in the brain following application of the antiserum preadsorbed with the control TRPV6 peptide (Fig. 1C). Several sensory neurons in the DRG showed TRPV6 immunoreactivity (Fig. 1D). Using this antiserum, the manufacturer (Alomone Labs) has also demonstrated TRPV6 immunofluorescence in the sensory neurons of the rat DRG. Application of the TRPV6 antiserum on sections of the mouse kidney showed immunofluorescence in the cells of renal tubules. In the hypothalamic tissue, while Western blot analysis detected a prominent band of ~95 kDa (Fig. 1E), corresponding to the molecular weight of TRPV6, RT-PCR analysis showed TRPV6 mRNA expression (Fig. 1F).

Organization of TRPV6-immunoreactivity in the brain

Diagrammatic representation of the organization of TRPV6-immunoreactive cell bodies and fibers in the mouse brain is shown in Fig. 2. The relative number of TRPV6 cells and fibers in different regions of the brain is given in Table 1.

Telencephalon

Moderately labelled TRPV6-immunoreactive cells were observed in the ventral tectum (Figs. 2A, 3A), ventral pallidum (Fig. 2A), and piriform cortex (Figs. 2C, 3B). In

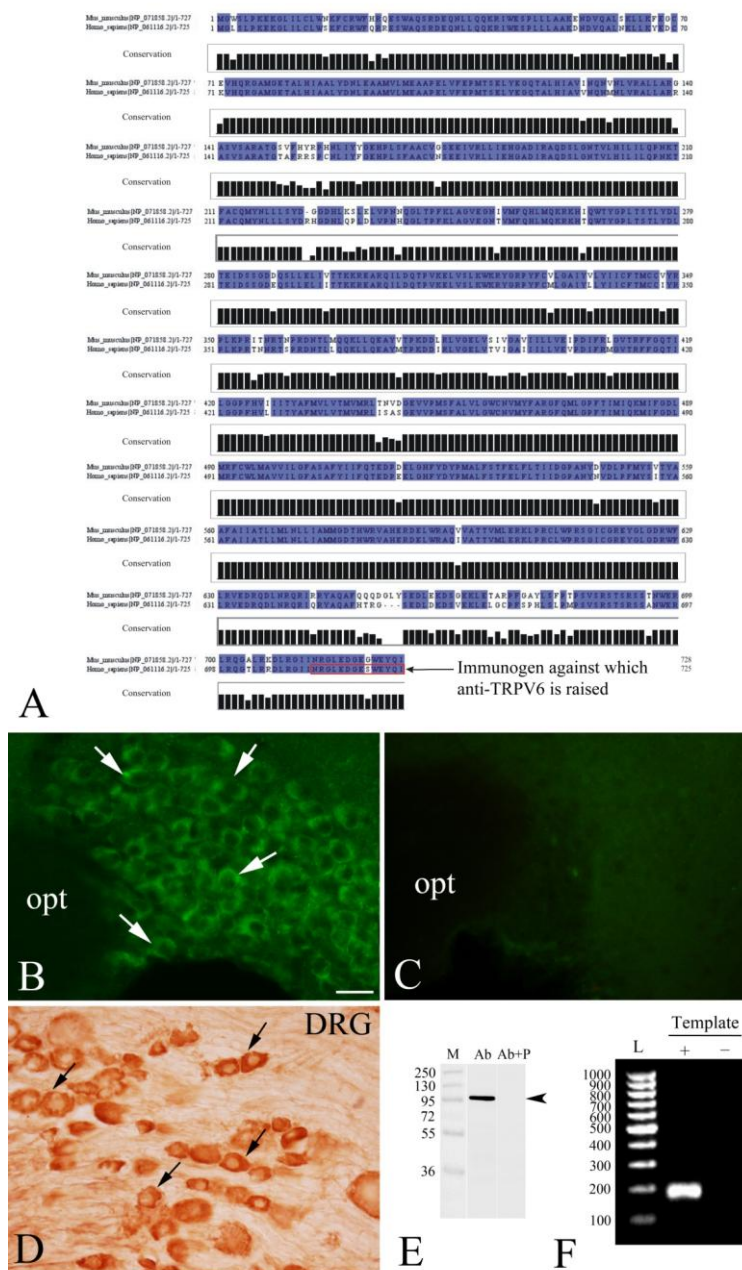


Figure 1: Specificity of the TRPV6 antiserum in the mouse brain. (A) CLUSTAL-OMEGA analysis of sequences of human and mouse TRPV6. The fragment of human TRPV6 against which the antiserum is raised show 92.9 % sequence identity with mouse TRPV6 (red rectangle). (B) TRPV6 labelled neurons (arrows) are seen in the hypothalamic supraoptic nucleus (SON) but (C) no immunofluorescence is seen in SON after application of the preadsorbed TRPV6 antiserum with control peptide. (D) Sensory neurons in the dorsal root ganglion (DRG) showing TRPV6 immunoreactive cell bodies (arrows). (E) Western blot analysis of the hypothalamus showing a band at ~95-100 kDa. No band is seen following application of the preadsorbed antiserum. (F) RT-PCR analysis showing TRPV6 transcript in the hypothalamus. Ab, TRPV6 antibody; Ab+P, TRPV6 antiserum preadsorbed with control peptide; L, DNA ladder; M, protein molecular weight marker. Scale bar = 20 μ m.

amygdala, TRPV6-immunoreactive cell bodies and fibers were observed in the medial amygdaloid nucleus, anterodorsal subdivision (MeAD) (Figs. 2D, 3C). In the hippocampus, immunoreactive cells were also observed in the molecular (Figs. 2E, F, 3D) and granule (Figs. 2F, 3E) layers of the dentate gyrus. Immunoreactive cells and fibers were seen in the nucleus of horizontal limb of the diagonal band (HDB) and ventral part of the lateral septal nucleus (Figs. 2B,C).

Diencephalon

TRPV6-immunoreactive cell bodies and fibers were observed in the preoptic area (POA) and hypothalamus (Fig. 2B-F). The cells and fibers of vascular organ of the lamina terminalis (VOLT) showed distinct TRPV6-immunofluorescence (Figs. 2B, 3F, G). TRPV6-immunoreactive cells were seen in the subfornical organ (Figs. 2D, 3I) and choroid plexus (Figs. 2E, F, 3J). TRPV6-immunoreactive cells and fibers were seen in the septohypothalamic nucleus (Figs. 2B, C, 4A). While several neurons in the hypothalamic supraoptic nucleus (SON) showed intense TRPV6 immunofluorescence (Figs. 2D, 4B), isolated weakly immunoreactive neurons were observed in the anterior hypothalamic area, posterior part (AHP) (Fig. 2E, 4C) and anterior hypothalamic area, central part (AHC) (Figs. 2D, 4D). No immunoreactivity was detected in the hypothalamic paraventricular nucleus (PVN). TRPV6 immunoreactive cell bodies and fibers were observed in the peduncular part of the lateral hypothalamus (PLH) (Figs. 2D-F, 4E), hypothalamic dorsomedial nucleus (DMN) (Figs. 2F, 4F-H), and subincertal nucleus (SubI) (Fig. 4I). In DMN, while the immunoreactive cells and fibers were organized in the dorsal (DMD, Figs. 2F, 4F, G) and ventral (DMV, Figs. 2F, 4H) subdivisions; the compact part of DMD was devoid of TRPV6 immunofluorescence (DMC, Fig. 2F). In the hypothalamic arcuate nucleus (ARC), several TRPV6 cells were observed; no TRPV6 fibers were observed in this area (Figs. 2E, F, 4J).

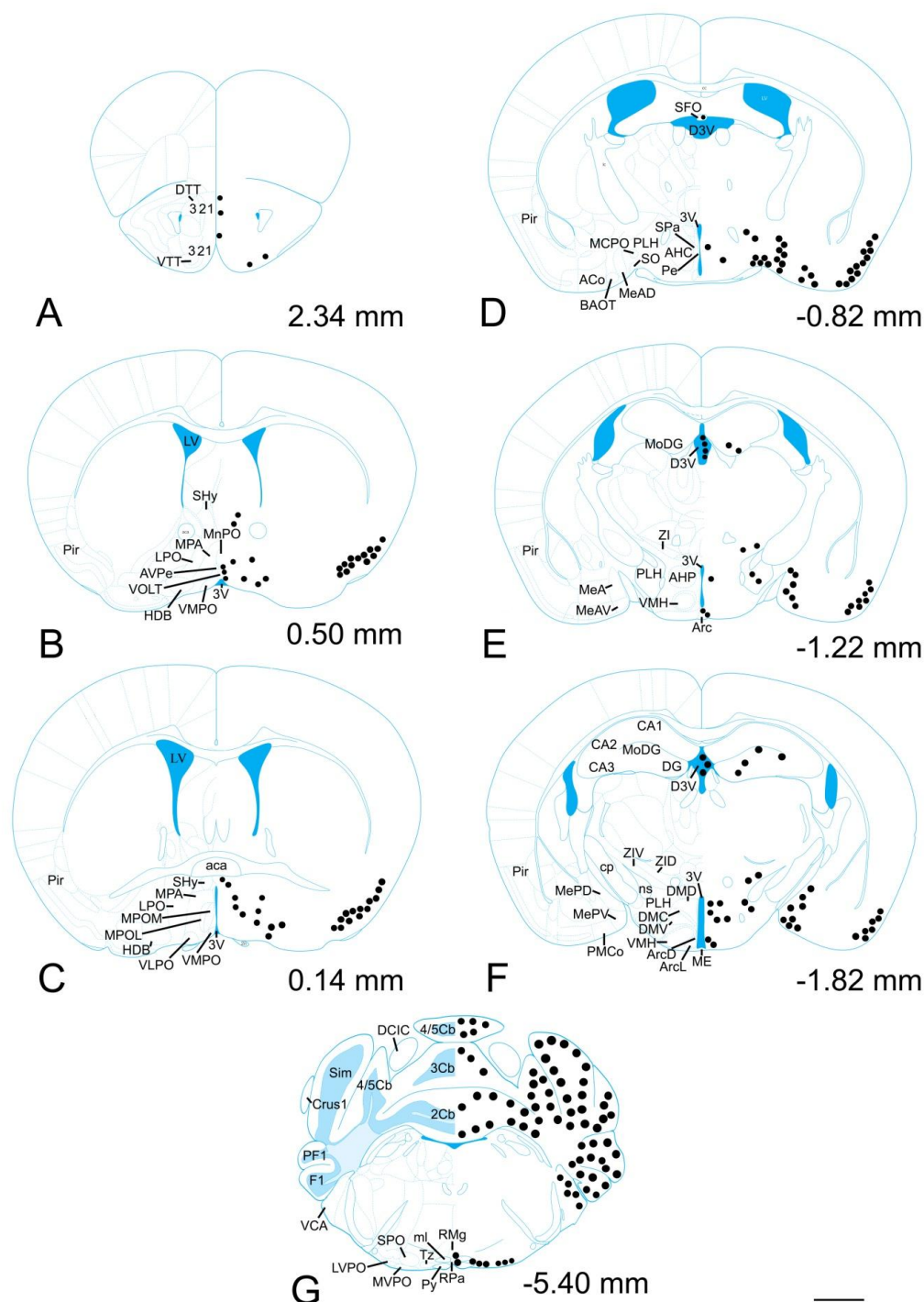


Figure 2: Schematics showing the organization of TRPV6-immunoreactive elements in the mouse brain. Schematic drawings of the rostrocaudal series of transverse sections (A-G) of the mouse brain [A: 2.34, B: 0.50, C: 0.14, D: -0.82, E: -1.22, F: -1.82, and G: -5.40 relative to bregma] showing cytoarchitectonic areas on the left [adopted from Franklin and Paxinos (2007)] and TRPV6 cells (circles) on the right. Please refer abbreviations for details of the nuclei and brain regions. Scale bar = 1 mm.

Table 1: Distribution of TRPV6-immunoreactive neuronal cell bodies and fibers/terminals in the mouse brain and pituitary gland

Areas of the brain	Cells	Fibers/terminals
Telencephalon		
Olfactory bulb		
Ventral tenia tecta	+	-
Ventral pallidum	+	-
Piriform cortex	+++	-
Amygdala		
Medial amygdaloid nucleus, anterodorsal (MeAD)	+++	++
Hippocampus (Hp)		
Granule cell layer of dentate gyrus (GrDG)	+	+
Molecular layer of dentate gyrus (MoDG)	+	-
Nucleus of the horizontal limb of the diagonal band (HDB)	+	-
Diencephalon		
Preoptic area (POA)		
Medial preoptic area (MPA)	+	-
Lateral preoptic area (LPO)	+	-
Septohypothalamic nucleus (SHy)	++	++
Hypothalamus		
Supraoptic nucleus (SON)	+++	+
Paraventricular nucleus (PVN)	-	-
Anterior hypothalamic area (AH)		
AH, central part (AHC)	+	+
AH, posterior part (AHP)	+	+
Dorsomedial hypothalamic nucleus (DM)		
DM, dorsal part (DMD)	++	+++
DM, ventral part (DMV)	++	+++
Hypothalamic arcuate nucleus (ARC)	+++	++
Peduncular part of lateral hypothalamus (PLH)	+++	+++
Subincertal nucleus (Subl)	++	++
Median eminence (ME)	-	++
Zona incerta (ZI)	+	+
Vascular organ of the lamina terminalis (VOLT)	+++	+++
Subfornical organ (SFO)	++	-
Choroid plexus (CP)	+++	-
Mesencephalon		
p1 periaqueductal gray (p1PAG)	-	+

Metencephalon and myelencephalon		
Raphe pallidus nucleus (RPa)	++	-
A11 dopamine cells	+	+
Lateroventral periolivary nucleus (LVPO)	++	-
Medioventral periolivary nucleus (MVPO)	++	-
Nucleus of trapezoid body (Tz)	+++	-
Ventral cochlear nucleus anterior part (VCA)	++	-
Cerebellum (Purkinje cells)	+++	-
Pituitary gland		
Pars tuberalis (PT)	++	-
Pars distalis (PD)	+	-

Number of cell bodies and fibers/terminals: +, few; ++, moderate; +++, high; -, negative

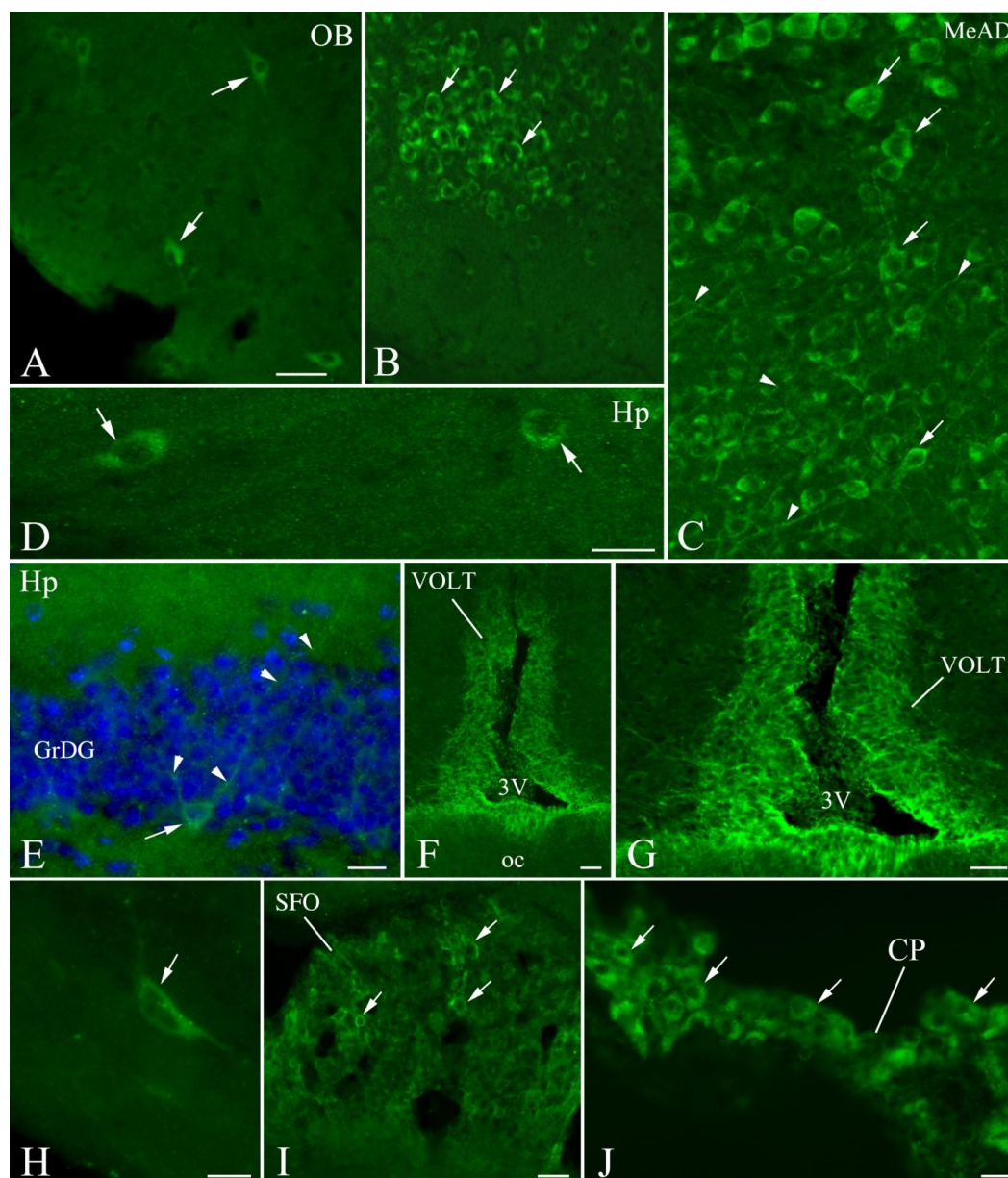


Figure 3: Organization of TRPV6-immunoreactive elements in the forebrain of mouse. Fluorescence photomicrographs showing TRPV6-immunoreactive cells (arrows) and fibers (arrowheads) in (A) tenia tecta, (B) piriform cortex, (C) medial amygdaloid nucleus anterodorsal subdivision, (D) hippocampus (Hp), (E) granule layer dentate gyrus (GrDG), (F) vascular organ of the lamina terminalis (VOLT) around the third ventricle (3V), (G) high magnification image of a region in F, (H) horizontal limb of the diagonal band (HDB), (I) subfornical organ, and (J) choroid plexus (CP) of mouse. Scale bar = 25 μm in A-C, F, G, I, and 10 μm in D, E, H, and J.

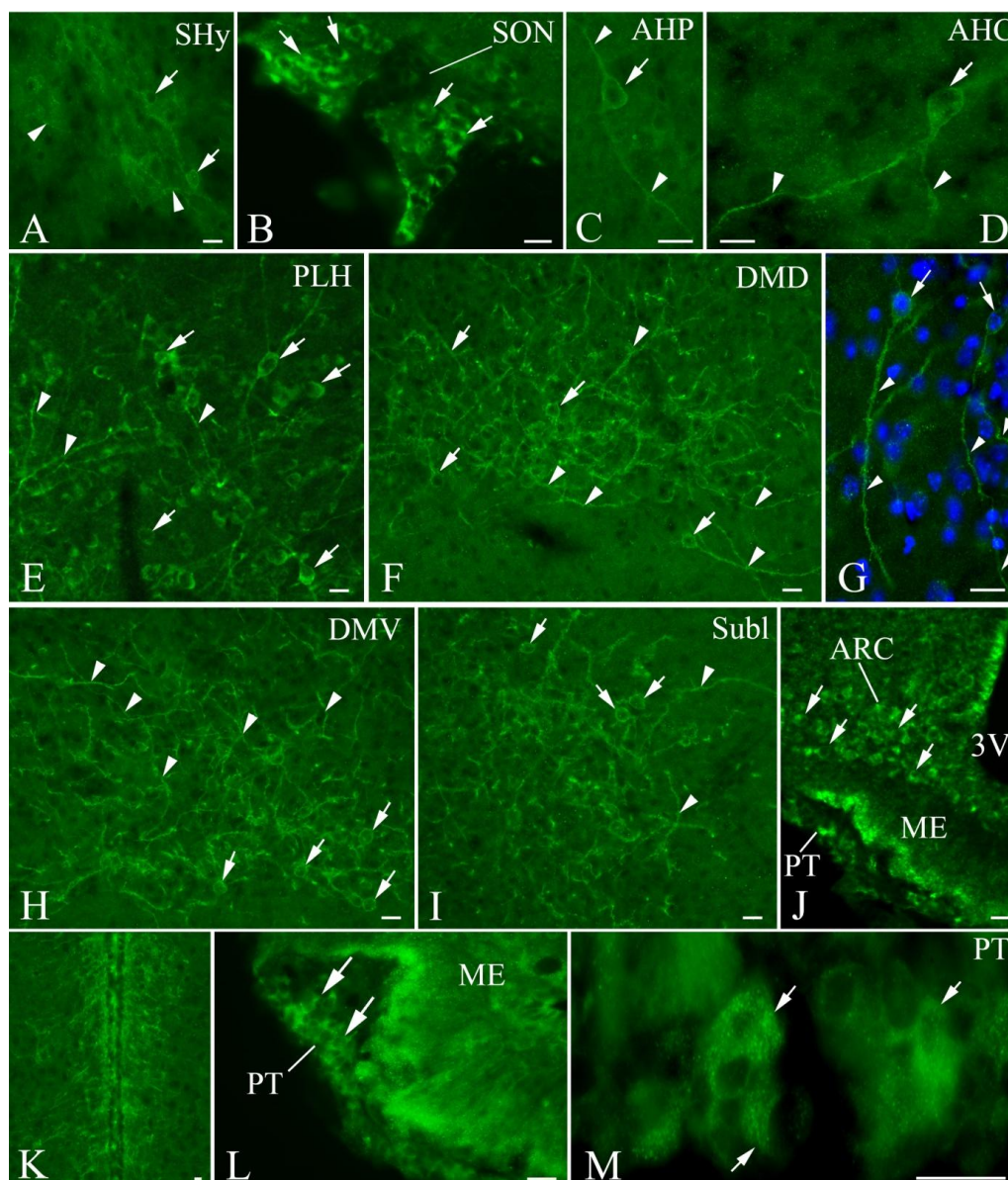


Figure 4: Organization of TRPV6-immunoreactive elements in the hypothalamus and pars tuberalis of mouse. Fluorescence photomicrographs showing TRPV6-immunoreactive cells (arrows) and fibers (arrowheads) in (A) septohypothalamic nucleus (SHy), (B) supraoptic nucleus (SON), (C) anterior hypothalamic area, anterior part (AHA), (D) anterior hypothalamic area, central part (AHC), (E) peduncular part of the lateral hypothalamus (PLH), (F) dorsomedial nucleus, dorsal subdivision (DMD), (G) enlarged region of DMD showing TRPV6-immunoreactive cells and processes, (H) dorsomedial nucleus, ventral subdivision (DMV), (I) subincertal nucleus (SubI), (J) hypothalamic arcuate nucleus (ARC), (K) around third ventricle in the hypothalamus, (L) external zone of the median eminence (ME) and pars tuberalis (PT), (M) enlarged view of PT. TRPV6-immunoreactive cells are seen in the PT. opt, optic tract; 3V, third ventricle. Scale bar = 25 μ m in A, B, E, F, H-L, and 10 μ m in C, D, G, and M.

Tanycytes lining the wall of third ventricle showed TRPV6 immunofluorescence (Figs. 2B-F, 4K). TRPV6 immunoreactive terminals were observed in the external zone of median eminence (Fig. 4L). Distinct TRPV6-immunoreactive cells were seen in the pars tuberalis around the median eminence (Figs. 4J, L, M).

Mesencephalon

Isolated beaded TRPV6 labelled fibers were observed in the p1 periaqueductal gray (p1PAG) (Fig. 5A). Other mesencephalic nuclei were devoid of TRPV6.

Metencephalon and myelencephalon

TRPV6-immunoreactive cells were observed in the A11 region (Fig. 5B), raphe pallidus (RPa) (Figs. 2G, 5C), medio- (MVPO) and lateroventral (LVPO) periolivary nucleus (Figs. 2G, 5D), nucleus of trapezoid body (tz) (Figs. 2G, 5E), and anterior part of the ventral cochlear nucleus (VCA) (Figs. 2G, 5F). Purkinje cells in the cerebellum were TRPV6-immunoreactive (Figs. 2G, 5G).

TRPV6-immunoreactive cells in ARC co-express ER α and TRPV6 protein expression in MBH show correlation with estrous cycle

TRPV6- (Fig. 6A) and ER α - (Fig. 6B) immunoreactive cells were seen in ARC (Fig. 6A, B). Application of double immunofluorescence showed TRPV6-immunoreactive cells co-expressing ER α (Fig. 6C). By semi-quantitative analysis, approximately 62 % TRPV6-immunoreactive cells in ARC showed ER α -immunoreactivity in their nuclei. Intense TRPV6-immunoreactive band was detected in the MBH tissue of mice during proestrus stage (Fig. 6D, E). Compared to the proestrus stage, a significant reduction ($P < 0.01$) in the percent intensity of the TRPV6-immunoreactive band was observed in MBH

of mice in the metestrus and diestrus stages (Fig. 6D, E). TRPV6 protein levels in the MBH during proestrus and estrus was comparable ($P>0.05$) (Fig. 6D, E).

TRPV6 equipped neurons in ARC innervates preoptic area and majority of TRPV6-immunoreactive cells in ARC co-express NPY

Majority of NPY neurons in the ARC showed TRPV6-immunoreactivity (Fig. 7G-I, arrow), whereas very few ARC CART neurons showed TRPV6-immunoreactivity (Fig. 7A-C, arrowhead). To ensure that the secondary antibody used for detecting CART neurons in ARC are not binding to the TRPV6 labelled neurons, few TRPV6-labeled sections of ARC were incubated in Alexa Fluor-594-conjugated anti-rabbit IgG. No Alexa Fluor-594 immunofluorescence was seen in TRPV6 labelled neurons (Fig. 7D-F). The iontophoretic injection of CtB in AVPe (Fig. 8A) and MnPO (Fig. 9A) resulted in retrograde accumulation of CtB in ARC neurons (Figs. 8B, B', 9B, B'). The CtB/TRPV6 neurons in ARC contained few or no CART-immunoreactivity (Figs. 8B-E, B'-E', 9B-E, B'-E').

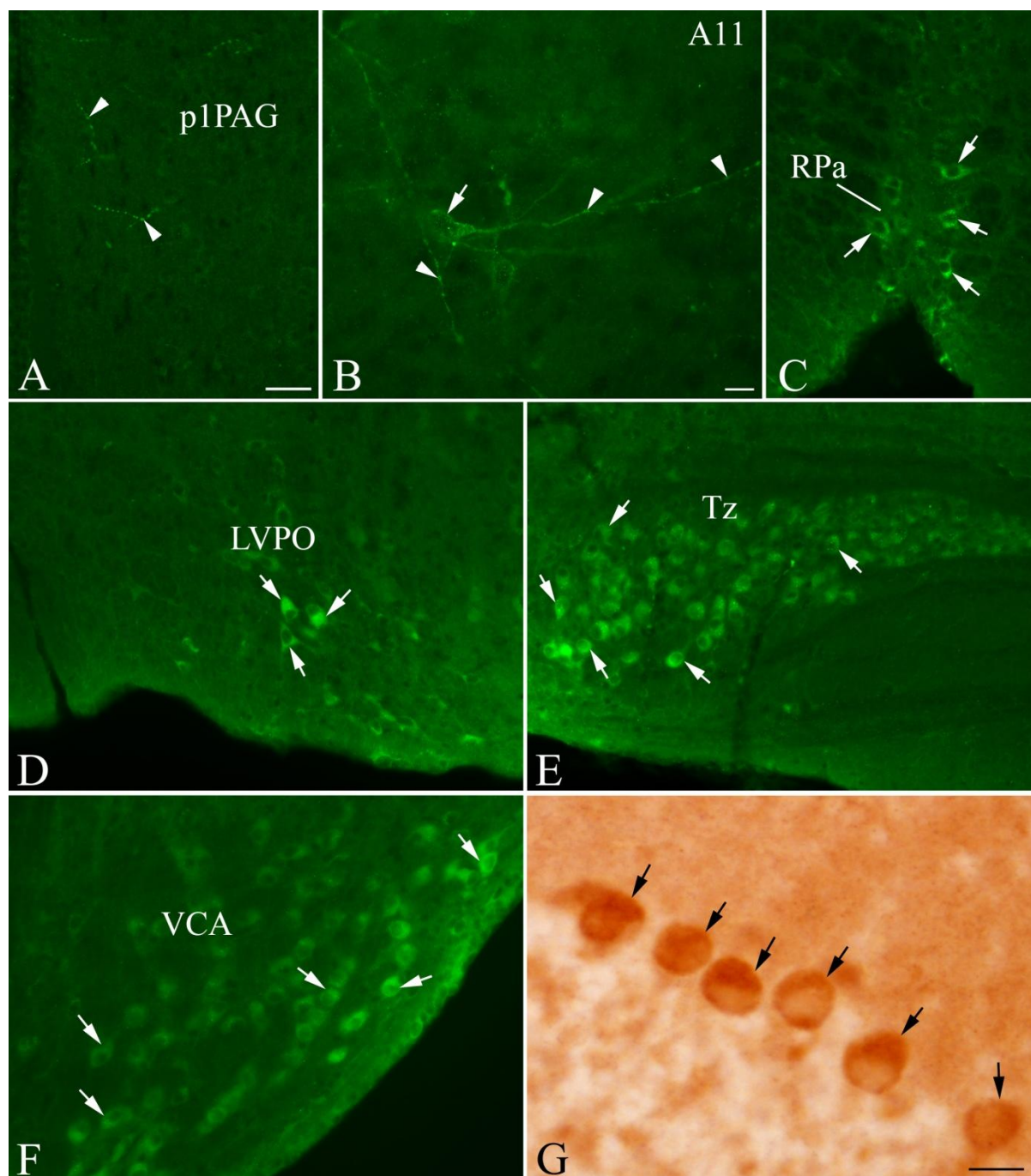


Figure 5: Organization of TRPV6-immunoreactive elements in the midbrain and cerebellum of mouse. Fluorescence photomicrographs showing TRPV6-immunoreactive cells (arrows) and fibers (arrowheads) in (A) p1 periaqueductal gray (p1PAG), (B) A11 region, (C) raphe pallidus (RPa), (D) lateroventral periolivary nucleus (LVPO), (E) nucleus of trapezoid body (Tz), and (F) anterior part of the ventral cochlear nucleus (VCA). (G) Distinct TRPV6-immunoreactivity is seen in purkinje cells of cerebellum. Scale bar = 25 μm in A-F and 10 μm in G.

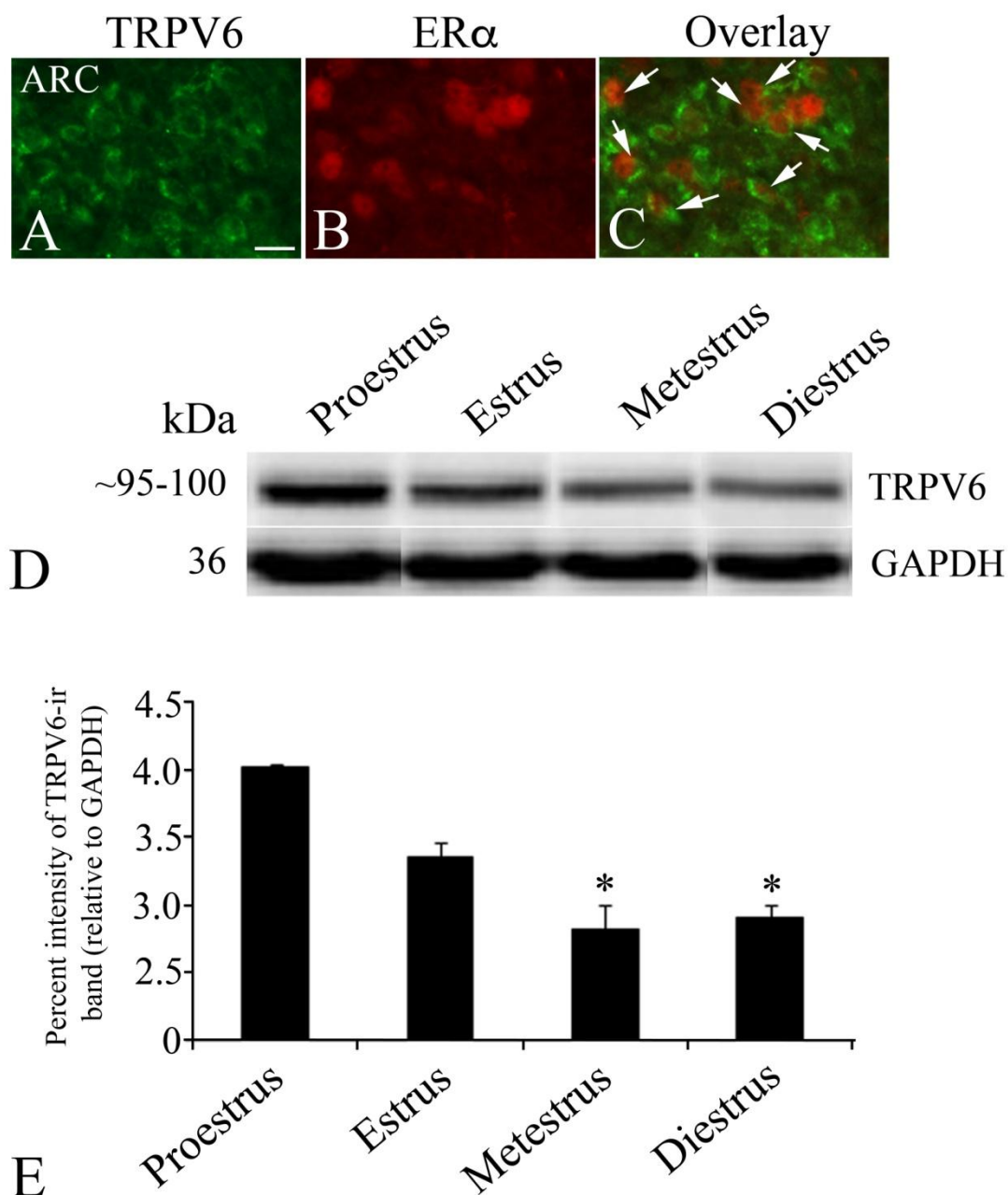


Figure 6: TRPV6-immunoreactive cells in the arcuate nucleus co-express ER α and TRPV6 protein in mediobasal hypothalamus show correlation with estrous cycle. (A-C) Double immunofluorescence photomicrographs showing TRPV6-immunoreactive cells (green, arrows) in the hypothalamic arcuate nucleus (ARC) co-expressing estrogen receptor alpha (ER α , red). (D, E) Western blot and analysis of the percent intensity of TRPV6-immunoreactive bands in the mediobasal hypothalamus (MBH) of mice collected during different phases of the estrous cycle. *, P < 0.01 compared to proestrus phase. Scale bar = 25 μ m.

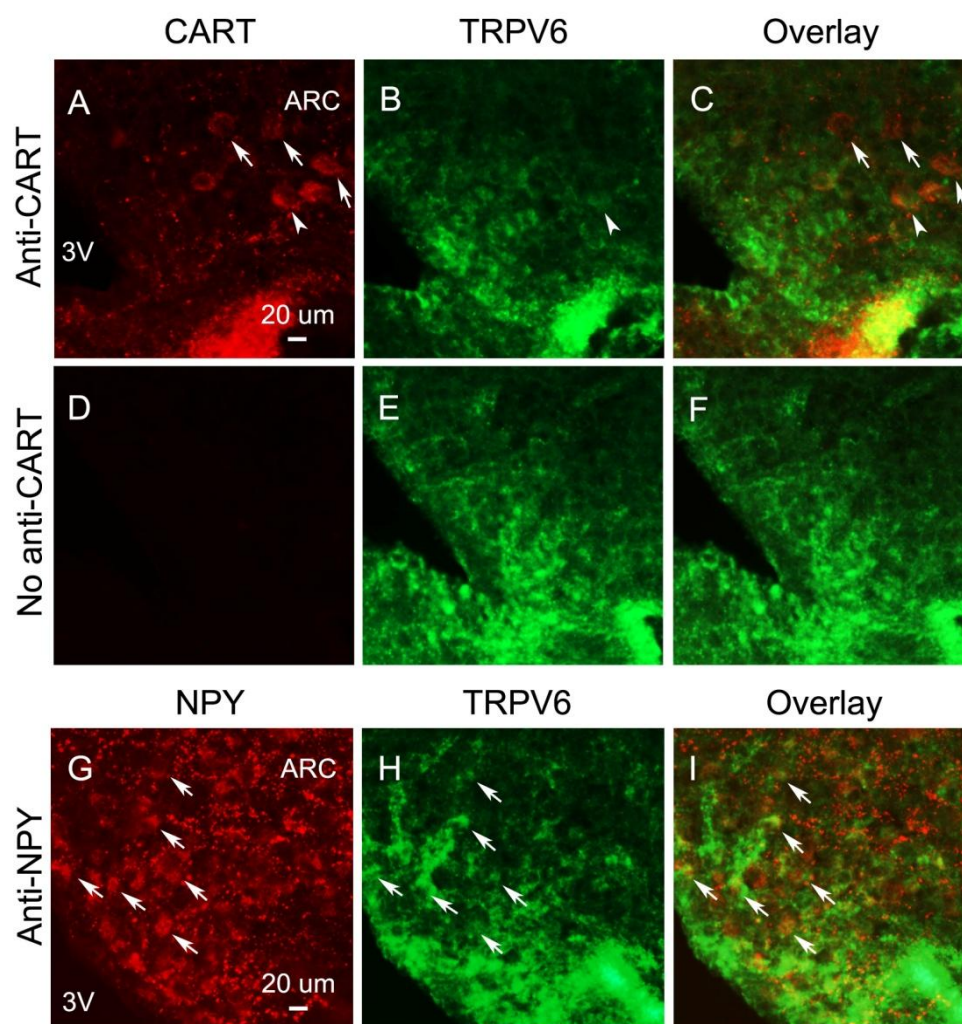


Figure 7: Majority of the TRPV6-immunoreactive cells in the arcuate nucleus (ARC) co-express neuropeptide Y (NPY) but not CART. Double immunofluorescence photomicrographs showing TRPV6-immunoreactive cells (B, E, H) in ARC co-expressing CART (A-C, arrowhead in C) and NPY (G-I, arrows). In the absence of CART- antibody, no co-localization is seen (D-F).

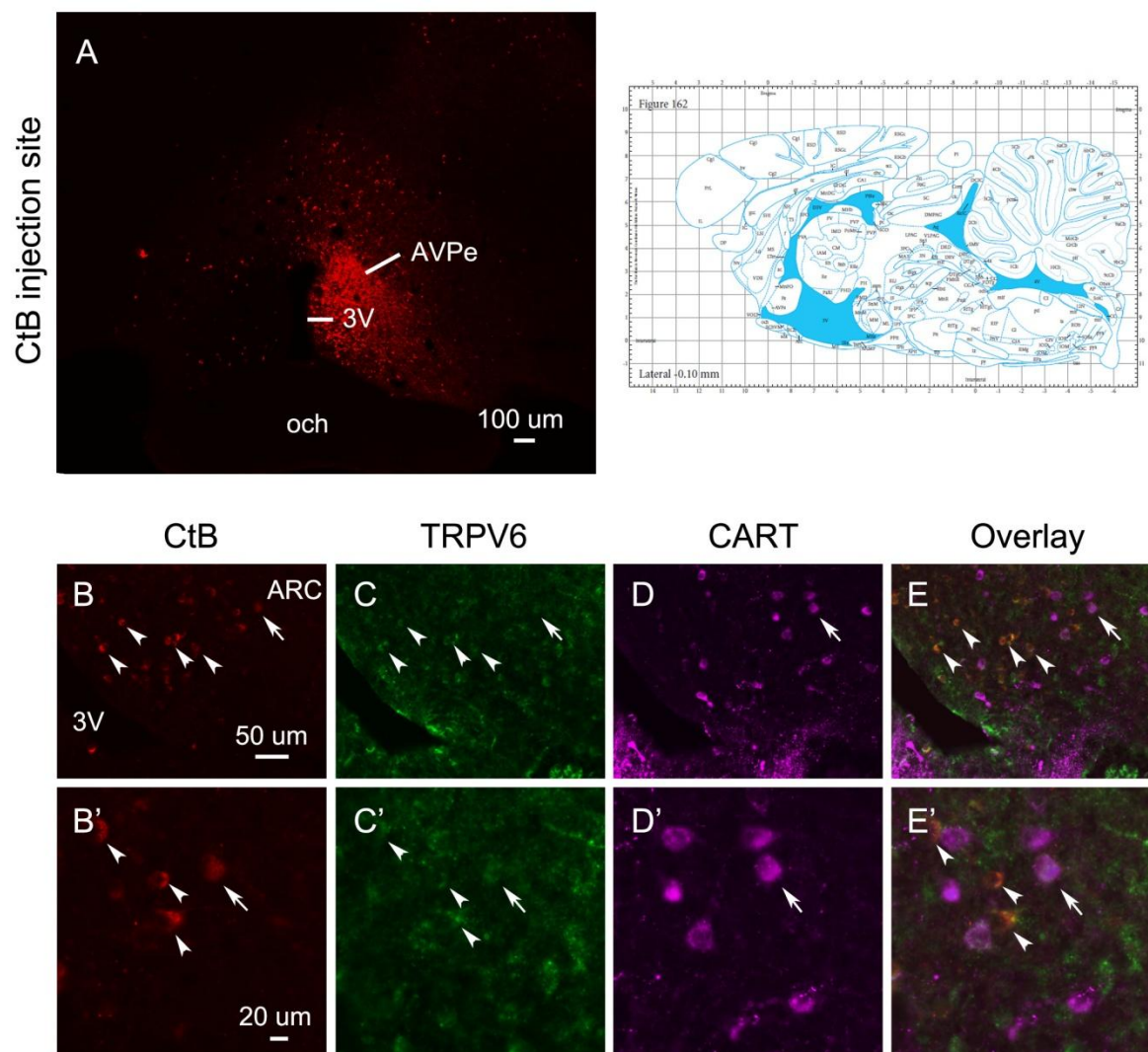


Figure 8: TRPV6-equipped neurons in the arcuate nucleus (ARC) innervate anteroventral periventricular nucleus (AVPe) in the preoptic area. (A-E, B'-E') CART neurons (magenta) in ARC equipped with TRPV6 (green) showing retrograde accumulation of cholera toxin beta subunit (red) injected in (A) AVPe. Note CtB/TRPV6/CART the triple labelled neurons in ARC (arrows).

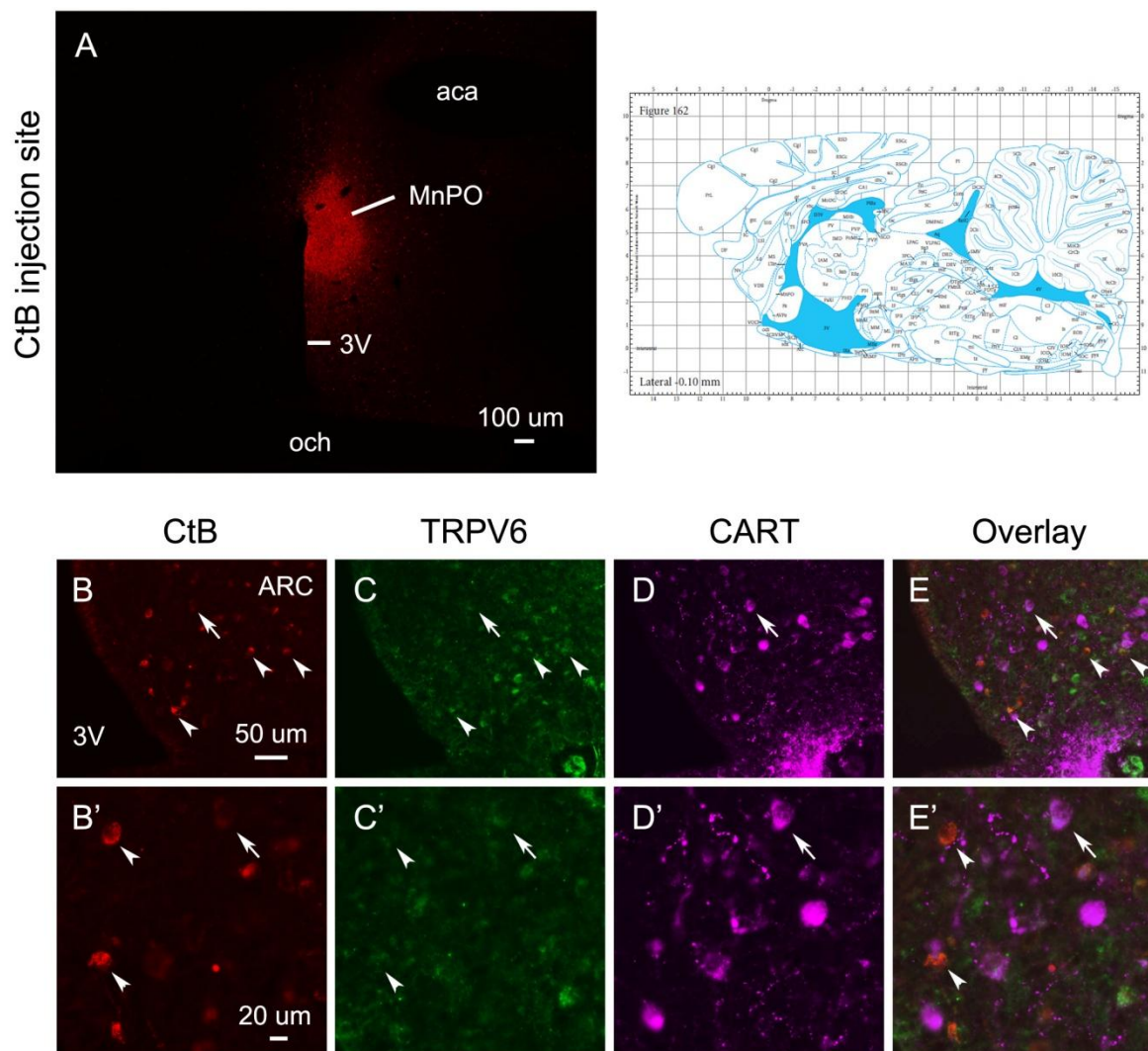


Figure 9: TRPV6-equipped neurons in the arcuate nucleus (ARC) innervate median preoptic nucleus (MnPO) in the preoptic area. (A-E, B'-E') CART neurons (magenta) in ARC equipped with TRPV6 (green) showing retrograde accumulation of cholera toxin beta subunit (red) injected in (A) MnPO. Note CtB/TRPV6/CART the triple labelled neurons in ARC (arrows).

DISCUSSION

TRPV ion channels have emerged as novel cationic channels and their significance in neural regulation is increasingly being appreciated. In contrast to TRPV1-4, TRPV5/TRPV6 are highly Ca^{2+} selective but temperature insensitive and their significance in the brain is not known. Using RT-PCR analysis, Nijenhuis et al. [314] observed the presence of TRPV5 and TRPV6 in the mouse brain; TRPV6 seem to be highly expressed as compared to TRPV5. Compared to other tissues, brain showed lower expression of TRPV6 [315]. We observed TRPV6 mRNA and protein expression in the hypothalamus of mouse. The cells/fibers expressing these ion channels proteins were observed in the hypothalamus, brainstem, cerebellum, and pituitary gland. While TRPV6 and $\text{ER}\alpha$ double immunofluorescence labelling showed their colocalization in ARC neurons, TRPV6 protein expression in MBH showed correlation with the estrous cycle. This is the first study describing the neuroanatomical architecture of TRPV6-expressing elements in the brain. Regulation of TRPV6 in the MBH by circulating levels of estradiol during estrous cycle might play a role in feedback regulation.

Using multiple sequence alignment, the human TRPV6 epitope against which the antiserum was raised showed a high degree of sequence similarity with mouse TRPV6. Specificity of the TRPV6 antiserum used in the present study is well established using range of approaches including Western blot analysis and transfection [310,311]. Using this antiserum, our control procedures like the preadsorption control and Western blot analysis produced convincing results. Further, the antiserum labelled DRG neurons and kidney cortex and served as positive controls. Using the same antiserum, the manufacturer has demonstrated TRPV6 immunoreactivity in DRG neurons of rat and the antiserum is known to label the cells of renal distal tubules [316]. In the present study, using TRPV6 antiserum the Western blot analysis of the hypothalamic tissue showed a distinct band of desired

molecular mass. In human prostate carcinoma cell line (LNCaP) endogenously expressing the ion channels, Western blot analysis using the TRPV6 antiserum has been shown to recognize ~95 kDa band [311]. Recently, HEK293 cells were transfected with pTRPV6-YFP or pIRES-TRPV6 plasmid and using immunofluorescence and Western blot the specificity of the antiserum was established [310]. While the immunofluorescence application of TRPV6 antiserum labelled the transfected HEK293 cells, Western blot analysis of TRPV6 transfected HEK293 cells showed a ~95-100 kDa band [310]. Yet another study used the same TRPV6 antiserum as used in our study and established its specificity [317]. In immunoblotting, application of TRPV6 antiserum on HEK cells stably overexpressing TRPV6 detected a distinct TRPV6 band and the siRNA-TRPV6 treatment reduced the intensity of the band [317]. Further the application of the TRPV6 antiserum from Alomone Labs on leukemia K562 cells [318], the intestinal tissue of mouse [319], and human colon tissue [209], consistently produced a band of predicted molecular mass. Application of TRPV6 antiserum on the LNCaP cells treated with siRNA-TRPV6, resulted in reduced TRPV6 immunofluorescence compared to the cells treated with functional non-coding siRNA [320]. The TRPV6 antiserum from Alomone labs has been shown to recognize mouse TRPV6 [312,313]. In mouse, the application of TRPV6 immunohistochemistry and TRPV6 *in situ* hybridization histochemistry on yolk sac tissue sections resulted in strong labelling of the intraplacental yolk sac [313]. Hatano et al. have established the specificity of TRPV6 antiserum using the lysate from HEK and Caco-2 cells transiently transfected with mouse TRPV6-expressing vector [312]. Our Western blot analysis of TRPV6 in the hypothalamus of mouse is in agreement with the above reports, suggesting that the TRPV6 antiserum is specific and recognizing TRPV6 in the mouse brain.

TRPV6-immunoreactive neurons were observed in the POA, cortex, hippocampus, amygdala, circumventricular organ, brainstem, and cerebellum. Hypothalamus contained distinct TRPV6-expressing cells and fibers. TRPV6-immunoreactive neurons were observed in SON but no immunoreactive signal was detected in the PVN. The neurons in SON have also been shown to express other members of the TRPV subfamily including TRPV1 [251], TRPV2 [202], and TRPV4 [250]. While the magnocellular vasopressin neurons in SON of wild type mice showed increased neuronal firing following capsaicin (a TRPV1-agonist) treatment, these neurons in TRPV1 knockout mice did not respond to capsaicin treatment [321]. While the vasopressin neurons in SON and PVN of rat co-express TRPV2 [202], both vasopressin and oxytocin neurons in the hypothalamus of monkey co-express TRPV2 [203]. Neurochemical identity of the TRPV6-immunoreactive neurons in the SON is not known. We suggest that, like other TRPV ion channels, TRPV6 may also play a role in regulation of SON neurons. The ARC contain neurons expressing TRPV1 [213] and TRPV2 [202] and role of TRPV2 in the regulation of feeding has been suggested [202]. Although no TRPV6-immunoreactive cells were observed in the PVN, distinct TRPV6 immunoreactive cells and fibers were observed in the DMNd and DMNv. The DMN serve as important integrative center in the hypothalamus and part of the ARC-DMN-PVN multisynaptic pathway [322]. Retrograde neuronal tracer study in rat has demonstrated that DMN neurons project to PVN and these neurons are innervated by α -melanocyte stimulating hormone-containing axons originating from ARC [322]. While we do not know the neurochemical phenotype of TRPV6-expressing cells in the DMN, we suggest that the TRPV6 equipped neurons in DMN may innervate and regulate the activity of PVN neurons. TRPV6-immunoreactivity was observed in the cells and fibers in the VOLT. The VOLT contains osmosensory neurons [268]. While the neurons in VOLT in wild type mice showed increased neuronal firing in response to increased osmolality, the

response was absent in TRPV1^{-/-} mice [282]. We speculate that the TRPV6 equipped elements in the VOLT may play a role in osmosensing.

The TRPV6-immunoreactive neurons were observed in ARC of mouse and these neurons co-expressed ER α . Western blot analysis of the TRPV6 protein expression in MBH of mice during different phases of the estrus cycle showed an interesting correlation. During estrous cycle, low but slowly increasing level of estradiol was observed during the metestrus and diestrus phases, and remain elevated during the proestrus phase [323]. During the proestrus phase, we observed a higher TRPV6 expression in MBH. Compared to proestrus phase, a significant reduction in TRPV6 expression was seen in MBH of mice in the metestrus and diestrus phases. The TRPV6 gene promoter contain estrogen response element [34] and estradiol has emerged as potential regulator of TRPV6 [316]. Although information pertaining to the interaction between estradiol and TRPV6 in neural tissue is not available, studies conducted on peripheral tissues have demonstrated a strong correlation between estrogen and TRPV6. The duodenal TRPV6 mRNA expression was reduced after ovariectomy in rat and in ER α knockout mice [211]. The TRPV6 mRNA expression in the duodenum of ovariectomized rat was upregulated following 17- β -estradiol treatment [141]. TRPV6 mRNA in the uterus showed correlation with estrous cycle and highest levels were detected during estrus phase and pregnancy [206,212]. Estradiol treatment-induced increase in TRPV6 mRNA expression in the uterus was blocked by pre-treatment with estrogen receptor antagonist [206]. In human T84 colonic cells, estradiol treatment rapidly enhanced [Ca²⁺]_i through TRPV6 ion channels [209]. The ARC contains ER α -expressing neurons [305,307] and the nucleus serve as site for negative feedback effect of estradiol [307]. Since the effect of estradiol on TRPV6 expression has been suggested to be mediated via ER α dependent pathway [206], we suggest that the higher estradiol levels during proestrus phase may upregulate TRPV6 expression in neurons of ARC and play a role in feedback regulation.

Further, using retrograde neuronal tracing, we observed majority of TRPV6 equipped neurons in ARC projects to AVPe and MnPO but none or few co-express CART. Double immunofluorescence studies showed ARC TRPV6 neurons co-express NPY suggesting role of TRPV6 ion channels in the modulation of NPY-GnRH pathway.

In summary, TRPV6-expressing elements seem to be discretely organized in the brain of mouse. TRPV6-immunoreactive ARC neurons contain ER α and the ion channel protein expression in MBH showed correlation with estrous cycle. The neuroanatomical organization of TRPV6-equipped elements in the brain would further help in exploring the functional significance of the ion channel in neural regulation.

CHAPTER 5

CART- AND TRPV1-INDUCED GROWTH HORMONE SECRETION MAY SERVE AS NOVEL COMPONENT OF THE CENTRAL REGULATION OF ENERGY BALANCE AND REPRODUCTION

S. Kumar, U. Singh, O. Singh, and P.S. Singru. (2017). Transient receptor potential vanilloid (TRPV1-6) in the pituitary gland of rat: organization and relevance to growth hormone secretion (manuscript under preparation).

INTRODUCTION

CART is a widely distributed neuropeptide in the brain [19,133] and regulates a range of physiological processes by its actions on central as well as peripheral tissues [128,146]. In Chapter 1, we have observed projections of the arcuate nucleus CART neurons in the CNS of rat. Although several brain regions dense/moderately innervated by CART axons originating from ARC, these neurons do not seem to project to the posterior pituitary gland. In addition, we did not find presence of ARC CART axons in the external zone of median eminence. While the ARC CART neurons may modulate the energy balance and reproduction by its central action, presence of CART peptide has also been observed in the peripheral circulation [128,324]. In addition to other peripheral sources of CART, hypothalamic neuroendocrine neurons secreting CART in portal circulation and CART synthesizing cells in the anterior pituitary gland may serve as important contributors for serum CART. CART in the external layer of medial eminence seem to play a role in the regulation of anterior pituitary gland secretion [325,326]. In addition, presence of CART-expressing cells has been reported in the anterior pituitary gland [327]. CART-(55-102) seems to be the predominant form of CART peptide reported in the anterior pituitary gland [127]. The CART-expressing cells have been shown to be colocalized with prolactin (PRL, 82%), growth hormone (GH, 10%), adrenocorticotrophic hormone (5%), and thyroid stimulating hormone and follicle stimulating hormone [$< 1\%$] in the anterior pituitary gland of rat [327]. While no CART-ir was observed in the pars intermedia, dense CART-ir fibers were seen in the posterior pituitary [327]. The CART-ir fibers in the pars nervosa seem to originate from neurons of hypothalamic supraoptic (SON) and paraventricular (PVN) nuclei since presence of CART/oxytocin and CART/AVP double labelled fibers were observed in the posterior pituitary [327]. The role of CART in the modulation of pituitary hormones has also been reported. CART peptide treatment has been shown to inhibit TSH, stimulate PRL,

and decrease LH release [175]. Recently, the CART-ir cells in the mouse pituitary at postnatal day P8 were TSH β - (16-21%) and GH- (57-68%) immunoreactive [40]. This percentage showed drastic change in the pituitary gland of a 12 week old adult mouse where approximately 67-76% TSH β but no GH cells co-expressed CART [40]. These observations suggest a role for CART peptide in pituitary hormone secretion.

GH plays an important role in the regulation of metabolism. GH regulate glucose production in liver by gluconeogenesis and glycogenolysis [328–332], lipolysis in the adipose tissue [333–336], and free fatty acid (FFA) uptake in skeletal muscles [337,338]. Evidence suggests role of GH in reproduction. As compared to the wild type mice, the growth hormone receptor knockout (GHR-KO) mice showed longer estrous cycle duration and reduced number of preovulatory follicles, corpora lutea, plasma estradiol level, and ovarian insulin-like growth factor I (IGF-I) mRNA expression [36]. The effect of GnRH on LH secretion as well as testicular function was also altered in GHR-KO mice [38]. GH levels are sexually dimorphic and the differential effects of androgens and estrogens in the hypothalamus might be the cause of sexual dimorphism in GH secretion [339]. The role of CART in the regulation of GH secretion has been suggested. Although CART-ir cells are present in the pituitary, only a small population of GH cells co-express CART. Furthermore, the icv CART peptide treatment significantly increased GH secretion and the external zone of median eminence contain dense CART innervations, suggesting role of hypophysiotropic CART system in modulation of GH secretion. Whether ARC CART contributes to the hypophysiotropic regulation, how CART controls GH release, and controls energy balance, however has remained unexplored.

The role of TRP channels for the currents present in pituitary cells has been suggested [340]. The nature of Ca²⁺-activated non-selective cationic currents in GH3 cells [341] and gonadotrophs [342], and TTX-insensitive Na⁺ conductance present in all endocrine

pituitary cells [343,344] is unknown and could be mediated by TRP channels. TRP ion channels have been speculated to be responsible for mediating Ca^{2+} -activated non-selective cationic currents in GH3 cells and gonadotrophs [340]. Ca^{2+} signalling is critical component of pituitary hormone secretion and the importance of TRPV ion channels in hormonal secretion has been suggested [340]. Few studies have demonstrated the presence of TRPV ion channels in the pituitary gland of mammals (Table 1) and their relevance in endocrine regulation. RT-PCR analysis has demonstrated the presence of TRPV3 in the human pituitary [217]. Followed by CNS, pituitary seems to be a high TRPV3 mRNA expressing tissue [217]. Using immunohistochemistry, TRPV2 immunoreactivity was observed in the pars nervosa (PN) of macaque [203] and rat [202]. TRPV5 and TRPV6 transcripts and protein expression were observed in the human parathyroid gland [285]. Reports from the non-mammalian vertebrate also support the relevance of TRPV ion channels in endocrine regulation. TRPV4 is expressed in the pituitary pars distalis of the teleost fish, *Oreochromis mossambicus* and mediate hyposmolality-induced prolactin release [345]. Presence of TRPV1 and TRPV4 was observed in the pituitary and pineal gland of the teleost fish, *Oncorhynchus mykiss* and these ion channels modulate melatonin secretion *in vitro* [346]. Poor understanding about these ion channels expression and organization of TRPV-equipped elements in the pituitary has posed a major impediment in exploring the role of these ion channels in the regulation of pituitary gland.

In this background, we studied expression and organization of TRPV subfamily members viz. TRPV1-6 in the rat pituitary. In a pilot study, we have observed TRPV1 immunoreactivity in GH cells in pars distalis. We have therefore explored the role of TRPV1 in GH secretion. Since CART peptide has been shown to modulate GH secretion, we determined whether this effect of CART is mediated *via* TRPV1. The pituitary cells were isolated from rat and treated with either CART or TRPV1 agonist, RTX. To test the

involvement of TRPV1 in GH release, the pituitary cells were treated with TRPV1 inhibitor, IRTX followed by RTX and the GH levels were measured using ELISA.

MATERIALS AND METHODS

Animals

Adult, male, Sprague-Dawley rats (220-250 g) were housed under standard temperature and humidity of the animal facility in a 12 h light and 12 h dark cycle. Standard rodent chow and fresh water were provided *ad libitum*. All the experimental protocols were reviewed and approved by the Institutional Animal Ethical Committee (IAEC) at the National Institute of Science Education and Research (NISER), Bhubaneswar, under the Committee for the Purpose of Control and Supervision of Experiments for Animals (CPCSEA), New Delhi, India.

Tissue collection

Rats (n = 5 for quantitative real-time PCR; n = 3 for Western blotting; n = 3 immunofluorescence) were anaesthetized intraperitoneally with a mixture of ketamine (100 mg/kg) and xylazine (10 mg/kg). For qRT-PCR and western blotting, anaesthetized rats were subjected to cervical dislocation followed by decapitation. The pituitaries were isolated, frozen in dry ice and stored at -80°C till processed further. For immunofluorescence, rats were transcardially perfused with 200 ml phosphate buffered saline (PBS, pH 7.4) followed by 100 ml 4% paraformaldehyde in phosphate buffer (PB, pH 7.4). The pituitary glands were isolated, post-fixed in 4% paraformaldehyde in PB and cryoprotected in 25% sucrose in PBS. Pituitary cell culture protocol was employed to study the effect of TRPV1 agents on GH cells. The procedure was carried out in sterile conditions. Anaesthetized rats (n = 6) were subjected to cervical dislocation followed by decapitation. The pituitary glands from each rat were immediately isolated. The processing of tissue for each protocol is described below.

Quantitative real-time PCR (qRT-PCR)

The relative abundance of TRPVs mRNA in rat pituitary was studied using quantitative real-time PCR. In brief, pituitary glands were disrupted and homogenized in 1 ml QIAzol lysis reagent using TissueLyser (Qiagen) at 50 Hz for 2 mins. Total RNA was isolated using RNeasy Lipid Tissue Mini Kit (Cat. # 74804, Qiagen). RNA was quantified in NanoDrop 2000 Spectrophotometer (Thermo Scientific). One μg of the total RNA was reverse transcribed into cDNA using QuantiTect Reverse Transcription Kit (Cat. # 205313, Qiagen). cDNA was added to a 20 μl reaction of KAPA SYBR Fast qPCR master mix (2X) (Cat. # KK4601, KAPA Biosystems) along with the primers (200 nM each) for rat TRPVs and HPRT (Table 1). TRPVs and HPRT cDNAs respectively were amplified in 7500 Real Time PCR System (Applied Biosystems). The qRT-PCR amplified products were finally run on 1.4 % agarose gel in order to confirm the amplification of single correct sized fragment. The relative expressions of TRPVs mRNA were normalized by HPRT mRNA (endogenous control) and reported as relative C_T values (C_T of TRPV/ C_T of HPRT), as previously described [231].

Western blotting

Pituitary glands collected for WB were disrupted and homogenized in 10 mM Tris-Cl, pH 8.0 buffer in the presence of HaltTM protease inhibitor cocktail (1:100, Thermo Scientific) using TissueLyser (Qiagen) at 50 Hz for 2 mins. The homogenate was kept in ice for 10 mins, centrifuged at 14000 x g for 30 mins at 4°C, and the supernatant was collected and stored at -20 °C [285]. Total protein was estimated using Bradford reagent (Sigma). 40 μg of the protein along with the protein marker (Fermentas) were resolved in 9% SDS-PAGE and transferred to Immobilon®-P Polyvinylidene difluoride (PVDF, Sigma) membrane using wet-transfer (Bio-Rad) at constant 350 mA for 1 h. The blots were incubated in blocking

Table 1: Primer sequences used in quantitative real-time PCR of the rat TRPVs (target genes) and HPRT (endogenous control gene).

Target gene	Primer	Primer sequence (5'--->3')	Amplicon length (bp)
TRPV1	F	GTTTCAGGGTGGACGAGGTA	173
	R	ATCCCTCAGAAGGGGAACCA	
TRPV2	F	GTTTGACCGTGACCGACTCT	131
	R	TTCCAGTGGAGCCTTCTGTG	
TRPV3	F	AGAGACCCCATCCAATCCA	197
	R	GCATGAGGAAGTCAGACGCA	
TRPV4	F	TCGGGGTCTTTCAGCACATC	197
	R	CTCATGGCGGTTCTCGATCT	
TRPV5	F	CTTACGGGTTGAACACCACCA	163
	R	TTGCAGAACCACAGAGCCTCTA	
TRPV6	F	GGGGTTAATACTCTGCCTATGG	191
	R	GCACCTCACATCCTTCAAACCTT	
HPRT	F	TTATCAGACTGAAGAGCTACTGTAATGATC	127
	R	TTACCAGTGTCAATTATATCTTCAACAATC	

buffer (3 % BSA, 0.05 % Tween 20 in PBS, pH 7.4) for 1 h, followed by incubation with TRPVs antisera (50 ng/ml, Table 2) for 1 h at room temperature. In addition, the TRPVs antisera were preadsorbed with their respective control peptides (1:1) for 1 h and the blots were incubated with the preadsorbed antisera. After washing in TBST buffer, the blots were incubated in goat anti-rabbit horseradish peroxidase-conjugated antibody (1:10000; Cell Signaling) for 1 h at room temperature. The blots were washed in TBST buffer and the signal was detected using Chemiluminescent HRP substrate (Millipore) in Gel Doc system (BioRad). All the conditions including chemicals, dilution, treatment time, and exposure time for capturing the images were kept constant to minimize the errors.

Immunofluorescence

The pituitary glands were coronally sectioned (18 μm thick) on a cryostat (Leica CM3050 S, Leica Microsystems, Nussloch GmbH, Germany). Sections were collected in PBS, transferred to the antifreeze solution (30% ethylene glycol and 25% glycerol in 0.05 M PB), and stored at $-20\text{ }^{\circ}\text{C}$ until processed further. The details of the antibodies used in the study are given in Appendix 1. Sections were processed for immunofluorescence as described previously [159,201]. Since the application of TRPV1-6 antiserum at 1:1000-1:2500 dilutions followed by incubation in Alexa Fluor 488-conjugated anti-rabbit IgG (1:1000) resulted in a weak immunofluorescence labelling, tyramide amplification protocol was employed for signal amplification of TRPV1-6 signal. Briefly, the sections of the pituitary gland were treated with 0.5% Triton X-100 in PBS for 20 min followed by 3% normal horse serum in PBS for 30 min. Each set of sections were separately incubated in TRPV1-6 antisera for 24 h at $4\text{ }^{\circ}\text{C}$. The sections were washed in PBS and incubated in biotinylated donkey anti-rabbit IgG (Vector Laboratories, Burlingame; 1:400) for 4 h followed by streptavidin-peroxidase (ABC, 1:1000) for 2 h. The immunoreaction was amplified using

Tyramide Signal Amplification kit as per the instructions of the manufacturer (New England Nuclear Life Science Products, USA). Sections were incubated in DTAF-avidin D (1:300, Jackson ImmunoResearch) for 2 h, rinsed in Tris buffer (pH 7.6), and mounted with Vectashield mounting medium containing DAPI (Vector).

A set of TRPV1 labelled pituitary sections from each animal were processed for GH immunofluorescence. The sections were incubated in polyclonal rabbit anti-GH antiserum overnight at 4 °C. The sections were washed in PBS and incubated in Alexa Fluor 594-conjugated anti-rabbit IgG (1:1000, Life Technologies) for 4 h at room temperature. After rinsing in Tris buffer, sections were mounted on glass slides and coverslipped with Vectashield mounting medium with DAPI (Vector).

Pituitary cell culture

The pituitary glands were kept in fresh ice-cold HBSS buffer, rinsed in 0.1 M PBS, pH 7.4, followed by gentle trituration in growth plating media [Neurobasal medium, 1X; B-27 supplement, 1X; GlutaMax, 1X; FBS, 0.5%; Penicillin-Streptomycin, 1X (Thermo Fisher Scientific)] [281]. The suspension was passed through the cell strainer (40 µm) and centrifuged at 1000 rpm for 5 mins. The pellet was resuspended in growth plating media. Approximately 2×10^5 cells per well were seeded on poly-d lysine coated coverslips and were placed in the CO₂ incubator (5% CO₂, 37 °C) for 2 days to allow cells to adhere. After 2 days, the coverslips containing adhered cells were used for immunofluorescence, ELISA, and Ca²⁺-imaging as described below.

The coverslips containing adhered pituitary cells were processed for GH and TRPV1 double-immunofluorescence labelling. In brief, coverslips were washed once with PBS, fixed in 4% paraformaldehyde in PB for 10 mins, and rinsed in PBS. The cells on coverslips were immersed in 0.2% Triton X-100 for 5 mins followed by washing in PBS. The cells were

blocked with 3% normal horse serum in PBS for 30 mins and incubated in polyclonal rabbit anti-TRPV1 antiserum for 2 h. The cells were washed with PBS and incubated in biotinylated donkey anti-rabbit IgG (1:400, Vector Laboratories) for 2 h followed by streptavidin-peroxidase (ABC, 1:1000). The immunoreaction was amplified as described above and detected using DTAF-avidin D. The cells were rinsed in PBS and incubated in GH antiserum for 2 h. After washing with PBS, the cells were incubated in Alexa Fluor 594-conjugated goat anti-rabbit IgG (1:1000) for 1 h. The cells were rinsed with Tris buffer (pH 7.6), and mounted in Vectashield mounting medium containing DAPI (Vector).

Growth hormone ELISA

The coverslips containing adhered pituitary cells were rinsed with serum-free media [Neurobasal medium, 1X; B-27 supplement, 1X; GlutaMax, 1X; Penicillin-Streptomycin, 1X] and incubated in the same fresh serum-free media for 1 h in CO₂ incubator (5 % CO₂, 37 °C) prior to experiment. After 1 h, the media was replaced with serum-free media containing 0.1 μM resiniferatoxin (RTX, TRPV1 agonist, CAT # 1137/1, Tocris Bioscience), 1 μM 5'-iodoresiniferatoxin (5'-iRTX, TRPV1 antagonist, CAT # 1362/1, Tocris Bioscience), and vehicle (containing DMSO; solvent for RTX and 5'-iRTX). The no-treatment group received only the serum-free media. Experiment was conducted in triplicate. The media were collected and stored at – 80 °C from the RTX, vehicle and no-treatment groups after 1 h of treatment. In the 5'-iRTX group, cells were rinsed in serum-free media followed by incubation with serum-free media containing RTX (0.1 μM). The media was collected after 1 h of treatment and stored at – 80 °C. Ten μl media from each group was assayed for GH levels using rat/mouse GH ELISA kit (Cat # EZRMGH-45K, Millipore) along with the equivalent amount of the quality controls (Cat # E6045-K, Millipore) and rat/mouse GH standard supplied, in duplicates as per the manufacturer's instructions. The absorbances were

read at 450 nm and 590 nm in ELISA plate reader within 5 mins and the difference in absorbance values (450 nm – 590 nm) were used to obtain the standard curve. The data was analysed using MasterPlex ReaderFit, a Curve-Fitting Software for ELISA Analysis.

All the quality control values fall within the calculated quality control range. The dose-response curve for this assay fits best to a 5-parameter logistic equation which was used to calculate the GH levels in different groups.

Ca²⁺ imaging

To test whether the release of GH in rat pituitary cell culture by TRPV1 activation is dependent or independent of Ca²⁺ ions, Ca²⁺-imaging was performed using Fluo-4 AM as previously described [347] with modifications.

Briefly, Pluronic F-127 (Cat. # P3000MP, Thermo Fisher Scientific) was mixed with Fluo-4 AM (Cat. No. F14201, Thermo Fisher Scientific) in 1:1 ratio such that the final concentration of Pluronic F-127 was below 0.1 %. The cells on coverslips were loaded with 2 µM Fluo-4 AM calcium indicator dye containing Pluronic F-127 in Ca²⁺-free HBSS buffer (Cat. # TL1098, HiMedia) for 45 mins in CO₂ incubator (5 % CO₂, 37 °C). The cells were rinsed in Ca²⁺-free HBSS buffer containing 1 mM probenecid (Cat. No. P8761, Sigma) followed by incubation with Hibernate A supplemented with GlutaMax, B-27, and 1 mM probenecid for 30 mins in CO₂ incubator (5 % CO₂, 37 °C). Fluorescence measurements were taken up to 36.4 mins at every 3 sec using a 490 nm excitation and 543 nm emission filter block in laser-scanning confocal microscope (LSM780, Carl Zeiss, Germany). Vehicle (containing DMSO) and RTX (0.1 µM) were given after 2 mins of the start of fluorescence measurements. The change in fluorescence intensity at a given time relative to average fluorescence intensity before stimulus ($\Delta F/F$) was plotted as a function of time [348].

Image capturing and image analysis

The image analysis system consisted of a fluorescence microscope equipped with a CCD camera. Images were captured using AxioCam digital camera (Carl Zeiss) by switching the filter sets. In Adobe Photoshop CS4 (Adobe Systems, Inc., USA), the images were superimposed, and adjusted for the brightness and contrast. In addition, the pituitary sections and coverslips containing pituitary cells were also analyzed under laser-scanning confocal microscope (LSM780, Carl Zeiss, Germany). Immunofluorescence signal was detected at excitation/emission wavelengths of 495/517 nm (DTAF, green), 590/619 nm (Alexa Fluor 594, red), and 358/463 nm (DAPI, blue). The series of optical slices from each coverslip were analysed using LSM software.

The immunoreactivity of each ion channel was visually scored [+ , low; ++, moderate; +++, high; +++++, intense; -, absent] based on the relative density in different compartments of the pituitary (Table 2).

Specificity of the antisera

The specificity of TRPV1 [349,350], TRPV2 [202], TRPV3 [215], TRPV4 [351], TRPV5 [159], and TRPV6 [201] antisera is well established. Stringent control procedures including omission of the primary antisera from the reaction, replacement of the primary antiserum with normal serum, and application of the preadsorbed antiserum with the respective control peptides at 1:1, were employed.

Statistical analysis

The various groups in different experiments were analyzed in GraphPad Prism 7.02 (trial version) software using One-way ANOVA followed by Bonferroni's multiple comparison test. A $P < 0.05$ was considered statistically significant.

RESULTS

TRPV1-6 mRNA expression in the rat pituitary

The TRPV1-6 mRNA expression was observed in the rat pituitary. Higher expression of TRPV1 followed by TRPV2 and TRPV4, TRPV3 and TRPV5, with lower levels of TRPV6 was seen in the pituitary gland (Fig. 1).

TRPV1-6 immunoreactivity in the rat pituitary

No immunofluorescence was observed in the pituitary sections following omission of the primary antisera from the reaction and replacement of the primary antiserum with normal serum. Further, the application of the preadsorbed antiserum with the respective control TRPV peptide did not produce any immunoreactivity in the pituitary gland sections (Fig. 2). The pituitary gland of rat consists of three lobes viz. PD, PN, and PI. In addition, PT has been suggested as a structural subdivision of PD and share similar ontogenic origin [352]. A discrete organization of TRPV1-6 immunoreactive elements was observed in each lobe of the pituitary gland. The diagrammatic representation of TRPV1-6-ir elements in the pituitary gland is shown in Figure 3, the relative immunoreactivity of each ion channel in different pituitary compartments is given in Table 2, and details of organization of TRPV-equipped cells/fibers in pituitary are described below.

TRPV1

Distribution of TRPV1-equipped elements in the rat pituitary is shown in Figs. 3A, 4A-D, and 5A. TRPV1 immunoreactivity was observed in the PD, PN, and PI (Fig. 3A, 4A-D). Weak TRPV1-ir fibers/terminals were seen in the PN (Figs. 3A, 4A, B). While several moderately TRPV1-ir cells were observed in the PI and PD (Figs. 3A, 4A, C, D), intense

immunoreactive cells were localized in PT (Fig. 5A). TRPV1-ir was seen in the periphery of the cells (Fig. 4D).

TRPV2

Organization of TRPV2-ir elements in the pituitary of rat is shown in Figs. 3B, 4E-H, and 5B. Dense and intensely labelled TRPV2-ir fibers were observed in the PN (Fig. 3B, 4E, F). Intensely labelled TRPV2-ir stellate cells were observed in the PD (Figs. 3B, 4E, H). No distinct immunofluorescence signal was detected in the PI (Figs. 3B, 4E, G) and PT (Fig. 5B).

TRPV3

The distribution of TRPV3-expressing elements in the pituitary is shown in Figs. 3C, 4I-L, and 5C. Isolated TRPV3-ir terminals and weak immunofluorescence signal was noticed in the PN (Figs. 3C, 4I, J). The PI showed diffuse TRPV3 immunofluorescence (Figs. 3C, 4I, K). In the PD, scattered TRPV3-ir cells were observed (Figs. 3C, 4I, L). No distinct TRPV3-ir was seen in the PT (Fig. 5C).

TRPV4

The organization of TRPV4-ir in the pituitary of rat is shown in Figs. 3D, 4M-P, and 5D. Isolated terminals and weak immunofluorescence signal were observed in the PN (Figs. 3D, 4M, N). While intensely labelled distinct TRPV4-ir cells were seen in the PI (Figs. 3D, 4M, O), isolated weak cells were present in the PD (Figs. 3D, 4M, P). No immunofluorescence signal was observed in the PT (Fig. 5D).

TRPV5

Organization of TRPV5-ir elements in the pituitary gland of rat is shown in Figs. 3E, 4Q-T, and 5E. TRPV5-ir was observed in all subdivisions of the pituitary gland. While several intensely labelled cells were observed in the PI (Figs. 3E, 4Q, S), isolated cells were seen in the PD (Figs. 3E, 4Q, T). The PN showed the presence of moderately immunoreactive terminal fields (Figs. 3E, 4Q, R) whereas intensely labelled cells were seen in the PT (Fig. 5E).

TRPV6

The distribution of TRPV6-ir cells/terminals in the different lobes of the pituitary gland of rat is shown in Figs. 3F, 4U-X, and 5F. TRPV6-ir fibers/terminals were observed in the PN (Figs. 3F, 4U, V). The PI showed the presence of compactly organized TRPV6-ir cells (Figs. 3F, 4U, W). Moderate to intensely immunoreactive cells were observed in the PD (Figs. 3F, 4U, X) and PT (Fig. 5F).

GH secreting cells in PD co-express TRPV1

Application of GH/TRPV1 double immunofluorescence method on pituitary gland showed co-expression of GH and TRPV1 in vast majority of cells in PD (Fig. 6A-C) as well as in the isolated rat pituitary primary cells (Figs. 6D-F). By semi-quantitative analysis of the pituitary sections for double labelled cells with GH+TRPV1, approximately 87% GH cells showed co-expression of TRPV1.

Activation of TRPV1 increases GH secretion *in vitro*

Compared to vehicle and no treatment groups, while the rat pituitary primary cells treated with 0.1 μ M RTX resulted in significant increase in GH secretion (Fig. 7), cells treated with 1 μ M IRTX followed by 0.1 μ M RTX blocked the RTX-induced increase in GH

release (Fig. 7). Compared to vehicle and no treatment, 0.1 μM CART peptide treatment significantly increased GH release from the pituitary cells (Fig. 7). The GH release observed by treatment with 0.1 μM RTX was significantly higher than that by 0.1 μM CART peptide, suggesting TRPV1-mediated GH release in rat pituitary primary cells is more potent than CART-induced GH release (Fig. 7). The GH levels in cells pre-treated with IRTX followed CART peptide and CART peptide alone was comparable (Fig. 7).

Effect of TRPV1 activation on $[\text{Ca}^{2+}]_i$ activity in rat pituitary primary cells

The $[\text{Ca}^{2+}]_i$ activity in rat pituitary primary cells prior (Fig. 8A), during (Fig. 8B), and after (Fig. 8C, D) application of 0.1 μM RTX were comparable. No change was observed in $\Delta\text{F}/\text{F}$ prior or after the application of RTX (Fig. 8E).

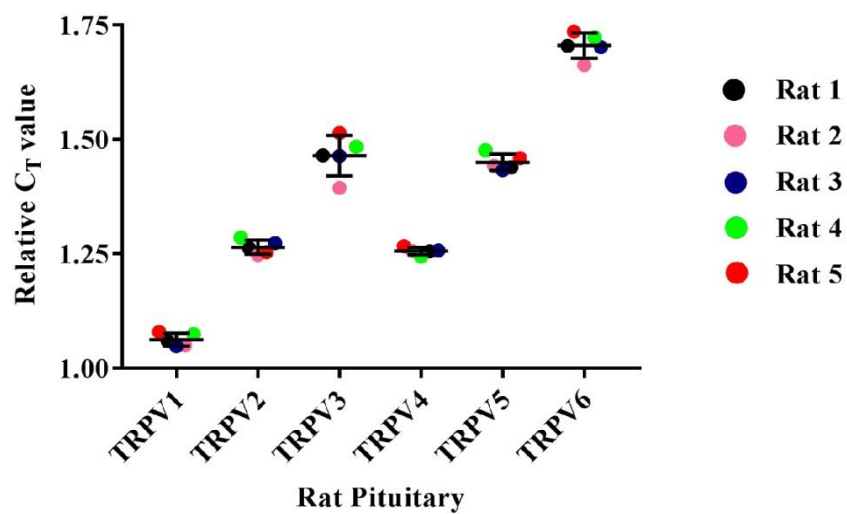


Figure 1: TRPV1-6 mRNA expression in the pituitary gland of rat. The relative C_T values for TRPV1-6 in the rat pituitary are represented as mean \pm SD. Coloured circles represent the relative C_T values for individual rats and the horizontal lines represent the mean relative C_T values from five rats. $P > 0.05$ TRPV2 vs TRPV4 and TRPV3 vs TRPV5.

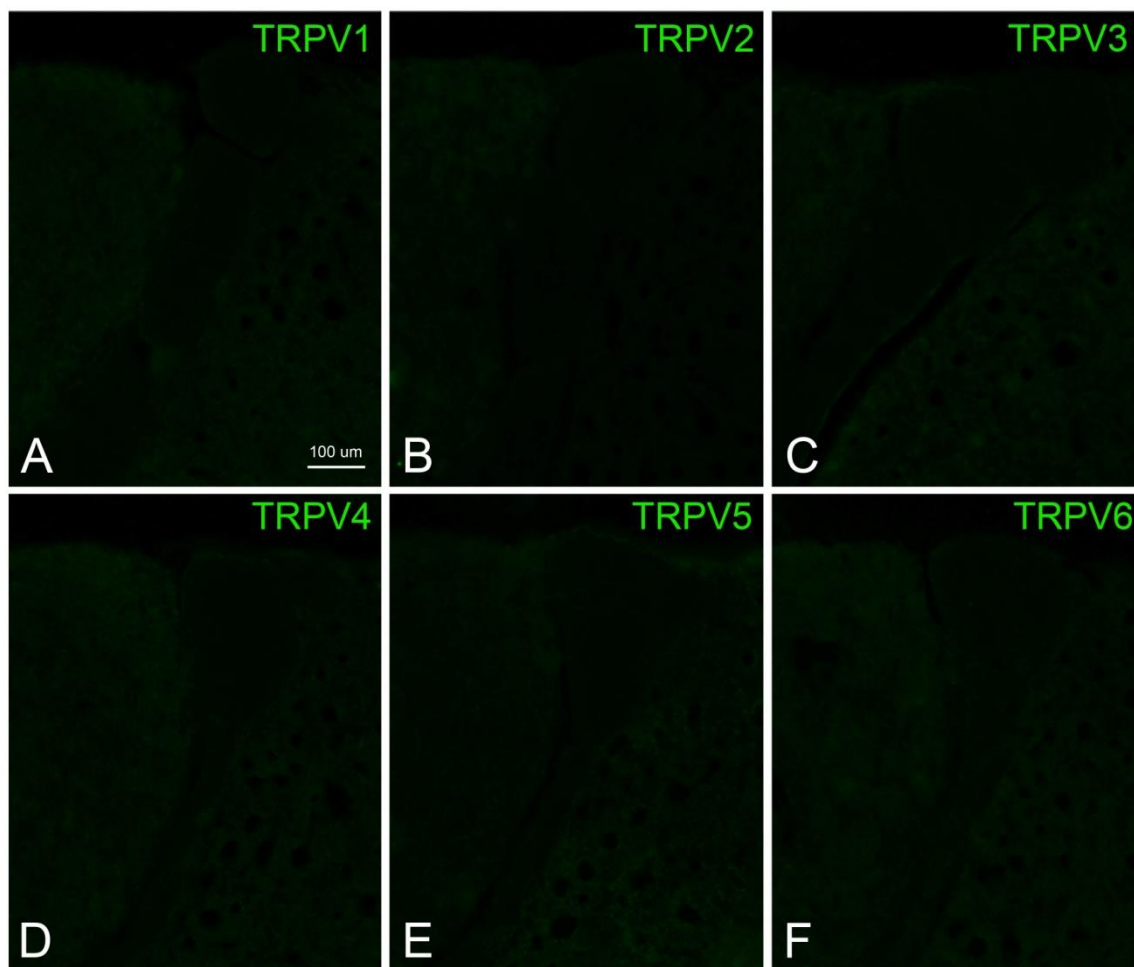


Figure 2: Specificity of the TRPV1-6 antisera in the pituitary gland of rat. Immunofluorescence photomicrographs of the sections of the rat pituitary gland incubated in (A) TRPV1, (B) TRPV2, (C) TRPV3, (D) TRPV4, (E) TRPV5, and (F) TRPV6 antisera preadsorbed with respective control peptide. No immunofluorescence is seen in the pituitary gland. Scale bar = 100 μ m.

Table 2: Qualitative analysis of TRPV1-6 immunoreactivity in the pituitary gland of rat

Organization of TRPV channels in the pituitary gland of rat				
TRPV subfamily	Pituitary gland			
	Pars nervosa	Pars intermedia	Pars distalis	Pars tuberalis
TRPV1	++	++	++++	++++
TRPV2	++++	-	+++	-
TRPV3	+	++	++	-
TRPV4	+	++	+	-
TRPV5	++	++++	+	++
TRPV6	+++	++++	+++	+++

Score based on relative density of TRPV channels immunoreactivity in different pituitary compartments: +, low; ++, moderate; +++, high; +++++, intense; -, absent

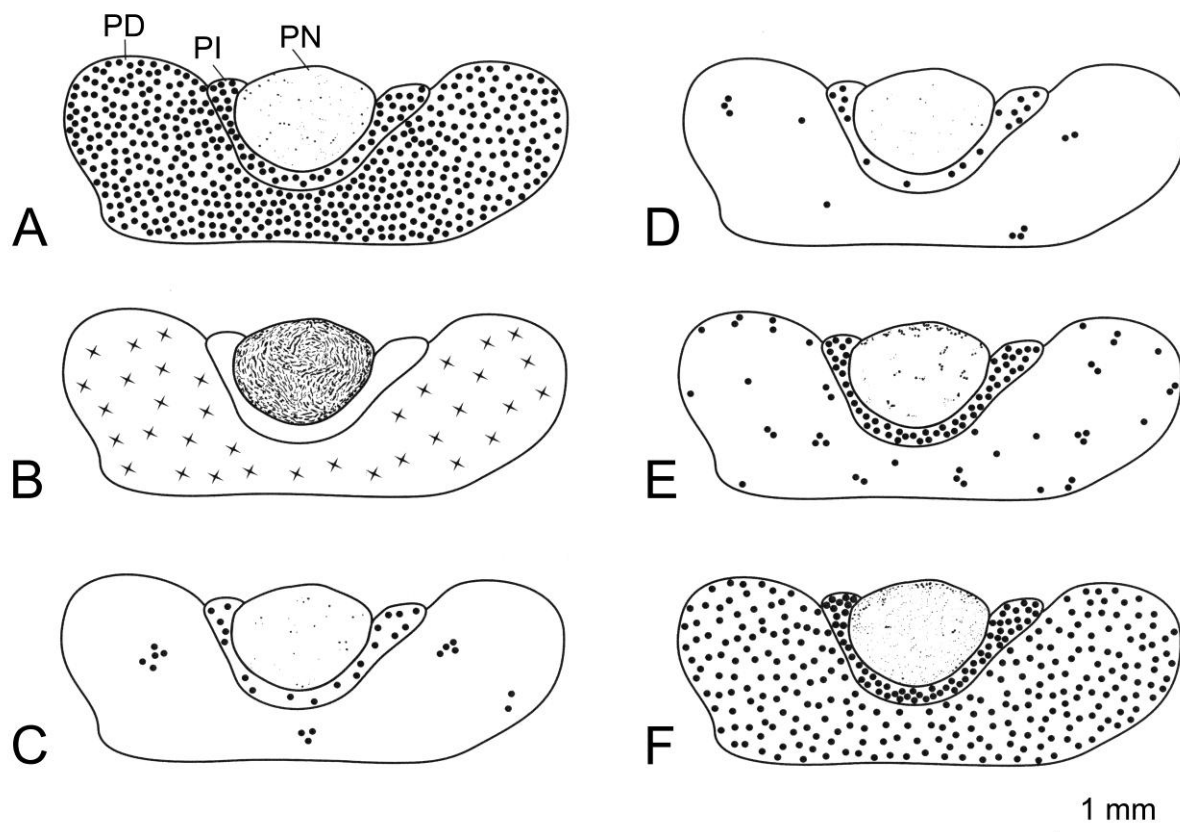


Figure 3: Schematics showing the organization of TRPV1-6 immunoreactive elements in the pituitary gland of rat. Schematics showing organization of (A) TRPV1-, (B) TRPV2-, (C) TRPV3-, (D) TRPV4-, (E) TRPV5-, and (F) TRPV6-equipped elements in pars distalis (PD), pars nervosa (PN) and pars intermedia (PI) of the rat pituitary gland. Immunoreactive fibers/terminals are shown with dots/dotted lines and cells with closed circles. The star shaped cells represent TRPV2-ir stellate cells in PD. Scale bar = 1 mm.

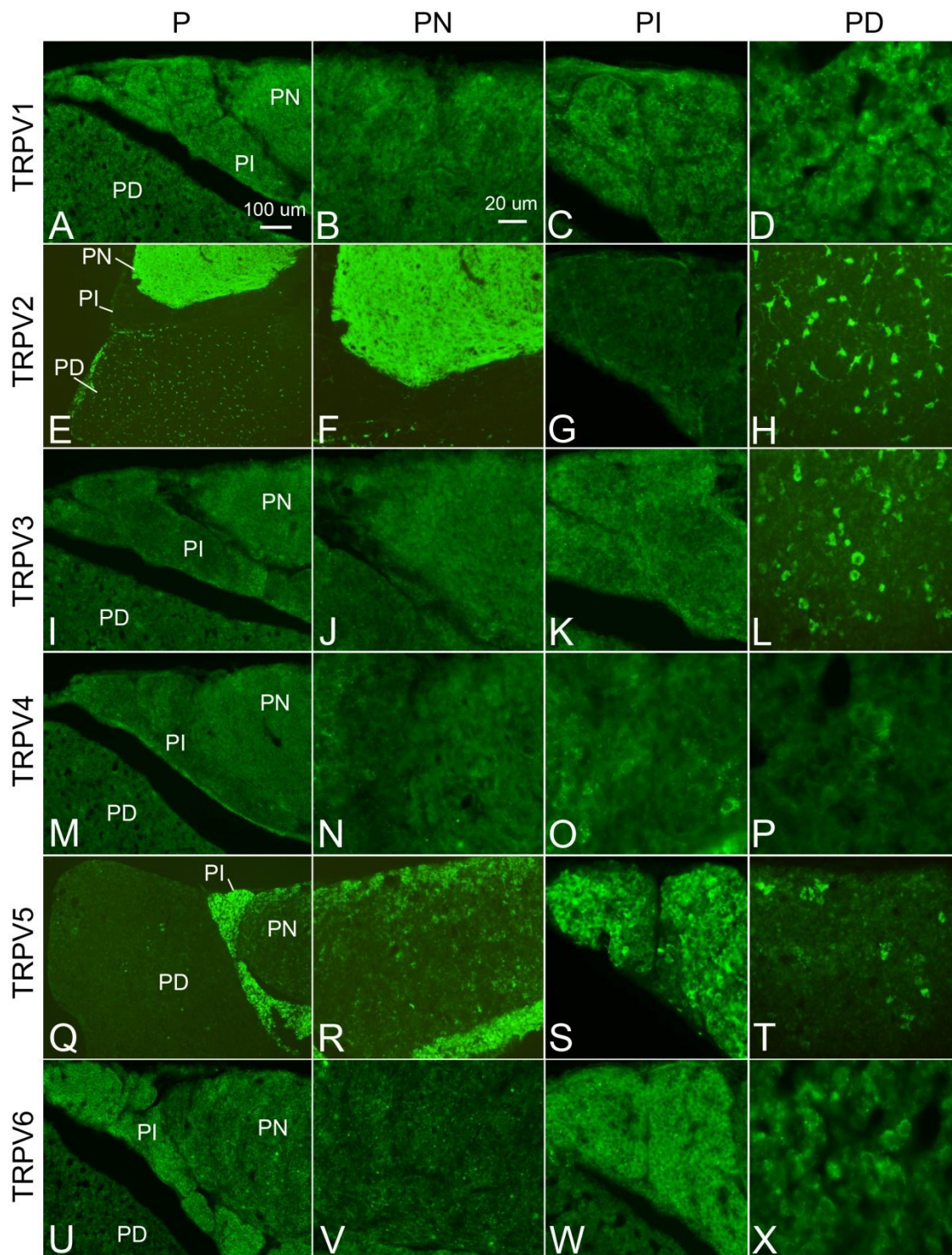


Figure 4: TRPV1-6 immunoreactivity in the pituitary gland of rat. Immunofluorescence photomicrographs of the sections of the pituitary gland showing (A-D) TRPV1, (E-H) TRPV2, (I-L) TRPV3, (M-P) TRPV4, (Q-T) TRPV5, and (U-X) TRPV6 immunoreactive cells or fibers in the pars nervosa (PN, B, F, J, N, R, V), pars intermedia (PI, C, G, K, O, S, W), and pars distalis (PD, D, H, L, P, T, X). The low magnification images of the pituitary gland are shown in the first column (A, E, I, M, Q, U). Scale bar = 100 μm (A, E, I, M, Q, U) and 20 μm (B-D, F-H, J-L, N-P, R-T, V-X).

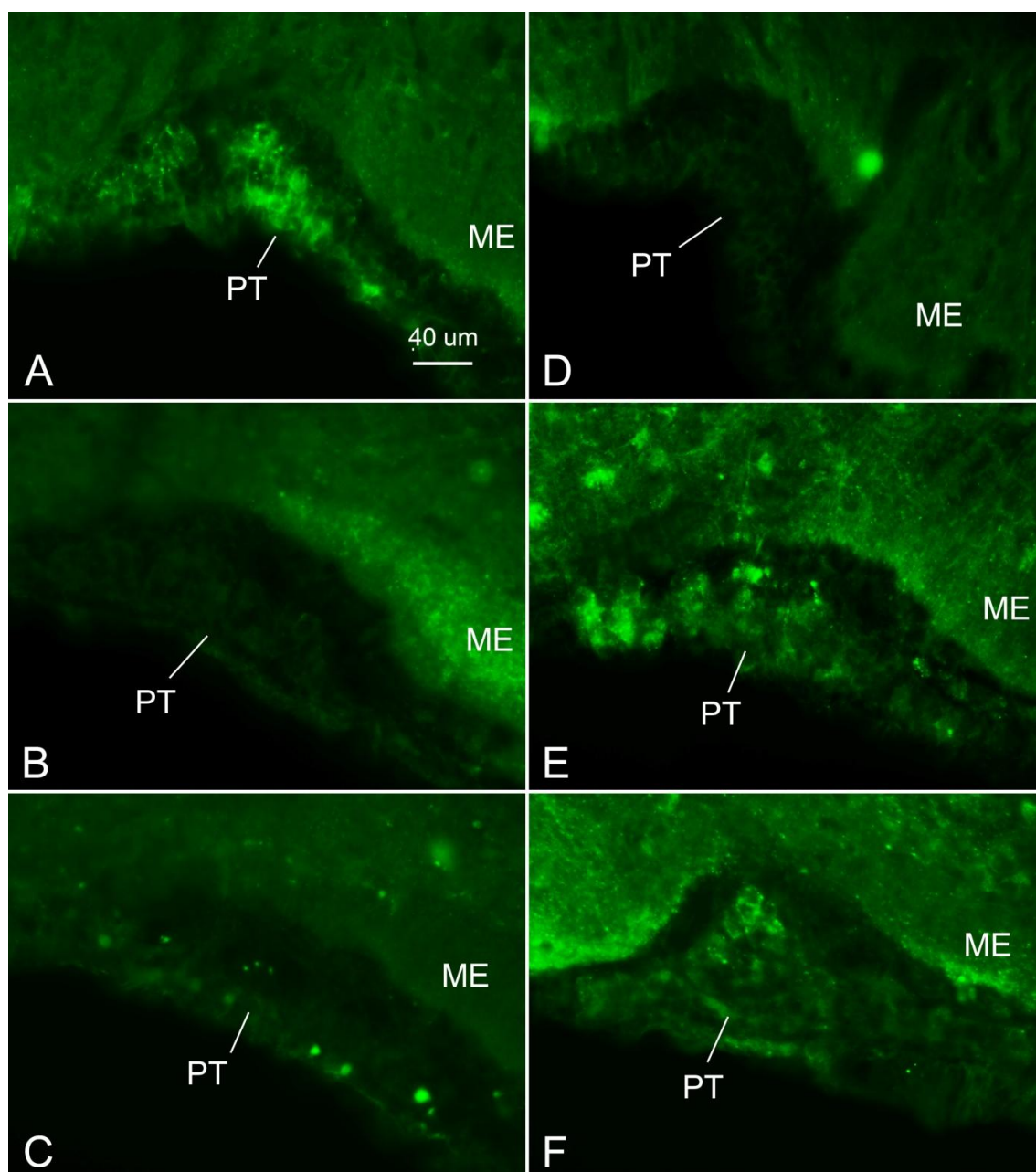


Figure 5: TRPV1-6 immunoreactivity in the pars tuberalis (PT) of rat. Immunofluorescence photomicrographs of the hypothalamic sections at the level of median eminence (ME) showing (A) TRPV1, (B) TRPV2, (C) TRPV3, (D) TRPV4, (E) TRPV5, and (F) TRPV6 immunoreactivity in the PT. Scale bar = 40 μm .

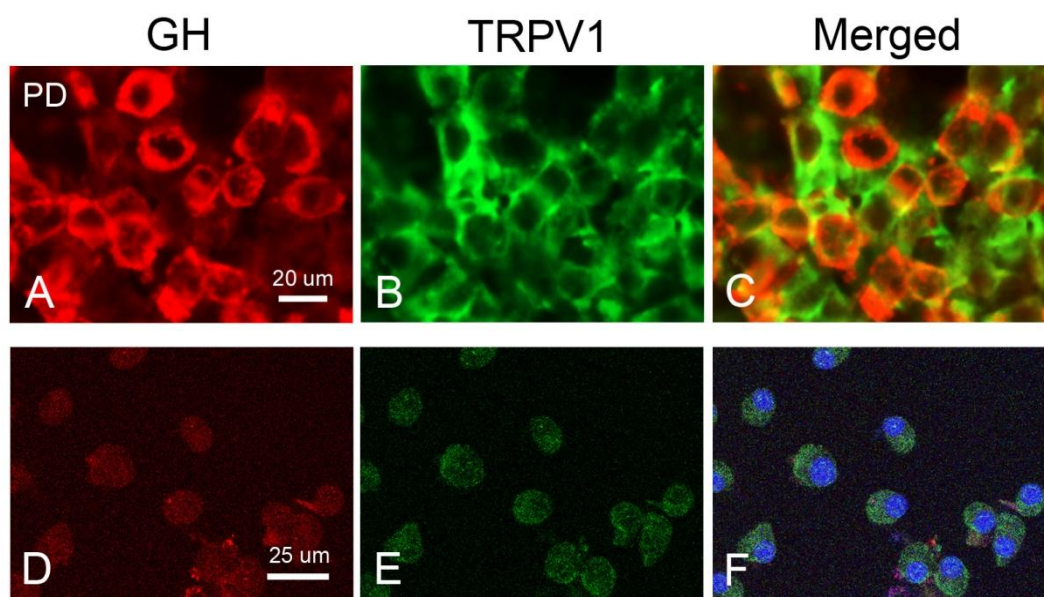


Figure 6: Growth hormone (GH) secreting cells in the rat pars distalis (PD) and pituitary primary cells co-express TRPV1. Double immunofluorescence photomicrographs of the sections of PD of the pituitary gland of rat (A-C) as well as the isolated rat pituitary primary cells (D-F) showing growth hormone (GH, red, A, D) and TRPV1 (green, B, E) immunoreactive cells. The co-localized cells (C, F) appear yellow due to colour mixing. Scale bar = 20 μm (A-C) and 25 μm (D-F).

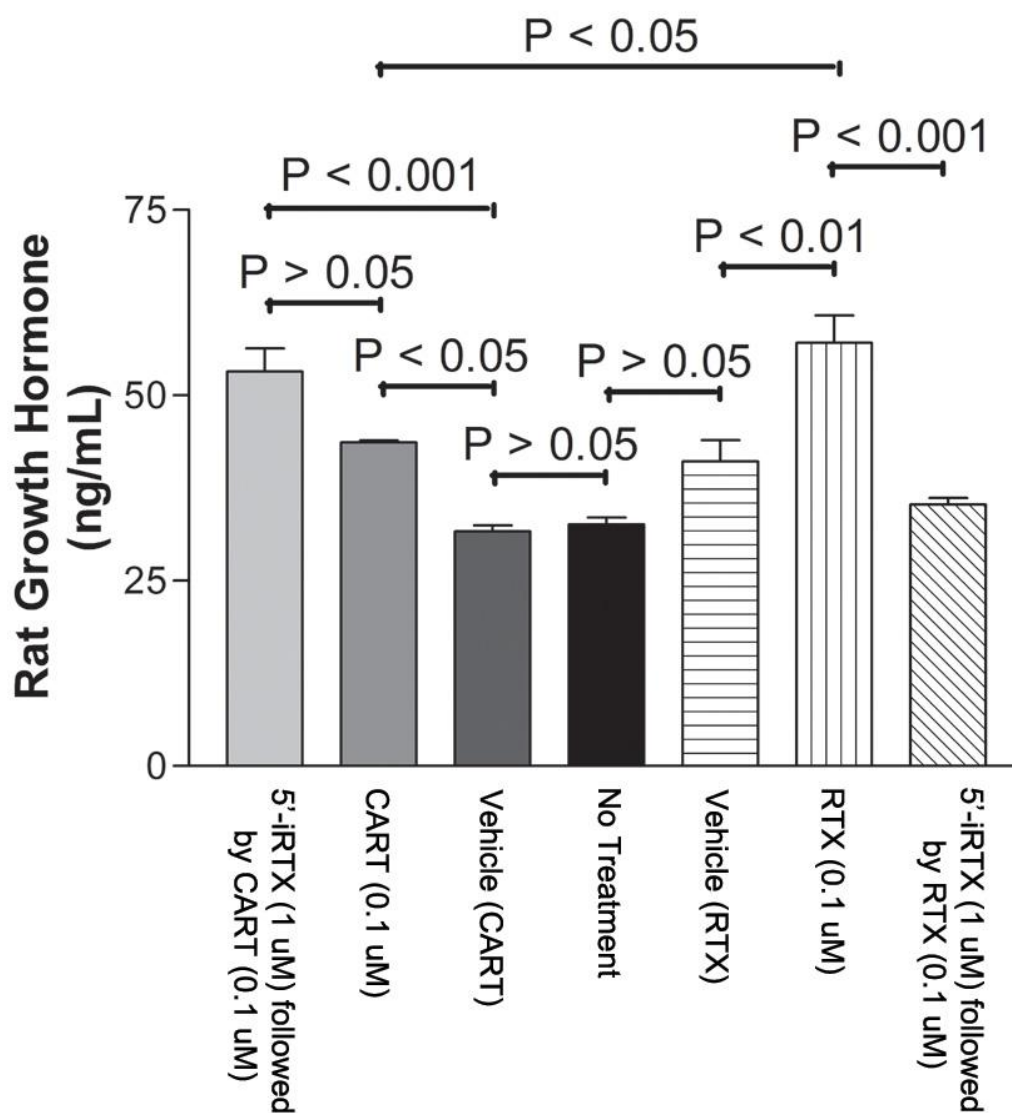


Figure 7: Effect of CART peptide treatment and TRPV1 agonist on growth hormone secretion. Effect of CART peptide and TRPV1 agonist, resiniferatoxin (RTX) on growth hormone (GH) release (ng/ml) from the rat pituitary primary cells. CART peptide or RTX significantly increase GH release. Pre-treatment of the cells with TRPV1 antagonist, iodoresiniferatoxin (iRTX) blocked TRPV1- but not CART-induced GH release.

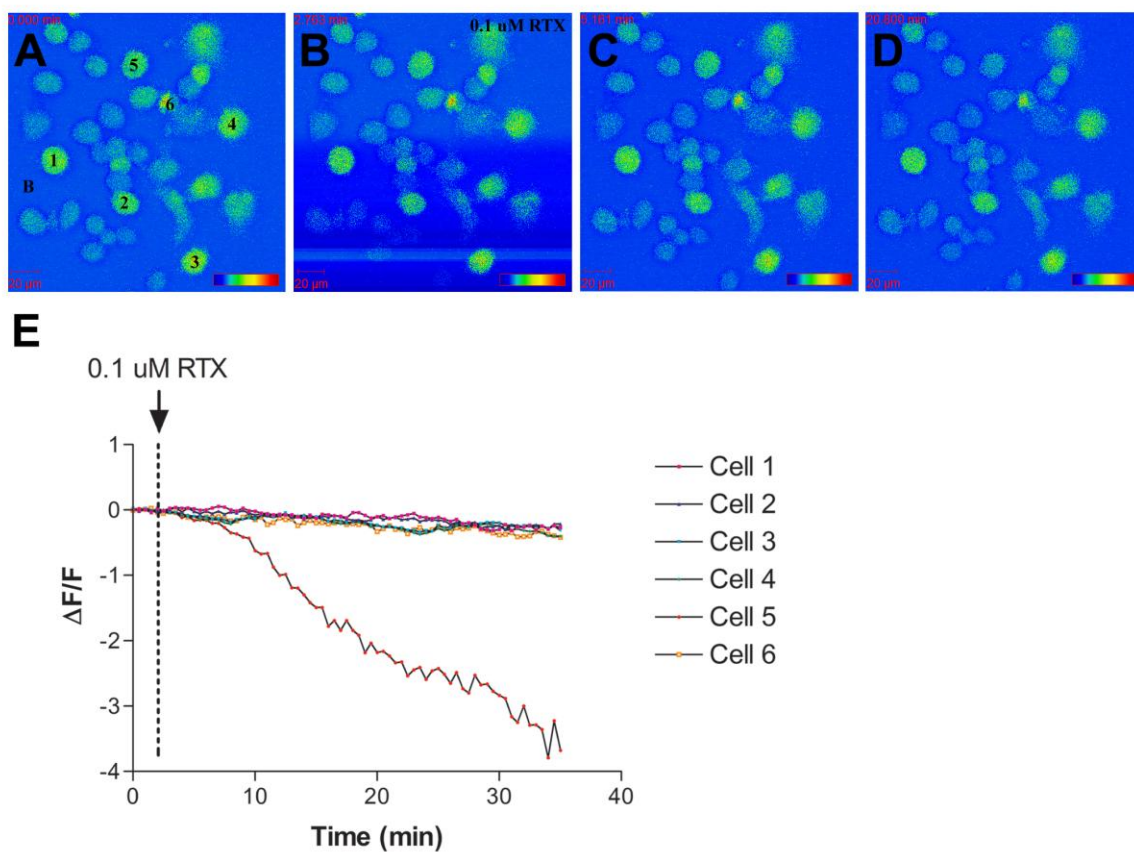


Figure 8: Effect of TRPV1 agonist on $[Ca^{2+}]_i$ activity in the rat pituitary primary cells. Photomicrographs showing intracellular Ca^{2+} concentration, $[Ca^{2+}]_i$ in rat pituitary primary cells prior (A), during (B), and after (C, D) application of TRPV1 agonist, resiniferatoxin (RTX). The change in $[Ca^{2+}]_i$ in RTX-treated rat cells (1-6) is shown in E. $[Ca^{2+}]_i$ is measured in terms of change in fluorescence intensity at a given time relative to average fluorescence intensity before stimulus ($\Delta F/F$). B = Background, Scale bar = 20 μm

DISCUSSION

Information on TRPV ion channels in the pituitary is scanty and functional significance of these channels in the regulation of pituitary hormones unexplored. Presence of TRPV1- and TRPV2-immunoreactivity was observed in the pars nervosa of the pituitary gland of rat [202] and monkey [203]. While we have recently described presence of TRPV6-ir cells in the pars tuberalis of mouse pituitary gland, Smith et al. [217] observed presence of TRPV3 transcript in the pituitary gland of rat. In the present study, expression of TRPV1-6 mRNA was detected in the pituitary gland of rat. The TRPV1 mRNA was highly expressed but low level of TRPV6 was seen in the pituitary. Our immunofluorescence data showed distinct cells in the PD and PI equipped with TRPV, whereas in the PN fibers/terminals containing TRPV1-6-ir were observed. The PD contained several TRPV1 and TRPV6-ir cells and PI showed the presence of TRPV5- and TRPV6-ir cells. The GH cells in PD showed co-expression of TRPV1, and treatment of the primary pituitary cells with TRPV1 agonist resulted in release of GH. This is the first report demonstrating discretely organized TRPV1-6-equipped elements in different compartment of the pituitary gland and significance of TRPV1 in the regulation of GH secretion.

Specific antisera against TRPV1-6 were employed for localization of the respective ion channels in the rat pituitary gland. These antisera have been used in previous studies to localize TRPV1-6 in different tissues. For example, TRPV1 antiserum was used to localize TRPV1 in DRG neurons of rat [350] and mice [353]. The TRPV2 antiserum was used for localization of TRPV2 in the brain and pituitary of rat and the specificity established using tissue obtained from TRPV2 knock out mice [202]. TRPV3 antiserum has been demonstrated to recognize its antigen in rat brain and in TRPV3 transfected cells [215]. The specificity of the TRPV4 was established in TRPV4-transfected HEK cells and mouse kidney

[351,354]. Recently, we have established the specificities of the TRPV5 and TRPV6 antisera in mouse/rat brain [159,201]. We further validated the specificity of each antiserum in the rat pituitary using preadsorption control protocol. We suggest that the TRPV1-6 antisera are specific and recognizing respective antigens in the pituitary gland of rat. Using qRT-PCR, distinct expression of each member of TRPV subfamily was observed in the pituitary gland of rat. Compared to other channels, TRPV1 mRNA was highly expressed whereas lowest level of TRPV6 mRNA was observed. The channel synthesis, trafficking, and recycling might a factor for the discrepancy in the results obtained with qRT-PCR and immunofluorescence. Further, we have used entire pituitary gland for qRT-PCR analysis, whereas immunofluorescence localization of TRPV1-6 was studied in each pituitary lobe.

While abundant TRPV2-ir was observed in the PN of rat, scattered TRPV1, TRPV3-6-ir fibers/terminals were seen in this region. The fibers/terminals in PN of rat [202] and monkey [203] are known to express TRPV2-immunoreactivity. The PN contains axon terminals of magnocellular neurons of the hypothalamic paraventricular (PVN) and supraoptic (SON) nuclei which synthesizes nonapeptides, oxytocin and vasopressin [42]. The oxytocin and vasopressin neurons in the PVN and SON co-express TRPV2 and importance of TRPV2 as a cation conducting channel in neurohypophyseal neurons to regulate lactation, diuresis, and parturition has been suggested [203]. The oxytocin-dependent Ca^{2+} signalling in PVN neurons is mediated *via* TRPV2 activation [355]. TRPV2 at the axonal endings of magnocellular neurons might regulate release of the nonapeptides from posterior pituitary. In addition to the PN, intensely TRPV2 labelled folliculo-stellate cells were seen in the PD. These cells are stellate/sustentacular/star shaped, their processes contact blood vessels and endocrine cells [356,357]. These cells express S-100 protein, glial fibrillary acidic protein, and vimentin and their neuroendocrine origin was proposed [357]. These cells have been considered as supporting cells for endocrine cells in PD [356–360]. Acosta et al

[357]studied the ultrastructure of folliculo-stellate cells and their association with different endocrine cells in PD of a rodent, *Viscacha*. In this animal, the folliculo-stellate cells were associated with lactotrophs, gonadotrophs, and corticotrophs [357]. The folliculo-stellate cells are known to secrete follistatin which may mediate paracrine regulation in pituitary [359]. While we do not know the significance of TRPV2 in folliculo-stellate cells, we speculate a role for this ion channel in regulation of other endocrine cells in PD.

We observed the presence of distinct TRPV1-, TRPV5-, and TRPV6-ir cells in the PT of the pituitary gland. The PT forms incomplete collar on pituitary/infundibular stalk [361]. Although PT has been considered as one of the major compartments of the adenohypophysis [362–364], it has been suggested that the PT is merely an extension of PD [365]. Using immunohistochemistry, while Gross [366] detected gonadotrophs (LH and FSH) and TSH in the PT of rats, TSH cells contribute a major population of cells of PT. The significance of the TSH cells in PT, however is not well established. The PT also express melatonin receptors and play a role in seasonal physiology [362,367]. Further studies are required to characterize the phenotype of TRPV expressing PT cells and their functional significance.

Exercise is known to stimulate GH secretion [368–373]. Bridge et al. [374] observed a linear increase in rectal temperature and plasma GH levels during exercise. The authors suggested core temperature as major stimulus for GH release [374]. This was further supported by Christensen [375], suggesting that it is mainly the core and not cutaneous temperature which modulate GH release. Although evidences strongly indicate that the exercise-induced rise in body temperature stimulate GH release, the molecular mechanism is still not known. In the present study, we observed the presence of a thermosensitive TRPV1 in GH cells in PD. The ion channels in GH cells seem functional since treatment with TRPV1 agonist, RTX significantly increase GH release from the primary pituitary cells.

While TRPV1 is rapidly activated at 33-39 °C, full opening of the ion channel was observed at 42 °C in the presence of 2.5 µM phosphatidylinositol 4,5-bisphosphate [376]. Bridge et al [374] observed an increase of up to 39 °C in rectal temperature during exercise and temperature of the blood perfusing the brain. The rectal temperature is generally slightly lower than that in the oesophagus [374]. We suggest that the rising central core temperature as a result of exercise may activate TRPV1 leading to increased GH release.

Our Ca^{2+} imaging results showed that the release of GH in rat pituitary cell culture by RTX mediated activation of TRPV1 is independent of change in activity of $[\text{Ca}^{2+}]_i$. Few reports have demonstrated TRPV1 mediated processes without any significant change in $[\text{Ca}^{2+}]_i$. For example the RTX mediated activation of TRPV1 in mouse DRG explants which cause varicosity formation and growth cone retraction seems independent of Ca^{2+} mobilization from the endoplasmic reticulum and partially independent of Ca^{2+} influx [377]. Although the proteins involved in exocytosis machinery in different cells are of similar, the molecular composition is different in different cell types. The stimulus based secretion where in neurons and endocrine cells has been shown to be Ca^{2+} dependent, it is independent of Ca^{2+} in epithelial and blood cells [378]. However, there are evidences where the secretion by neurons and endocrine cells has been observed without affecting intracellular Ca^{2+} levels [378]. For example, the release of vasopressin from isolated neurohypophysial nerve endings can be evoked by Na^+ without rise in the intracellular Ca^{2+} [379]. Corticotropin-releasing factor (CRF) stimulation has been shown to be both Ca^{2+} -dependent as well as Ca^{2+} -independent in primary cultured anterior pituitary cells of the rat [380]. While the GnRH-induced LH secretion from rat gonadotropes is Ca^{2+} -dependent [381], phorbol myristate acetate stimulates LH secretion without detectable $[\text{Ca}^{2+}]_i$ elevation [382]. The activation of G-protein *via* intracellular dialysis of non-hydrolysable analogues of GTP can directly stimulate a component of exocytosis that is independent of $[\text{Ca}^{2+}]_i$ elevation, as well as the

activation of the cAMP or PKC pathway [383]. This G-protein-mediated and Ca^{2+} -independent exocytosis appears to be acting on a pool of vesicles or granules that is distinct from the Ca^{2+} -dependent pool [383].

Since CART stimulate GH release when given intracerebroventricularly or intravenously [39], we explored the involvement of TRPV1 in CART's action on GH cells. Treatment of the primary rat pituitary cells with CART peptide resulted in significant increase in GH release. Although CART serves as regulator of GH cells, the origin of CART stimulation to the pituitary is still unclear. Intense CART immunoreactivity is observed in the median eminence. CART-ir cells are present in the pituitary but only 10 % GH cells co-express CART. We presume that the hypophysiotropic neurons synthesizing CART may significantly contribute to the action of CART on GH cells. The effect of CART on GH release, however, does not seem to be mediated via TRPV1 since blockage of TRPV1 with its antagonist could not prevent CART-induced GH release. We suggest that in addition to the central control, the GH cells might be equipped with mechanism to regulate the hormone secretion independent of the hypothalamic regulation. TRPV1-6 ion channels therefore seem to be the novel elements in the regulatory control of pituitary gland and their differential distribution in pituitary lobes suggest their involvement in precise control of endocrine or neuroendocrine regulation.

SUMMARY AND CONCLUSIONS

The reproductive success of any species depends on nutritional status and a perfect balance between energy balance and reproduction is crucial. Improper nourishment and imbalance in the energy balance may lead to infertility. In rodents, acute or chronic food deprivation or food restriction delays puberty, lengthens estrous cycles and reduces reproductive behavior [1,2]. One of the important factors responsible for the infertility due to inadequate nutrition is the suppression of pulsatile luteinizing hormone (LH) secretion from the pituitary [3]. While GnRH regulates LH secretion, GnRH in turn is regulated by a complex neural circuitry in the hypothalamus. GnRH neurons in the preoptic area have been found to be responsive to glucose treatment and the sensitivity of GnRH neurons was dependent on ovarian steroids [28]. Furthermore, the neural circuitry that regulates feeding, satiety and energy balance also resides in the hypothalamus. Evidence suggesting a complex interplay between the neuronal systems regulating reproduction and energy balance are emerging. It is therefore important to understand the central mechanism that link reproduction and energy balance to design strategies to address the question. The neural pathways and mechanisms regulating reproduction and energy balance are well established. Two subpopulations of neurons residing in the ARC orchestrate the central regulation of energy balance. While the AgRP/NPY-containing neurons inhibit energy expenditure but stimulates food intake, CART/ α -MSH-producing neurons are known to inhibit food intake and stimulate energy expenditure [62–64]. These neurons seem to exert their effect by acting on TRH neurons in the hypothalamic PVN as well as other neuronal elements in the brain [12]. The evidence like suppression in LH and reproductive behaviour during fasting, and regulation of GnRH neurons by peripheral metabolites [3,21,26–28], has raised a possibility of crosstalk between neural pathways regulating energy balance and reproduction. While studies have demonstrated role of CART peptide in energy balance, importance of this

peptide in the regulation of GnRH neurons and reproduction is also available. In this thesis, I have investigated role of ARC CART in weighing reproductive strategies versus energy availability and identified the regulators of CART neurons. An overall representation of the neural circuitry in the hypothalamus involving CART as key messenger linking pathways of reproduction and energy balance, and key regulatory players in the circuitry is shown in Figure 1. The ARC CART neurons showed expression of gonadal steroid receptor, ER α and these neurons respond to changes in energy status. The ARC CART neurons project to several different brain region and distinct innervation of CART-ir fibers was observed in the POA. Using triple immunofluorescence, we identified the innervation of GnRH neurons in POA by CART-ir fibers of ARC origin and the CART-GnRH contacts showed correlation with estrous cycle. We further demonstrate that the CART neurons of ARC co-express highly Ca²⁺-selective TRPV channels viz. TRPV5 and TRPV6. These ion channels genes contain putative estrogen receptor binding elements in their promoters. TRPV5/6 mRNA expression showed estrous cycle-related changes. Interestingly, these ion channel equipped CART neurons project to POA. In addition to the central modulation, CART may also serve as regulator of energy balance by its action on pituitary GH cells. While CART treatment stimulated GH release from the primary rat pituitary cells, the action was not mediated *via* TRPV1.

CART neurons in ARC have emerged as crucial regulators of energy balance. CART neurons senses the peripheral metabolic cues and are believed to serve as the first order neurons in the neural circuitry of central regulation of energy balance [12,13]. We observed the expression of ER α in ARC CART neurons, suggesting role of estrogen in modulating these neurons. The ER α -expressing CART neurons showed activation when the fasted rats were refed for a short interval. These studies suggest that CART neurons in ARC may link two intricate functions of integrating estradiol signalling and modulating food intake/energy

balance. This is further supported by the studies demonstrating role of leptin as well as estrogen in influencing energy balance and reproduction. Since ARC CART neurons express both LepR and ER α , these neurons may play a crucial role in mediating the cross talk. We have also explored the CNS projections of the ARC CART. Not only the regions which processes the energy balance or reproduction related information, ARC CART neurons innervate various regions in the brain and spinal cord, suggesting a complex inputs of ARC CART neurons provided to the CNS. We observed dense innervations of ARC CART neurons in the POA where the CART fibers contacted GnRH neurons. The intensity of GnRH-ir neurons as well as the CART-ir fibers and contacts show energy status- as well as estrous cycle-dependent plasticity. In view of the higher estradiol levels and reduced expression of ER α in ARC [122–124] observed during proestrus, we presume that rising estradiol levels during proestrus may activate ARC CART neurons which then alter the food intake and triggers GnRH neurons. During fasting, by suppressing CART mRNA expression in ARC neurons, the activity of GnRH neurons might be altered. It is important, however, to note that the acute or chronic food deprivation or food restriction in rodent delays puberty, lengthens estrous cycles, and reduces reproductive behaviour [1,2].

TRPV subfamily of cationic channels has emerged as novel players of neuroendocrine regulation. The activation of these channels by various stimuli enables an individual cell to receive information from different signals and accordingly regulate the function of cell. While we observed the presence of putative functional ERE in the promoter regions of TRPV genes, changes in the mRNA expression levels of TRPV genes in different brain regions of mouse across the estrous cycle suggesting importance of estradiol-TRPV interaction in the central control of reproduction. The TRPV5 and TRPV6 channels are distinct from other members of the TRPV subfamily. These ion channels have been suggested temperature insensitive but highly selective for Ca²⁺ ions with P_{Ca}/P_{Na} ratio more

than 100 compared to other TRP channels [248,255]. Despite their high selectivity for Ca²⁺ ions, we could not find evidence of distribution of these ion channels-equipped elements in the CNS. We observed the TRPV5- and TRPV6-ir elements widely distributed in the brain of mice/rat. While TRPV6 was localized in neurons, TRPV5-ir was observed in neurons as well as glial cells. In addition to other brain regions, presence of these ion channel expressing elements was observed in ARC, where a great majority of CART neurons co-express TRPV5, and NPY neurons showed TRPV6-ir. The ARC CART neurons are anorexigenic whereas NPY neurons are orexigenic, and these neuronal populations constitute the major part of the hypothalamic pathways regulating food intake and energy balance [8,9,62–64]. To gain insight into the functional significance of these ion channels in ARC, we employed retrograde neuronal tracing protocol. Following neuronal tracer CtB injection in the POA, we observed accumulation of the tracer in CART neurons co-expressing TRPV5/6. Further, the POA projecting ARC CART neurons co-expressing TRPV5 showed estrous cycle dependent changes. The TRPV5-ir astrocytes in the ARC also showed estrous cycle-dependent changes. The ARC TRPV6-ir neurons coexpressed ER α and their expression showed estrous cycle-dependent changes in the medio-basal hypothalamus. These observations suggest the involvement of TRPV5/6 channels in the regulation of neural circuitry linking energy balance with that regulating reproduction. These ion channels expressions seem to be modulated by circulating levels of estradiol and thereby regulate ARC CART or NPY neurons which in turn regulate the GnRH neurons. In addition to its role in the regulation of ARC CART neurons, hypothalamic neuroendocrine neurons synthesizing oxytocin and vasopressin also seem to be equipped with these ion channels. Further studies are essential to elucidate the functional significance of these ion channels in the regulation of neuroendocrine pathways.

In addition to the role of TSH in regulation of energy expenditure, and importance of LH and FSH in reproduction, the GH secreted by the anterior pituitary gland seem to play an essential role in controlling energy balance as well as reproduction. The GH is a crucial regulator of metabolism and reproduction, and therefore may serve as important player in the cross talk between the two distinct functions. We observed dense CART-ir fibers in the external zone of ME. Hypophysiotropic CART neurons release the peptide in the ME and transported to the anterior pituitary via portal vessels and may trigger GH secretion. Intracerebroventricular administered CART peptide has been shown causes GH release in rats [39]. Since we could not find the CART/ α -MSH double labelled fibers in the ME, we suggest that ARC CART neurons do not contribute directly to the pituitary gland regulation. Treatment of the primary rat pituitary cells with CART peptide resulted in significant increase in GH release. While exploring the CART-GH interaction and role of TRPV in the regulation of ARC CART neurons, we encountered TRPV ion channel expression in the rat pituitary gland. While TRPV1 mRNA was highly expressed, lowest expression of TRPV6 was observed in the pituitary gland. Application of TRPV1-6 immunofluorescence showed discrete organization of these ion channel expressing elements in the pituitary gland. The GH cells in the pituitary co-expressed TRPV1 and treatment with TRPV1-agonist stimulated GH release from rat pituitary primary cells. We further observed that the CART mediated GH release is independent of TRPV1, suggesting different mechanism are employed for GH release by CART and TRPV1 modulators. The TRPV1 induced GH release was more potent than the CART-mediated GH release. These findings seem to have paramount importance in regulation of GH secretion by body temperature. TRPV1 is a thermosensor and GH release has been shown to increase with an increase in the core body temperature as seen during exercise [374]. Activation of TRPV1 and release of GH thus provide an important non-neural mechanism for cross talk between the energy balance and reproduction. Although

presence of six members of TRPV subfamily in three different compartments of pituitary gland was exciting, understanding the significance of each of these ion channels in the regulation of pituitary was challenging. The study might help to further explore the functional significance of TRPV1-6 in the pituitary gland.

Taken together, we suggest that ARC neurons serve as common neural substrate to link pathways regulating energy balance and reproduction, and CART as common messenger employed by these pathways. For the first time we have demonstrated the neuroanatomical organization of TRPV5 and TRPV6-ir elements in the brain. With TRPV ion channels expressed in ARC CART neurons, the regulation of these neurons seem to interesting. CART neurons in ARC contain ER α , and TRPV5. Further, the promoters of TRPV5/6 genes are equipped with putative ERE and their expression changes with changes in circulating levels of estradiol during estrous cycle. We propose that the TRPV5 and TRPV6 may function like ionotropic receptor for estradiol's action. These ion channels seem to be important in the regulation of CART-GnRH pathway since they are present on ARC CART neurons and these neurons project to POA and innervate GnRH neurons to regulate reproduction. In addition to its central action on pathways regulating energy balance and reproduction, CART seems to be a potent regulator of GH cells in pituitary gland. Given the discretely organized TRPV1-6-ir elements in different lobes of the pituitary gland, we speculate that TRPV ion channels as novel endocrine regulators of pituitary gland. With TRPV1-6 in different compartments and polymodal nature of these ion channels, the pituitary hormone secretion might also be regulated independent of the hypophysiotropic regulation. This is evident from the comparable response of GH secretion elicited by CART peptide and TRPV1 agonist treatments, but inability of TRPV1 antagonist to block GH releasing action of CART.

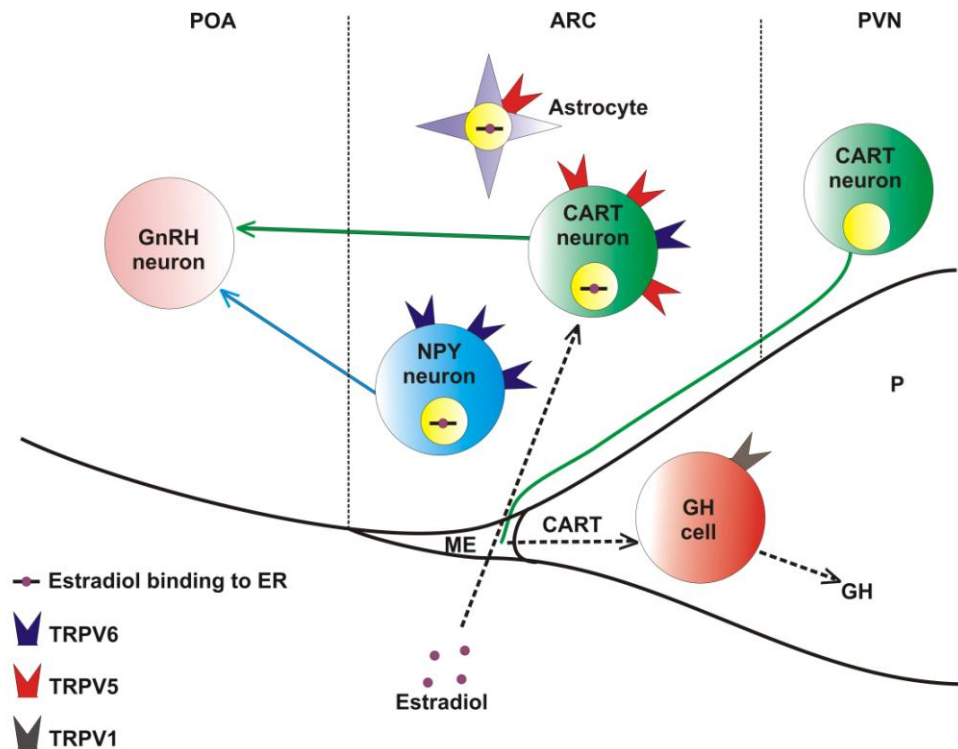


Figure 1: Organization and proposed mechanism of the regulation of neural pathways in the brain wherein the cocaine- and amphetamine-regulated transcript (CART)-containing neurons of the hypothalamic arcuate nucleus (ARC) serve as a common messenger in the crosstalk between circuits regulating energy balance and reproduction. CART neurons residing in the ARC express estrogen receptor ($ER\alpha$) and respond to changes in energy status. The $ER\alpha$ -expressing CART neurons receive estradiol feedback signals and project to preoptic area (POA) to innervate the gonadotropin-releasing hormone (GnRH) neurons. Majority of ARC CART neurons are equipped with TRPV5, innervate GnRH neurons in the POA, and the CART-GnRH contacts show estrous cycle-dependent plasticity. The astrocytes in ARC also express TRPV5 and estradiol may modulate their activity to regulate reproduction. Unlike TRPV5, TRPV6 is expressed by only few ARC CART neurons but the majority of the ARC neuropeptide Y (NPY) neurons co-express TRPV6. The hypophysiotropic CART neurons residing in the paraventricular nucleus (PVN) which project to the external zone of median eminence (ME) may regulate growth hormone (GH) release from the somatotrophs in the pituitary gland (P). GH is a crucial regulator of metabolism. The GH cells in the pituitary are equipped with TRPV1 and the hypophysiotropic regulation of GH by CART seems independent of TRPV1 activation.

REFERENCES

1. Bronson FH: Food-restricted, prepubertal, female rats: rapid recovery of luteinizing hormone pulsing with excess food, and full recovery of pubertal development with gonadotropin-releasing hormone. *Endocrinology* 1986 Jun;118:2483–7.
2. Wade GN, Schneider JE: Metabolic fuels and reproduction in female mammals. [Internet]. . *Neurosci Biobehav Rev* 1992;16:235–72.
3. Wade GN, Jones JE: Neuroendocrinology of nutritional infertility. *Am J Physiol Regul Integr Comp Physiol* 2004;287:R1277-96.
4. Shander D, Barraclough CA: Role of the preoptic brain in the regulation of preovulatory gonadotropin surges in the hamster [Internet]. . *Exp Brain Res* 1980;40:123–130.
5. Silverman AJ, Witkin JW: Biosynthesis of gonadotropin-releasing hormone during the rat estrous cycle: a cellular analysis. [Internet]. . *Neuroendocrinology* 1994 Jun;59:545–51.
6. Bliss SP, Navratil AM, Xie J, Roberson MS: GnRH signaling, the gonadotrope and endocrine control of fertility. *Front Neuroendocr* 2010;31:322–340.
7. King JC, Tobet SA, Snavely FL, Arimura AA: LHRH immunopositive cells and their projections to the median eminence and organum vasculosum of the lamina terminalis. *J Comp Neurol* 1982;209:287–300.
8. Elmquist JK, Coppari R, Balthasar N, Ichinose M, Lowell BB: Identifying hypothalamic pathways controlling food intake, body weight, and glucose homeostasis. *J Comp Neurol* 2005;493:63–71.
9. Meister B: Neurotransmitters in key neurons of the hypothalamus that regulate feeding behavior and body weight. *Physiol Behav* 2007;92:263–271.
10. Toni R, Lechan RM: Neuroendocrine regulation of thyrotropin-releasing hormone

- (TRH) in the tuberoinfundibular system. *J Endocrinol Invest* 1993;16:715–753.
11. Danforth Jr. E, Burger A: The role of thyroid hormones in the control of energy expenditure [Internet]. . *Clin Endocrinol Metab* 1984;13:581–595.
 12. Lechan RM, Fekete C: The TRH neuron: a hypothalamic integrator of energy metabolism. *Prog Brain Res* 2006;153:209–235.
 13. Cone RD, Cowley MA, Butler AA, Fan W, Marks DL, Low MJ: The arcuate nucleus as a conduit for diverse signals relevant to energy homeostasis. *Int J Obes Relat Metab Disord* 2001;25 Suppl 5:S63-7.
 14. Frank A, Brown LM, Clegg DJ: The role of hypothalamic estrogen receptors in metabolic regulation. *Front Neuroendocrinol* 2014 Oct;35:550–7.
 15. Schneider JE: Energy balance and reproduction. *Physiol Behav* 2004 Apr;81:289–317.
 16. Clarke IJ: Control of GnRH secretion: one step back. *Front Neuroendocrinol* 2011 Aug;32:367–75.
 17. Nestor CC, Kelly MJ, Ronnekleiv OK: Cross-talk between reproduction and energy homeostasis: central impact of estrogens, leptin and kisspeptin signaling. *Horm Mol Biol Clin Investig* 2014;17:109–128.
 18. Simonian SX, Spratt DP, Herbison AE: Identification and characterization of estrogen receptor alpha-containing neurons projecting to the vicinity of the gonadotropin-releasing hormone perikarya in the rostral preoptic area of the rat. *J Comp Neurol* 1999;411:346–358.
 19. Douglass J, McKinzie AA, Couceyro P: PCR differential display identifies a rat brain mRNA that is transcriptionally regulated by cocaine and amphetamine [Internet]. . *J Neurosci* 1995;15:2471–2481.
 20. Rondini TA, Baddini SP, Sousa LF, Bittencourt JC, Elias CF: Hypothalamic cocaine- and amphetamine-regulated transcript neurons project to areas expressing

- gonadotropin releasing hormone immunoreactivity and to the anteroventral periventricular nucleus in male and female rats. *Neuroscience* 2004;125:735–48.
21. Parent AS, Lebrethon MC, Gérard A, Vandersmissen E, Bourguignon JP: Leptin effects on pulsatile gonadotropin releasing hormone secretion from the adult rat hypothalamus and interaction with cocaine and amphetamine regulated transcript peptide and neuropeptide Y. [Internet]. . *Regul Pept* 2000 Aug 25;92:17–24.
 22. Fekete C, Lechan RM: Neuroendocrine implications for the association between cocaine- and amphetamine regulated transcript (CART) and hypophysiotropic thyrotropin-releasing hormone (TRH). *Peptides* 2006 Aug;27:2012–8.
 23. Lambert PD, Couceyro PR, McGirr KM, Dall Vechia SE, Smith Y, Kuhar MJ: CART peptides in the central control of feeding and interactions with neuropeptide Y. *Synapse* 1998 Aug;29:293–8.
 24. Vrang N, Larsen PJ, Clausen JT, Kristensen P: Neurochemical characterization of hypothalamic cocaine- amphetamine-regulated transcript neurons. *J Neurosci* 1999;19:RC5.
 25. Elias CF, Saper CB, Maratos-Flier E, Tritos NA, Lee C, Kelly J, et al.: Chemically defined projections linking the mediobasal hypothalamus and the lateral hypothalamic area. *J Comp Neurol* 1998;402:442–459.
 26. Lebrethon MC, Vandersmissen E, Gérard A, Parent AS, Bourguignon JP: Cocaine and amphetamine-regulated-transcript peptide mediation of leptin stimulatory effect on the rat gonadotropin-releasing hormone pulse generator in vitro. [Internet]. . *J Neuroendocrinol* 2000 May;12:383–5.
 27. Nagatani S, Bucholtz DC, Murahashi K, Estacio MA, Tsukamura H, Foster DL, et al.: Reduction of glucose availability suppresses pulsatile luteinizing hormone release in female and male rats. *Endocrinology* 1996 Apr;137:1166–70.

28. Roland A V, Moenter SM: Glucosensing by GnRH neurons: inhibition by androgens and involvement of AMP-activated protein kinase. *Mol Endocrinol* 2011 May;25:847–58.
29. Silva LECM, Castro M, Amaral FC, Antunes-Rodrigues J, Elias LLK: Estradiol-induced hypophagia is associated with the differential mRNA expression of hypothalamic neuropeptides. [Internet]. . *Brazilian J Med Biol Res = Rev Bras Pesqui medicas e Biol* 2010 Aug;43:759–66.
30. Strassburg S, Pfluger PT, Chaudhary N, Tso P, Tschöp MH, Anker SD, et al.: Action profile of the antiobesity drug candidate oleoyl-estrone in rats. *Obesity (Silver Spring)* 2010 Dec;18:2260–7.
31. Vennekens R, Menigoz A, Nilius B: TRPs in the brain. *Rev Physiol Biochem Pharmacol* 2012;163:27–64.
32. Venkatachalam K, Montell C: TRP channels. *Annu Rev Biochem* 2007;76:387–417.
33. Kauer JA, Gibson HE: Hot flash: TRPV channels in the brain. *Trends Neurosci* 2009;32:215–224.
34. Weber K, Erben RG, Rump A, Adamski J: Gene Structure and Regulation of the Murine Epithelial Calcium Channels ECaC1 and 2. *Biochem Biophys Res Commun* 2001;289:1287–1294.
35. Berryman DE, Christiansen JS, Johannsson G, Thorner MO, Kopchick JJ: Role of the GH/IGF-1 axis in lifespan and healthspan: lessons from animal models. *Growth Horm IGF Res* 2008;18:455–471.
36. Zaczek D, Hammond J, Suen L, Wandji S, Service D, Bartke A, et al.: Impact of growth hormone resistance on female reproductive function: new insights from growth hormone receptor knockout mice [Internet]. . *Biol Reprod* 2002;67:1115–1124.
37. Vijayakumar A, Yakar S, Leroith D: The intricate role of growth hormone in

- metabolism. *Front Endocrinol* 2011;2:32.
38. Chandrashekar V, Bartke A, Coschigano KT, Kopchick JJ: Pituitary and testicular function in growth hormone receptor gene knockout mice. *Endocrinology* 1999;140:1082–1088.
 39. Baranowska B, Wolinska-Witort E, Martynska L, Chmielowska M, Baranowska-Bik A: Effects of cocaine-amphetamine regulated transcript (CART) on hormone release. *Regul Pept* 2004;122:55–59.
 40. Mortensen AH, Camper SA: Cocaine-and Amphetamine Regulated Transcript (CART) Peptide Is Expressed in Precursor Cells and Somatotropes of the Mouse Pituitary Gland. *PLoS One* 2016;11:e0160068.
 41. Lechan RM, Toni R: Functional Anatomy of the Hypothalamus and Pituitary [Internet]. 2000.Available from: <http://www.ncbi.nlm.nih.gov/pubmed/25905349>
 42. Baribeau DA, Anagnostou E: Oxytocin and vasopressin: linking pituitary neuropeptides and their receptors to social neurocircuits. *Front Neurosci* 2015;9:335.
 43. Le Tissier PR, Hodson DJ, Lafont C, Fontanaud P, Schaeffer M, Mollard P: Anterior pituitary cell networks. *Front Neuroendocrinol* 2012 Aug;33:252–66.
 44. Lim CT, Grossman A, Khoo B: Normal Physiology of ACTH and GH Release in the Hypothalamus and Anterior Pituitary in Man [Internet]. 2000.Available from: <http://www.ncbi.nlm.nih.gov/pubmed/25905340>
 45. Liposits Z: Ultrastructure of hypothalamic paraventricular neurons. [Internet]. . *Crit Rev Neurobiol* 1993;7:89–162.
 46. Luther JA, Tasker JG: Voltage-gated currents distinguish parvocellular from magnocellular neurones in the rat hypothalamic paraventricular nucleus. [Internet]. . *J Physiol* 2000 Feb 15;523 Pt 1:193–209.
 47. Garcia-Garcia RM: Integrative control of energy balance and reproduction in females.

- ISRN Vet Sci 2012;2012:121389.
48. Arita J, Kojima Y, Kimura F: Lactotrophs secreting small amounts of prolactin reveal great responsiveness to thyrotropin-releasing hormone: analysis by the sequential cell immunoblot assay. *Endocrinology* 1992 Jun;130:3167–74.
 49. Schwarz JR, Bauer CK: Ionic mechanisms underlying TRH-induced prolactin secretion in rat lactotrophs. [Internet]. . *Russ Fiziol zhurnal Im IM Sechenova* 1999 Jan;85:195–204.
 50. Hall J.E. and Guyton A.C.: *Textbook of medical physiology*. ed 12 Philadelphia, Pa.: Saunders/Elsevier, 2011.
 51. Roa J: Role of GnRH Neurons and Their Neuronal Afferents as Key Integrators between Food Intake Regulatory Signals and the Control of Reproduction. *Int J Endocrinol* 2013;2013:518046.
 52. Filicori M, Crowley WF: The study of GnRH control of reproductive function. [Internet]. . *Ups J Med Sci* 1984;89:13–8.
 53. Ohlsson B: Gonadotropin-Releasing Hormone and Its Role in the Enteric Nervous System. *Front Endocrinol (Lausanne)* 2017;8:110.
 54. Roa J, García-Galiano D, Castellano JM, Gaytan F, Pinilla L, Tena-Sempere M: Metabolic control of puberty onset: new players, new mechanisms. *Mol Cell Endocrinol* 2010 Aug 5;324:87–94.
 55. Hill JO, Wyatt HR, Peters JC: Energy balance and obesity. *Circulation* 2012 Jul 3;126:126–32.
 56. Davies MJ: Evidence for effects of weight on reproduction in women. [Internet]. . *Reprod Biomed Online* 2006 May;12:552–61.
 57. Qin D-D, Yuan W, Zhou W-J, Cui Y-Q, Wu J-Q, Gao E-S: Do reproductive hormones explain the association between body mass index and semen quality? *Asian J Androl*

- 2007 Nov;9:827–34.
58. Jokela M, Elovainio M, Kivimäki M: Lower fertility associated with obesity and underweight: the US National Longitudinal Survey of Youth. [Internet]. . Am J Clin Nutr 2008 Oct;88:886–93.
 59. Broberger C, De Lecea L, Sutcliffe JG, Hökfelt T: Hypocretin/orexin- and melanin-concentrating hormone-expressing cells form distinct populations in the rodent lateral hypothalamus: relationship to the neuropeptide Y and agouti gene-related protein systems. [Internet]. . J Comp Neurol 1998 Dec 28;402:460–74.
 60. Hahn TM, Breininger JF, Baskin DG, Schwartz MW: Coexpression of Agrp and NPY in fasting-activated hypothalamic neurons. Nat Neurosci 1998 Aug;1:271–2.
 61. Elias CF, Lee C, Kelly J, Aschkenasi C, Ahima RS, Couceyro PR, et al.: Leptin activates hypothalamic CART neurons projecting to the spinal cord. [Internet]. . Neuron 1998 Dec;21:1375–85.
 62. Bell CG, Walley AJ, Froguel P: The genetics of human obesity. Nat Rev Genet 2005 Mar;6:221–34.
 63. Schwartz MW: Central nervous system regulation of food intake. Obesity (Silver Spring) 2006 Feb;14 Suppl 1:1S–8S.
 64. Morton GJ, Cummings DE, Baskin DG, Barsh GS, Schwartz MW: Central nervous system control of food intake and body weight. Nature 2006 Sep 21;443:289–95.
 65. Cheung CC, Clifton DK, Steiner RA: Proopiomelanocortin neurons are direct targets for leptin in the hypothalamus. Endocrinology 1997 Oct;138:4489–92.
 66. Cowley MA, Smart JL, Rubinstein M, Cerdán MG, Diano S, Horvath TL, et al.: Leptin activates anorexigenic POMC neurons through a neural network in the arcuate nucleus. Nature 2001 May 24;411:480–4.
 67. Könnner AC, Janoschek R, Plum L, Jordan SD, Rother E, Ma X, et al.: Insulin action in

- AgRP-expressing neurons is required for suppression of hepatic glucose production. *Cell Metab* 2007 Jun;5:438–49.
68. Hill JW: Gene Expression and the Control of Food Intake by Hypothalamic POMC/CART Neurons. [Internet]. . *Open Neuroendocrinol J* 2010;3:21–27.
69. Considine R V, Sinha MK, Heiman ML, Kriauciunas A, Stephens TW, Nyce MR, et al.: Serum immunoreactive-leptin concentrations in normal-weight and obese humans. *N Engl J Med* 1996 Feb 1;334:292–5.
70. Pelleymounter MA, Cullen MJ, Baker MB, Hecht R, Winters D, Boone T, et al.: Effects of the obese gene product on body weight regulation in ob/ob mice. [Internet]. . *Science* 1995 Jul 28;269:540–3.
71. van de Wall E, Leshan R, Xu AW, Balthasar N, Coppari R, Liu SM, et al.: Collective and individual functions of leptin receptor modulated neurons controlling metabolism and ingestion. *Endocrinology* 2008 Apr;149:1773–85.
72. Fu Z, Gilbert ER, Liu D: Regulation of insulin synthesis and secretion and pancreatic Beta-cell dysfunction in diabetes. [Internet]. . *Curr Diabetes Rev* 2013 Jan 1;9:25–53.
73. Fontana R, Della Torre S: The Deep Correlation between Energy Metabolism and Reproduction: A View on the Effects of Nutrition for Women Fertility. *Nutrients* 2016 Feb 11;8:87.
74. Brüning JC, Gautam D, Burks DJ, Gillette J, Schubert M, Orban PC, et al.: Role of brain insulin receptor in control of body weight and reproduction. [Internet]. . *Science* 2000 Sep 22;289:2122–5.
75. Qiu J, Zhang C, Borgquist A, Nestor CC, Smith AW, Bosch MA, et al.: Insulin excites anorexigenic proopiomelanocortin neurons via activation of canonical transient receptor potential channels. *Cell Metab* 2014 Apr 1;19:682–93.
76. Varela L, Horvath TL: Leptin and insulin pathways in POMC and AgRP neurons that

- modulate energy balance and glucose homeostasis. *EMBO Rep* 2012 Dec;13:1079–86.
77. Hill JW, Elias CF, Fukuda M, Williams KW, Berglund ED, Holland WL, et al.: Direct insulin and leptin action on pro-opiomelanocortin neurons is required for normal glucose homeostasis and fertility. *Cell Metab* 2010 Apr 7;11:286–97.
78. Balthasar N, Coppari R, McMinn J, Liu SM, Lee CE, Tang V, et al.: Leptin receptor signaling in POMC neurons is required for normal body weight homeostasis. *Neuron* 2004 Jun 24;42:983–91.
79. Mesaros A, Koralov SB, Rother E, Wunderlich FT, Ernst MB, Barsh GS, et al.: Activation of Stat3 signaling in AgRP neurons promotes locomotor activity. *Cell Metab* 2008 Mar;7:236–48.
80. Hill JW, Williams KW, Ye C, Luo J, Balthasar N, Coppari R, et al.: Acute effects of leptin require PI3K signaling in hypothalamic proopiomelanocortin neurons in mice. *J Clin Invest* 2008 May;118:1796–805.
81. Plum L, Ma X, Hampel B, Balthasar N, Coppari R, Münzberg H, et al.: Enhanced PIP3 signaling in POMC neurons causes KATP channel activation and leads to diet-sensitive obesity. *J Clin Invest* 2006 Jul;116:1886–901.
82. Niswender KD, Morrison CD, Clegg DJ, Olson R, Baskin DG, Myers MG, et al.: Insulin activation of phosphatidylinositol 3-kinase in the hypothalamic arcuate nucleus: a key mediator of insulin-induced anorexia. [Internet]. . *Diabetes* 2003 Feb;52:227–31.
83. True C, Verma S, Grove KL, Smith MS: Cocaine- and amphetamine-regulated transcript is a potent stimulator of GnRH and kisspeptin cells and may contribute to negative energy balance-induced reproductive inhibition in females. *Endocrinology* 2013 Aug;154:2821–32.
84. Serke H, Nowicki M, Kosacka J, Schröder T, Klötting N, Blüher M, et al.: Leptin-

- deficient (ob/ob) mouse ovaries show fatty degeneration, enhanced apoptosis and decreased expression of steroidogenic acute regulatory enzyme. *Int J Obes (Lond)* 2012 Aug;36:1047–53.
85. Swerdloff RS, Batt RA, Bray GA: Reproductive hormonal function in the genetically obese (ob/ob) mouse. *Endocrinology* 1976 Jun;98:1359–64.
86. Chehab FF, Lim ME, Lu R: Correction of the sterility defect in homozygous obese female mice by treatment with the human recombinant leptin. *Nat Genet* 1996 Mar;12:318–20.
87. Barash IA, Cheung CC, Weigle DS, Ren H, Kabigting EB, Kuijper JL, et al.: Leptin is a metabolic signal to the reproductive system. *Endocrinology* 1996 Jul;137:3144–7.
88. Mounzih K, Lu R, Chehab FF: Leptin treatment rescues the sterility of genetically obese ob/ob males. *Endocrinology* 1997 Mar;138:1190–3.
89. Kühn-Velten N, Codjambopoulo P, Herberg L, Kley HK, Staib W: In-vitro studies of the development of pituitary and testicular functions in diabetes (C57Bl/KsJ-db/db) mutant mice. *Horm Metab Res* 1985 Nov;17:576–9.
90. Garris DR, Garris BL: Diabetes (db/db) mutation-induced ovarian involution: progressive hypercytolipidemia. [Internet]. . *Exp Biol Med (Maywood)* 2003 Oct;228:1040–50.
91. Zhang Y, Hu M, Ma H, Qu J, Wang Y, Hou L, et al.: The impairment of reproduction in db/db mice is not mediated by intraovarian defective leptin signaling. *Fertil Steril* 2012 May;97:1183–91.
92. de Luca C, Kowalski TJ, Zhang Y, Elmquist JK, Lee C, Kilimann MW, et al.: Complete rescue of obesity, diabetes, and infertility in db/db mice by neuron-specific LEPR-B transgenes. *J Clin Invest* 2005 Dec;115:3484–93.
93. Kowalski TJ, Liu SM, Leibel RL, Chua SC: Transgenic complementation of leptin-

- receptor deficiency. I. Rescue of the obesity/diabetes phenotype of LEPR-null mice expressing a LEPR-B transgene. [Internet]. . *Diabetes* 2001 Feb;50:425–35.
94. Navarro VM, Kaiser UB: Metabolic influences on neuroendocrine regulation of reproduction. *Curr Opin Endocrinol Diabetes Obes* 2013 Aug;20:335–41.
 95. Quennell JH, Mulligan AC, Tups A, Liu X, Phipps SJ, Kemp CJ, et al.: Leptin indirectly regulates gonadotropin-releasing hormone neuronal function. *Endocrinology* 2009 Jun;150:2805–12.
 96. Kim HH, DiVall SA, Deneau RM, Wolfe A: Insulin regulation of GnRH gene expression through MAP kinase signaling pathways. *Mol Cell Endocrinol* 2005 Oct 20;242:42–9.
 97. Salvi R, Castillo E, Voirol M-J, Glauser M, Rey J-P, Gaillard RC, et al.: Gonadotropin-releasing hormone-expressing neurons immortalized conditionally are activated by insulin: implication of the mitogen-activated protein kinase pathway. *Endocrinology* 2006 Feb;147:816–26.
 98. Divall SA, Williams TR, Carver SE, Koch L, Brüning JC, Kahn CR, et al.: Divergent roles of growth factors in the GnRH regulation of puberty in mice. *J Clin Invest* 2010 Aug;120:2900–9.
 99. Mauvais-Jarvis F: Estrogen and androgen receptors: regulators of fuel homeostasis and emerging targets for diabetes and obesity. *Trends Endocrinol Metab* 2011 Jan;22:24–33.
 100. Mauvais-Jarvis F, Clegg DJ, Hevener AL: The role of estrogens in control of energy balance and glucose homeostasis. *Endocr Rev* 2013 Jun;34:309–38.
 101. Monteiro R, Teixeira D, Calhau C: Estrogen signaling in metabolic inflammation. *Mediators Inflamm* 2014;2014:615917.
 102. Micevych PE, Wong AM, Mittelman-Smith MA: Estradiol Membrane-Initiated

- Signaling and Female Reproduction. *Compr Physiol* 2015 Jul 1;5:1211–22.
103. Skynner MJ, Sim JA, Herbison AE: Detection of estrogen receptor alpha and beta messenger ribonucleic acids in adult gonadotropin-releasing hormone neurons. *Endocrinology* 1999 Nov;140:5195–201.
104. Lehman MN, Karsch FJ: Do gonadotropin-releasing hormone, tyrosine hydroxylase-, and beta-endorphin-immunoreactive neurons contain estrogen receptors? A double-label immunocytochemical study in the Suffolk ewe. *Endocrinology* 1993 Aug;133:887–95.
105. Herbison AE, Horvath TL, Naftolin F, Leranath C: Distribution of estrogen receptor-immunoreactive cells in monkey hypothalamus: relationship to neurones containing luteinizing hormone-releasing hormone and tyrosine hydroxylase. [Internet]. . *Neuroendocrinology* 1995 Jan;61:1–10.
106. Sullivan KA, Witkin JW, Ferin M, Silverman AJ: Gonadotropin-releasing hormone neurons in the rhesus macaque are not immunoreactive for the estrogen receptor. [Internet]. . *Brain Res* 1995 Jul 10;685:198–200.
107. Warembourg M, Leroy D, Peytevin J, Martinet L: Estrogen receptor and progesterone receptor-immunoreactive cells are not co-localized with gonadotropin-releasing hormone in the brain of the female mink (*Mustela vison*). [Internet]. . *Cell Tissue Res* 1998 Jan;291:33–41.
108. Cheong RY, Porteous R, Chambon P, Abrahám I, Herbison AE: Effects of neuron-specific estrogen receptor (ER) α and ER β deletion on the acute estrogen negative feedback mechanism in adult female mice. *Endocrinology* 2014 Apr;155:1418–27.
109. Wintermantel TM, Campbell RE, Porteous R, Bock D, Gröne H-J, Todman MG, et al.: Definition of estrogen receptor pathway critical for estrogen positive feedback to gonadotropin-releasing hormone neurons and fertility. *Neuron* 2006 Oct 19;52:271–80.

110. Naulé L, Robert V, Parmentier C, Martini M, Keller M, Cohen-Solal M, et al.: Delayed pubertal onset and prepubertal Kiss1 expression in female mice lacking central oestrogen receptor beta. *Hum Mol Genet* 2015 Dec 20;24:7326–38.
111. Kalra SP: Mandatory neuropeptide-steroid signaling for the preovulatory luteinizing hormone-releasing hormone discharge. *Endocr Rev* 1993;14:507–538.
112. Herbison AE: Multimodal influence of estrogen upon gonadotropin-releasing hormone neurons. *Endocr Rev* 1998;19:302–330.
113. Eyigor O, Lin W, Jennes L: Identification of neurones in the female rat hypothalamus that express oestrogen receptor-alpha and vesicular glutamate transporter-2. *J Neuroendocr* 2004;16:26–31.
114. Cooke PS, Naaz A: Role of estrogens in adipocyte development and function. [Internet]. . *Exp Biol Med (Maywood)* 2004 Dec;229:1127–35.
115. Shen M, Kumar SPDS, Shi H: Estradiol regulates insulin signaling and inflammation in adipose tissue. *Horm Mol Biol Clin Investig* 2014 Feb;17:99–107.
116. Yasrebi A, Rivera JA, Krumm EA, Yang JA, Roepke TA: Activation of Estrogen Response Element-Independent ER α Signaling Protects Female Mice From Diet-Induced Obesity. *Endocrinology* 2017;158:319–334.
117. Jones ME, Thorburn AW, Britt KL, Hewitt KN, Wreford NG, Proietto J, et al.: Aromatase-deficient (ArKO) mice have a phenotype of increased adiposity. *Proc Natl Acad Sci U S A* 2000 Nov 7;97:12735–40.
118. Geary N, Asarian L, Korach KS, Pfaff DW, Ogawa S: Deficits in E2-dependent control of feeding, weight gain, and cholecystokinin satiation in ER-alpha null mice. *Endocrinology* 2001 Nov;142:4751–7.
119. ter Haar MB: Circadian and estrual rhythms in food intake in the rat. [Internet]. . *Horm Behav* 1972 Sep;3:213–9.

120. BROBECK JR, WHEATLAND M, STROMINGER JL: Variations in regulation of energy exchange associated with estrus, diestrus and pseudopregnancy in rats. *Endocrinology* 1947 Feb;40:65–72.
121. Fungfuang W, Nakada T, Nakao N, Terada M, Yokosuka M, Gizurason S, et al.: Serum leptin concentrations, leptin mRNA expression, and food intake during the estrous cycle in rats. *Lab Anim Res* 2013 Mar;29:1–6.
122. Lauber AH, Romano GJ, Mobbs C V, Pfaff DW: Estradiol Regulation of Estrogen Receptor Messenger Ribonucleic Acid in Rat Mediobasal Hypothalamus: An in situ Hybridization Study. *J Neuroendocrinol* 1990 Oct 1;2:605–11.
123. Hou Y, Yang S-P, Voogt JL: Changes in estrogen receptor-alpha expression in hypothalamic dopaminergic neurons during proestrous prolactin surge. *Endocrine* 2003;20:131–8.
124. Hawkins RA, Freedman B, Marshall A, Killen E: Oestradiol-17 beta and prolactin levels in rat peripheral plasma. [Internet]. . *Br J Cancer* 1975 Aug;32:179–85.
125. Fontana R, Della Torre S, Meda C, Longo A, Eva C, Maggi AC: Estrogen replacement therapy regulation of energy metabolism in female mouse hypothalamus. *Endocrinology* 2014 Jun;155:2213–21.
126. Spiess J, Villarreal J, Vale W: Isolation and sequence analysis of a somatostatin-like polypeptide from ovine hypothalamus. [Internet]. . *Biochemistry* 1981 Mar 31;20:1982–8.
127. Thim L, Kristensen P, Nielsen PF, Wulff BS, Clausen JT: Tissue-specific processing of cocaine- and amphetamine-regulated transcript peptides in the rat. [Internet]. . *Proc Natl Acad Sci U S A* 1999 Mar 16;96:2722–7.
128. Rogge G, Jones D, Hubert GW, Lin Y, Kuhar MJ: CART peptides: regulators of body weight, reward and other functions. *Nat Rev Neurosci* 2008 Oct;9:747–58.

129. Zhang M, Han L, Xu Y: Roles of cocaine- and amphetamine-regulated transcript in the central nervous system. *Clin Exp Pharmacol Physiol* 2012 Jun;39:586–92.
130. Lebrethon MC, Vandersmissen E, Gérard A, Parent AS, Junien JL, Bourguignon JP: In vitro stimulation of the prepubertal rat gonadotropin-releasing hormone pulse generator by leptin and neuropeptide Y through distinct mechanisms. *Endocrinology* 2000 Apr;141:1464–9.
131. Koylu EO, Couceyro PR, Lambert PD, Kuhar MJ: Cocaine- and amphetamine-regulated transcript peptide immunohistochemical localization in the rat brain. [Internet]. . *J Comp Neurol* 1998 Feb 2;391:115–32.
132. Koylu EO, Couceyro PR, Lambert PD, Ling NC, DeSouza EB, Kuhar MJ: Immunohistochemical localization of novel CART peptides in rat hypothalamus, pituitary and adrenal gland. [Internet]. . *J Neuroendocrinol* 1997 Nov;9:823–33.
133. Vrang N: Anatomy of hypothalamic CART neurons. *Peptides* 2006 Aug;27:1970–80.
134. Füzesi T, Sánchez E, Wittmann G, Singru PS, Fekete C, Lechan RM: Regulation of cocaine- and amphetamine-regulated transcript-synthesising neurons of the hypothalamic paraventricular nucleus by endotoxin; implications for lipopolysaccharide-induced regulation of energy homeostasis. *J Neuroendocrinol* 2008 Sep;20:1058–66.
135. Briski KP, Sylvester PW: Role of endogenous opiates in glucoprivic inhibition of the luteinizing hormone surge and fos expression by preoptic gonadotropin-releasing hormone neurones in ovariectomized steroid-primed female rats. [Internet]. . *J Neuroendocrinol* 1998 Oct;10:769–76.
136. Murahashi K, Bucholtz DC, Nagatani S, Tsukahara S, Tsukamura H, Foster DL, et al.: Suppression of luteinizing hormone pulses by restriction of glucose availability is mediated by sensors in the brain stem. *Endocrinology* 1996 Apr;137:1171–6.

137. Zheng J: Molecular mechanism of TRP channels. *Compr Physiol* 2013 Jan;3:221–42.
138. Montell C, Rubin GM: Molecular characterization of the *Drosophila* *trp* locus: a putative integral membrane protein required for phototransduction. [Internet]. . *Neuron* 1989 Apr;2:1313–23.
139. Montell C, Birnbaumer L, Flockerzi V: The TRP channels, a remarkably functional family. [Internet]. . *Cell* 2002 Mar 8;108:595–8.
140. van Abel M, Hoenderop JGJ, Dardenne O, St Arnaud R, Van Os CH, Van Leeuwen HJPTM, et al.: 1,25-dihydroxyvitamin D(3)-independent stimulatory effect of estrogen on the expression of ECaC1 in the kidney. *J Am Soc Nephrol* 2002 Aug 1;13:2102–9.
141. van Abel M, Hoenderop JGJ, van der Kemp AWCM, van Leeuwen JPTM, Bindels RJM: Regulation of the epithelial Ca²⁺ channels in small intestine as studied by quantitative mRNA detection. *Am J Physiol Gastrointest Liver Physiol* 2003 Jul;285:G78-85.
142. Kuhar MJ, Jaworski JN, Hubert GW, Philpot KB, Dominguez G: Cocaine- and amphetamine-regulated transcript peptides play a role in drug abuse and are potential therapeutic targets. *AAPS J* 2005 Sep 2;7:E259-65.
143. Kuhar MJ, Dall Vechia SE: CART peptides: novel addiction- and feeding-related neuropeptides. [Internet]. . *Trends Neurosci* 1999 Jul;22:316–20.
144. Subhedar NK, Nakhate KT, Upadhyaya MA, Kokare DM: CART in the brain of vertebrates: Circuits, functions and evolution. *Peptides* 2014;54:108–130.
145. Kuhar MJ, Adams LD, Hunter RG, Vechia SD, Smith Y: CART peptides. [Internet]. . *Regul Pept* 2000 May 10;89:1–6.
146. Kuhar MJ, Adams S, Dominguez G, Jaworski J, Balkan B: CART peptides. [Internet]. . *Neuropeptides* 2002 Feb;36:1–8.
147. Vrang N, Tang-Christensen M, Larsen PJ, Kristensen P: Recombinant CART peptide

- induces c-Fos expression in central areas involved in control of feeding behaviour. [Internet]. . Brain Res 1999 Feb 13;818:499–509.
148. Fekete C, Singru PS, Sanchez E, Sarkar S, Christoffolete MA, Riberio RS, et al.: Differential effects of central leptin, insulin, or glucose administration during fasting on the hypothalamic-pituitary-thyroid axis and feeding-related neurons in the arcuate nucleus. Endocrinology 2006 Jan;147:520–9.
 149. Asnicar MA, Smith DP, Yang DD, Heiman ML, Fox N, Chen YF, et al.: Absence of cocaine- and amphetamine-regulated transcript results in obesity in mice fed a high caloric diet. Endocrinology 2001 Oct;142:4394–400.
 150. Wierup N, Richards WG, Bannon AW, Kuhar MJ, Ahrén B, Sundler F: CART knock out mice have impaired insulin secretion and glucose intolerance, altered beta cell morphology and increased body weight. Regul Pept 2005 Jul 15;129:203–11.
 151. Moffett M, Stanek L, Harley J, Rogge G, Asnicar M, Hsiung H, et al.: Studies of cocaine- and amphetamine-regulated transcript (CART) knockout mice. Peptides 2006 Aug;27:2037–45.
 152. Jones JE, Wade GN: Acute fasting decreases sexual receptivity and neural estrogen receptor-alpha in female rats. [Internet]. . Physiol Behav 2002 Sep;77:19–25.
 153. Lima FB, Henderson JA, Reddy AP, Tokuyama Y, Hubert GW, Kuhar MJ, et al.: Unique responses of midbrain CART neurons in macaques to ovarian steroids. Brain Res 2008 Aug 28;1227:76–88.
 154. Cavalcante JC, Bittencourt JC, Elias CF: Female odors stimulate CART neurons in the ventral premammillary nucleus of male rats. Physiol Behav 2006 Jun 15;88:160–6.
 155. Yoon YS, Lee JS, Lee HS: Retrograde study of CART- or NPY-neuronal projection from the hypothalamic arcuate nucleus to the dorsal raphe and/or the locus coeruleus in the rat. Brain Res 2013 Jun 26;1519:40–52.

156. Elmquist JK: Hypothalamic pathways underlying the endocrine, autonomic, and behavioral effects of leptin. [Internet]. . *Physiol Behav* 2001;74:703–8.
157. Fekete C, Mihály E, Luo LG, Kelly J, Clausen JT, Mao Q, et al.: Association of cocaine- and amphetamine-regulated transcript-immunoreactive elements with thyrotropin-releasing hormone-synthesizing neurons in the hypothalamic paraventricular nucleus and its role in the regulation of the hypothalamic-pituitary-thyroid axis [Internet]. . *J Neurosci* 2000 Dec 15;20:9224–34.
158. Joseph SA, Pilcher WH, Bennett-Clarke C: Immunocytochemical localization of ACTH perikarya in nucleus tractus solitarius: evidence for a second opiocortin neuronal system. [Internet]. . *Neurosci Lett* 1983 Aug 8;38:221–5.
159. Kumar S, Singh U, Goswami C, Singru PS: Transient receptor potential vanilloid 5 (TRPV5), a highly Ca(2+) -selective TRP channel in the rat brain: relevance to neuroendocrine regulation. *J Neuroendocrinol* 2017 Apr;29. DOI: 10.1111/jne.12466
160. Marcondes FK, Bianchi FJ, Tanno AP: Determination of the estrous cycle phases of rats: some helpful considerations. [Internet]. . *Braz J Biol* 2002 Nov;62:609–14.
161. Singru PS, Sánchez E, Fekete C, Lechan RM: Importance of melanocortin signaling in refeeding-induced neuronal activation and satiety. *Endocrinology* 2007 Feb;148:638–46.
162. Cao X, Xu P, Oyola MG, Xia Y, Yan X, Saito K, et al.: Estrogens stimulate serotonin neurons to inhibit binge-like eating in mice. *J Clin Invest* 2014 Oct;124:4351–62.
163. Singh P, Krishna A, Sridaran R, Tsutsui K: Immunohistochemical localization of GnRH and RFamide-related peptide-3 in the ovaries of mice during the estrous cycle. *J Mol Histol* 2011 Oct;42:371–81.
164. Dandekar MP, Singru PS, Kokare DM, Lechan RM, Thim L, Clausen JT, et al.: Importance of cocaine- and amphetamine-regulated transcript peptide in the central

- nucleus of amygdala in anxiogenic responses induced by ethanol withdrawal. *Neuropsychopharmacology* 2008 Apr;33:1127–36.
165. Paxinos George and Watson Charles: *The Rat Brain in Stereotaxic Coordinates*. ed 4 Academic Press, 1998.
166. Bolte S, Cordelières FP: A guided tour into subcellular colocalization analysis in light microscopy. *J Microsc* 2006 Dec;224:213–32.
167. Kumar S, Singh U, Saha S, Singru PS: Tyrosine hydroxylase in the olfactory system, forebrain and pituitary of the Indian major carp, *Cirrhinus cirrhosus*: organisation and interaction with neuropeptide Y in the preoptic area. *J Neuroendocrinol* 2014 Jun;26:400–11.
168. Wade GN, Schneider JE, Li HY: Control of fertility by metabolic cues. [Internet]. . *Am J Physiol* 1996 Jan;270:E1-19.
169. Kumar S, Kaur G: Intermittent fasting dietary restriction regimen negatively influences reproduction in young rats: a study of hypothalamo-hypophysial-gonadal axis. *PLoS One* 2013;8:e52416.
170. Zhang C, Bosch MA, Levine JE, Rønnekleiv OK, Kelly MJ: Gonadotropin-releasing hormone neurons express K(ATP) channels that are regulated by estrogen and responsive to glucose and metabolic inhibition. *J Neurosci* 2007 Sep 19;27:10153–64.
171. Xu Y, Faulkner LD, Hill JW: Cross-Talk between Metabolism and Reproduction: The Role of POMC and SF1 Neurons. *Front Endocrinol (Lausanne)* 2011;2:98.
172. Yeo S-H, Herbison AE: Estrogen-negative feedback and estrous cyclicity are critically dependent upon estrogen receptor- α expression in the arcuate nucleus of adult female mice. *Endocrinology* 2014 Aug;155:2986–95.
173. Fekete C, Mihály E, Luo LG, Kelly J, Clausen JT, Mao Q, et al.: Association of cocaine- and amphetamine-regulated transcript-immunoreactive elements with

- thyrotropin-releasing hormone-synthesizing neurons in the hypothalamic paraventricular nucleus and its role in the regulation of the hypothalamic-pituitary-thyroid axis. *J Neurosci* 2000;20:9224–34.
174. Silverman AJ, Jhamandas J, Renaud LP: Localization of luteinizing hormone-releasing hormone (LHRH) neurons that project to the median eminence. [Internet]. . *J Neurosci* 1987 Aug;7:2312–9.
175. Baranowska B, Wolińska-Witort E, Chmielowska M, Martyńska L, Baranowska-Bik A: Direct effects of cocaine-amphetamine-regulated transcript (CART) on pituitary hormone release in pituitary cell culture. [Internet]. . *Neuro Endocrinol Lett* 2003;24:224–6.
176. True C, Verma S, Grove KL, Smith MS: Cocaine- and amphetamine-regulated transcript is a potent stimulator of GnRH and kisspeptin cells and may contribute to negative energy balance-induced reproductive inhibition in females. *Endocrinology* 2013;154:2821–2832.
177. Baranowska B, Wolińska-Witort E, Martyńska L, Chmielowska M, Baranowska-Bik A: Effects of cocaine-amphetamine regulated transcript (CART) on hormone release. *Regul Pept* 2004 Oct 15;122:55–9.
178. Barsagade VG, Mazumdar M, Singru PS, Thim L, Clausen JT, Subhedar N: Reproductive phase-related variations in cocaine- and amphetamine-regulated transcript (CART) in the olfactory system, forebrain, and pituitary of the female catfish, *Clarias batrachus* (Linn.). *J Comp Neurol* 2010 Jul 1;518:2503–24.
179. Hill JW, Elmquist JK, Elias CF: Hypothalamic pathways linking energy balance and reproduction. *Am J Physiol Endocrinol Metab* 2008 May;294:E827-32.
180. Nestor CC, Coolen LM, Nesselrod GL, Valent M, Connors JM, Hileman SM, et al.: Evidence that orphanin FQ mediates progesterone negative feedback in the ewe.

- Endocrinology 2013 Nov;154:4249–58.
181. Adachi S, Yamada S, Takatsu Y, Matsui H, Kinoshita M, Takase K, et al.: Involvement of anteroventral periventricular metastin/kisspeptin neurons in estrogen positive feedback action on luteinizing hormone release in female rats. [Internet]. . J Reprod Dev 2007 Apr;53:367–78.
 182. Wittmann G, Füzesi T, Singru PS, Liposits Z, Lechan RM, Fekete C: Efferent projections of thyrotropin-releasing hormone-synthesizing neurons residing in the anterior parvocellular subdivision of the hypothalamic paraventricular nucleus. J Comp Neurol 2009 Jul 20;515:313–30.
 183. Sobrino Crespo C, Perianes Cachero A, Puebla Jiménez L, Barrios V, Arilla Ferreiro E: Peptides and food intake. Front Endocrinol (Lausanne) 2014;5:58.
 184. Zséli G, Vida B, Szilvásy-Szabó A, Tóth M, Lechan RM, Fekete C: Neuronal connections of the central amygdalar nucleus with refeeding-activated brain areas in rats. Brain Struct Funct 2018 Jan;223:391–414.
 185. Malik KF, Silverman AJ, Morrell JI: Gonadotropin-releasing hormone mRNA in the rat: distribution and neuronal content over the estrous cycle and after castration of males. Anat Rec 1991 Dec;231:457–66.
 186. Berriman SJ, Wade GN, Blaustein JD: Expression of Fos-like proteins in gonadotropin-releasing hormone neurons of Syrian hamsters: effects of estrous cycles and metabolic fuels. Endocrinology 1992 Nov;131:2222–8.
 187. Ronnekleiv OK, Kelly MJ: Luteinizing hormone-releasing hormone neuronal system during the estrous cycle of the female rat: effects of surgically induced persistent estrus. [Internet]. . Neuroendocrinology 1986;43:564–76.
 188. Park OK, Gugneja S, Mayo KE: Gonadotropin-releasing hormone gene expression during the rat estrous cycle: effects of pentobarbital and ovarian steroids.

- Endocrinology 1990 Jul;127:365–72.
189. Suzuki M, Nishihara M, Takahashi M: Hypothalamic gonadotropin-releasing hormone gene expression during rat estrous cycle. [Internet]. . Endocr J 1995 Dec;42:789–796.
 190. Arroyo A, Kim BS, Biehl A, Yeh J, Bett GCL: Expression of kv4.3 voltage-gated potassium channels in rat gonadotrophin-releasing hormone (GnRH) neurons during the estrous cycle. Reprod Sci 2011 Feb;18:136–44.
 191. Han S-K, Lee K, Bhattarai JP, Herbison AE: Gonadotrophin-releasing hormone (GnRH) exerts stimulatory effects on GnRH neurons in intact adult male and female mice. J Neuroendocrinol 2010 Mar;22:188–95.
 192. Silveira MA, Burger LL, DeFazio RA, Wagenmaker ER, Moenter SM: GnRH Neuron Activity and Pituitary Response in Estradiol-Induced vs Proestrous Luteinizing Hormone Surges in Female Mice. Endocrinology 2017;158:356–366.
 193. Nilius B, Owsianik G: The transient receptor potential family of ion channels. Genome Biol 2011;12:218.
 194. Diaz-Franulic I, Poblete H, Miño-Galaz G, González C, Latorre R: Allosterism and Structure in Thermally Activated Transient Receptor Potential Channels. Annu Rev Biophys 2016;45:371–398.
 195. Nilius B, Sage SO: TRP channels: novel gating properties and physiological functions. J Physiol 2005 Aug;567:33–34.
 196. Gees M, Colsoul B, Nilius B: The role of transient receptor potential cation channels in Ca²⁺ signaling. Cold Spring Harb Perspect Biol 2010;2.
 197. Akopian A: Role of TRP ion channels in physiology and pathology. Semin Immunopathol 2016 May 12;38:275–6.
 198. Nilius B, Voets T: A TRP channel-steroid marriage. Nat Cell Biol 2008;10:1383–1384.

199. Pike JW, Zella LA, Meyer MB, Fretz JA, Kim S: Molecular actions of 1,25-dihydroxyvitamin D₃ on genes involved in calcium homeostasis. *J Bone Miner Res* 2007 Dec;22 Suppl 2:V16-9.
200. Müller D, Hoenderop JG, Merkx GF, van Os CH, Bindels RJ: Gene structure and chromosomal mapping of human epithelial calcium channel. *Biochem Biophys Res Commun* 2000 Aug 18;275:47–52.
201. Kumar S, Singh U, Singh O, Goswami C, Singru PS: Transient receptor potential vanilloid 6 (TRPV6) in the mouse brain: Distribution and estrous cycle-related changes in the hypothalamus. *Neuroscience* 2017;344:204–216.
202. Nedungadi TP, Dutta M, Bathina CS, Caterina MJ, Cunningham JT: Expression and distribution of TRPV2 in rat brain. *Exp Neurol* 2012;237:223–237.
203. Wainwright A, Rutter AR, Seabrook GR, Reilly K, Oliver KR: Discrete expression of TRPV2 within the hypothalamo-neurohypophysial system: Implications for regulatory activity within the hypothalamic-pituitary-adrenal axis. *J Comp Neurol* 2004 Jun 14;474:24–42.
204. Ramírez-Barrantes R, Marchant I, Olivero P: TRPV1 may increase the effectiveness of estrogen therapy on neuroprotection and neuroregeneration. *Neural Regen Res* 2016;11:1204–1207.
205. Yan T, Liu B, Du D, Eisenach JC, Tong C: Estrogen Amplifies Pain Responses to Uterine Cervical Distension in Rats by Altering Transient Receptor Potential-1 Function. *Anesth Analg* 2007 May;104:1246–1250.
206. Lee G-S, Jeung E-B: Uterine TRPV6 expression during the estrous cycle and pregnancy in a mouse model. *Am J Physiol Endocrinol Metab* 2007;293:E132–E138.
207. Irnaten M, Blanchard-Gutton N, Praetorius J, Harvey BJ: Rapid effects of 17beta-estradiol on TRPV5 epithelial Ca²⁺ channels in rat renal cells. *Steroids* 2009

- Aug;74:642–649.
208. Choi Y, Seo H, Kim M, Ka H: Dynamic Expression of Calcium-Regulatory Molecules, TRPV6 and S100G, in the Uterine Endometrium During Pregnancy in Pigs. *Biol Reprod* 2009 Dec 1;81:1122–1130.
 209. Irnaten M, Blanchard-Gutton N, Harvey BJ: Rapid effects of 17beta-estradiol on epithelial TRPV6 Ca²⁺ channel in human T84 colonic cells. *Cell Calcium* 2008 Nov;44:441–52.
 210. Chen F, Ouyang Y, Ye T, Ni B, Chen A: Estrogen inhibits RANKL-induced osteoclastic differentiation by increasing the expression of TRPV5 channel. *J Cell Biochem* 2014 Apr;115:651–8.
 211. Van Cromphaut SJ, Rummens K, Stockmans I, Van Herck E, Dijcks FA, Ederveen AGH, et al.: Intestinal calcium transporter genes are upregulated by estrogens and the reproductive cycle through vitamin D receptor-independent mechanisms. *J Bone Miner Res* 2003 Oct;18:1725–36.
 212. Lee B-M, Lee G-S, Jung E-M, Choi K-C, Jeung E-B: Uterine and placental expression of TRPV6 gene is regulated via progesterone receptor- or estrogen receptor-mediated pathways during pregnancy in rodents. *Reprod Biol Endocrinol* 2009 May 21;7:49.
 213. Cavanaugh DJ, Chesler AT, Jackson AC, Sigal YM, Yamanaka H, Grant R, et al.: Trpv1 reporter mice reveal highly restricted brain distribution and functional expression in arteriolar smooth muscle cells. *J Neurosci* 2011 Mar 30;31:5067–77.
 214. Liedtke W: Transient receptor potential vanilloid channels functioning in transduction of osmotic stimuli. *J Endocrinol* 2006 Dec 1;191:515–523.
 215. Singh U, Kumar S, Shelkar GP, Yadav M, Kokare DM, Goswami C, et al.: Transient receptor potential vanilloid 3 (TRPV3) in the ventral tegmental area of rat: Role in modulation of the mesolimbic-dopamine reward pathway. *Neuropharmacology* 2016

- Nov;110:198–210.
216. Xu H, Ramsey IS, Kotecha SA, Moran MM, Chong JA, Lawson D, et al.: TRPV3 is a calcium-permeable temperature-sensitive cation channel. *Nature* 2002 Jul 11;418:181–6.
217. Smith GD, Gunthorpe MJ, Kelsell RE, Hayes PD, Reilly P, Facer P, et al.: TRPV3 is a temperature-sensitive vanilloid receptor-like protein. *Nature* 2002 Jul 11;418:186–90.
218. Pohóczky K, Kun J, Szalontai B, Szőke É, Sággy É, Payrits M, et al.: Estrogen-dependent up-regulation of TRPA1 and TRPV1 receptor proteins in the rat endometrium. *J Mol Endocrinol* 2016 Feb;56:135–49.
219. Gofflot F, Chartoire N, Vasseur L, Heikkinen S, Dembele D, Le Merrer J, et al.: Systematic gene expression mapping clusters nuclear receptors according to their function in the brain. *Cell* 2007 Oct 19;131:405–18.
220. Mahfouz A, Lelieveldt BPF, Grefhorst A, van Weert LTCM, Mol IM, Sips HCM, et al.: Genome-wide coexpression of steroid receptors in the mouse brain: Identifying signaling pathways and functionally coordinated regions. *Proc Natl Acad Sci U S A* 2016 Mar 8;113:2738–43.
221. Merchenthaler I, Lane M V, Numan S, Dellovade TL: Distribution of estrogen receptor alpha and beta in the mouse central nervous system: in vivo autoradiographic and immunocytochemical analyses. *J Comp Neurol* 2004 May 24;473:270–91.
222. Pérez SE, Chen E-Y, Mufson EJ: Distribution of estrogen receptor alpha and beta immunoreactive profiles in the postnatal rat brain. *Brain Res Dev Brain Res* 2003 Oct 10;145:117–39.
223. Stell A, Belcredito S, Ciana P, Maggi A: Molecular imaging provides novel insights on estrogen receptor activity in mouse brain. *Mol Imaging* 2008;7:283–92.
224. Wu Y-W, Bi Y-P, Kou X-X, Xu W, Ma L-Q, Wang K-W, et al.: 17-Beta-estradiol

- enhanced allodynia of inflammatory temporomandibular joint through upregulation of hippocampal TRPV1 in ovariectomized rats. *J Neurosci* 2010 Jun 30;30:8710–9.
225. Greaves E, Grieve K, Horne AW, Saunders PTK: Elevated peritoneal expression and estrogen regulation of nociceptive ion channels in endometriosis. *J Clin Endocrinol Metab* 2014 Sep;99:E1738-43.
226. Xu S, Cheng Y, Keast JR, Osborne PB: 17beta-estradiol activates estrogen receptor beta-signalling and inhibits transient receptor potential vanilloid receptor 1 activation by capsaicin in adult rat nociceptor neurons. *Endocrinology* 2008 Nov;149:5540–8.
227. Cho T, Chaban V V: Expression of P2X3 and TRPV1 receptors in primary sensory neurons from estrogen receptors- α and estrogen receptor- β knockout mice. *Neuroreport* 2012 Jun 20;23:530–4.
228. Bajic VB, Tan SL, Chong A, Tang S, Ström A, Gustafsson J-A, et al.: Dragon ERE Finder version 2: A tool for accurate detection and analysis of estrogen response elements in vertebrate genomes. *Nucleic Acids Res* 2003 Jul 1;31:3605–7.
229. Essack M, MacPherson CR, Schmeier S, Bajic VB: Identification of estrogen responsive genes using esophageal squamous cell carcinoma (ESCC) as a model. *BMC Syst Biol* 2012 Oct 26;6:135.
230. Caligioni CS: Assessing reproductive status/stages in mice. *Curr Protoc Neurosci* 2009 Jul;Appendix 4:Appendix 4I.
231. Jang Y, Lee Y, Kim SM, Yang YD, Jung J, Oh U: Quantitative analysis of TRP channel genes in mouse organs. *Arch Pharm Res* 2012 Oct;35:1823–30.
232. Dreos R, Ambrosini G, Cavin Périer R, Bucher P: EPD and EPDnew, high-quality promoter resources in the next-generation sequencing era. *Nucleic Acids Res* 2013 Jan;41:D157-64.
233. Mezey E, Tóth ZE, Cortright DN, Arzubi MK, Krause JE, Elde R, et al.: Distribution

- of mRNA for vanilloid receptor subtype 1 (VR1), and VR1-like immunoreactivity, in the central nervous system of the rat and human. *Proc Natl Acad Sci U S A* 2000 Mar 28;97:3655–60.
234. Han SK, Park SA, Jeon JG, Chang KW, Ahn DK, Oh SB, et al.: Functional type I vanilloid receptor expression by substantia gelatinosa neurons of trigeminal subnucleus caudalis in mice. *Neurosci Lett* 2009 Mar 20;452:228–31.
235. Liapi A, Wood JN: Extensive co-localization and heteromultimer formation of the vanilloid receptor-like protein TRPV2 and the capsaicin receptor TRPV1 in the adult rat cerebral cortex. *Eur J Neurosci* 2005 Aug;22:825–34.
236. Tóth A, Boczán J, Kedei N, Lizanecz E, Bagi Z, Papp Z, et al.: Expression and distribution of vanilloid receptor 1 (TRPV1) in the adult rat brain. *Brain Res Mol Brain Res* 2005 Apr 27;135:162–8.
237. Cristino L, de Petrocellis L, Pryce G, Baker D, Guglielmotti V, Di Marzo V: Immunohistochemical localization of cannabinoid type 1 and vanilloid transient receptor potential vanilloid type 1 receptors in the mouse brain. *Neuroscience* 2006;139:1405–15.
238. Luo J, Hu H: Thermally activated TRPV3 channels. *Curr Top Membr* 2014;74:325–64.
239. Shibasaki K, Ikenaka K, Tamalu F, Tominaga M, Ishizaki Y: A novel subtype of astrocytes expressing TRPV4 (transient receptor potential vanilloid 4) regulates neuronal excitability via release of gliotransmitters. *J Biol Chem* 2014 May 23;289:14470–80.
240. Shibasaki K, Suzuki M, Mizuno A, Tominaga M: Effects of body temperature on neural activity in the hippocampus: regulation of resting membrane potentials by transient receptor potential vanilloid 4. *J Neurosci* 2007 Feb 14;27:1566–75.

241. Lee JC, Joo KM, Choe SY, Cha CI: Region-specific changes in the immunoreactivity of TRPV4 expression in the central nervous system of SOD1(G93A) transgenic mice as an in vivo model of amyotrophic lateral sclerosis. *J Mol Histol* 2012 Dec;43:625–31.
242. Jung E-M, Kim J-H, Yang H, Hyun S-H, Choi K-C, Jeung E-B: Duodenal and renal transient receptor potential vanilloid 6 is regulated by sex steroid hormones, estrogen and progesterone, in immature rats. *J Vet Med Sci* 2011 Jun;73:711–6.
243. Yang H, Choi K-C, Hyun S-H, Jeung E-B: Coexpression and estrogen-mediated regulation of TRPV6 and PMCA1 in the human endometrium during the menstrual cycle. *Mol Reprod Dev* 2011 Apr;78:274–82.
244. Boychuk CR, Zsombok A, Tasker JG, Smith BN: Rapid Glucocorticoid-Induced Activation of TRP and CB1 Receptors Causes Biphasic Modulation of Glutamate Release in Gastric-Related Hypothalamic Preautonomic Neurons. *Front Neurosci* 2013;7:3.
245. Chen S-C, Chang T-J, Wu F-S: Competitive inhibition of the capsaicin receptor-mediated current by dehydroepiandrosterone in rat dorsal root ganglion neurons. *J Pharmacol Exp Ther* 2004 Nov;311:529–36.
246. Chen S-C, Wu F-S: Mechanism underlying inhibition of the capsaicin receptor-mediated current by pregnenolone sulfate in rat dorsal root ganglion neurons. *Brain Res* 2004 Nov 19;1027:196–200.
247. Liedtke W, Kim C: Functionality of the TRPV subfamily of TRP ion channels: Add mechano-TRP and osmo-TRP to the lexicon! *Cell Mol Life Sci* 2005;62:2985–3001.
248. Mensenkamp AR, Hoenderop JGJ, Bindels RJM: TRPV5, the gateway to Ca²⁺ homeostasis. *Handb Exp Pharmacol* 2007;179:207–220.
249. Sudbury JR, Bourque CW: Dynamic and Permissive Roles of TRPV1 and TRPV4

- Channels for Thermosensation in Mouse Supraoptic Magnocellular Neurosecretory Neurons. *J Neurosci* 2013;33:17160–17165.
250. Nedungadi TP, Carreño FR, Walch JD, Bathina CS, Cunningham JT: Region-specific changes in transient receptor potential vanilloid channel expression in the vasopressin magnocellular system in hepatic cirrhosis-induced hyponatraemia. *J Neuroendocrinol* 2012;24:642–652.
251. Sharif Naeini R, Witty M-F, Séguéla P, Bourque CW: An N-terminal variant of Trpv1 channel is required for osmosensory transduction. *Nat Neurosci* 2006;9:93–98.
252. Toth A, Boczan J, Kedei N, Lizanecz E, Bagi Z, Papp Z, et al.: Expression and distribution of vanilloid receptor 1 (TRPV1) in the adult rat brain. *Brain Res Mol Brain Res* 2005;135:162–168.
253. Dunn KM, Hill-Eubanks DC, Liedtke WB, Nelson MT: TRPV4 channels stimulate Ca²⁺-induced Ca²⁺ release in astrocytic endfeet and amplify neurovascular coupling responses. *Proc Natl Acad Sci U S A* 2013;110:6157–62.
254. Mannari T, Morita S, Furube E, Tominaga M, Miyata S: Astrocytic TRPV1 ion channels detect blood-borne signals in the sensory circumventricular organs of adult mouse brains. *Glia* 2013;61:957–971.
255. Vennekens R, Hoenderop JGJ, Prenen J, Stuver M, Willems PHGM, Droogmans G, et al.: Permeation and gating properties of the novel epithelial Ca²⁺ channel. *J Biol Chem* 2000;275:3963–3969.
256. van Abel M, Hoenderop JGJ, Bindels RJM: The epithelial calcium channels TRPV5 and TRPV6: regulation and implications for disease. *Naunyn Schmiedebergs Arch Pharmacol* 2005 Apr;371:295–306.
257. Nijenhuis T, Hoenderop JGJ, van der Kemp AWCM, Bindels RJM: Localization and regulation of the epithelial Ca²⁺ channel TRPV6 in the kidney. *J Am Soc Nephrol*

- 2003;14:2731–2740.
258. Hoenderop JG, Vennekens R, Müller D, Prenen J, Droogmans G, Bindels RJ, et al.: Function and expression of the epithelial Ca(2+) channel family: comparison of mammalian ECaC1 and 2. *J Physiol* 2001;537:747–761.
259. Hoenderop JGJ, Dardenne O, Van Abel M, Van Der Kemp AWCM, Van Os CH, St - Arnaud R, et al.: Modulation of renal Ca²⁺ transport protein genes by dietary Ca²⁺ and 1,25-dihydroxyvitamin D₃ in 25-hydroxyvitamin D₃-1alpha-hydroxylase knockout mice. *FASEB J* 2002 Sep;16:1398–406.
260. Song Y, Peng X, Porta A, Takanaga H, Peng J-B, Hediger MA, et al.: Calcium transporter 1 and epithelial calcium channel messenger ribonucleic acid are differentially regulated by 1,25 dihydroxyvitamin D₃ in the intestine and kidney of mice. *Endocrinology* 2003 Sep;144:3885–94.
261. Eyles DW, Smith S, Kinobe R, Hewison M, McGrath JJ: Distribution of the vitamin D receptor and 1 alpha-hydroxylase in human brain. *J Chem Neuroanat* 2005 Jan;29:21–30.
262. Jirikowski GF, Kaunzner UW, Kauntzer UW, Dief AEE, Caldwell JD: Distribution of vitamin D binding protein expressing neurons in the rat hypothalamus. *Histochem Cell Biol* 2009 Mar;131:365–70.
263. Garcia-Segura LM, Lorenz B, DonCarlos LL: The role of glia in the hypothalamus: implications for gonadal steroid feedback and reproductive neuroendocrine output. *Reproduction* 2008 Apr;135:419–29.
264. Della Torre S, Benedusi V, Fontana R, Maggi A: Energy metabolism and fertility: a balance preserved for female health. *Nat Rev Endocrinol* 2014 Jan;10:13–23.
265. Dandekar MP, Nakhate KT, Kokare DM, Subhedar NK: Involvement of CART in estradiol-induced anorexia. *Physiol Behav* 2012 Jan 18;105:460–9.

266. Liedtke W, Choe Y, Martí-Renom MA, Bell AM, Denis CS, Sali A, et al.: Vanilloid receptor-related osmotically activated channel (VR-OAC), a candidate vertebrate osmoreceptor. *Cell* 2000;103:525–535.
267. Zsombok A, Gao H, Miyata K, Issa A, Derbenev A V.: Immunohistochemical localization of transient receptor potential vanilloid type 1 and insulin receptor substrate 2 and their co-localization with liver-related neurons in the hypothalamus and brainstem. *Brain Res* 2011;1398:30–39.
268. Bourque CW: Central mechanisms of osmosensation and systemic osmoregulation. *Nat Rev Neurosci* 2008;9:519–531.
269. Lewinter RD, Scherrer G, Basbaum AI: Dense transient receptor potential cation channel, vanilloid family, type 2 (TRPV2) immunoreactivity defines a subset of motoneurons in the dorsal lateral nucleus of the spinal cord, the nucleus ambiguus and the trigeminal motor nucleus in rat. *Neuroscience* 2008 Jan 2;151:164–73.
270. Hu J, Choo HJ, Ma S-X: Infrared heat treatment reduces food intake and modifies expressions of TRPV3-POMC in the dorsal medulla of obesity prone rats. *Int J Hyperthermia* 2011;27:708–16.
271. Güler AD, Lee H, Iida T, Shimizu I, Tominaga M, Caterina M: Heat-evoked activation of the ion channel, TRPV4. *J Neurosci* 2002;22:6408–6414.
272. Lee JC, Choe SY: Age-related changes in the distribution of transient receptor potential vanilloid 4 channel (TRPV4) in the central nervous system of rats. *J Mol Histol* 2014;45:497–505.
273. Gutekunst C-A, Stewart EN, Gross RE: Immunohistochemical Distribution of PlexinA4 in the Adult Rat Central Nervous System. *Front Neuroanat* 2010;4. DOI: 10.3389/fnana.2010.00025
274. Brailoiu GC, Dun SL, Brailoiu E, Inan S, Yang J, Chang JK, et al.: Nesfatin-1:

- distribution and interaction with a G protein-coupled receptor in the rat brain. *Endocrinology* 2007 Oct;148:5088–94.
275. Dabrowska J, Hazra R, Ahern TH, Guo J-D, McDonald AJ, Mascagni F, et al.: Neuroanatomical evidence for reciprocal regulation of the corticotrophin-releasing factor and oxytocin systems in the hypothalamus and the bed nucleus of the stria terminalis of the rat: Implications for balancing stress and affect. *Psychoneuroendocrinology* 2011 Oct;36:1312–26.
276. Ben-Barak Y, Russell JT, Whitnall MH, Ozato K, Gainer H: Neurophysin in the hypothalamo-neurohypophysial system. I. Production and characterization of monoclonal antibodies. *J Neurosci* 1985;5:81–97.
277. Gómez-Nicola D, Fransen NL, Suzzi S, Perry VH: Regulation of microglial proliferation during chronic neurodegeneration. *J Neurosci* 2013 Feb 6;33:2481–93.
278. Sanchez E, Vargas MA, Singru PS, Pascual I, Romero F, Fekete C, et al.: Tanycyte pyroglutamyl peptidase II contributes to regulation of the hypothalamic-pituitary-thyroid axis through glial-axonal associations in the median eminence. *Endocrinology* 2009;150:2283–2291.
279. Nakajima H, Kubo T, Semi Y, Itakura M, Kuwamura M, Izawa T, et al.: A rapid, targeted, neuron-selective, in vivo knockdown following a single intracerebroventricular injection of a novel chemically modified siRNA in the adult rat brain. *J Biotechnol* 2012 Jan 20;157:326–33.
280. Wang D, Yan B, Rajapaksha WRAKJS, Fisher TE: The expression of voltage-gated ca^{2+} channels in pituicytes and the up-regulation of L-type ca^{2+} channels during water deprivation. *J Neuroendocrinol* 2009 Oct;21:858–66.
281. Kim GL, Wang X, Chalmers JA, Thompson DR, Dhillon SS, Koletar MM, et al.: Generation of immortal cell lines from the adult pituitary: role of cAMP on

- differentiation of SOX2-expressing progenitor cells to mature gonadotropes. *PLoS One* 2011;6:e27799.
282. Sharif-Naeini R, Ciura S, Zhang Z, Bourque CW: Contribution of TRPV channels to osmosensory transduction, thirst, and vasopressin release. *Kidney Int* 2008;73:811–815.
283. Loh NY, Bentley L, Dimke H, Verkaart S, Tammaro P, Gorvin CM, et al.: Autosomal dominant hypercalciuria in a mouse model due to a mutation of the epithelial calcium channel, TRPV5. *PLoS One* 2013;8:e55412.
284. Kennedy BG, Torabi AJ, Kurzawa R, Echtenkamp SF, Mangini NJ: Expression of transient receptor potential vanilloid channels TRPV5 and TRPV6 in retinal pigment epithelium. *Mol Vis* 2010;16:665–675.
285. Giusti L, Cetani F, Da Valle Y, Pardi E, Ciregia F, Donadio E, et al.: First evidence of TRPV5 and TRPV6 channels in human parathyroid glands: possible involvement in neoplastic transformation. *J Cell Mol Med* 2014 Oct;18:1944–52.
286. Hoenderop JGJ, Voets T, Hoefs S, Weidema F, Prenen J, Nilius B, et al.: Homo- and heterotetrameric architecture of the epithelial Ca²⁺ channels TRPV5 and TRPV6. *EMBO J* 2003;22:776–785.
287. Yamauchi D, Nakaya K, Raveendran NN, Harbidge DG, Singh R, Wangemann P, et al.: Expression of epithelial calcium transport system in rat cochlea and vestibular labyrinth. *BMC Physiol* 2010 Jan 29;10:1.
288. Wolf MTF, An S-W, Nie M, Bal MS, Huang C-L: Klotho up-regulates renal calcium channel transient receptor potential vanilloid 5 (TRPV5) by intra- and extracellular N-glycosylation-dependent mechanisms. *J Biol Chem* 2014 Dec 26;289:35849–57.
289. Zhang W, Na T, Peng J-B: WNK3 positively regulates epithelial calcium channels TRPV5 and TRPV6 via a kinase-dependent pathway. *Am J Physiol Renal Physiol*

- 2008 Nov;295:F1472-84.
290. Hoenderop JG, Hartog A, Stuver M, Doucet A, Willems PH, Bindels RJ: Localization of the epithelial Ca(2+) channel in rabbit kidney and intestine. [Internet]. . J Am Soc Nephrol 2000 Jul;11:1171–8.
291. Gkika D, Topala CN, Hoenderop JGJ, Bindels RJM: The immunophilin FKBP52 inhibits the activity of the epithelial Ca²⁺ channel TRPV5. Am J Physiol Renal Physiol 2006 May;290:F1253-9.
292. Leunissen EHP, Nair A V, Büll C, Lefeber DJ, van Delft FL, Bindels RJM, et al.: The epithelial calcium channel TRPV5 is regulated differentially by klotho and sialidase. J Biol Chem 2013 Oct 11;288:29238–46.
293. Harikai N, Tomogane K, Sugawara T, Tashiro S: Differences in hypothalamic Fos expressions between two heat stress conditions in conscious mice. [Internet]. . Brain Res Bull 2003 Oct 15;61:617–26.
294. Guatteo E, Chung KKH, Bowala TK, Bernardi G, Mercuri NB, Lipski J: Temperature sensitivity of dopaminergic neurons of the substantia nigra pars compacta: involvement of transient receptor potential channels. J Neurophysiol 2005;94:3069–3080.
295. Bjorklund A, Lindvall O: Dopamine-containing systems in the CNS. In Handbook of Chemical Neuroanatomy vol. 2: Classical Transmitters in the CNS, Part I. Bjorklund Elsevier, Amsterdam, 1984.
296. Benfenati V, Amiry-Moghaddam M, Caprini M, Mylonakou MN, Rapisarda C, Ottersen OP, et al.: Expression and functional characterization of transient receptor potential vanilloid-related channel 4 (TRPV4) in rat cortical astrocytes. Neuroscience 2007;148:876–892.
297. Shibasaki K, Ishizaki Y, Mandadi S: Astrocytes express functional TRPV2 ion

- channels. *Biochem Biophys Res Commun* 2013;441:327–332.
298. Clapham DE: TRP channels as cellular sensors. [Internet]. . *Nature* 2003;426:517–524.
299. Peng J Bin: TRPV5 and TRPV6 in transcellular Ca²⁺ transport: Regulation, gene duplication, and polymorphisms in African populations; in : *Advances in Experimental Medicine and Biology*. 2011, pp 239–275.
300. Owsianik G, Talavera K, Voets T, Nilius B: Permeation and selectivity of TRP channels. [Internet]. . *Annu Rev Physiol* 2006;68:685–717.
301. Woudenberg-Vrenken TE, Lameris a. L, Weissgerber P, Olausson J, Flockerzi V, Bindels RJM, et al.: Functional TRPV6 channels are crucial for transepithelial Ca²⁺ absorption. *AJP Gastrointest Liver Physiol* 2012;303:G879–G885.
302. Bianco SDC, Peng J-B, Takanaga H, Suzuki Y, Crescenzi A, Kos CH, et al.: Marked Disturbance of Calcium Homeostasis in Mice With Targeted Disruption of the Trpv6 Calcium Channel Gene [Internet]. . *J Bone Miner Res* 2007;22:274–285.
303. Weissgerber P, Kriebs U, Tsvilovsky V, Olausson J, Kretz O, Stoerger C, et al.: Male fertility depends on Ca²⁺ absorption by TRPV6 in epididymal epithelia. [Internet]. . *Sci Signal* 2011;4:ra27.
304. Caraty A, Fabre-Nys C, Delaleu B, Locatelli A, Bruneau G, Karsch FJ, et al.: Evidence that the mediobasal hypothalamus is the primary site of action of estradiol in inducing the preovulatory gonadotropin releasing hormone surge in the ewe. *Endocrinology* 1998;139:1752–1760.
305. Saito K, He Y, Yan X, Yang Y, Wang C, Xu P, et al.: Visualizing estrogen receptor- α -expressing neurons using a new ER α -ZsGreen reporter mouse line. *Metabolism* 2016;65:522–532.
306. Yang JA, Mamounis KJ, Yasrebi A, Roepke TA: Regulation of gene expression by 17 β -estradiol in the arcuate nucleus of the mouse through ERE-dependent and ERE-

- independent mechanisms. *Steroids* 2016;in press.
307. Yeo SH, Herbison AE: Estrogen-negative feedback and estrous cyclicity are critically dependent upon estrogen receptor- α expression in the arcuate nucleus of adult female mice. *Endocrinology* 2014;155:2986–2995.
308. Singh U, Kumar S, Singru PS: Interaction between dopamine- and isotocin-containing neurones in the preoptic area of the catfish, *Clarias batrachus*: role in the regulation of luteinising hormone cells. *J Neuroendocrinol* 2012;24:1398–1411.
309. Franklin KBJ, Paxinos G: *The mouse brain in stereotaxic coordinates*. ed 3 San Diego, Academic Press, 2007.
310. Raphaël M, Lehen'kyi V, Vandenberghe M, Beck B, Khalimonchik S, Vanden Abeele F, et al.: TRPV6 calcium channel translocates to the plasma membrane via Orail-mediated mechanism and controls cancer cell survival. [Internet]. . *Proc Natl Acad Sci U S A* 2014;111:E3870-9.
311. Lallet-Daher H, Roudbaraki M, Bavencoffe A, Mariot P, Gackiere F, Bidaux G, et al.: Intermediate-conductance Ca^{2+} -activated K^{+} channels (IKCa1) regulate human prostate cancer cell proliferation through a close control of calcium entry. *Oncogene* 2009;28:1792–1806.
312. Hatano R, Fujii E, Segawa H, Mukaisho K, Matsubara M, Miyamoto K-I, et al.: Ezrin, a membrane cytoskeletal cross-linker, is essential for the regulation of phosphate and calcium homeostasis. [Internet]. . *Kidney Int* 2013;83:41–9.
313. Suzuki Y, Kovacs CS, Takanaga H, Peng J-B, Landowski CP, Hediger MA: Calcium channel TRPV6 is involved in murine maternal-fetal calcium transport. *J Bone Miner Res* 2008;23:1249–1256.
314. Nijenhuis T, Hoenderop JGJ, Nilius B, Bindels RJM: (Patho)physiological implications of the novel epithelial Ca^{2+} channels TRPV5 and TRPV6. *Pflugers Arch*

- Eur J Physiol 2003;446:401–409.
315. Muller D, Hoenderop JG, Meij IC, van den Heuvel LP, Knoers N V, den Hollander AI, et al.: Molecular cloning, tissue distribution, and chromosomal mapping of the human epithelial Ca²⁺ channel (ECAC1) [Internet]. . Genomics 2000;67:48–53.
316. Hoenderop JGJ, Nilius B, Bindels RJM: Calcium Absorption Across Epithelia [Internet]. . Physiol Rev 2005;85:373–422.
317. Lehen'kyi V, Beck B, Polakowska R, Charveron M, Bordat P, Skryma R, et al.: TRPV6 is a Ca²⁺ entry channel essential for Ca²⁺-induced differentiation of human keratinocytes. J Biol Chem 2007;282:22582–22591.
318. Semenova SB, Vassilieva IO, Fomina AF, Runov AL, Negulyaev Y a: Endogenous expression of TRPV5 and TRPV6 calcium channels in human leukemia K562 cells. Am J Physiol Cell Physiol 2009;296:C1098–C1104.
319. Cui M, Li Q, Johnson R, Fleet JC: Villin promoter-mediated transgenic expression of TRPV6 increases intestinal calcium absorption in wild-type and VDR knockout mice [Internet]. . J Bone Miner Res 2012;27:2097–2107.
320. Lehen'kyi V, Flourakis M, Skryma R, Prevarskaya N: TRPV6 channel controls prostate cancer cell proliferation via Ca(2+)/NFAT-dependent pathways. Oncogene 2007;26:7380–7385.
321. Sharif-Naeini R, Ciura S, Bourque CW: TRPV1 gene required for thermosensory transduction and anticipatory secretion from vasopressin neurons during hyperthermia. Neuron 2008;58:179–185.
322. Singru PS, Fekete C, Lechan RM: Neuroanatomical evidence for participation of the hypothalamic dorsomedial nucleus (DMN) in regulation of the hypothalamic paraventricular nucleus (PVN) by ??-melanocyte stimulating hormone. Brain Res 2005;1064:42–51.

323. Miller BH, Takahashi JS: Central circadian control of female reproductive function. *Front Endocrinol (Lausanne)* 2014;5.
324. Larsen PJ, Seier V, Fink-Jensen A, Holst JJ, Warberg J, Vrang N: Cocaine- and amphetamine-regulated transcript is present in hypothalamic neuroendocrine neurones and is released to the hypothalamic-pituitary portal circuit. [Internet]. . *J Neuroendocrinol* 2003 Mar;15:219–26.
325. Dall Vechia S, Lambert PD, Couceyro PC, Kuhar MJ, Smith Y: CART peptide immunoreactivity in the hypothalamus and pituitary in monkeys: analysis of ultrastructural features and synaptic connections in the paraventricular nucleus. [Internet]. . *J Comp Neurol* 2000 Jan 17;416:291–308.
326. Armbruszt S, Abraham H, Figler M, Kozicz T, Hajnal A: Cocaine- and amphetamine-regulated transcript (CART) peptide immunoreactivity in feeding- and reward-related brain areas of young OLETF rats. *J Chem Neuroanat* 2013 May;50–51:75–84.
327. Smith SM, Vaughan JM, Donaldson CJ, Fernandez RE, Li C, Chen A, et al.: Cocaine- and amphetamine-regulated transcript is localized in pituitary lactotropes and is regulated during lactation. *Endocrinology* 2006 Mar;147:1213–23.
328. Brooks AJ, Wooh JW, Tunny KA, Waters MJ: Growth hormone receptor; mechanism of action. *Int J Biochem Cell Biol* 2008;40:1984–9.
329. Lindberg-Larsen R, Møller N, Schmitz O, Nielsen S, Andersen M, Orskov H, et al.: The impact of pegvisomant treatment on substrate metabolism and insulin sensitivity in patients with acromegaly. *J Clin Endocrinol Metab* 2007 May;92:1724–8.
330. Sakharova AA, Horowitz JF, Surya S, Goldenberg N, Harber MP, Symons K, et al.: Role of growth hormone in regulating lipolysis, proteolysis, and hepatic glucose production during fasting. *J Clin Endocrinol Metab* 2008 Jul;93:2755–9.
331. Fan Y, Menon RK, Cohen P, Hwang D, Clemens T, DiGirolamo DJ, et al.: Liver-

- specific deletion of the growth hormone receptor reveals essential role of growth hormone signaling in hepatic lipid metabolism. *J Biol Chem* 2009 Jul 24;284:19937–44.
332. Kaplan W, Sunehag AL, Dao H, Haymond MW: Short-term effects of recombinant human growth hormone and feeding on gluconeogenesis in humans. *Metabolism* 2008 Jun;57:725–32.
333. Chen XL, Lee K, Hartzell DL, Dean RG, Hausman GJ, McGraw RA, et al.: Adipocyte insensitivity to insulin in growth hormone-transgenic mice. *Biochem Biophys Res Commun* 2001 May 18;283:933–7.
334. Berryman DE, List EO, Coschigano KT, Behar K, Kim JK, Kopchick JJ: Comparing adiposity profiles in three mouse models with altered GH signaling. *Growth Horm IGF Res* 2004 Aug;14:309–18.
335. Pasarica M, Zachwieja JJ, Dejonge L, Redman S, Smith SR: Effect of growth hormone on body composition and visceral adiposity in middle-aged men with visceral obesity. *J Clin Endocrinol Metab* 2007 Nov;92:4265–70.
336. Freda PU, Shen W, Heymsfield SB, Reyes-Vidal CM, Geer EB, Bruce JN, et al.: Lower visceral and subcutaneous but higher intermuscular adipose tissue depots in patients with growth hormone and insulin-like growth factor I excess due to acromegaly. *J Clin Endocrinol Metab* 2008 Jun;93:2334–43.
337. Khalfallah Y, Sassolas G, Borson-Chazot F, Vega N, Vidal H: Expression of insulin target genes in skeletal muscle and adipose tissue in adult patients with growth hormone deficiency: effect of one year recombinant human growth hormone therapy. [Internet]. . *J Endocrinol* 2001 Nov;171:285–92.
338. Oscarsson J, Ottosson M, Vikman-Adolfsson K, Frick F, Enerbäck S, Lithell H, et al.: GH but not IGF-I or insulin increases lipoprotein lipase activity in muscle tissues of

- hypophysectomised rats. [Internet]. . J Endocrinol 1999 Feb;160:247–55.
339. Ohlsson C, Mohan S, Sjögren K, Tivesten A, Isgaard J, Isaksson O, et al.: The role of liver-derived insulin-like growth factor-I. *Endocr Rev* 2009 Aug;30:494–535.
340. Stojilkovic SS, Tabak J, Bertram R: Ion channels and signaling in the pituitary gland. *Endocr Rev* 2010 Dec;31:845–915.
341. Wu SN, Li HF, Jan CR: Regulation of Ca²⁺-activated nonselective cationic currents in rat pituitary GH3 cells: involvement in L-type Ca²⁺ current. [Internet]. . *Brain Res* 1998 Nov 23;812:133–41.
342. Vergara L, Rojas E, Stojilkovic SS: A novel calcium-activated apamin-insensitive potassium current in pituitary gonadotrophs. *Endocrinology* 1997 Jul;138:2658–64.
343. Sankaranarayanan S, Simasko SM: A role for a background sodium current in spontaneous action potentials and secretion from rat lactotrophs. [Internet]. . *Am J Physiol* 1996 Dec;271:C1927-34.
344. Kucka M, Kretschmannova K, Murano T, Wu C-P, Zemkova H, Ambudkar S V, et al.: Dependence of multidrug resistance protein-mediated cyclic nucleotide efflux on the background sodium conductance. *Mol Pharmacol* 2010 Feb;77:270–9.
345. Watanabe S, Seale AP, Grau EG, Kaneko T: Stretch-activated cation channel TRPV4 mediates hyposmotically induced prolactin release from prolactin cells of mozambique tilapia *Oreochromis mossambicus*. *Am J Physiol Regul Integr Comp Physiol* 2012 Apr 15;302:R1004-11.
346. Nisembaum LG, Besseau L, Paulin C-H, Charpantier A, Martin P, Magnanou E, et al.: In the Heat of the Night: Thermo-TRPV Channels in the Salmonid Pineal Photoreceptors and Modulation of Melatonin Secretion. *Endocrinology* 2015 Dec;156:4629–38.
347. Bhaskaracharya A, Dao-Ung P, Jalilian I, Spildrejorde M, Skarratt KK, Fuller SJ, et

- al.: Probenecid blocks human P2X7 receptor-induced dye uptake via a pannexin-1 independent mechanism. *PLoS One* 2014;9:e93058.
348. Kim S, Jung U, Baek J, Kang S, Kim J: Simultaneous measurement of neural spike recordings and multi-photon calcium imaging in neuroblastoma cells. *Sensors (Basel)* 2012 Nov 8;12:15281–91.
349. Urata K, Shinoda M, Honda K, Lee J, Maruno M, Ito R, et al.: Involvement of TRPV1 and TRPA1 in incisional intraoral and extraoral pain. *J Dent Res* 2015 Mar;94:446–54.
350. Isensee J, Diskar M, Waldherr S, Buschow R, Hasenauer J, Prinz A, et al.: Pain modulators regulate the dynamics of PKA-RII phosphorylation in subgroups of sensory neurons. *J Cell Sci* 2014 Jan 1;127:216–29.
351. Berrout J, Jin M, Mamenko M, Zaika O, Pochynyuk O, O’Neil RG: Function of transient receptor potential cation channel subfamily V member 4 (TRPV4) as a mechanical transducer in flow-sensitive segments of renal collecting duct system. *J Biol Chem* 2012 Mar 16;287:8782–91.
352. Morgan PJ: The pars tuberalis: the missing link in the photoperiodic regulation of prolactin secretion? [Internet]. . *J Neuroendocrinol* 2000 Apr;12:287–95.
353. Devesa I, Ferrándiz-Huertas C, Mathivanan S, Wolf C, Luján R, Changeux J-P, et al.: α CGRP is essential for algescic exocytotic mobilization of TRPV1 channels in peptidergic nociceptors. *Proc Natl Acad Sci U S A* 2014 Dec 23;111:18345–50.
354. Jin M, Wu Z, Chen L, Jaimes J, Collins D, Walters ET, et al.: Determinants of TRPV4 activity following selective activation by small molecule agonist GSK1016790A. *PLoS One* 2011 Feb 14;6:e16713.
355. van den Burg EH, Stindl J, Grund T, Neumann ID, Strauss O: Oxytocin Stimulates Extracellular Ca²⁺ Influx Through TRPV2 Channels in Hypothalamic Neurons to Exert Its Anxiolytic Effects. *Neuropsychopharmacology* 2015 Dec;40:2938–47.

356. Pires M, Tortosa F: Update on Pituitary Folliculo-Stellate Cells. *Int Arch Endocrinol Clin Res* 2016;2:006.
357. Acosta M, Filippa V, Mohamed F: Folliculostellate cells in pituitary pars distalis of male viscacha: immunohistochemical, morphometric and ultrastructural study. [Internet]. . *Eur J Histochem* 2010 Jan 20;54:e1.
358. Allaerts W, Vankelecom H: History and perspectives of pituitary folliculo-stellate cell research. *Eur J Endocrinol* 2005 Jul;153:1–12.
359. Bilezikjian LM, Leal AMO, Blount AL, Corrigan AZ, Turnbull A V, Vale WW: Rat anterior pituitary folliculostellate cells are targets of interleukin-1beta and a major source of intrapituitary follistatin. *Endocrinology* 2003 Feb;144:732–40.
360. Yamashita M, Qian ZR, Sano T, Horvath E, Kovacs K: Immunohistochemical study on so-called follicular cells and folliculostellate cells in the human adenohypophysis. *Pathol Int* 2005 May;55:244–7.
361. Childs GV: Pituitary Gland (Cell Types, Mediators, Development) [Internet]; in : *Encyclopedia of Neuroscience*. Elsevier, 2009, pp 719–726.
362. Morgan PJ, Williams LM: The pars tuberalis of the pituitary: a gateway for neuroendocrine output. [Internet]. . *Rev Reprod* 1996 Sep;1:153–61.
363. Walling BE, Picut CA, Remick AK: The Endocrine System [Internet]; in : *Atlas of Histology of the Juvenile Rat*. Elsevier, 2016, pp 257–291.
364. Rosol TJ, DeLellis RA, Harvey PW, Sutcliffe C: Endocrine System [Internet]; in : *Haschek and Rousseaux's Handbook of Toxicologic Pathology*. Elsevier, 2013, pp 2391–2492.
365. Norris DO, Carr JA: Organization of the Mammalian Hypothalamus–Pituitary Axes [Internet]; in : *Vertebrate Endocrinology*. Elsevier, 2013, pp 93–150.
366. Gross DS: Hormone production in the hypophysial pars tuberalis of intact and

- hypophysectomized rats. *Endocrinology* 1983 Feb;112:733–44.
367. Morgan PJ, Barrett P, Howell HE, Helliwell R: Melatonin receptors: localization, molecular pharmacology and physiological significance. [Internet]. . *Neurochem Int* 1994 Feb;24:101–46.
368. Thomas GA, Kraemer WJ, Comstock BA, Dunn-Lewis C, Maresh CM, Volek JS: Obesity, growth hormone and exercise. *Sports Med* 2013 Sep;43:839–49.
369. Lassarre C, Girard F, Durand J, Raynaud J: Kinetics of human growth hormone during submaximal exercise. [Internet]. . *J Appl Physiol* 1974 Dec;37:826–30.
370. Raynaud J, Capderou A, Martineaud JP, Bordachar J, Durand J: Intersubject viability in growth hormone time course during different types of work. [Internet]. . *J Appl Physiol* 1983 Dec;55:1682–7.
371. Felsing NE, Brasel JA, Cooper DM: Effect of low and high intensity exercise on circulating growth hormone in men. *J Clin Endocrinol Metab* 1992 Jul;75:157–62.
372. Vanhelder WP, Goode RC, Radomski MW: Effect of anaerobic and aerobic exercise of equal duration and work expenditure on plasma growth hormone levels. [Internet]. . *Eur J Appl Physiol Occup Physiol* 1984;52:255–7.
373. Lim C, Grossman A, Khoo B: Normal Physiology of ACTH and GH Release in the Hypothalamus and Anterior Pituitary in Man. [Internet]. *Endotext* [Internet]. South Dartmouth (MA): MDText.com, Inc., 2014. Available from: <https://www.ncbi.nlm.nih.gov/books/NBK279116/>
374. Bridge MW, Weller AS, Rayson M, Jones DA: Ambient temperature and the pituitary hormone responses to exercise in humans. [Internet]. . *Exp Physiol* 2003 Sep;88:627–35.
375. Christensen SE, Jørgensen OL, Møller N, Orskov H: Characterization of growth hormone release in response to external heating. Comparison to exercise induced

- release. [Internet]. . *Acta Endocrinol (Copenh)* 1984 Nov;107:295–301.
376. Sun X, Zakharian E: Regulation of the temperature-dependent activation of transient receptor potential vanilloid 1 (TRPV1) by phospholipids in planar lipid bilayers. *J Biol Chem* 2015 Feb 20;290:4741–7.
377. Goswami C, Schmidt H, Hucho F: TRPV1 at nerve endings regulates growth cone morphology and movement through cytoskeleton reorganization. *FEBS J* 2007 Feb;274:760–72.
378. Hille B, Billiard J, Babcock DF, Nguyen T, Koh D-S: Stimulation of exocytosis without a calcium signal. *J Physiol* 1999 Oct;520:23–31.
379. Stuenkel EL, Nordmann JJ: Sodium-evoked, calcium-independent vasopressin release from rat isolated neurohypophysial nerve endings. [Internet]. . *J Physiol* 1993 Aug;468:357–78.
380. Dave JR, Eiden LE, Lozovsky D, Waschek JA, Eskay RL: Calcium-independent and calcium-dependent mechanisms regulate corticotropin-releasing factor-stimulated proopiomelanocortin peptide secretion and messenger ribonucleic acid production. *Endocrinology* 1987 Jan;120:305–10.
381. Tse A, Tse FW, Almers W, Hille B: Rhythmic exocytosis stimulated by GnRH-induced calcium oscillations in rat gonadotropes. [Internet]. . *Science* 1993 Apr 2;260:82–4.
382. Billiard J, Koh DS, Babcock DF, Hille B: Protein kinase C as a signal for exocytosis. [Internet]. . *Proc Natl Acad Sci U S A* 1997 Oct 28;94:12192–7.
383. Tse FW, Tse A: Stimulation of Ca²⁺-independent exocytosis in rat pituitary gonadotrophs by G-protein. *J Physiol* 2000 Jul;526:99–108.

Appendix 1: Details of the primary antibodies/antisera used

Antigen	Host	Antibody type	Immunogen	Source	Dilution
Cocaine-and amphetamine -regulated transcript (CART)	Mouse	Monoclonal	Purified recombinant CART (54-102)	Kind gift of Drs. Lars Thim and J.T. Clausen, Novonordisk, Denmark	1:2000
CART	Rabbit	Polyclonal	CART (54-102)	Phoenix Pharmaceuticals, USA Cat. # H-003-62	1:5000
Alpha-melanocyte-stimulating hormone (α -MSH)	Sheep	Polyclonal	α -MSH conjugated to bovine thyroglobulin	Jeffrey B. Tatro, Tufts Medical Center, Boston, MA	1:10000
Neuropeptide Y (NPY)	Sheep	Polyclonal	Synthetic NPY peptide conjugated to bovine thyroglobulin	Chemicon® Cat. # AB1583	1:1000
Gonadotropin-releasing hormone (GnRH)	Guinea pig	Polyclonal	Mammalian GnRH conjugated to bovine thyroglobulin	Kind gift of Dr. Erik Hrabovszky, Hungarian Academy of Sciences, Hungary (#1018)	1:1000
cFos	Rabbit	Polyclonal	A synthetic peptide (SGFNADYEASSRC) (Cat. No. PP10) corresponding to amino acids 4-17 of human c-Fos	Calbiochem® Cat. # PC38	1:50,000
Oxytocin	Mouse	Monoclonal	Oxytocin conjugated to thyroglobulin.	Millipore, USA Cat. # MAB5296	1:500
Vasopressin	Mouse	Monoclonal	Vasopressin neurophysin	Kind gift of Dr. H. Gainer	1:500
Glial fibrillary acidic protein (GFAP)	Mouse	Monoclonal	Purified GFAP from porcine spinal cord.	EMD Millipore, Cat. # MAB360	1:500
Vimentin	Mouse	Monoclonal	Purified vimentin from pig eye lens.	EMD Millipore, Cat. # MAB3400	1:1000

Estrogen receptor alpha (ER α)	Rabbit	Polyclonal	KLH-conjugated synthetic peptide corresponding to 15 amino acids of rat ER α (TYIYIPPEAEGFPNTI).	EMD Millipore, Cat. # 06-935	1:1000
Cholera Toxin B Subunit (CtB)	Goat	Polyclonal	Purified CtB isolated from <i>Vibrio cholerae</i>	List Biological Laboratories, Campbell, CA, USA Cat. # 703	1:5000
GAPDH	Mouse	Monoclonal	A partial length recombinant GAPDH protein (amino acids 120-320)	Abgenex Cat. # 10-10011	1:8000
β -Actin	Rabbit	Monoclonal	A synthetic peptide corresponding to residues near the amino terminus of human β -actin protein	Cell Signaling Cat. # 4970	1:8000
GH	Rabbit	Polyclonal	Rat GH	National Hormone and Pituitary Program (NHPP), NIH, USA	1:1000 (IF); 1:2000 (IF cells)
TRPV1	Rabbit	Polyclonal	Peptide EDAEVFKDSMVPGEK, corresponding to the amino acid residues 824-838 of rat TRPV1 (Accession O35433) from C-terminus region.	Alomone Labs, Jerusalem, Israel Cat. # ACC-030	1:1000 (IF); 1:2000 (IF cells); 50 ng/ml (WB)
TRPV2	Rabbit	Polyclonal	Peptide (KNSASEEDHLPLQVLQSP) corresponding to amino acids 744-761 of rat vanilloid receptor like protein 1, conjugated to KLH	Calbiochem, Cat. # PC421	1:1000 (IF); 50 ng/ml (WB)
TRPV2	Rabbit	Polyclonal	Peptide KKNPTSKPGKNSASEE, corresponding to the amino acid residues 735-750 of rat TRPV2 (Accession Q9WUD2) from C-terminus region.	Alomone Labs, Jerusalem, Israel Cat. # ACC-032	1:1000 (IF); 50 ng/ml (WB)

TRPV3	Rabbit	Polyclonal	KLH conjugated synthetic peptide selected from the N-terminal region of mouse TRPV3 (NP_659567, 95-129)	Sigma-Aldrich Cat. # SAB1300539	1:1000 (IF); 50 ng/ml (WB)
TRPV4	Rabbit	Polyclonal	Peptide CDGHQQGYAPKWRA EDAPL, corresponding to the amino acid residues 853-871 of rat TRPV4 (Accession Q9ERZ8) from C-terminus region.	Alomone Labs, Jerusalem, Israel Cat. # ACC-034	1:1000 (IF); 50 ng/ml (WB)
TRPV5	Rabbit	Polyclonal	Peptide GLNLSEGDGEEVYHF, corresponding to the amino acid residues 715-729 of human TRPV5 (Accession Q8NDW5) from C-terminus region.	Alomone Labs, Jerusalem, Israel Cat. # ACC-035	1:1000 (IF); 50 ng/ml (WB)
TRPV5	Goat	Polyclonal	Peptide C-SHRGWEILRQNT corresponding to amino acids 697-708 of human TRPV5.	Abcam, USA Cat. # ab77351	1:2000
TRPV6	Rabbit	Polyclonal	Peptide NRGLEDGESWEYQI, corresponding to the amino acid residues 712-725 of human TRPV6 (Accession Q9H1D0) from C-terminus region.	Alomone Labs, Jerusalem, Israel Cat. # ACC-036	1:1000 (IF); 50 ng/ml (WB)